UNIVERSITY OF CANTERBURY

Department of Mechanical Engineering
Christchurch, New Zealand

The Design of Resonant Absorbers

by

Timothy D Whitehead

Master of Engineering Thesis

July 2005

The Design of Resonant Absorbers

by

Timothy D Whitehead

A thesis submitted in partial fulfilment
of the requirements for the degree of

Master of Engineering

in the

Department of Mechanical Engineering
University of Canterbury
Christchurch, New Zealand

July 2005

Abstract

The purpose of this project was to investigate the acoustic performance of a range of resonant absorbers as typically used in automotive applications. A literature review considering sources of exhaust noise, muffler types and components, sound measurement, and prediction techniques was undertaken. Test facilities were constructed that allowed testing of muffler systems with either an engine or a speaker as the source of excitation. This enabled measurements made with a speaker to be compared to those made with an engine, the latter including flow, temperature and pressure effects. A number of different muffler systems were tested and their acoustic performance predicted using a scattering matrix technique. Comparing measured and predicted results allowed assessment of the accuracy of the predictions, the performance of various muffler components and the reliability of measurements. The model adequately predicted muffler performance for all muffler systems tested apart from those containing Helmholtz resonators. This was attributed to pressure and flow effects not included in the model. Using the modelling procedure presented, muffler systems can be quickly designed and optimised.

Acknowledgements

I would like to extend special thanks to Dr John Pearse and Professor Cliff Stevenson of the Department of Mechanical Engineering at the University of Canterbury. Their supervision, support and technical knowledge throughout the course of the project was invaluable.

I would like to thank the staff in the Product Engineering Department at Southward Engineering Company Limited for their enthusiasm and support of the project, for supplying the hardware required, and for reviewing my results and progress.

I would also like to thank the technicians and workshop staff in the Mechanical Engineering Department for their help. In particular I would like to thank Eric Cox for his help in the Automotive Laboratory setting up the experimental arrangement and running the test engine.

I would like to thank my sister Emma Bassett for her help with the project and for her support and guidance. I would like to thank Vanessa Cammell for her support during the project; the time spent with her away from University helped me to stay relaxed and productive throughout the project. Finally, I would thank my mum Heather Bassett for providing me with the opportunity to come to university and for her support over the years.

Table of Contents

Chapter 1
Introduction

1.1 Project objectives

The objective of this project was to assess the performance of resonant absorbers as used in automotive muffler systems. A number of parameters were investigated including tuned resonators, temperature, pressure, inlet pipe length, flow, engine load, and chamber curvature. A model was developed and refined to predict the acoustic performance of resonant absorbers.

The outcome of this project was a tool which allows the fast and accurate prediction of muffler performance for use in the development of muffler systems.

1.2 Project outline

This thesis is arranged in seven chapters: Introduction, Literature Review, Experimental Arrangement, Muffler Testing, Modelling, Project Findings and Analysis, and Conclusion and Recommendations. Following Chapter 1, this introduction, a literature review is presented in Chapter 2. The literature review considers established findings concerning the sources of exhaust noise and its propagation, muffler types and their attenuation characteristics, measurement of exhaust noise, and modelling techniques. Chapter 3 describes the experimental arrangement and tests conducted to ensure accuracy and repeatability of measurements. Chapter 4 presents the experimental procedure and results gathered using the experimental arrangement described in the previous chapter. Chapter 5 presents theory and modelling procedure used to predict muffler performance. The predicted and measured results are presented in Chapter 6. These are discussed in terms of the accuracy of the model, the validity of results, and the changes in muffler performance observed. The final chapter contains overall conclusions to the project and recommendations for further work. Following this are appendices containing drawings of the mufflers tested and figures showing the measured and predicted performance of each muffler system tested.

1.3 Nomenclature

A complete list of symbols used in this thesis together with meanings and units (if applicable) is shown in this section. As some symbols have multiple definitions, for ease of use and clarity all symbols are defined when they are first used in each chapter listed below formulas and diagrams.

A	area (m²)
a	radius (m)
c	speed of sound (m/s)
cyl	number of cylinders
d	diameter (m/mm)
f	frequency (Hz)
f_r	resonant frequency (Hz)
h	thermal convection coefficient
i	imaginary operator
IL	insertion loss (dB)
k	acoustic wave number
ka	Helmholtz number
K,C,n	coefficients
l	length (m)
M	Mach number
m	expansion ratio
N	engine speed (RPM)
P	denotes function of pressure
PWL	sound power level
p	sound pressure (Pa)
Q	directivity
R	gas constant / real component of impedance / reflection coefficient
r	radius (m)
RMS	root mean square
R_s	flow resistance (mks rayls)
S	surface area (m²)
SPL	sound pressure level
St	Strouhal number
T	temperature (°C, K) / denotes function of time / reverberation time (s)
T_x	Transfer matrix for element x in the system

t	time (s) / connecting tube length (m/mm)
TL	transmission loss (dB)
u	velocity (m/s)
V	volume (m^3)
v	particle velocity
W	acoustic power (W)
X	imaginary component of impedance
x	length / distance on along the x-axis (m/mm)
Z	impedance
$\bar{}$	denotes average value
$\begin{bmatrix} A & B \\ C & D \end{bmatrix}$	four pole parameters
α	resonator resistance / room constant
β	resonator reactance
γ	ratio of specific heats
δ	mass end correction
ε	emissivity
λ	wave length (m)
μ	viscosity
ρ	density (kg/m^3)
σ	Plancks constant / expansion ratio
φ	End correction factor (non-dimensional)
ψ	phase angle (rad)
ω	angular frequency (rad/s)

Subscripts:

$_b$	branch
$_g$	gas
$_i$	incident
$_r$	reflected
$_m$	measured
$_{tr}$	transmitted
$_w$	wall
$_0$	main passage
$_{1,2,3\ etc}$	denotes specific points in a system

Chapter 2
Literature Review

Summary

The performance of an exhaust system is assessed by a number of factors; the two most important being the backpressure and the attenuation of the system. High backpressure in an exhaust system affects the performance of the engine, decreasing power and increasing fuel consumption, and hence emissions. Exhaust noise is a large contributor to traffic noise, a significant source of noise pollution. An exhaust system must therefore achieve somewhat conflicting goals of low backpressure and high attenuation, while also taking into account cost, manufacturing, materials, weight, and space issues.

Exhaust noise can be classified into two categories: pulsating noise from the engine, and flow noise from high speed exhaust gasses flowing though and exiting the exhaust system. Pulsating noise is generated when exhaust gases at high pressure are released from the engine cylinders through the exhaust valves. Flow noise is created by exhaust gas flow eddying, oscillating and impacting inside the exhaust system as well as jet noise as the flow exits the system. Flow noise can be both tonal and broadband in nature, with broadband flow noise having frequency components predominantly over 500 Hz. Comparatively, pulsating exhaust noise is relatively low frequency.

Pulsating noise can be attenuated through the use of reactive or dissipative mufflers, or more commonly a combination of the two. Flow noise generated by the components of the exhaust system itself can be avoided through careful design, or can be attenuated using a muffler downstream of the flow noise source. Techniques for the prediction of exhaust noise have been the focus of a large amount research over the years with modelling ranging from simple one-dimensional calculations for individual elements to three-dimensional system models solved using computational techniques.

Techniques for the measurement of noise emitted from vehicle exhaust systems and for total vehicle noise are set out in both ISO (International Standard) and SAE (Society of Automotive Engineers) standards and recommended practices. Exhaust noise is regulated by legislation in Australia with the maximum limit being 90 dB(A) for a stationary test. In New Zealand the Traffic Regulations of 1976 set out a drive-by noise limit for new passenger vehicles at 81 dB(A). There is currently no objective noise limit in New Zealand for exhaust noise itself. A significant proportion of the noise emitted during a drive-by test is emitted directly from the exhaust outlet or radiated from the exhaust structure.

Table of Contents

List of Figures and Tables

2.1 Introduction

This chapter reviews current literature available on automotive exhaust noise and in particular the prediction and measurement of noise attenuation through the use of mufflers. The review is organised into the following sections:

- Sources of exhaust noise and its propagation
- Muffler components and their attenuation characteristics
- Sound measurement techniques
- An overview of modelling techniques

2.2 Sources of exhaust noise and its propagation

2.2.1 Introduction

Weltens, Bressler and Krause [1] stated that in vehicle drive-by tests the dominant source of noise is from the engine itself, with a large contribution from the exhaust system being noise either directly from the exhaust outlet or radiated from the exhaust structure (shell noise). Figure 2.2-1 below shows the relative magnitudes of noises produced from a drive-by test of a small car [2].

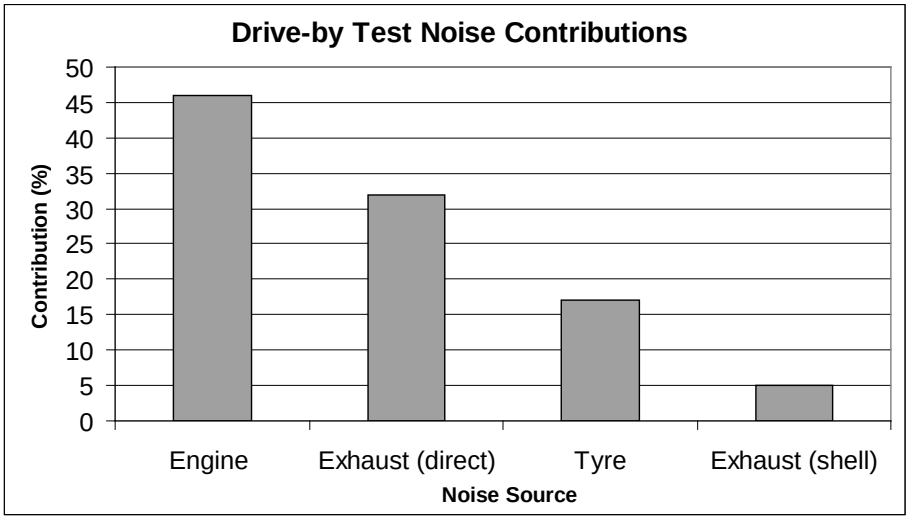

Figure 2.2-1 Drive-by noise contributions, adapted from Kim et al. [2]

Phillips and Orchard [3] defined four sources of noise as being inherent to motor vehicles, being: power plant (engine/transmission), induction, exhaust and tyre noise. Exhaust noise is primarily generated by the discharge of combustion products at high pressure and temperature from the engine cylinders through the exhaust valves, producing a pulsating noise. As exhaust gases flow through the

exhaust system and as they exit the exhaust outlet, flow noise is produced [4]. Secondary sources of exhaust noise involve the transmission of mechanical noise from the engine, such as piston slap and valve train noise. In addition to these sources, if the engine is equipped with a supercharger or a turbocharger there will be associated noise components related to the engine and turbine speeds respectively [5]. This section will focus on the generation of pulsating noise and flow noise and its propagation to the surroundings either directly from the exhaust outlet or radiated from the exhaust structure.

2.2.2 Pulsating noise

Pulsating exhaust noise is generated by the periodic release of exhaust gases from the engine cylinders. Pulsating noise is characteristically low frequency and is directly related to the number of cylinders in the engine and the speed of rotation of the engine [6]. The fundamental frequency component of pulsating noise is generally described by the following equation (for a four stroke engine):

$$f = \frac{N}{60} \times \frac{cyl}{2} \ (Hz) \qquad (2.2\text{-}1)$$

Where: f = frequency (Hz)
N = engine speed (rpm)
cyl = number of cylinders

There will be components present at multiples of this frequency known as higher engine orders or firing harmonics. The equation stated above is very general with the actual frequency dependent on the design of the exhaust manifold. If the length of each exhaust manifold is not equal, then the noise emitted will change due to the pulsations from each cylinder interacting. As a result, the system must be analysed per engine cycle rather than as a series of identical pulses [7]. The size and characteristic of the exhaust pulse is primarily dependant on exhaust valve timing. However, it is also influenced by a number of engine parameters such as cylinder volume, compression ratio and air/fuel ratio [1]. There is little information available on the influence of these parameters on the behaviour of an engine as a noise source. As each engine type varies in configuration and timing the size and characteristic of the exhaust pulse from each engine type will be different [7]. Levels of exhaust noise vary with engine load typically increasing 15 dB from no load to full load [8].

2.2.3 Flow noise

Flow noise is generated by turbulent exhaust gas flow eddying, impacting and oscillating within the exhaust system and as the exhaust flow exits the system. Flow noise can be both broadband and tonal in nature depending on the mechanism of generation. Tonal flow noise of specific frequency arises when a free stream flow passes an obstacle creating swirling vortices that shed at a specific frequency given by the equation:

$$f = St\frac{u}{d}\ (Hz) \qquad (2.2\text{-}2)$$

Where: f = frequency (Hz)
St = Strouhal number
u = flow velocity (m/s)
d = critical diameter (m)

Flow noise of the same type is produced by vortex generation inside closed pipe systems at area discontinuities and at sharp edges such as baffles. The basic frequency of noise is the same as that for an object in free flow given by equation 2.2-2. Flow noise generated by vortex shedding from discontinuities in the exhaust system has been shown to exhibit staging where the frequency of generation jumps from one discrete frequency to another as flow speed is increased. Davies [9] attributed this to a feedback interaction between the vortex generation and the flow. Figure 2.2-2 below shows flow noise generated at the entrance of an expansion chamber and its transmission to the tailpipe.

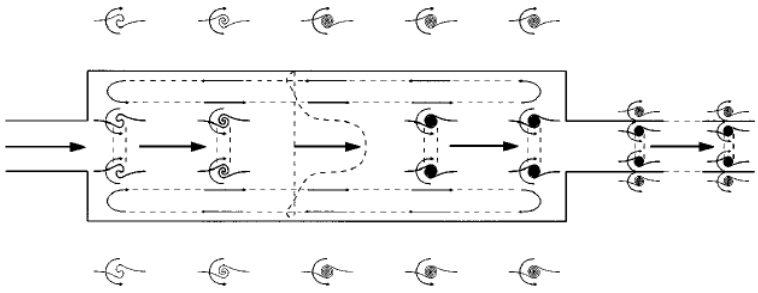

Figure 2.2-2 Expansion chamber showing ring vortices and flow circulation [9]

Flow noise is more commonly broadband in nature caused by turbulent flow through the system. Erhard [10] showed that the lower the Reynolds Number of the flow the smaller the bandwidth of the flow noise created. Broadband flow noise is also generated at the exhaust outlet when the exiting jet of exhaust gas interacts with the surrounding atmosphere. Studies [9-12] have shown that flow noise generated in exhaust systems can be amplified by resonances within the system.

Lighthill's [13, 14] acoustic theory relates pressure fluctuations in flows to the generation of acoustic waves, this is the basis of flow noise. Kunz [15] presented a solution to Lighthill's equation for noise in an exhaust flow. However, the solution is restricted to the special case of a dipole source in a narrow channel. Tanaka and Harara [4] presented a more general solution for the sound power produced by flow. As flow noise is a type of aerodynamic noise its acoustic power can be expressed by the equation:

$$PWL = \frac{K\rho^2 \overline{U}^{2n} A}{\rho_0 c^{2n-3}} = \frac{K\rho^2 c^3 M^{2n} A}{\rho_0} \ (W) \qquad (2.2\text{-}3)$$

Where: PWL = acoustic power (W)
ρ_0 = atmospheric air density (kg/m³)
ρ = air density of noise source (kg/m³)
$\bar{U}$ = mean flow velocity (m/s)
c = sound velocity in atmospheric air (m/s)
A = area of exhaust outlet (m²)
$M = \bar{U}/c$ = Mach number
K = dimensionless coefficient
n = index, 1 to 4

For flow noise generated at the exit of exhaust gas into a larger chamber $n = 3$. For flow noise generated from exhaust gas leaving the exhaust outlet as a jet $n = 4$.

The exhaust gas speed of modern engines can be up to Mach 0.25 [16]. Area discontinuities within the exhaust system may increase local flow velocities to multiples of the mean velocity and shock waves can be formed. Seknine et al. [17] conducted a study into the development of shock waves in exhaust systems. The study found local exhaust gas speeds at an area expansion of up to Mach 1.1 causing shockwaves to develop. This was related to the generation of a metallic noise in the system.

A compression ratio over two will typically produce supersonic flow if the pressure is suddenly released. As modern engines have compression ratios up to 14:1, the pressure ratio is high enough for supersonic flow to occur. However, as the exhaust valve opening is not instantaneous and choked flow occurs; supersonic flow from the exhaust valves is uncommon. Wave steepening is more likely to occur as the pressure wave travels through the exhaust system. As the distance between discontinuities in exhaust systems is usually quite short, significant wave steepening does not commonly occur [18].

2.2.4 Noise propagation

Exhaust noise will propagate from the exhaust system to the surroundings by either direct discharge from the exhaust outlet, or by emanating from the exhaust structure itself (shell noise). It is of paramount importance that the exhaust system is sealed along its length to the exhaust outlet. Small openings before the outlet can be very detrimental to the acoustic performance of the system, not to mention the possibility of leaking poisonous exhaust gases.

Studies [1, 19] have shown that the noise radiated from the exhaust structure itself predominantly arises when large flat surfaces are present in the exhaust system. In recent years increasing space restrictions underneath cars have led to the use of thin half pressings and elliptical shaped mufflers. Mufflers of this type have large flat surfaces that are acoustically efficient at radiating sound. Shell noise can be reduced by stiffening or increasing the transmission loss of the walls of the system. Figure 2.2-3 shows a summary of various methods that can be used to reduce the propagation of shell noise and their approximate effect over a standard thickness single case.

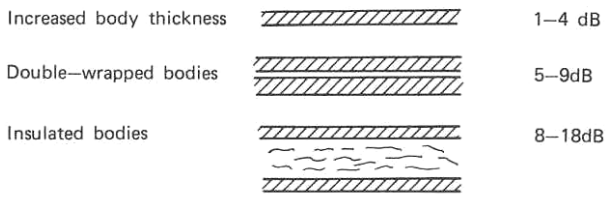

Figure 2.2-3 Shell noise control techniques [8]

2.3 Muffler elements

2.3.1 Introduction

Most modern vehicles use a number of mufflers to reduce the exhaust noise to a level less than or equal to that of other noise sources present, such as: engine noise, tyre noise and wind noise. In general, the components of automotive mufflers can be split into two basic categories that reflect the process by which the sound is primarily attenuated:

1. Reactive or resonant mufflers.
2. Absorptive or dissipative mufflers.

Most modern exhaust systems use a combination of reactive and dissipative mufflers, and often have a number of muffler elements tightly packed into one case. Reactive mufflers can be tuned to attenuate specific frequencies of noise, or be tuned for a broad frequency range dependant on muffler design. Reactive mufflers are most effective at lower frequencies. Dissipative mufflers tend to provide broadband attenuation predominantly at higher frequencies (above about 1000 Hz) and become increasing effective as frequency rises [16]. In this section, the basic reactive and dissipative elements of automotive mufflers are presented. The process by which they attenuate sound is discussed along with some examples of muffler systems as used in the automotive industry.

2.3.2 Perforates

Perforates are present in most modern exhaust systems, either as flow through, or flow past elements. Flow through elements are generally used to dissipate the pulsations in the flow. Flow past elements are used in expansion chamber type mufflers where the perforate is used to direct flow, reduce flow noise, provide an acoustic coupling to the reactive chambers and structurally connect the inlet(s) and outlet(s) of the muffler. Perforated sections are also used to contain packing material in absorptive style mufflers.

The acoustic performance of a perforated section of pipe in an exhaust system is highly dependant on its percentage open area. If the percentage open area of a perforate is over about 20 percent, in the direction of propagation, the perforate can be said to be acoustically transparent. For percentage open areas below 20 percent, at higher frequencies the perforate will act somewhat like a Helmholtz resonator with an attenuation peak associated with the primary resonance of the chamber and

associated higher order secondary peaks. At low frequencies, the perforate will appear somewhat acoustically transparent. These effects are shown in Figure 2.3-1 below.

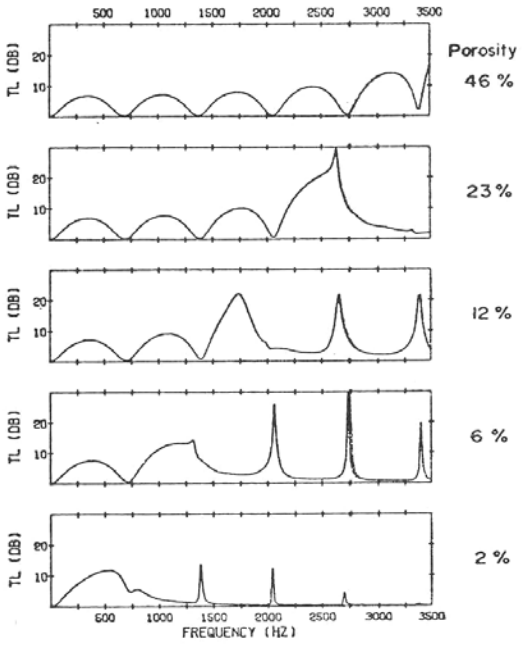

Figure 2.3-1 Effect of perforate percentage open area on muffler performance [8]

2.3.3 Reactive mufflers

2.3.3.1 Introduction

The performance of a reactive muffler is determined by its internal geometry. This will define the attenuation characteristic of the muffler that can range from sharply tuned narrow band attenuation to broadband attenuation across wide frequency bands. The one or more chambers, resonators, or finite sections of pipe that collectively make up a reactive muffler provide an impedance mismatch. This impedance mismatch results in a reflection of part of the incident acoustic energy back towards the source of the sound or back and forth between chambers, where it is eventually dissipated. The cut-off frequency of a muffler relates to the point where the presence of only one dimensional plane waves can no longer be assumed. At frequencies above the cut-off frequency, higher order waves will propagate through the muffler and dramatically decrease its performance. For this reason reactive mufflers are most effective at attenuating low frequency noise. In the following sections, a range of reactive mufflers that are in common use in automotive exhaust systems will be described along with their attenuation characteristics. Only the performance of the muffler itself will be considered, neglecting inlet and outlet conditions that will be considered separately.

2.3.3.2 Expansion chamber mufflers

The simplest reactive muffler is the expansion chamber muffler, which as the name suggests is simply a section of increased area. If the wavelength (λ) of the sound of interest corresponds to the length of the chamber, and at half order multiples of this (e.g. λ/2, λ, 3λ/2…), the expansion chamber is a perfect impedance match to the pipe and no sound is attenuated. For frequencies other than this, the discontinuity reflects a portion of the acoustic energy back towards its source resulting in destructive interference [6]. Examples of expansion chamber mufflers are shown in Figure 2.3-2 along with their attenuation characteristics predicted using equation 2.3-1. Experimentally determined attenuation is shown at point values.

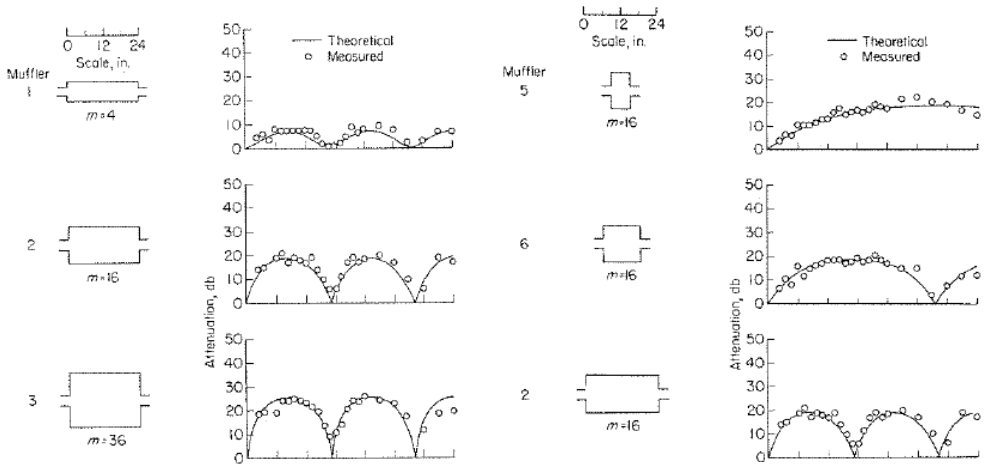

Figure 2.3-2 Characteristic curves for expansion chamber mufflers [20]

Figure 2.3-2 shows that the performance of the expansion chamber muffler is only dependant on two factors: the length of the expansion chamber, which serves to change the periodicity of the attenuation characteristic; and the expansion ratio, which affects the magnitude of the attenuation. The transmission loss (*TL*) of an expansion chamber muffler as shown in Figure 2.3-2 can be calculated using the equation developed by Davis [20] below:

$$TL = 10\log\left[1+\frac{1}{4}\left(m-\frac{1}{m}\right)^2 \sin^2 kl\right] \ (dB) \qquad (2.3\text{-}1)$$

Where: m = expansion ratio
$kl = 2\pi l / \lambda$
l = length of expansion chamber (m)
λ = wavelength of sound of interest (m)

Connection of two of more expansion chambers in series yields an increase in attenuation. As the number of chambers connected in series is increased, the rate of improvement in attenuation is decreased. The length of the tube connecting the chambers has a significant effect on the attenuation characteristic. An increase in the length of the connection tube leads to higher attenuation and wider regions of approximately zero attenuation centred about the resonant frequencies. These effects are illustrated in Figure 2.3-3 below.

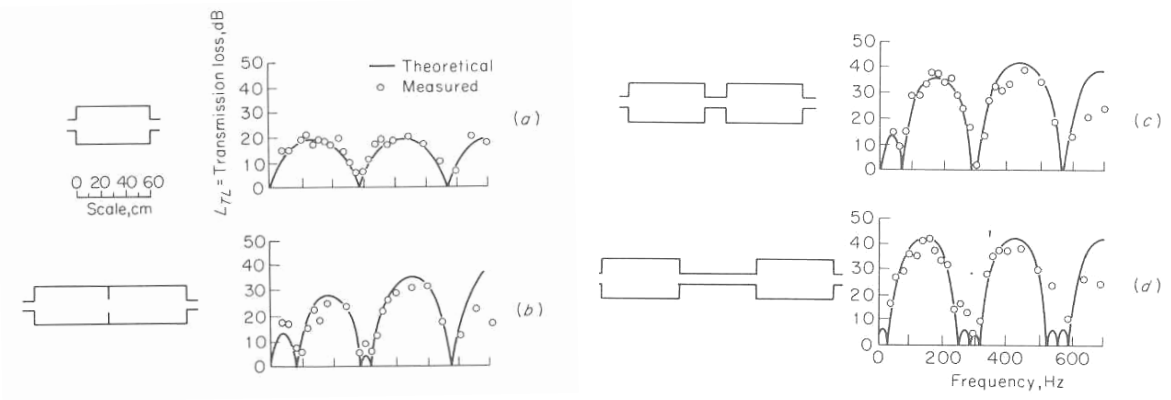

Figure 2.3-3 Effect of connection tube length between two expansion chamber resonators [20]

2.3.3.3 Extended tube resonators

Extended tube resonators are characterised by the protuberance of inlet or outlet pipes into an expansion chamber. At certain frequencies all the incoming acoustic energy is used to resonate the closed end cavity and almost none is transmitted downstream. Four examples of extended tube resonators are shown in Figure 2.3-4 below.

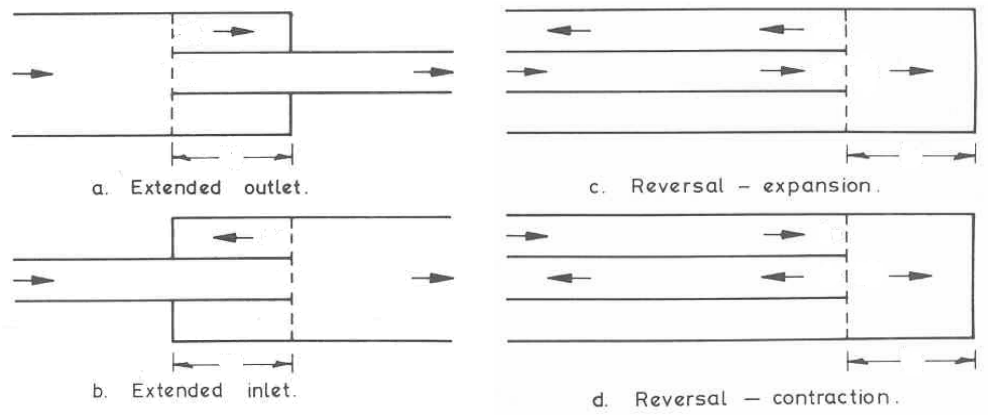

Figure 2.3-4 Extended tube resonators [21]

The frequencies at which resonance occurs are given by the simple relation:

$$\frac{l}{\lambda} = \frac{(2n+1)}{4},\ n = 0, 1, 2, 3\ldots \qquad (2.3\text{-}2)$$

Where: l = length of extended tube (m)
λ = wavelength of resonance (m)

As the length of the extended tube resonator corresponds to ¼ of the wave length at which resonance occurs, extended tube resonators are also called quarter wave resonators. The transmission loss of an extended tube resonator at its resonance frequency is given by the following equation:

$$TL = 10\log_{10}\left(1 + \frac{\rho c}{2R_s m}\right)^2 \ (dB) \qquad (2.3\text{-}3)$$

Where: ρ = density of gas (kg/m³)
c = speed of sound in gas (m/s)
R_s = specific acoustic resistance of the resonator (mks rayls)
m = expansion ratio

The attenuation of an extended tube resonator is however, significantly lowered by the presence of mean flow. It is common for extended tube resonators to be combined with an expansion chamber as shown in Figure 2.3-5 below. Selamet and Ji [22, 23] showed that by tuning the extensions to the pass bands of an expansion chamber it is possible to produce a combination of the broad band attenuation domes of an expansion chamber with the resonant peaks of the extended tube resonator.

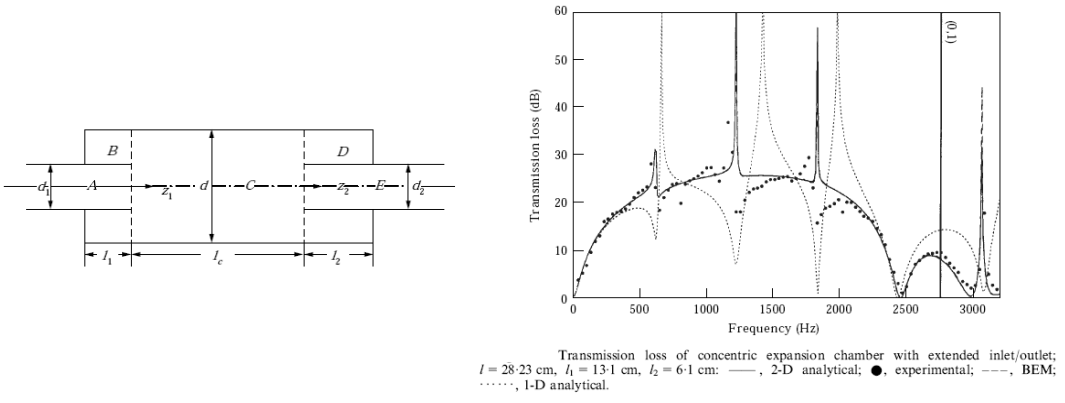

Transmission loss of concentric expansion chamber with extended inlet/outlet; l = 28·23 cm, l_1 = 13·1 cm, l_2 = 6·1 cm: ——, 2-D analytical; ●, experimental; – – –, BEM; · · · · · ·, 1-D analytical.

Figure 2.3-5 Attenuation characteristic extended inlet and outlet/expansion muffler [22]

2.3.3.4 Helmholtz resonators

Helmholtz resonators, also known as side branch or volume resonators, differ from expansion chamber or extended tube resonators in that there is no gas flow through the chamber. A Helmholtz resonator consists of a small opening or neck connected to a larger chamber. The basic principle is that a small mass of gas oscillates in the neck of the resonator causing compression and expansion of the volume of gas inside the chamber. At the resonant frequency of the chamber, the impedance reduces to zero preventing any transmission of noise. Figure 2.3-6 below shows the components of a simple Helmholtz resonator.

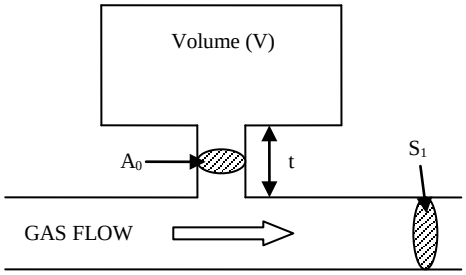

Figure 2.3-6 Helmholtz resonator schematic

Where: A_o = area of connection tube (m²)
V = volume (m³)
S_1 = area of main pipe (m²)
t = length of connection tube (m)

Assuming that the dimensions of the cavity are less than 1/10th of the wavelength of the highest frequency of interest, the transmission loss of a Helmholtz resonator can be expressed as follows [24]:

$$TL = 10\log_{10}\left[1 + \frac{\alpha + 0.25}{\alpha^2 + \beta^2(f/f_r - f_r/f)^2}\right] \ (dB) \qquad (2.3\text{-}4)$$

Where: α = resonator resistance = $S_1 R_s / A_0 \rho c$
β = resonator reactance = $S_1 c / 2\pi f_r V$
S_1 = area of main duct (m²)
R_s = flow resistance in resonator tubes (mks rayls)
V = volume of resonator (m³)
A_0 = total aperture area (m²)
f_r = resonance frequency (Hz)
ρ = density of gas (kg/m³)
c = speed of sound in gas (m/s)

The resonant frequency is given by:

$$f_r = \frac{c}{2\pi}\sqrt{\frac{A_0}{Vt'}} \quad (Hz) \qquad (2.3\text{-}5)$$

Where: t' = the equivalent neck length = $t + \varphi\sqrt{4A_0/\pi}$ (m)

φ = the end correction factor

At resonance the impedance of the resonator is reduced to zero and equation 2.3-4 simplifies to:

$$TL = 20\log_{10}\left(\frac{\alpha + 0.5}{\alpha}\right) \quad (dB) \qquad (2.3\text{-}6)$$

Davis et al. [20] described the parameters for the chamber openings using a single parameter called the conductivity (c_o) which is equal to A_0/t'. Two examples of the attenuation characteristics of Helmholtz resonators as described above are shown below in Figure 2.3-7. Note the finely tuned attenuation peak that would not be of much use on its own to attenuate the broadband noise from an internal combustion engine which has many peaks that vary depending on engine speed and load. A broadening of the attenuation region can be obtained by increasing the chamber volume and neck conductivity.

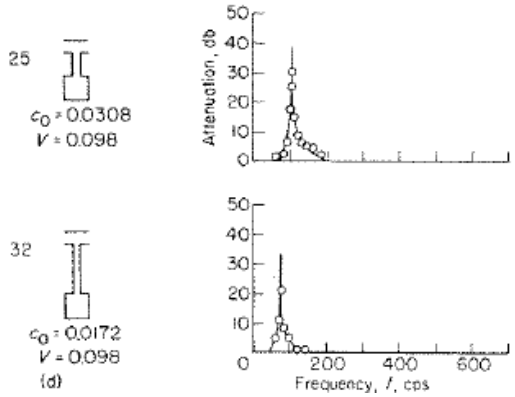

Figure 2.3-7 Attenuation characteristic of a side branch Helmholtz resonator [20]

Davis et al. [20] showed that as the dimensions of the resonator volume become sufficiently large, wave motion within the cavity cannot be neglected. The performance of the resonator then becomes dependant on the location of the entrance(s) to the cavity. In automotive applications Helmholtz resonators are commonly arranged in a concentric fashion with resonator cavities sufficiently large that wave motion inside the cavity takes place.

Figure 2.3-8 illustrates that wave motion in the cavity becomes the dominant effect. The resultant system is much like two parallel extended tube resonators with maximum attenuation occurring at a frequencies relating to the length from the neck opening(s) to the ends of the cavity. Davies [25] provided a simple way to analyse this by calculating the effective length of the resonator and treating it as a quarter wave resonator.

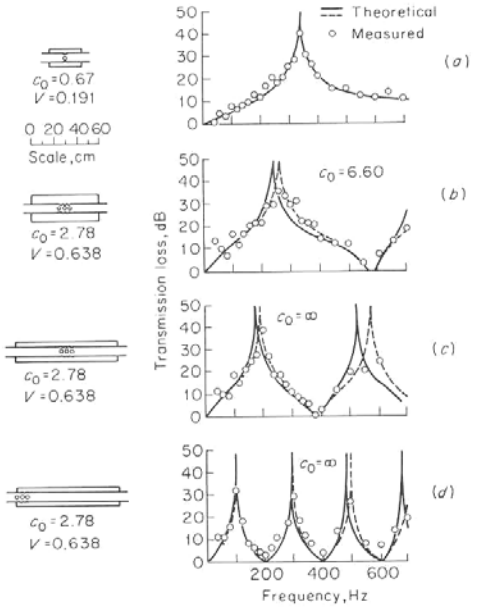

Figure 2.3-8 Wave motion effects in concentric tube Helmholtz resonators [20]

Wan and Soedel [26] analysed and experimentally tested two degree of freedom (2DOF) Helmholtz resonators. The 2DOF Helmholtz resonators tested had a second resonator connected to the volume of the first resonator. The result is a system with two natural frequencies and hence two attenuation peaks of the same size as a single degree of freedom system. It was observed in this study that grazing flow over the inlets to the resonant chamber increased the tuned peak frequency and decreased the level of attenuation. Sindhupak et al. [27] conducted a similar study on flow effects on the performance of single degree of freedom Helmholtz resonators and showed the performance of resonators is significantly reduced at a flow speeds over of 60 m/s.

2.3.4 Dissipative mufflers

A dissipative muffler works by smoothing out the pulsations of gas as they flow through the exhaust system. This can be performed in many ways, with the most common being to pass the gas flow through perforated sections, dispersing then recombining the flow. An example of a dissipative muffler is shown in Figure 2.3-9 below. This muffler also demonstrates some properties of expansion chamber and extended tube resonators due to the impedance changes at entry and exit of the muffler.

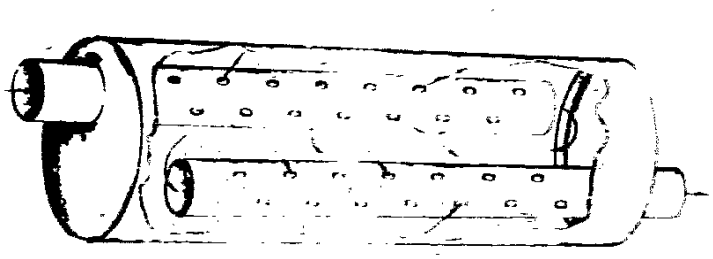

Figure 2.3-9 Dissipative type muffler [28]

2.3.5 Absorptive mufflers

An absorptive muffler is one whose acoustical performance is determined mainly by the presence of sound absorbing materials within the muffler. As the sound waves pass through the spaces between the tightly packed fibres of the absorptive material, the resulting viscous and inertia losses dissipate sound energy as small amounts of heat [16]. Absorptive mufflers usually have relatively broadband noise attenuation characteristics and perform most effectively at frequencies over 1000 Hz. The most common form of an absorptive muffler is an expansion chamber packed with absorption material. Two examples of this are shown in Figure 2.3-10 below. The absorption material is placed behind a perforated pipe to prevent it from blocking the gas flow or being blown out and a barrier layer such as stainless steel wool may also be used to prevent deterioration of the packing material.

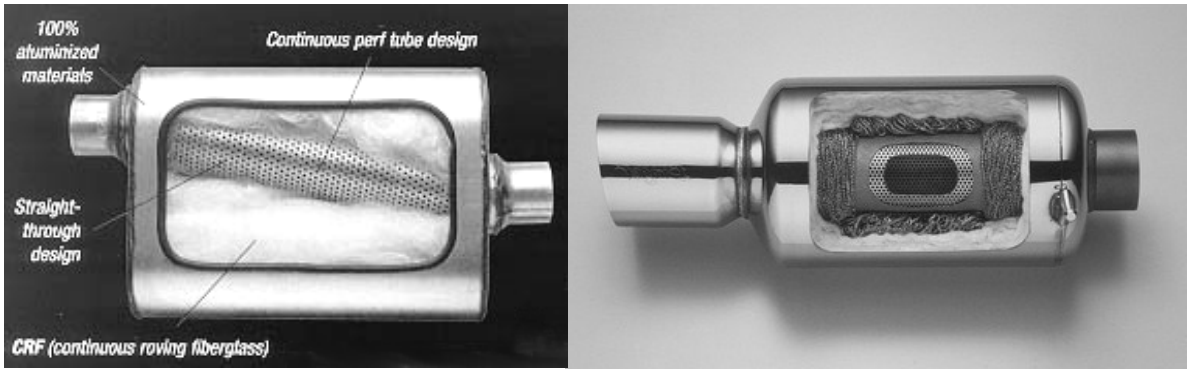

Figure 2.3-10 Absorptive style mufflers

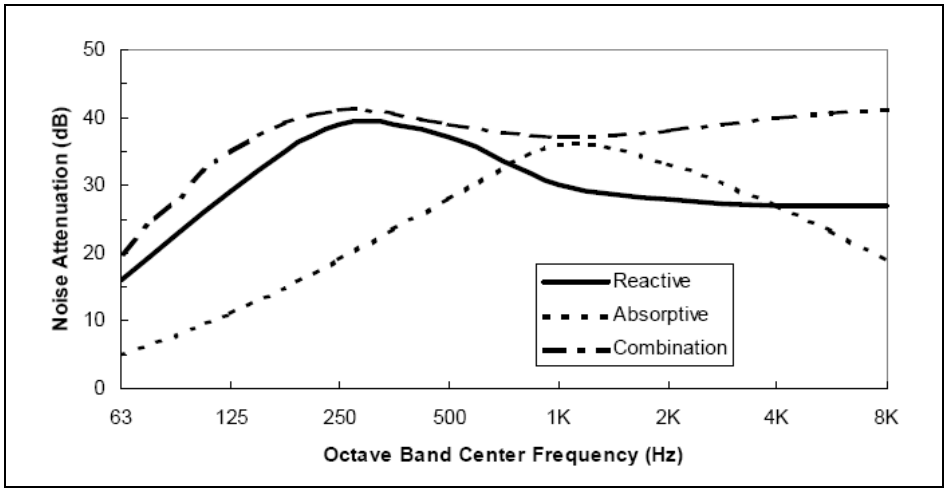

Figure 2.3-11 Comparison of reactive, absorptive and combination mufflers [29]

For straight through type absorptive silencers a change in cross section is inevitably required if the packing material is not to hinder the exhaust flow. The absorptive muffler will therefore have reactive qualities due to the change in impedance at the transition from solid to perforated/packed pipe. Figure 2.3-11 shows the increase in performance that can be gained using a packed style muffler. Lehringer [30] developed a model to calculate the attenuation of such a muffler that coupled the propagation of sound within the absorbing medium using its complex propagation constant and its characteristic impedance with the propagation of the sound through the perforations.

2.3.6 Active and semi-active mufflers

Active and semi-active mufflers differ from the mufflers described thus far in that the muffler reacts to changes in engine conditions, or to the incoming sound field, and changes its properties accordingly. Krause, Weltens and Hutchins [31] conducted a study into active and semi-active muffler systems in current use and defined active and semi-active mufflers as follows. An active muffler is a system where the noise field is measured by a sensor that is connected to a system that adds anti-noise or modulates the pulsating exhaust gas flow to smooth the gas flow and in this way provide sound attenuation. A semi-active muffler will in some way alter its internal geometry to change the performance of the muffler, either acoustically or flow wise, in relation to changes in engine conditions.

Most active noise cancellation systems are designed to cancel noise either inside the passenger compartment or at the exhaust outlet. The sensor of an active noise system will pick up both the sound it is trying to cancel as well as sound from the active system itself. It must therefore compensate for this feedback [32]. Kashani [33] discussed the effectiveness of an active noise control system to reduce a booming noise in a large sport utility vehicle.

Active noise attenuation systems in the exhaust system itself are still in a development stage. Due to the high sound pressure levels inside exhaust systems, extremely powerful speakers are required as the speaker must be able to produce sound levels comparable to the exhaust noise [31]. Also of consideration is the harsh environment of the exhaust system and the effect that this has on the life of active noise control components [34]. These factors make active noise control in the exhaust system itself impractical at this stage.

Semi-active noise systems are more practical for automotive exhaust systems with large manufacturers such as Subaru, Nissan, Mitsubishi and Toyota offering various semi-active systems on some vehicles. An example of a semi-active system is shown in Figure 2.3-12 below.

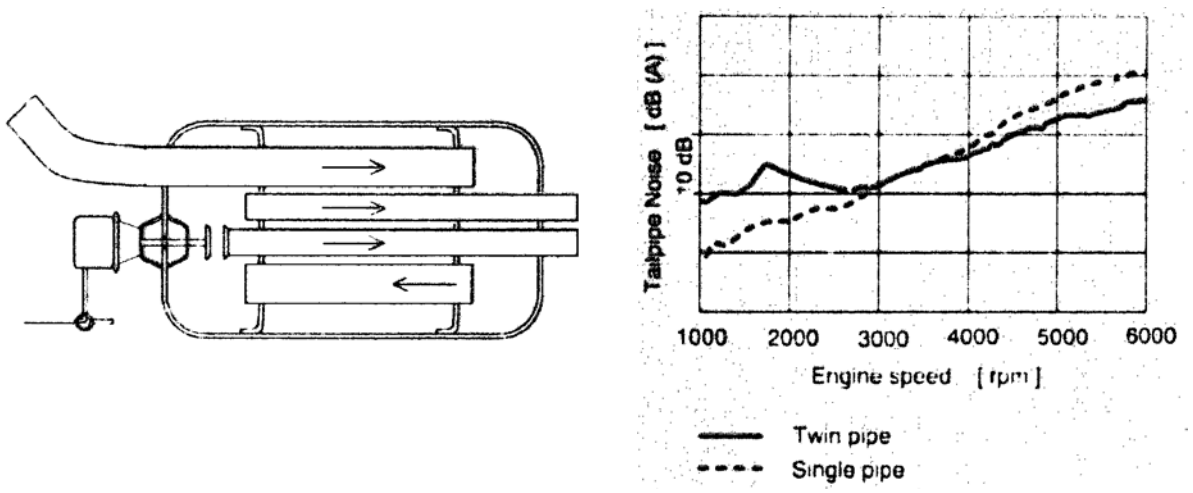

Figure 2.3-12 Semi-active exhaust system [31]

The above figure shows a muffler that uses a valve system to open and close one tailpipe inside the muffler. At low engine speeds, the single pipe provides better attenuation. As engine speed is increased, flow noise becomes the dominant factor and higher attenuation along with lower backpressure is achieved using the twin exhaust pipes. Other systems such as this use tuned tailpipes switching between a long tailpipe for low engine speeds and a short pipe for high engine speeds or simply switching between a single pipe in cruising mode for a quiet sound and twin pipes in performance mode for a sporty sound. In summary, the use of very simple semi-active noise systems provides an appreciable gain in muffler and/or engine performance.

2.3.7 Tailpipe effects

A similar impedance mismatch as the expansion chamber muffler occurs when the flow exits the exhaust outlet. The exhaust pipe ahead of the muffler and the tailpipe after the muffler resonate at certain frequencies amplifying the exhaust noise. This resonance is shown by negative insertion loss in Figure 2.3-13.

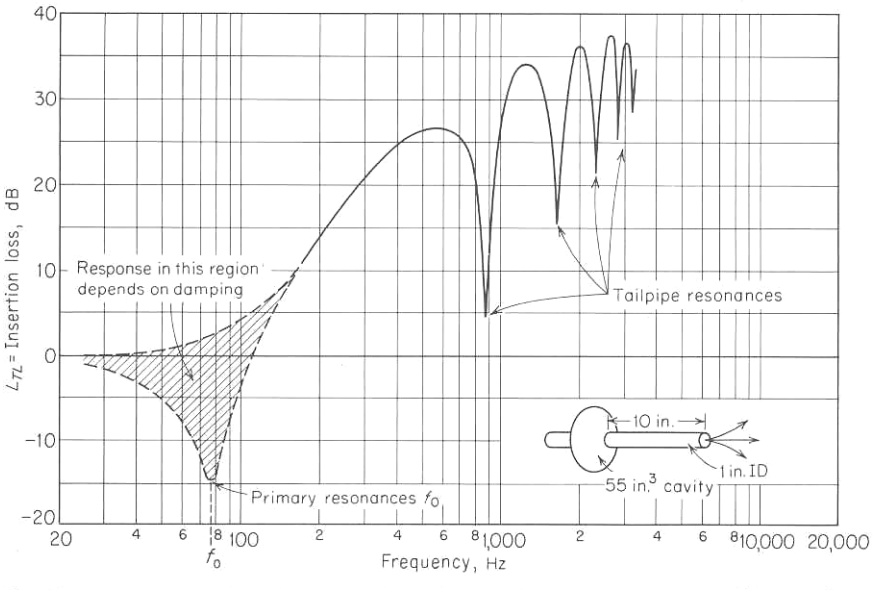

Figure 2.3-13 Effect of tailpipe on resonance of muffler [24]

The primary resonance occurs when the reactance of the tailpipe and muffler cavity are equal and opposite and therefore cancel. The only insertion loss occurring is due to the resistive impedance of the muffler. At higher frequencies half wavelength resonances within the tailpipe also occur [24]. The inlet and tailpipe lengths must be carefully selected so that resonance within them falls in a frequency range where little or no attenuation is required.

An approximation postulated by Davis et al. [20] for the tailpipe impedance is to add an end correction of 0.61 times the pipe radius to the length of the tailpipe and assume that the exhaust outlet is terminated with a zero impedance (a total reflection with a phase shift of 180°). Levine and Schwinger [35] provided a more complex formulation for the end correction that uses a piecewise function dependant on the diameter of the exhaust outlet and frequency of interest. The effect of flow through the tailpipe is to reduce negative insertion loss and improve attenuation at resonance frequencies.

2.4 Sound measurement

2.4.1 Introduction

This section describes measurement parameters and measurement techniques that are in current use for assessing the acoustic performance of exhaust systems and components. There are a number of different parameters that can be used to describe the acoustic performance of exhaust systems. The first part of this section will describe the parameters used and how they are measured. The second part will cover methods set out in SAE and ISO international standards for the measurement of exhaust noise and vehicle drive-by noise. The last part of this section will cover the subjective classification of exhaust noise components using objective measurements.

2.4.2 Measurement parameters for exhaust noise

2.4.2.1 Testing conditions

For the measurement of the acoustic performance of exhaust systems and components it is common to separate the exhaust system or specific exhaust components from the source of excitation. This is usually achieved by using an acoustically treated barrier or a wall. Figure 2.4-1 below shows the layout of one such test facility.

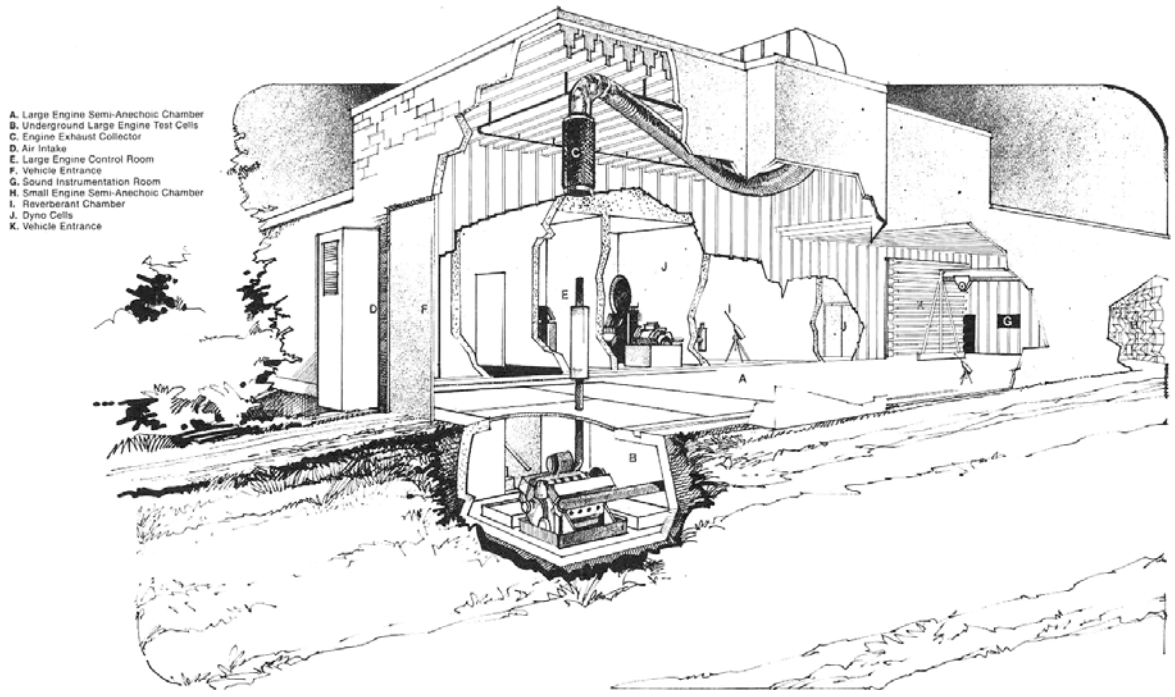

Figure 2.4-1 Exhaust test layout [8]

2.4.2.2 Transmission loss

Transmission loss (*TL*) is the difference in sound power between waves entering the muffler and transmitted past the muffler, assuming an anechoic termination. It is therefore a property of the muffler itself and is independent of upstream and downstream conditions [36]. Transmission loss is defined by the equation below:

$$TL = 10\log_{10}\frac{W_i}{W_t}\ (dB) \qquad (2.4\text{-}1)$$

Where: W_i = incident sound power
W_{tr} = transmitted sound power

There are a number of methods that can be used to measure the incident and transmitted sound power in order to calculate transmission loss. Tao and Seybert [37] reviewed the three most common methods being:

- The decomposition method
- The two source method
- The two load method

Figure 2.4-2 below shows the experimental set up required to measure transmission loss using the decomposition method. The sound power upstream of the test element is measured using a two microphone technique to separate incident and reflected waves. The sound power downstream of the element can be measured directly using a single microphone as the anechoic termination insures there are no reflected wave components from the outlet.

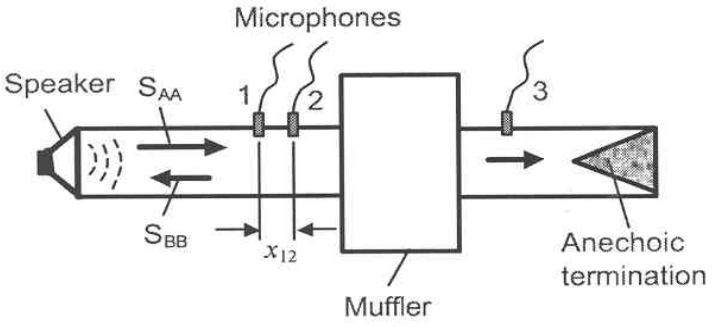

Figure 2.4-2 Test layout for determining transmission loss, decomposition method [37]

The sound pressure can be decomposed into incident (S_{AA}) and reflected (S_{BB}) components using the two-microphone technique and decomposition theory.

Using decomposition theory the auto spectrum of the incident wave is:

$$S_{AA} = \frac{S_{11} + S_{22} - 2C_{12}\cos kx_{12} + 2Q_{12}\sin kx_{12}}{4\sin^2 kx_{12}} \qquad (2.4\text{-}2)$$

Where: S_{11} and S_{22} = the auto spectra of the total acoustic pressure at points 1 and 2
C_{12} and Q_{12} = the real and imaginary parts of the cross spectrum between points 1 and 2
k = the wave number
x_{12} = the distance between the two microphones

The *RMS* amplitude of the incident wave sound pressure p_i can be found from:

$$p_i = \sqrt{S_{AA}} \qquad (2.4\text{-}3)$$

Using *RMS* pressure amplitudes for the incident wave (*i*) as calculated using equation 2.4-3 above and for the transmitted (*t*) wave pressure that is directly measured, the sound power for each wave is given by:

$$W_{i,t} = \frac{p_{i,tr}^2}{\rho c} A_{i,o} \qquad (2.4\text{-}4)$$

Where: $W_{i,tr}$ = the sound power of the incident or transmitted wave
$p_{i,tr}$ = the *RMS* incident or transmitted pressure amplitude
$A_{i,o}$ = muffler inlet area for incident wave and outlet area for the transmitted wave (m)
ρ = density of gas (kg/m³)
c = speed of sound in gas (m/s)

Inserting equation 2.4-4 for both the incident and transmitted waves into equation 2.4-1 yields the following expression for transmission loss:

$$TL = 20\log_{10}\frac{p_i}{p_{tr}} + 10\log_{10}\frac{A_i}{A_o} \qquad (2.4\text{-}5)$$

The main draw back of using the decomposition method and the primary source of error is that a fully anechoic termination is very difficult to construct, especially for low frequencies. Error will therefore be introduced as the microphone measuring the transmitted sound power will also be measuring some reflected component.

The two load and two source methods use four microphone positions and no anechoic termination as shown in Figure 2.4-3 below.

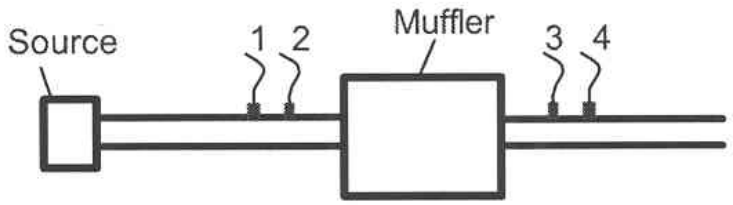

Figure 2.4-3 Test layout for determining transmission loss, two load method [37]

By either changing the location of the source (two source method) or by varying the load (two load method) the transmission loss can be calculated by solving for the four pole parameters, the four components of the pressure/volume velocity transfer matrix of the muffler. The transmission loss across the element can be expressed as a function of the four pole parameters as shown below:

$$TL = 20\log_{10}\left\{\frac{1}{2}\left|A_{23} + \frac{B_{23}}{\rho c} + \rho c \cdot C_{23} + D_{23}\right|\right\} + 10\log_{10}\left(\frac{A_i}{A_o}\right) \qquad (2.4\text{-}6)$$

Where: A_{23}, B_{23}, C_{23} and D_{23} = four pole parameters
c = speed of sound in medium
A_i, A_o = inlet and outlet areas of muffler

Tao and Seybert [37] showed that the two load and two source methods are highly accurate and the problems of requiring an anechoic termination as with the decomposition method are avoided. Other studies have shown that the spacing between the two microphones either side of the element is important and will determine the useable frequency range of the measurements.

2.4.2.3 Insertion loss

Insertion loss is the difference between sound pressure levels measured before and after a muffler has been inserted between the source and the measurement point. There are a number of different definitions for insertion loss measurements as shown in Figure 2.4-4, with definition (a) being the most common. Some authors have recently moved to using the term insertion impact as opposed to insertion loss as this more accurately describes the effect of introducing a new element into an acoustic system that can result in both an increase and a decrease in radiated sound.

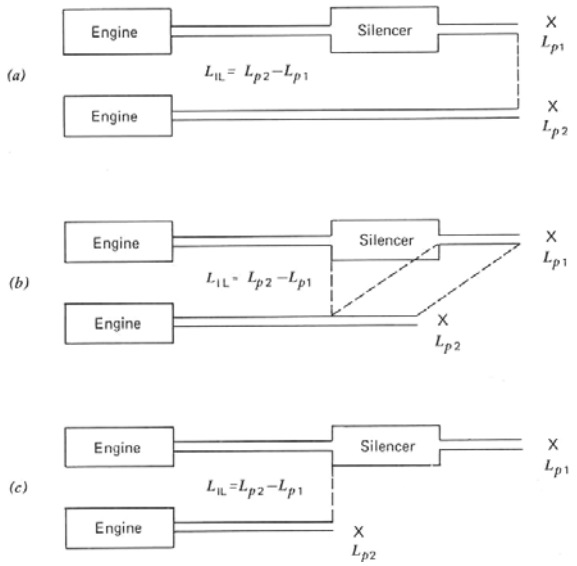

Figure 2.4-4 Insertion loss definitions [8]

2.4.2.4 Noise reduction

Noise reduction, also known by the more descriptive term of sound pressure level difference, is the difference between sound pressure levels measured at the input and output of a muffler. Noise reduction is affected by other elements in the system such as inlet and outlet pipe lengths. It is not a measure of the performance of a muffler itself but rather the performance of a muffler at a point in a single system.

2.4.2.5 Attenuation

Attenuation is the decrease in sound power between two points in an acoustic system. Attenuation is an especially useful quantity for describing wave propagation in lined ducts where acoustic material is continuously distributed along the direction that noise is travelling. Attenuation can be measured for mufflers by determining the decrease in sound pressure level per unit length of the duct measured inside the muffler away from the ends, and multiplying this by the total length of the muffler.

2.4.3 Standardised measurements

Legislation in New Zealand (and much of the world) specifies maximum levels for exhaust noise and total vehicle noise. Exhaust noise is commonly measured by a stationary test at either a fixed engine speed or by an engine speed sweep method. Total vehicle noise (of which exhaust noise is a significant contributor) is commonly measured by a drive-by test of an accelerating vehicle. This section will describe these techniques with reference to both ISO and SAE standards, which are somewhat similar and widely used.

2.4.3.1 Stationary measurements

Criteria for stationary measurements are specified in the following relevant standards and recommendations:

- Measurement of Light Vehicle Exhaust Sound Level Engine Sweep Method
  SAE Recommended Practice, J1492, May 1998.
- Measurement of Light Vehicle Exhaust Sound Level Under Stationary Conditions
  SAE Standard, J1169, May 1998.
- Acoustics – Measurement of noise emitted by stationary road vehicles – Survey method.
  ISO 5130 – 1982 (E).

A brief outline of the requirements of the above standards is:

- A sound level meter with an A-weighting network set up for the fast exponential time averaging characteristic should be used.
- The meter should be calibrated before and after the measurements are taken and any deviation noted.
- Accuracies of all recording equipment must be within specified limits.
- Measurements should be repeated until they fall within 2 dB of each other.
- For the engine sweep method the engine speed should be increased from idle to ¾ of maximum engine speed and held there for 1 to 2 seconds. The sound level should be measured over the entire test time. For the standard test at constant engine speed, the sound reading is measured at ¾ of the engine speed where the vehicle produces maximum power as stated by the manufacturer.
- The ambient sound level at the test site must be at least 10 dB lower than the sound level produced by the vehicle during the test. It is recommended that the background noise level is 15 dB lower than that produced by the vehicle during the test.

- The orientation of the microphone to the end of the muffler should be at a distance of 0.5m and at an angle of 45° measured from the uppermost point of the exhaust outlet and at a height in line with the highest point of the outlet itself. This is shown in Figure 2.4-5 below.

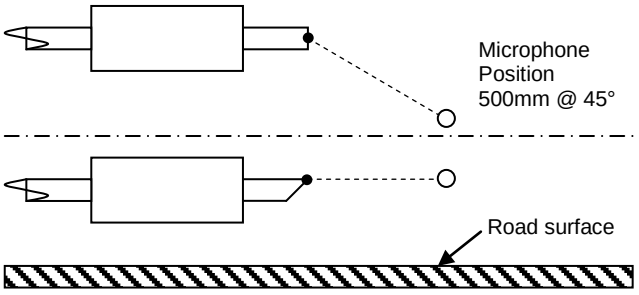

Figure 2.4-5 Microphone position

Although the above list outlines the general procedure for stationary tests it is by no means complete and the relevant standards and recommendations should be consulted for further details.

2.4.3.2 Drive-by measurements

Criteria for drive-by measurements are set out in the following relevant standards and recommendations:

- Sound Level for Passenger Cars and Light Trucks. SAE Recommended Practice, J986, 1998.
- Acoustics – Measurement of noise emitted by passenger cars under conditions representative of urban driving. ISO 7188:1994(E).
- Acoustics – Measurement of noise emitted by accelerating road vehicles – Engineering method. BS ISO 362:1998.

A brief outline of the requirements of the above standards is:

- The acceleration test is the primary test mode by which the test vehicle shall approach the measurement area at a specified speed. Once the front of the vehicle passes the start of the test section the accelerator should be fully depressed and the vehicle allowed to accelerate until either the highest rated engine speed is obtained, or the vehicle reaches the end of the test section.
- A deceleration test should also be conducted by which the reverse of the above occurs starting at the maximum engine speed attained in the acceleration test.
- A sound level meter with an A-weighting network set up for the fast exponential time averaging characteristic should be used.

- The ambient sound level at the test site must be at least 10 dB lower than the sound level produced by the vehicle during the test. It is recommended that the background noise level is 15 dB lower than that produced by the vehicle during the test.
- The test site should be a large flat (±0.05 m) open area, as shown in Figure 2.4-6 below, with no large reflecting surfaces within 30 m of the site. The measurement area must be concrete or nonporous asphalt, dry and free from extraneous material.

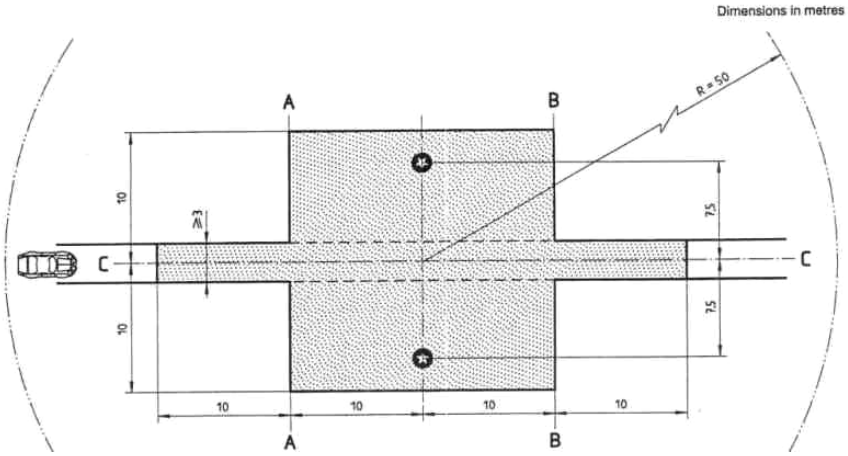

Figure 2.4-6 Test area with microphone layout from ISO Standard [38]

Although the above list outlines the general procedure for drive-by tests it is by no means complete and the relevant standards and recommendations should be consulted for further details. Various authors [2, 3, 39] have tried to simulate drive-by measurements by taking indoor measurements. The results from these tests are varied and the methods often more complicated than conducting the drive-by test itself.

2.4.4 Effects of ambient conditions engine noise

Ambient conditions affect engine performance that in turn affects the sound generated. Increasing inlet air temperature tends to reduce the pressure increase during fuel combustion resulting in less noise. As a guideline the change is given by [8]:

Δ = -0.54 to -1.08 dB per 10°C increase for naturally aspirated engines.
Δ = -0.18 to -0.54 dB per 10°C increase for forced induction engines.

As far as engine noise is concerned a higher inlet pressure, due to higher ambient pressure, tends to decrease ignition delay and reduce combustion noise. However, for the normal range of ambient pressure, the effect on exhaust noise is negligible.

2.4.5 Sound elements

Sound quality is an important aspect in exhaust design as the sound from an exhaust system helps to give a car its character. For example, a deep rumbling exhaust gives the impression of a powerful car whereas a quiet exhaust may give a car a feeling of refinement and quality. Sound quality can be separated into two categories: disturbing sound (e.g. boom, hollow sound) and the sound quality character (e.g. sporty, refined, four, six or eight cylinder).

Dedene et al. [40] produced a method to determine an objective measure of the disturbing sound elements of automotive exhaust noise. Metrics for disturbing sound elements were produced by using an artificial head to measure sound levels and then identifying the noise and applying a frequency range, description and engine operation to it. The aim of this study was to generate an objective list of sound parameters to replace current subjective analysis of sound components that is inaccurate and hard to quantify across different studies and languages. Also presented was a method to reproduce measurements independent of testing location and a detailed method to engineer sound metrics. Some examples of metrics presented in the study are shown in Table 2.4-1 below.

Table 2.4-1 Exhaust sound metrics [40]

Name	Description	Frequency range	Engine operation
Booming	Low frequency resonance	20-250 Hz	Run-up and run-down at low rpm
Flow noise	High frequency stochastic noise	800-5000 Hz	Run-up at middle and high rpm
Putter	Stochastic impulsive fluctuations	500-15000 Hz	Run-down at low rpm
Flutter	Middle and high frequencies modulated with an engine order	300-10000 Hz	Run-up at low rpm and full load
Whistle	Tonal or narrow band noise	Narrow band in a 1-20 kHz band	Run-up at middle and high rpm
Rumble	Intermittent low frequency noise	20-300Hz	Run-down at middle rpm
Crackle	Very short and sharp sound	> 3000 Hz	Throttle pulses

2.5 Modelling of exhaust noise

2.5.1 Introduction

In this section the applications, limits and accuracies of various modelling techniques as found in the literature are discussed. Modelling techniques can be split into two main categories: analytical modelling and computational modelling, which is how this section is divided.

2.5.2 Analytical modelling

2.5.2.1 One dimensional wave equation

Exhaust noise is primarily produced by pressure fluctuations generated by the periodic release of exhaust gasses from the cylinders. For many applications it has been found that the pressure fluctuations are relatively small compared to the mean pressure. Thus, the total pressure variation may be expressed by a linear equation containing a steady state term and a first-order fluctuating term. The basic one dimensional wave equation is shown below:

$$\frac{\partial^2 p(x:t)}{\partial x^2} + k^2 p(x:t) = 0 \qquad (2.5\text{-}1)$$

Where p is a function of x and t, k is the acoustic wave number = $\omega/c = (2\pi f)/c$. The general solution to this equation is:

$$p(x:t) = \tilde{P}_o^{+} e^{i(\omega t - kx)} + \tilde{P}_o^{-} e^{i(\omega t + kx)} \qquad (2.5\text{-}2)$$

One dimensional modelling is valid up to a cut-off frequency, which is the point where only one dimensional plane waves can no longer be assumed to propagate. Typically the propagation of higher order waves leads to a decrease in attenuation. One dimensional modelling can be used to model single exhaust components and calculate insertion loss, attenuation and transmission loss as presented in previous sections.

One dimensional modelling of exhaust systems can be performed through the use of matrix methods that use four element matrices to transfer between discontinuities in the system. The scattering and transfer matrix methods are utilised by various groups [18, 21, 25, 41] with matrices developed for a wide range of exhaust system elements.

The four pole or transfer matrix method uses plane wave approximations to develop transfer matrices between various acoustic elements. The transfer matrix relation is shown below:

$$\begin{bmatrix} p_1 \\ v_1 \end{bmatrix} = \begin{bmatrix} A_1 & B_1 \\ C_1 & D_1 \end{bmatrix} \begin{bmatrix} A_2 & B_2 \\ C_2 & D_2 \end{bmatrix} \begin{bmatrix} A_3 & B_3 \\ C_3 & D_3 \end{bmatrix} \begin{bmatrix} p_4 \\ v_4 \end{bmatrix} \qquad (2.5\text{-}3)$$

Where p_1 and p_4 are the acoustic pressures, v_1 and v_4 are the particle velocities at points 1 and 4 in the system. A transfer matrix for each exhaust component is used to modify the waveform between points 1 and 4. *A*, *B*, *C* and *D* are the transfer matrix elements which can be derived or obtained from literature for simple elements such as tubes, expansions or contractions, branch systems and perforations. The scattering matrix is similar to the transfer matrix method but uses a four element matrix to transfer positive and negative travelling pressure waves between points in the system.

Ji, Ma and Zhang [42] presented a boundary element scheme for the evaluation of the four pole parameters for ducts and mufflers in the presence of a low Mach number, non-uniform flow. This model was compared to existing one-dimensional flow models for validation. This study showed that there was noticeable non-uniform flow and non-plane waves in the muffler, which cause divergence from one-dimensional plane wave theory at higher frequencies.

2.5.2.2 Higher order modes

An automotive engine as a source of noise will excite all modes in a system. Many of these modes are cut-off and decay exponentially as they travel away from the source. At impedance changes in the system, such as area expansions, additional modes may be generated that may or may not be cut-off depending on the cross-sectional geometry of the section. If higher order modes are generated at impedance changes near the tailpipe, it is possible for them to propagate from the system before being fully attenuated.

Cut-off frequencies may be determined by noting that the radial component of the particle velocity must be reduced to zero at the walls, or the radial derivative of the wave equation in cylindrical form must go to zero at the walls. This results in a series of roots (x_{mn}) for the derivative of the radial wave function as shown with the nodal lines for each mode in Figure 2.5-1 [8].

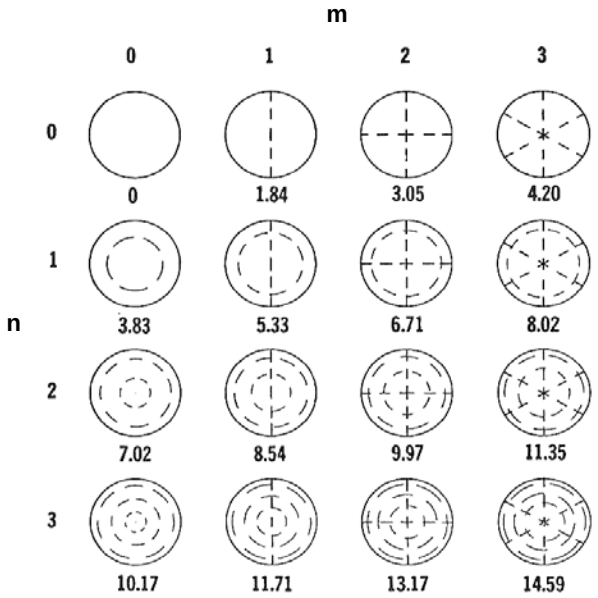

Figure 2.5-1 Pressure nodal lines for a circular duct with x_{mn} values for each mode [8]

The cut-off frequency may be calculated using the x_{mn} values from Figure 2.5-1.

$$f_c = \frac{x_{mn} c}{\pi d} \qquad (2.5\text{-}4)$$

Where: x_{mn} = roots of derivative of radial function
c = speed of sound in medium (m/s)
d = diameter of duct (m)

It is of note that literature commonly defines the cut-off frequency as the first circularly symmetric or radial (0,1) mode, as opposed to the first cross-sectional mode (1,0). Mean flow has the effect of reducing the cut-off frequency by a factor of $(1\text{-}M^2)^{1/2}$ where M is the Mach number.

2.5.2.3 Non-linear effects

Non-linear effects in exhaust systems refer to the point at which high amplitude pressure variations cause a steepening of the pressure pulse as it progresses through the exhaust system, tending to form a shock wave at the front of the disturbance. Wave steepening will begin to occur if noise levels in the exhaust system are above 140 dB. For levels below this, the performance of the resonator can be assumed linear for all frequencies [25]. El-Rahman, Sabry and Mobarak [43] presented a model based on the method of characteristics to account for non-linear wave effects. The predictions were compared to experimental data and previously published work, and in most cases provided good agreement.

2.5.3 Computational modelling

A number of programs using finite element analysis (FEA) and boundary element methods (BEM), both general and specific to exhaust systems have been written. A number of these are commercially available such as Ricardo Wave [5], Sysnoise [44] and Fluent. One, two and three dimensional computational techniques can be used to model entire exhaust systems or analyse singular exhaust system components. Computational modelling has a major advantage over analytical modelling as complex exhaust systems that can include the engine, higher order effects, flow noise and non-linear wave effects can be included in the analysis.

Lai [45] presented a study comparing various modelling techniques for the acoustic performance of mufflers. Models studied were the lumped parameter method, one-dimensional travelling wave method, and one, two and three-dimensional modelling schemes based on a modal expansion method. This study showed the allowable limits of each method and accuracy of the solution compared to experimental data. The three dimensional modal expansion method was shown to be the most accurate, however, it also had the largest computational requirement.

Mackey et al. [46] created a combined one and three dimensional model of an exhaust system comprising of a one dimensional inlet tube to model the flow entering the system with a three dimensional axis symmetric model of the muffler itself. The mufflers modelled in this situation were a simple expansion chamber muffler and a concentric tube resonator with and without absorptive material present. Experimental arrangements were constructed that produced single pressure pulses and cyclic pressure flows. The experimental results correlated well to those from the numerical model; however, the numerical model did not incorporate pressure effects.

Harrison [47, 48] presented a model that coupled a time variant source with a frequency domain analysis of the intake and exhaust systems through the use of a fast Fourier transform. Harrison's model allowed the radiated noise from the exhaust system to be predicted with a very low computational requirement. The prediction from the model was compared to experimental data with mixed success.

Patil et al. [49] summarised computational modelling by stating that

> "Three dimensional FEM techniques have proved to be successful for the analysis of geometrically complicated mufflers where one dimensional theory cannot be used due to the propagation of higher order modes during operation"

However, computational modelling is time intensive and the results should be validated in some form.

2.6 References

[1] H. Weltens, H. Bressler, and P. Krause, "Influence of Catalytic Converters on Acoustics of Exhaust Systems for European Cars," Society of Automotive Engineers, Technical Paper 910836, 1991.

[2] B.-K. Kim, H. Kim, S. Yoo, and K. Zwanzig, "Prediction of Vehicle Pass-By Noise Using Indoor Measurements," Society of Automotive Engineers, Technical Paper 2001-01-1563, 2001.

[3] A. V. Phillips and M. Orchard, "Drive-By Noise Prediction by Vehicle System Analysis," Society of Automotive Engineers, Technical Paper 2001-01-15632, 2001.

[4] T. Tanaka and M. Harara, "A Consideration on the Exhaust System of Passenger Cars," Mitsubishi Heavy Industries, Ltd. 1981.

[5] J. J. Silverstri, T. Morel, and M. Costello, "Study of Intake System Wave Dynamics and Acoustics by Simulation and Experiment," Society of Automotive Engineers, Technical Paper 940206, 1994.

[6] J. Happian-Smith, *An Introduction to Modern Vehicle Design*: Butterworth-Heinemann, 2002.

[7] A. J. Torregrosa, A. Broatch, and R. Payri, "On the Infulence of Manifold Geometry on Exhaust Noise," Society of Automotive Engineers, Technical Paper 1999-01-1650, 1999.

[8] D. E. Baxa, "Noise Control in Internal Combustion Engines." Wisconsin: Wiley, 1982.

[9] P. O. A. L. Davies, "The Observed Aeroacoustic Behaviour of Some Flow-Excited Expansion Chambers," *Journal of Sound and Vibration*, vol. 239, pp. 695-708, 2001.

[10] C. A. Erhard, "Flowdynamical and Acoustical Optimisation of Mufflers to Reduce High Frequrncy Flow Noise at the End Pipe Outlet," presented at Inter-Noise 95, Newport Beach, CA, USA, 1995.

[11] N. Kojima, B. Liu, and H. Zohu, "Relation Between the Predominance of Acoustic Resonance Noise and Air Flow in Muffler," Society of Automotive Engineers, Technical Paper 951262, 1995.

[12] N. Kojima and B. Z. Liu, "A Study on the Interaction between Acoustic Resonance and Turbulence in Mufflers," presented at Inter-Noise 94, Yokohama, Japan, 1994.

[13] M. J. Lighthill, "On sound generated aerodynamically; II. Turbulence as a source of sound," Proceedings of the Royal Society of London, vol. A222 no. 1148, pp 1-32, 1954.

[14] M. J. Lighthill, "On sound generated aerodynamically; I. General theory," Proceedings of the Royal Society of London, vol. A211 no. 1107, pp 546-587, 1952.

[15] F. H. Kunz, "Semi-Emprical Model for Flow Noise Prediction on Intake and Exhaust Systems," Society of Automotive Engineers, Technical Paper 1999-01-1654, 1999.

[16] K. Garrett, "Engine Silencing - Changes in Emphasis," in *Engineering*, 1975.

[17] N. Sekine, S. Matsumura, K. Takeuchi, O. Onodera, and K. Ito, "Shock Wave development and propagation in Automobile Exhaust Systems," Society of Automotive Engineers, Technical Paper 880082, 1988.

[18] P. O. A. L. Davies, "Piston Engine Intake and Exhaust System Design," *Journal of Sound and Vibration*, vol. 190, pp. 677-712, 1996.

[19] C. A. Erhard, "Acoustical and Gas Dynamical Investigations on Exhaust Systems to Get Further Knowledge on the Sound Generation Mechanism of Abnormal Exhaust Noise," Society of Automotive Engineers, Technical Paper 945134, 1994.

[20] D. D. J. Davis, G. M. Stokes, D. Moore, and G. L. J. Stevens, "Theoretical and Experimental Investigation of Mufflers: with Comments on Engine-Exhaust muffler Design," U.S National Advisory Committee for Aeronautics Langley Aeronautical Laboratory, Report 1192, 1954.

[21] M. L. Munjal, *Acoustics of ducts and mufflers with application to exhaust and ventilation system design*. New York: Wiley, 1987.

[22] A. Selamet and Z. L. Ji, "Acoustic Attenuation Performance of Circular Chambers with Extended Inlet/Outlet," *Journal of Sound and Vibration*, vol. 223(2), pp. 197-121, 1999.

[23] A. Selamet and Z. L. Ji, "Acoustic Behaviour of Circular Dual-Chamber Mufflers," *Journal of Sound and Vibration*, vol. 265, pp. 967-985, 2003.

[24] T. F. W. Embleton, "Mufflers," in *Noise and vibration control*, L. L. Beranek, Ed., Revised ed. Washington, D.C: Institute of Noise Control Engineering, 1988, pp. 362-405.

[25] P. O. A. L. Davies, "Practical Flow Duct Acoustics," *Journal of Sound and Vibration*, vol. 124, pp. 91-115, 1988.

[26] D. Wan and D. T. Soedel, "Two Degree of Freedom Helmholtz Resonator Analysis," Society of Automotive Engineers, Technical Paper 2004-10-0387, 2004.

[27] A. Sindhupak, M. Lokitsangtong, B. Silapakijwongkul, T. Wada, S. Murakami, M. Maeda, and S. Hagi, "Acoustical Characteristics of Helmholtz Type Resonators," Ladkrabag, Bangkok, Thailand.

[28] D. G. Thomas, "Muffler Selection and Design for Internal Combution Engines," Society of Automotive Engineers, Technical Paper 700737, 1970.

[29] Silex, "Exhaust Silencers," 2002.

[30] F. Lehringer, "Models for the calculation of Absorbtion Mufflers in Exhaust Systems - Part 1," *MTZ Worldwide*, pp. 2-4, 1998.

[31] P. Krause, H. Weltens, and S. M. Hutchins, "Advanced design of Automotive Exhaust Silencer Systems," Society of Automotive Engineers, Technical Paper 922088, 1992.

[32] A. Shoureshi, G. Alves, D. Novotry, L. Ogundipe, and M. Wheeler, "Mechatronically-Based Vibration and Noise Control in Automotive Systems," pp. 691-698, 1995.

[33] R. Kashani, "Active Boom Noise Damping of a Large Sport Utility Vehicle," Society of Automotive Engineers, Technical Paper 2003-01-1694, 2003.

[34] O'Connor, "Generating the Sounds of Science," *Journal of Mechnical Engineering*, pp. 54-58, 1994.

[35] H. Levine and J. Schwinger, "On the radiation of sound from an unflanged circular pipe," *Physics Review*, vol. 73, pp. 373, 1948.

[36] A. Lorea, A. Renzullo, L. Chiesa, and G. Guenna, "Acoustic Intensity Measurements in Exhaust Pipes," pp. 230-238.

[37] Z. Tao and A. F. Seybert, "Current Techniques for Measuring Muffler Transmission Loss," Society of Automotive Engineers, Technical Paper 2003-01-1653, 2003.

[38] "Acoustics - Measurement of noise emitted by accelerating road vehicles - Engineering method," International Standard BS ISO 362:1998(E), 1998.

[39] H. Onusic, M. A. M. Cano, R. M. T. Cheruti, M. M. Hage, and E. L. Baptista, "Pass By and Stationary Noises: Correlation and Evaluation," Society of Automotive Engineers, Technical Paper 1999-01-2991, 1999.

[40] L. Dedene, M. Van Overmeire, P. Guillaume, and R. Valgaeren, "Engineering Metrics for Disturbing Sound Elements of Automotive Exhaust Noise," Society of Automotive Engineers, Technical Paper 1999-01-1653, 1999.

[41] M. L. Munjal, "Automotive Noise - The Indian Scene in 2004," presented at ACOUSTICS 2004, Gold Coast, Australia, 2004.

[42] Z. L. Ji, Q. Ma, and Z. H. Zhang, "A Boundary Element Scheme for Evaluation of Four-Pole Parameters of Ducts and Mufflers with Low Mach Number Non-Uniform Flow.," *Journal of Sound and Vibration*, vol. 185, pp. 107-117, 1995.

[43] A. A. I. El-Rahman, A. S. Sabry, and A. Mobarak, "Non-Linear Simulation if Single Pass Perforated Tube Silencers Based on thr Method of Characteristics," *Journal of Sound and Vibration*, vol. 278, pp. 63-81, 2004.

[44] M. R. M. Kimura, C. Walber, and S. N. Y. Gerges, "Acoustical Modelling and Experimental Measurement for Plug Type Muffler," Society of Automotive Engineers, Technical Paper 962394, 1996.

[45] P. C. C. Lai, "Evaluation of several analytical methods on muffler acoustic modelling," *Noise Control Engineering Journal*, vol. 46, pp. 109-119, 1998.

[46] D. O. Mackey, G. P. Blair, and R. Fleck, "Correlation of Simulated and Measured noise Emission Using a combined 1D/3D Computational Technique," Society of Automotive Engineers, Technical Paper 970801, 1997.

[47] M. F. Harrison, "Time and Frequency Domain Modelling of Vehicle Intake and Exhaust Systems." Doctoral Thesis, Institute of Sound and Vibration Research, University of Southampton, 1994.

[48] M. F. Harrison and R. P. Arenas, "A Hybrid Boundary for the Prediction of Intake Wave Dynamics in IC Engines," *Journal of Sound and Vibration*, vol. 270, pp. 111-136, 2004.

[49] A. R. Patil, P. R. Sajanpawar, and V. V. Masurekar, "Acoustic Three Dimensional Finite Element Analysis of a Muffler," Society of Automotive Engineers, Technical Paper 960189, 1996.

Chapter 3
Experimental Arrangement

Summary

Experimental testing was conducted to determine the actual performance of resonant absorbers as used in automotive applications. Testing was conducted using either an engine or a speaker as the source of excitation. This permitted comparison between the two sources, with the engine including pressure, temperature and flow effects.

An experimental test arrangement was developed using existing facilities in the Automotive Laboratory at the University of Canterbury. The test arrangement was based on similar arrangements identified in the literature review. The exhaust system from the test engine was modified to pass through a wall into an adjacent room. The exhaust system was made up of a number of sections joined by flanges allowing mufflers and pipe lengths to be changed. The exhaust system was instrumented with pressure and temperature sensors, with the noise from the exhaust outlet measured 500 mm behind at 45° from the top of the exhaust outlet, in accordance with ISO and SAE standards. The sound from the exhaust was measured using a Brüel and Kjær 2260 Investigator with the BZ7208 FFT software package used for narrow band analysis.

As the acoustics of the test area were unknown, a number of tests were conducted to quantify them. The background noise and the reverberation time of the room were measured. From these measurements the effect on measurements taken in the room was calculated and determined to be insignificant. The lower cut-off frequency of the room was calculated to be 100 Hz, which compares well to commercial test facilities.

Table of Contents

List of Figures and Tables

3.1 Introduction

This chapter describes the experimental arrangement that was used to measure the performance of resonant type absorbers as used in automotive exhaust systems. Mufflers were tested using either an engine or a speaker as the sound source. This enabled the results to be compared and the effects of pressure, flow and temperature to be assessed. The results from the experimental tests performed using this test arrangement are presented in Chapter 4, and discussed in Chapter 6.

The Mechanical Engineering Department has both an engine dynamometer and a rolling road dynamometer located in adjacent rooms in the Automotive Laboratory. A 3S-GE four cylinder, two litre, normally aspirated engine from a Toyota MR2 was used as the test engine. The standard exhaust system of this engine consists of an equal length 4-2-1 exhaust manifold, a catalytic converter and a muffler. The standard system was just before the catalytic converter and a new system was constructed that passed through the wall to the rolling road room where the noise radiated from the exhaust outlet was measured. Test setups of this type are reported in the literature review and are preferred to having the engine and the exhaust outlet in the same room, as the noise from the engine and exhaust noise are separated. The engine test cell will be referred to as the source room and the rolling road dynamometer room will be referred to as the receiving room, indicating the noise generation and measurement locations respectively.

3.2 Test area

The engine and speaker testing was conducted in the Automotive Laboratory in the Mechanical Engineering Department at the University of Canterbury. The diagram below shows the general layout of the Automotive Laboratory. A false floor was constructed in the receiving room to simulate the height from the ground of a typical exhaust outlet on a passenger car.

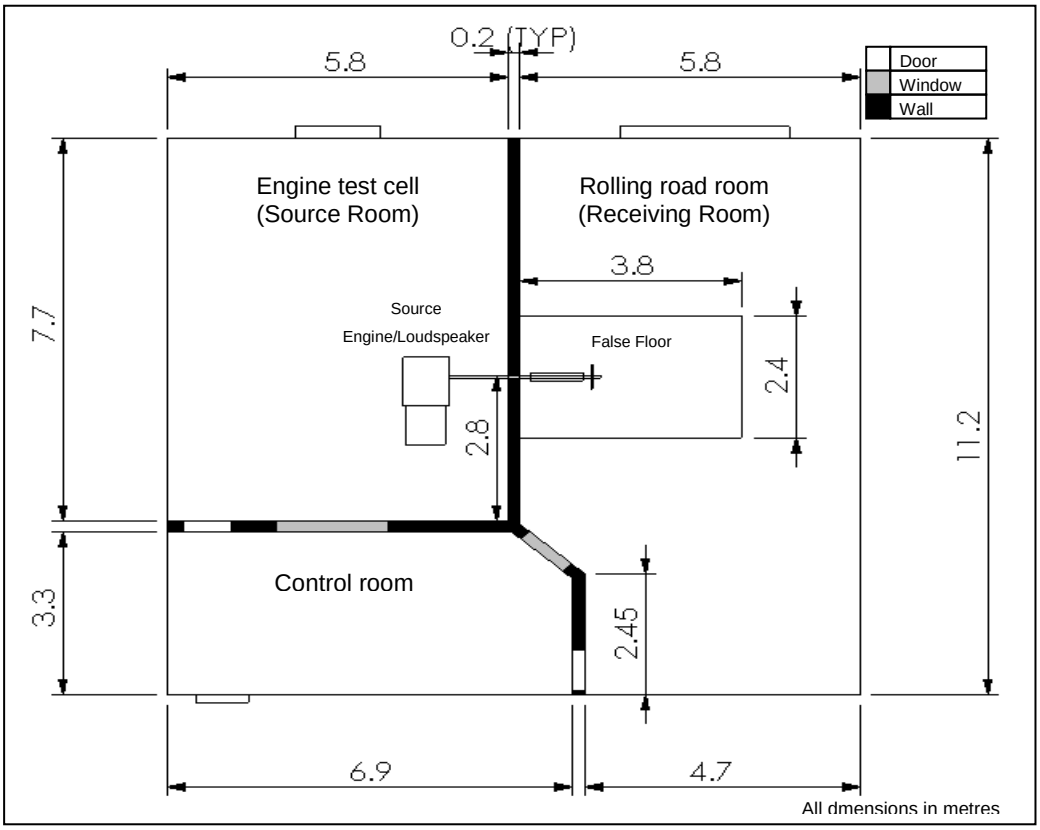

Figure 3.2-1 Automotive laboratory room layout

The details of the receiving room are shown in the table below:

Table 3.2-1 Receiving room properties

Surface Area	212.4 m²
Volume	171.0 m³

Both the source room and receiving room had been previously acoustically treated with fibreglass sound absorption material 50 mm in thickness spaced 20 mm from the wall. This absorption lined the entire room above a height of 1.2m. In addition to this, extra fibreglass absorption was installed in the receiving room as shown in Figure 3.2-2. Absorption was placed at each end of the room

perpendicular to the exhaust system axis as shown in Figures 3.2-3 and 3.3-1 to reduce standing waves in this direction. The acoustic properties of the receiving room are further discussed in section 3.3.

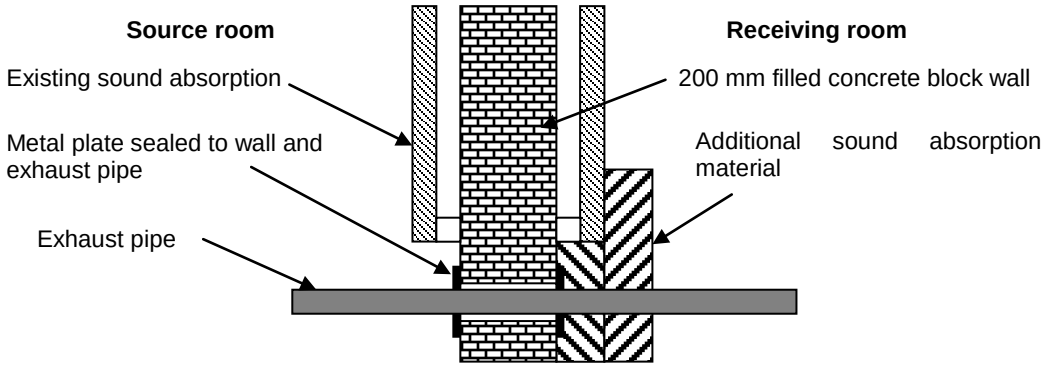

Figure 3.2-2 Acoustic treatment of wall between source and receiving rooms

Figure 3.2-3 Receiving room showing fibreglass absorption material

3.3 Quantification of test area acoustics

3.3.1 *Introduction*

The acoustic properties of the Automotive Laboratory were determined so their effect on measurements could be ascertained. Tests were to be conducted in relation to ISO and SAE standards which specify tests to be conducted in a large open area or a hemi-anechoic room, that is, an area with little to no reverberant field. For measurements to be accurate the background noise level must be significantly lower than that from the exhaust outlet. The first test conducted was to assess the effect of the reverberant field within the room; the second test was to determine the background noise level. The method of testing and the results obtained are discussed in the following sections.

3.3.2 *Reverberant field*

ISO and SAE standards specify a large open area or a hemi-anechoic room for exhaust sound measurements. This is so that only the direct sound field from the exhaust outlet, with reflections from the road, is measured. If testing is performed in a reverberant room, reflections from surfaces other than the 'road', the false floor this case, will result in artificially high measurements.

Reverberation times were measured in the receiving room and the cut-off frequency of the room was calculated. This is the lower frequency limit to which the room can be considered hemi-anechoic. From the reverberation times the increase in measurement caused by the reverberant field was calculated. Figure 3.3-1 below shows a schematic of the receiving room and the speaker and microphone positions used to measure the reverberation time of the room.

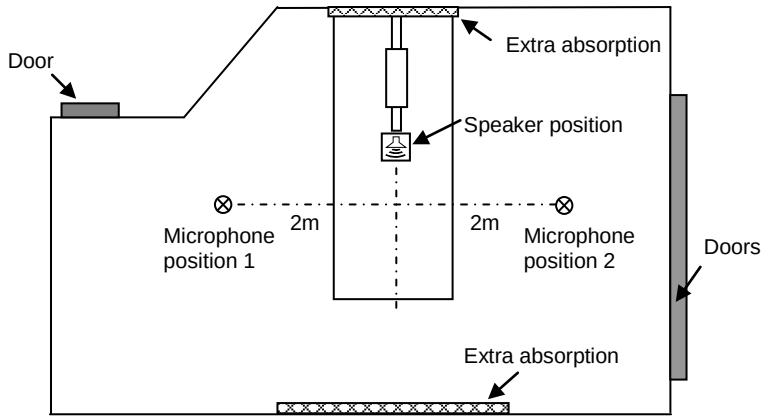

Figure 3.3-1 Measurement locations for reverberation time measurements

As it was desired to operate the test rig with the large doors located at the end of the receiving room open or closed, measurements were taken with the doors in both positions. It was found that the position of the doors did not have a significant effect on the reverberation time of the room. From the reverberation times, the effect of the reverberant field in the room on measurements taken at a specified distance was calculated as follows:

The room absorption coefficient was found from the reverberation time and room geometry:

$$\overline{\alpha} = \frac{0.161V}{ST} \qquad (3.3\text{-}1)$$

Where: $\overline{\alpha}$ = absorption coefficient
V = room volume (m³)
S = room surface area (m²)
T = reverberation time (s)

Using the absorption coefficient the room constant can be found:

$$R = \frac{S\overline{\alpha}}{1-\overline{\alpha}} \qquad (3.3\text{-}2)$$

Where: R = the room constant

The effect of the reverberant field was calculated by considering the difference between the sound pressure level and the sound power level at a specified distance from the source, with and without the reverberant field component:

$$SPL - PWL = 10\log_{10}\left[\left(\frac{Q}{4\pi r^2}\right)_{direct} + \left(\frac{4}{R}\right)_{reverberant}\right] \qquad (3.3\text{-}3)$$

Where: SPL = sound pressure level (dB)
PWL = sound power level (dB)
Q = directivity (1.0 in this case)
r = distance from source to measurement position (m)

This calculation was performed for each 1/3 octave frequency band. The effect that the reverberant field in the room will have on the measurements taken 500 mm and at 45° from the exhaust is shown in Figure 3.3-2.

Figure 3.3-2 Increase in measurement caused by reverberant field

The effect of the reverberant field on measurements is small at all frequencies above 100 Hz and will therefore have little effect on results. Below 100 Hz the reverberant field causes a significant increase in measurements. This frequency will therefore be nominated as the cut-off frequency of the room.

The 100 Hz cut-off frequency of the room compares well to that of the Lotus test facility at 120 Hz [1], suggesting that the room is sufficiently anechoic. The primary use of measurements is to calculate insertion loss by comparing the difference between two measurements. Due to this, any increase in measurement due to the reverberant field will largely cancel when the insertion loss is calculated.

3.3.3 *Background noise levels*

For accurate measurements to be taken it is required by ISO and SAE standards that background noise levels are at least 10 dB lower than that from the exhaust outlet. This ensures that the contribution of background noise to the measurement is insignificant (less than 0.5 dB). The total background noise in the receiving room with the engine running could not be measured directly due to the presence of the exhaust outlet in the receiving room. Two sources of background noise were identified being noise from the surroundings and noise from the engine and extraction fans in the source room.

The noise from the surroundings was measured simply by taking a measurement without the engine running. The background noise level in the receiving room due to the noise sources in the source room was found by measuring the noise level in the source room and the transmission loss of the wall

between the two rooms. The transmission loss was found by placing a speaker at the exhaust outlet, measuring the level at the engine in the source room, and comparing this to the level measured in the receiving room at the usual measurement location. The average noise level in the source room was found by making measurements with the engine running at a variety of speeds and loads with the extraction fan system running. From this data the resulting background noise level in the receiving can be simply calculated. These results are summarised in Figure 3.3-3 below.

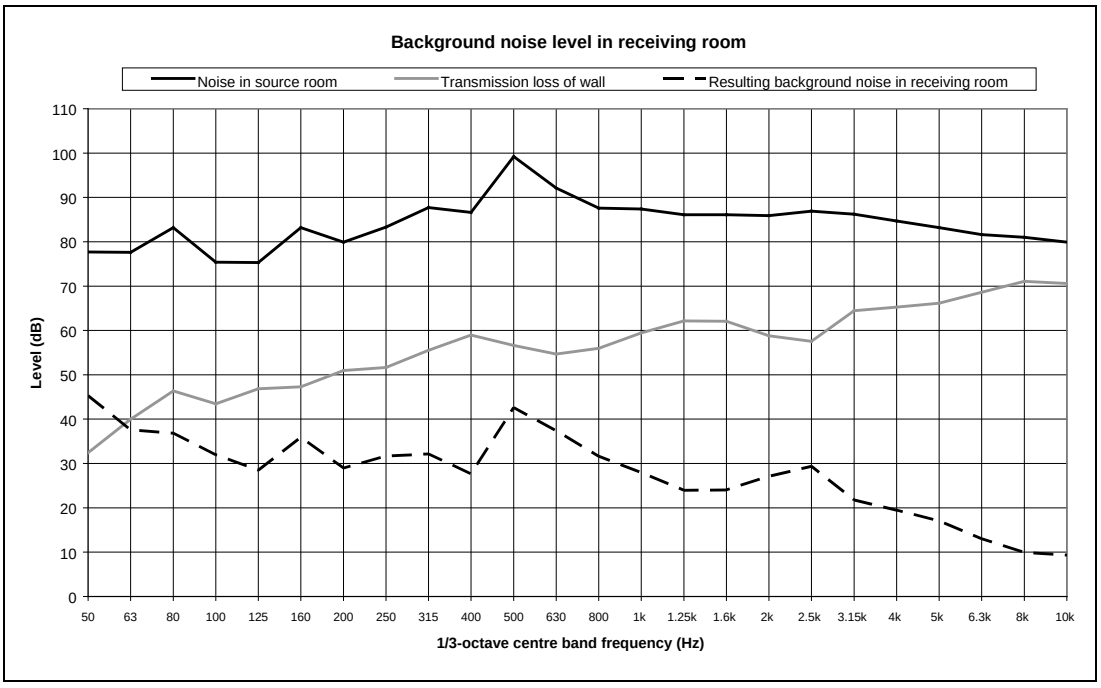

Figure 3.3-3 Background noise level in receiving room

Figure 3.3-3 shows that the background noise level across the frequency range of interest is less than 45 dB, with the total background noise level 49 dB. Levels measured in the receiving room with the engine running are over 70 dB across the frequency range of interest, with total levels over 110 dB. From this data, the background noise level in the receiving room when compared to the much higher levels from the exhaust outlet will not affect measurements.

3.4 Engine test arrangement

3.4.1 *Engine specifications*

The test engine used was a 3S-GE, four cylinder, spark ignition engine from a Toyota MR2. The engine is naturally aspirated and fuel injected with twin camshafts and four valves per cylinder producing a maximum of 175 hp. The specifications of the engine are shown in Table 3.4-1 below.

Table 3.4-1 Toyota 3S-GE engine specifications

Engine Model	3S-GE
Bore	86 mm
Stroke	86 mm
CC rating	1998
Compression Ratio	10.0:1
Cylinder Angle	50°
Engine speed limit	7000 RPM
Power	175 hp @ 6600 RPM
Torque (lb ft)	137 @ 4800 RPM

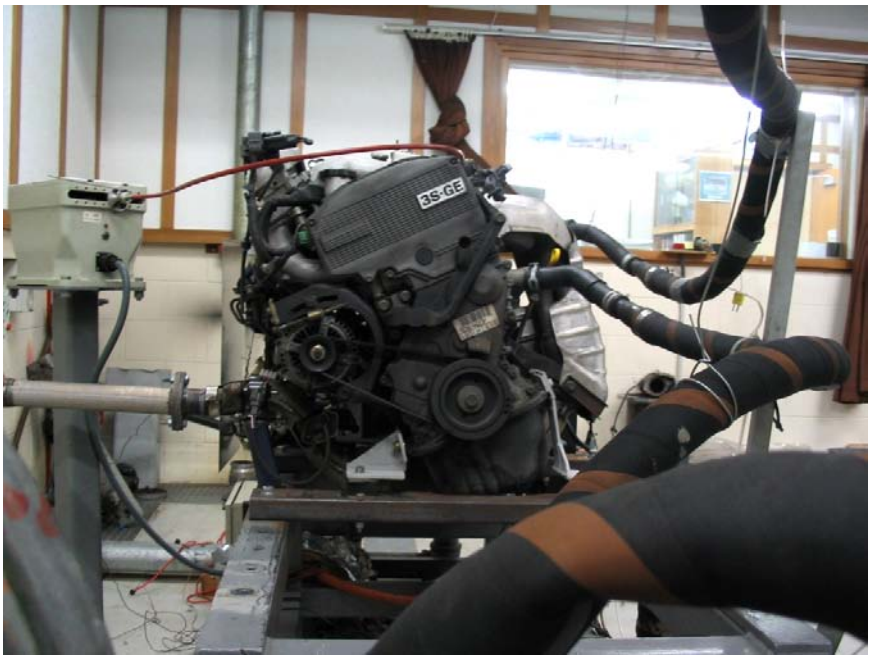

Figure 3.4-1 Toyota 3S-GE test engine

3.4.2 *Engine control system*

The engine test dynamometer was equipped with a control unit that could be run from the control console or connected to a desktop computer for automatic control. In manual control mode, two separate controls allowed the engine speed, throttle position and load to be set independently. In automatic control mode, throttle positions and target engine speeds can be set. At each target point the control unit will set the specified throttle position and vary the load to obtain the required engine speed. The automatic control system receives input in the form of a text file containing the throttle position set points and target engine speeds. The control console and the automatic control system display are shown in Figure 3.4-2 below.

Figure 3.4-2 Control console and automatic control system display

Both the manual and automatic control systems were used for testing muffler systems. Using the manual system, engine speeds and loads were set and the sound signal analysed using a Brüel and Kjær 2260 Investigator equipped with the BZ7208 FFT software package. Engine ramp-up or sweep tests were conducted with the control module in automatic mode using a Brüel and Kjær Pulse system to analyse the sound signal. Various engine sweeps were conducted using different throttle and hence load conditions.

3.4.3 *Exhaust system*

The exhaust system on the test engine is shown in Figure 3.4-3 below. The numbers relate to the centreline length of each exhaust section.

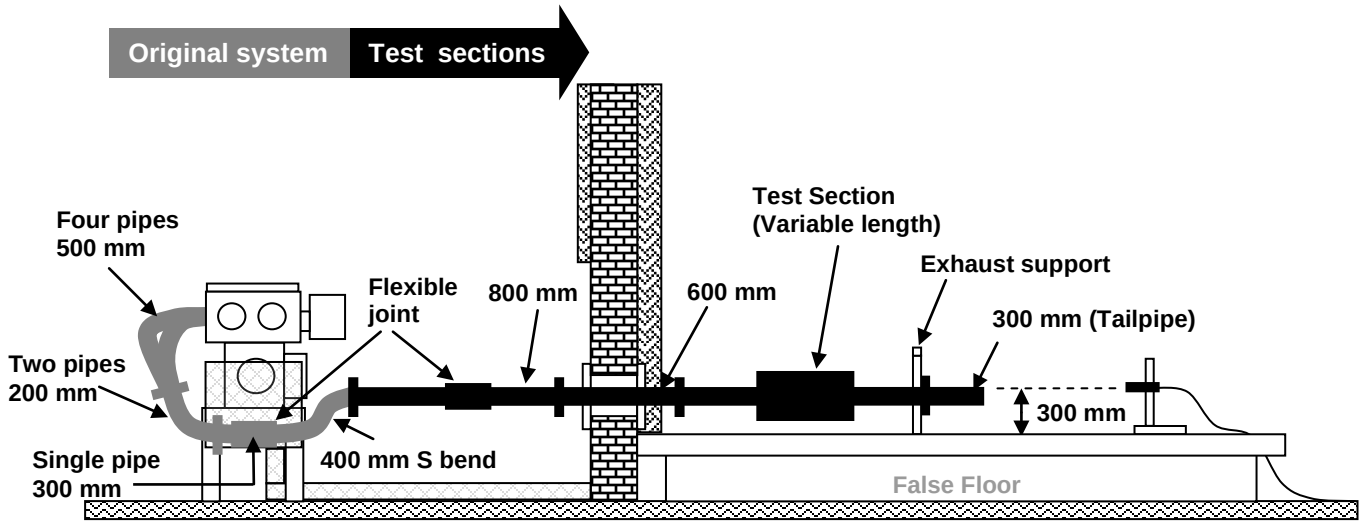

Figure 3.4-3 Exhaust system detail

The 3S-GE test engine uses tuned length extractors with four pipes of equal length from the exhaust manifold joining into two equal length pipes and then into one pipe further down the exhaust system. From this, a single pipe passes under the engine. It is to this pipe that the test exhaust system was fitted. The test exhaust system was passed through a tight fitting hole in the wall from the source room to the receiving room. The exhaust system was supported in the receiving room using standard exhaust hangers as shown in Figures 3.2-3 and 3.4-3.

3.4.4 *Exhaust gas temperature measurement*

As the speed of sound changes with temperature, and there is a large axial temperature gradient along the exhaust system, it was desired to measure the exhaust gas temperature at various locations within the exhaust system. A number of different methods were investigated [2, 3], and tests conducted to compare the accuracy of various configurations. K-type thermocouples were chosen as they allow temperature measurement up to 1400°C. K-type thermocouples come in a number of wire diameters, with diameters ranging from 0.125 mm to 0.8 mm suitable for use within an exhaust system. The use of shielded and unshielded thermocouples was considered and tests were conducted to determine which of the two provided the best response and accuracy.

The temperature measured by a thermocouple is the temperature of the junction between the two dissimilar wires. The temperature of the junction is a function of the heat transferred to it by convection from the exhaust gas, and the heat lost from it by radiation to the exhaust pipe walls and heat conducted away from the junction through the thermocouple wires. The thermal equilibrium of the junction is shown in the equation below:

$$T_g - T_m = -\frac{k_j d}{4h}\frac{\partial^2 T_m}{\partial x^2} + \frac{\varepsilon\sigma}{h}(T_m^4 - T_w^4) \qquad (3.4\text{-}1)$$

Where: T_g = temperature of the gas (K)
T_m = measured temperature (K)
T_w = temperature of the wall (K)
k = thermal conductivity of the wire (W/mK)
d = diameter of wire (m)
ε = emissivity of wire
σ = Plancks constant (W/m^2K^4)
h = thermal convection coefficient (m/s)
x = distance along wire from junction (m)

The measured temperature will be lower than the actual gas temperature due to heat lost by radiation and conduction, termed radiation and conduction errors. The thermocouples used were 0.5 mm in diameter with the junction located in the middle of the exhaust cross section as shown in Figure 3.4-4. As a relatively small diameter wire was used and the junction placed well away from the wall, conduction error will be minimal [2].

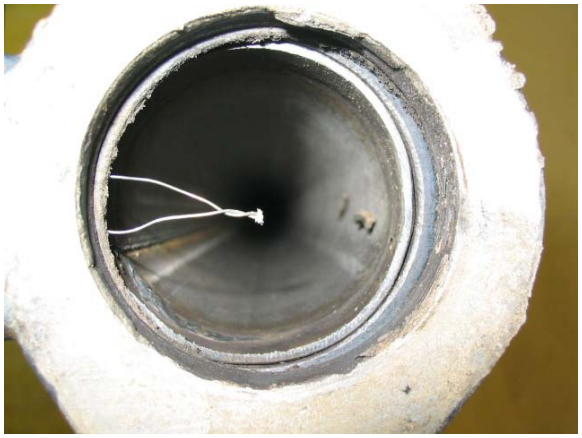

Figure 3.4-4 K-type 0.5 mm unshielded thermocouple as used for the test rig

Radiation error was assessed by placing a shielded thermocouple and an unshielded thermocouple at the same point in the system and comparing the measured temperatures. The shielded thermocouple measured consistently lower than the unshielded thermocouple and took significantly longer to respond. Analysing equation 3.4-1 the shielded thermocouple should, in theory, measure a higher temperature than the unshielded thermocouple, due to its lower radiation error. However, due to the

larger size of the shielded thermocouple and its larger contact area with the wall of the exhaust system, the conduction error of the shielded thermocouple would seem to be very high giving it a larger total error than the unshielded thermocouple. From these tests it was concluded that 0.5 mm unshielded thermocouples would give the least amount of error and also have the benefit of a fast response time.

The calibration of the thermocouples was checked by placing them in boiling water and measuring the temperature. The barometric pressure was measured and the actual boiling temperature calculated to be 99.3°C. The calculated and measured temperatures for all five thermocouples tested were in agreement to 0.1°C, which is the accuracy of the digital readout of the meter used.

3.4.5 *Pressure measurement*

The exhaust pressure pulse was measured as it travelled through the exhaust system using a fast response piezoresistive pressure sensor that measures both static and dynamic absolute pressure. The sensor was mounted in the test section of the exhaust system immediately before the rear muffler. Due to the high temperature in the exhaust system the pressure transducer was mounted in a cooling adapter as shown in Figure 3.4-5 below. The pressure transducer was calibrated using a dead weight tester and data was recorded using an 8 kHz 16 channel digital data acquisition system.

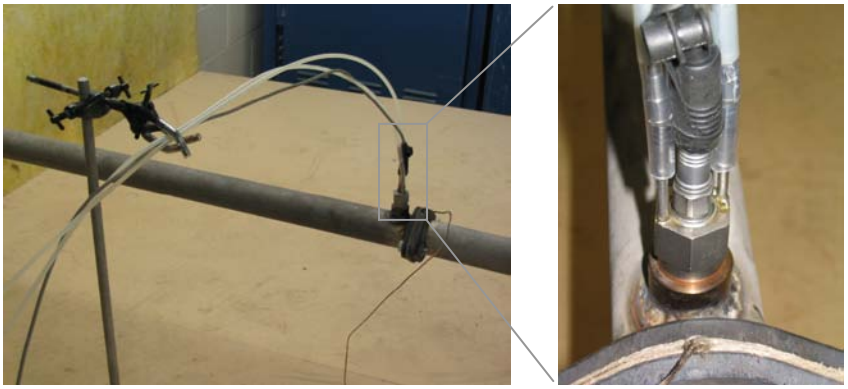

Figure 3.4-5 Pressure transducer mounting

3.5 Speaker test arrangement

3.5.1 *Speaker response*

The speaker response was tested to verify that the equipment used to generate noise at the input to the exhaust system would produce an adequate sound pressure level and frequency response. The speaker was driven using a Sony F210 amplifier with a Neutric Minirator MR1 used to generate pink noise. A Bruel and Kjær 2260 sound level meter equipped with the BZ7208 FFT software package was used to analyse the sound produced. The test setup is shown in Figure 3.5-1 below.

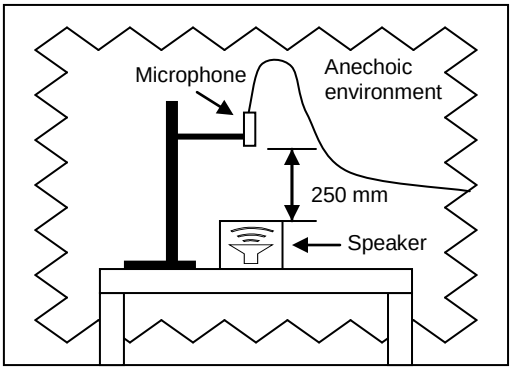

Figure 3.5-1 Speaker response test arrangement

The speaker was tested at five levels corresponding to settings 1 to 5 on the amplifier. The measured speaker output was considered adequate and is shown in Figure 3.5-2 below.

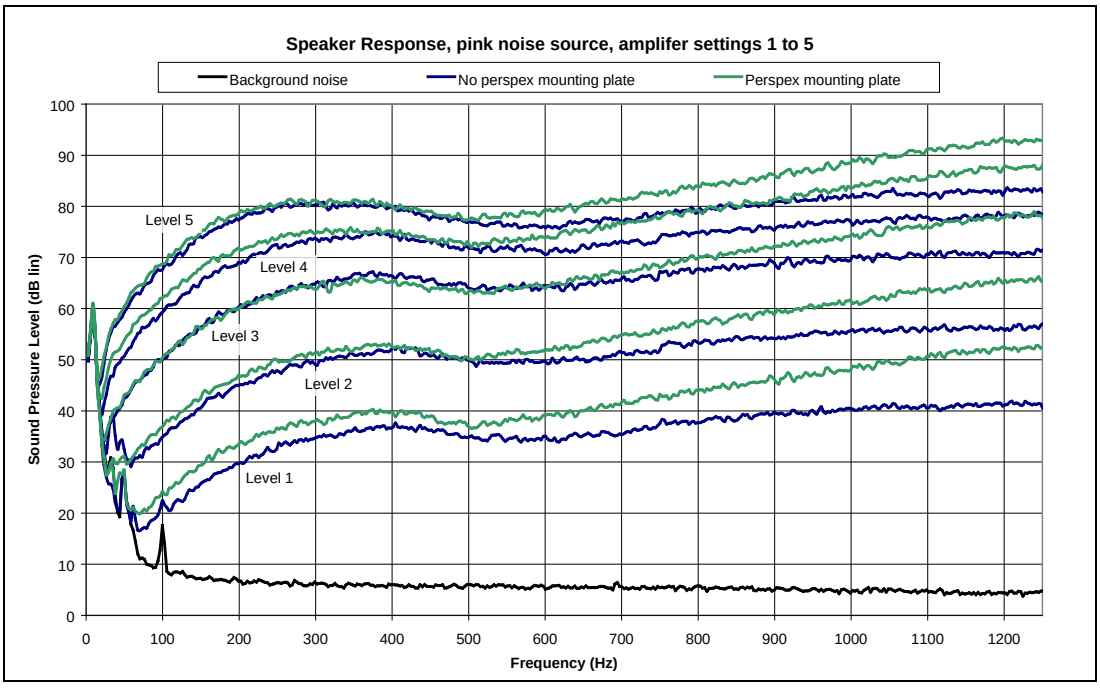

Figure 3.5-2 Speaker response

3.5.2 *Test arrangement*

The test arrangement used for the engine testing was modified to accommodate speaker testing. This was done by breaking the exhaust system and inserting a speaker in-between the original system and the test sections as shown in Figure 3.5-3 below.

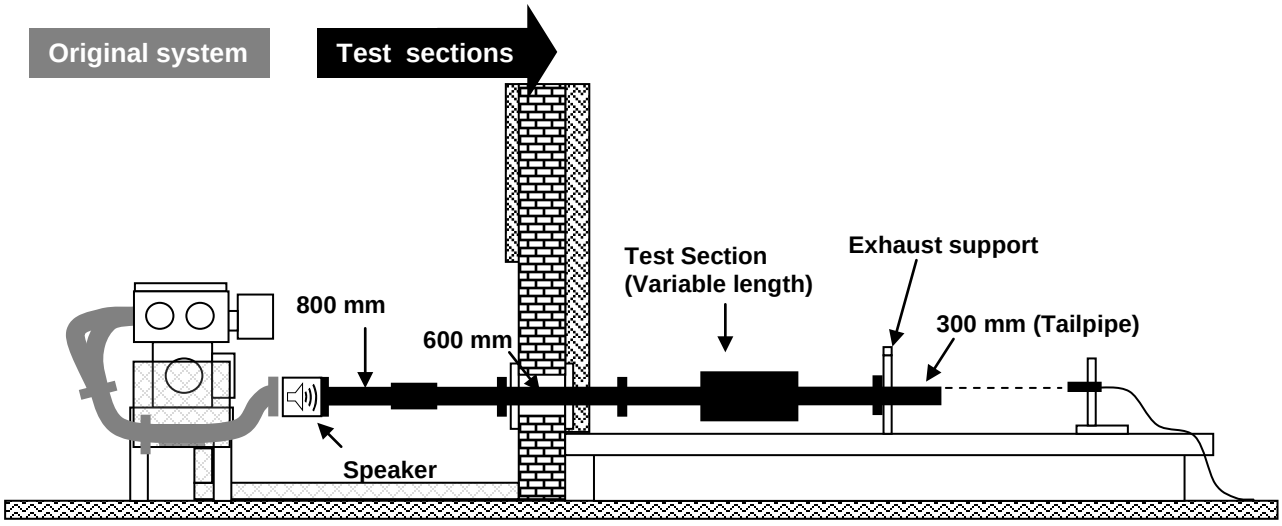

Figure 3.5-3 Loudspeaker testing arrangement

The speaker was mounted directly to the test sections via an adaptor plate as shown in Figure 3.5-4 and driven using a Sony F210 amplifier using a Neutric Minirator MR1 to generate pink noise. The microphone was placed as for the engine tests 500 mm behind and at 45° from the exhaust outlet.

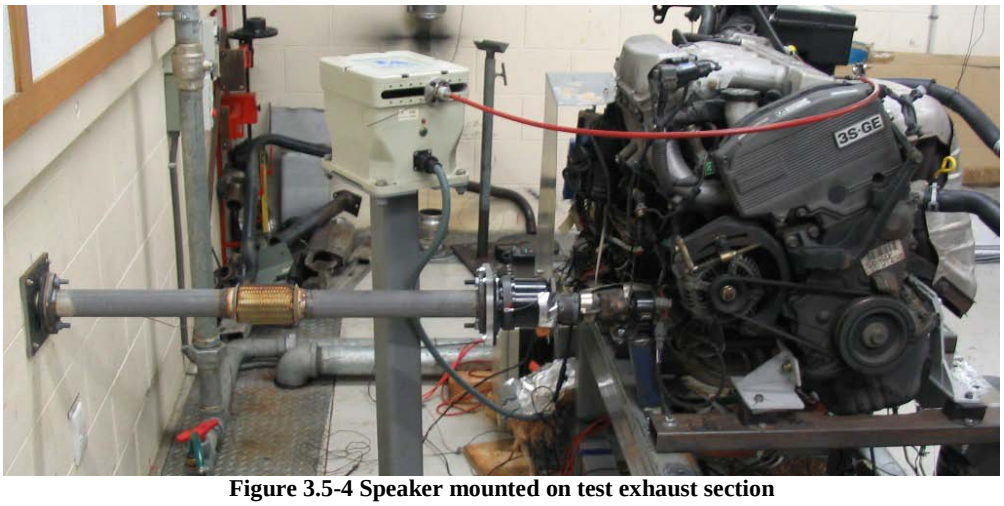

Figure 3.5-4 Speaker mounted on test exhaust section

3.6 References

[1] M. F. Harrison, "Time and Frequency Domain Modelling of Vehicle Intake and Exhaust Systems." Doctoral Thesis, Institute of Sound and Vibration Research, University of Southampton, 1994.

[2] R. J. Kee, P. G. O'Reilly, R. Fleck, and P. T. McEntee, "Measurement of Exhaust Gas Temperatures in a High Performance Two-Stroke Engine," Society of Automotive Engineers, Technical Paper 983072, 1998.

[3] J. A. Catom, "Comparasions of Thermocouple, Time-averaged and Mass-Averaged Exhaust Gas Temperatures for a Spark-Ignited Engine," Society of Automotive Engineers, Technical Paper 820050, 1982.

Chapter 4
Muffler Testing

Summary

Using the test arrangement described in the previous chapter, a number of muffler systems were tested using either an engine or a speaker as the source of excitation. Mufflers were tested to investigate changes in muffler cross-section, the length of connecting tubes between mufflers, and Helmholtz and quarter wave resonator performance. The noise emitted from the exhaust outlet was measured for each muffler system and the insertion loss of each system calculated by comparing the noise measured with and without the muffler present.

The noise measured with the engine as the source of excitation agreed well with that expected and reported in literature. Peaks at the fundamental firing frequency and at higher order harmonics were as predicted. Random noise attributed to flow was present at higher frequencies. Calculating insertion loss from the measured results showed some random variation. This variation was attributed primarily to slight changes in engine load and speed. To remove this variation so that trends in the data could be easily assessed, a moving average smoothing scheme was employed. To assess the repeatability of measurements, two nominally identical mufflers were constructed and tested. The insertion loss of these two mufflers was calculated and the results compared well with variation between the two cases increasing at frequencies above 500 Hz. With the speaker as the source of excitation, repeatability between tests was much improved due to the stable input signal.

The exhaust pressure pulse was analysed at various engine loads and speeds with a pressure transducer mounted at the inlet to the muffler. The data gathered agrees well with that measured at the exhaust outlet with the microphone. Analysing successive pressure pulses showed slight variations between the pressure pulses released from each of the four cylinders of the engine. These variations were attributed to differences in compression, fuelling and flow characteristics of each of the four cylinders. As these variations were small and consistent, they were not considered to affect the results.

Table of Contents

List of Figures and Tables

4.1 Introduction

A number of muffler systems were designed and tested in order to gain an appreciation of the factors that affect muffler performance. This chapter presents the experimental procedure, describes the mufflers tested, outlines the results gathered, and discusses the validity and repeatability of the results. All tests were conducted using the procedure described in Chapter 3. Insertion loss was calculated by comparing each test case to the un-muffled noise from the source. A complete discussion of the measured results, muffler performance characteristics and comparisons to predicted performance is contained in Chapter 6.

4.2 Muffler description

Eighteen mufflers were designed and constructed, their performance analysed, and an assessment of the accuracy of their predicted performance made. All mufflers tested were modifications to base case mufflers that were single expansion chamber, extended inlet and outlet mufflers. A summary of the mufflers tested is shown in Table 4.2-1 below. Drawings of all mufflers are presented in appendix A.

Table 4.2-1 Muffler description

Muffler	Description	Profile	Layout	Details
R1001	Base case round	155 Round	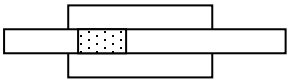	47.6 to 150.5 mm expansion 95.5 mm perforate, extended inlet (38.5 mm) and outlet (237 mm)
R1002 R1000	Modified tuned outlet extend tube	155 Round	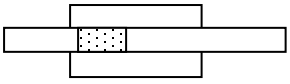	As per round base case with length of outlet extend tube decreased to 216 mm
R1003	Tuned Helmholtz chamber in series	155 Round	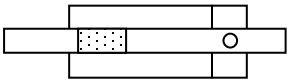	R1000 + Helmholtz chamber with Ø15.9 mm punched hole (series) 1145948 mm³ chamber volume
R1004	Tuned Helmholtz chamber in series	155 Round	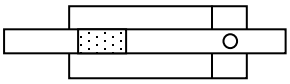	R1000 + Helmholtz chamber with 13.5 ID x 11 mm tube (series) 906355 mm³ chamber volume
R1005	Tuned Helmholtz chamber in parallel	155 Round	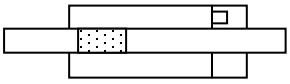	R1000 + Helmholtz chamber with Ø25.4 mm punched hole (parallel) 1145948 mm³ chamber volume
R1006	Tuned Helmholtz chamber in parallel	155 Round	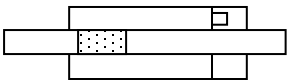	R1000 + Helmholtz chamber with 23 ID x 20 mm tube (parallel) 645594 mm³ chamber volume
R1011	Tuned Helmholtz chamber in series	155 Round	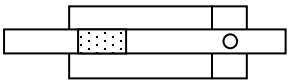	R1000 + Helmholtz chamber with 23 ID x 36 mm tube (series) 649419 mm³ chamber volume
R1012	Tuned Helmholtz chamber in series	155 Round	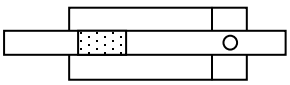	R1000 + Helmholtz chamber with Ø23 mm punched hole (series) 1713642 mm³ chamber volume
R1021 R1022	Intermediate muffler (two positions)	155 Round	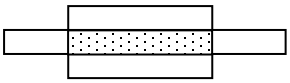	Perforated along entire length of expansion chamber (400 mm)
R2000 R2001	Base case oval	220x119 Oval	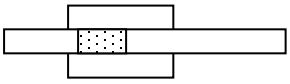	Ø50.9 to Ø150.5 mm expansion 95.5 mm perforate, extended inlet (38.5 mm) and outlet (166 mm)
R2002	Modified outlet extend tube	220x119 Oval	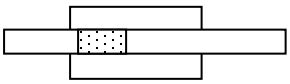	As per oval base case with length of outlet extend tube increased to 216 mm
R2003	Tuned Helmholtz chamber in series	220x119 Oval	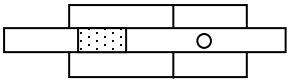	R2000 + Helmholtz chamber with Ø32 mm punched hole (series) 2405242 mm³ chamber volume
R2004	Tuned Helmholtz chamber in series	220x119 Oval	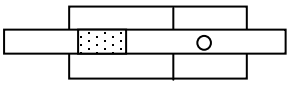	R2000 + Helmholtz chamber with 30.8 ID x 15 mm tube (series) 1442269 mm³ chamber volume
R2005	Tuned Helmholtz chamber in parallel	220x119 Oval	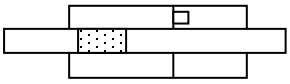	R2000 + Helmholtz chamber with Ø32 mm punched hole (parallel) 2405242 mm³ chamber volume
R2006	Tuned Helmholtz chamber in parallel	220x119 Oval	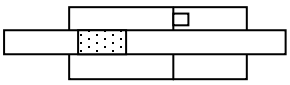	R2000 + Helmholtz chamber with 30.8 ID x 20 mm tube (parallel) 126447 mm³ chamber volume

4.3 Test procedure

4.3.1 Engine tests

The sound signal radiated from the exhaust outlet was measured at a variety of engine loads and speeds with each muffler installed. The test procedure was as follows:

1. The test muffler system was installed into the exhaust system of the engine.
2. The microphone was positioned 500 mm from the top of the tailpipe outlet at an angle of 45° to the centreline of the exhaust system in accordance with ISO 5130-1982 and SAE J1169 standards.
3. The microphone and sound analyser were calibrated to 114 dB using a Bruel and Kjær type 4231 calibrator.
4. The engine was started and warmed up to operating temperature.
5. Measurements of the sound signal and exhaust gas temperature were made with the engine speed and load stable going from low to high load and from 1000 to 5000 RPM at 500 RPM increments. A windshield was used on the microphone to reduce any noise due to the exhaust flow and a Bruel and Kjær type ZF0023 -20 dB filter was used between the microphone and preamp to allow sound measurements up to 149.9 dB. The loads applied to the engine for each engine speed and load case are shown in Table 4.3-1 below.

Table 4.3-1 Target engine loads

Load (kNm)	**Engine Speed (RPM)**								
	1000	**1500**	**2000**	**2500**	**3000**	**3500**	**4000**	**4500**	**5000**
Low	20	20	20	20	20	20	20	20	20
Half	52	70	70	70	70	70	70	70	70
High	80	100	115	125	140	150	155	160	160

The sound signal emitted from the exhaust was analysed using a Bruel and Kjær 2260 Investigator equipped with the BZ7208 FFT software package with the settings as per those shown in Table 4.3-2.

Table 4.3-2 Sound Analyser settings

Averaging	Linear
Number of measurements for average	200
Average measurement time	22.800 s
Full scale measurement	~150 dB (with ZF0023)
Weighting scale applied	None
Frequency span	1250 Hz
Central frequency	629.88 Hz
Frequency resolution	2.930 Hz
Noise bandwidth	4.395 Hz
Measurement window	Hanning
Measurement window overlap	67 %

4.3.2 Loudspeaker tests

Each muffler system was tested with a speaker installed at the inlet to the test section as described in section 3.6.2. The test procedure was as follows:

1. The test muffler system was installed on the test rig and the microphone positioned 500 mm from the top of the tailpipe orifice at an angle of 45° to the centreline of the exhaust system in accordance with ISO 5130-1982 and SAE J1169 standards.
2. The microphone and sound analyser were calibrated to 94 dB using a Bruel and Kjær type 4231 calibrator.
3. Pink noise generated with a Neutrik Minirator MR1 signal generator was amplified by a Sony F210 amplifier and played through a speaker to produce a sound pressure level of about 110 dB at the inlet to the test exhaust system.
4. The sound signal emitted from the tailpipe was analysed using a Bruel and Kjær 2260 Investigator equipped with the BZ7208 FFT analysis software with the settings as shown in Table 4.3-2 with the full scale measurement reduced to 109.9 dB.

4.4 Results and analysis

4.4.1 Engine testing

4.4.1.1 Un-muffled exhaust noise

To calculate the insertion loss of a muffler system the un-muffled noise from the source must first be measured. Figure 4.4-1 below shows the measured data for the un-muffled engine at 1000 RPM. The low, half and high load cases are shown in green, orange and red respectively. The light blue lines show the fundamental firing frequency and its higher order harmonics.

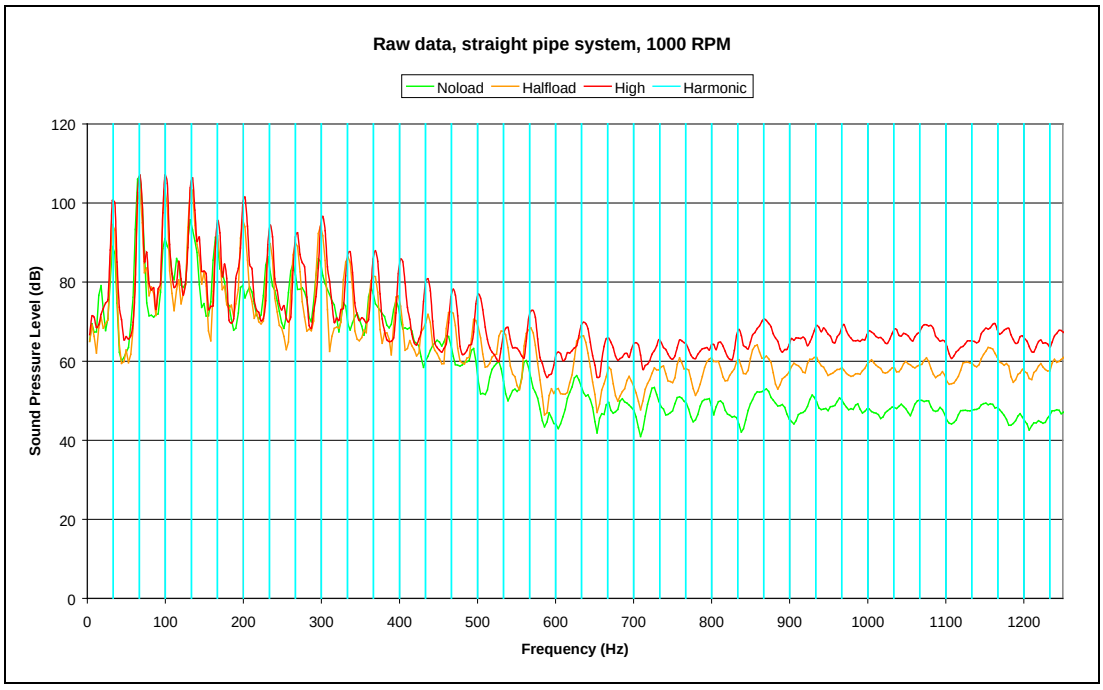

Figure 4.4-1 Un-muffled exhaust noise

The measured peaks shown above in Figure 4.4-1 show clear agreement with those predicted. The first peak present at 33.3 Hz is the fundamental firing frequency with associated higher order modes at integer multiplies of the fundamental. As the load is increased the noise level increases as expected. At frequencies above 500 Hz, the signal becomes random in nature due to flow noise. Increasing engine load leads to higher flow through the system and hence higher flow noise, as is evident when comparing the low, half and high load cases. Exhaust noise data is commonly shown on a waterfall plot as shown in Figure 4.4-2. Waterfall plots show data across the engine speed and frequency range of interest, with the sound pressure level indicated by the colour bar shown to the right of the plot. The firing harmonics are shown as red bands tracking diagonally across the plot.

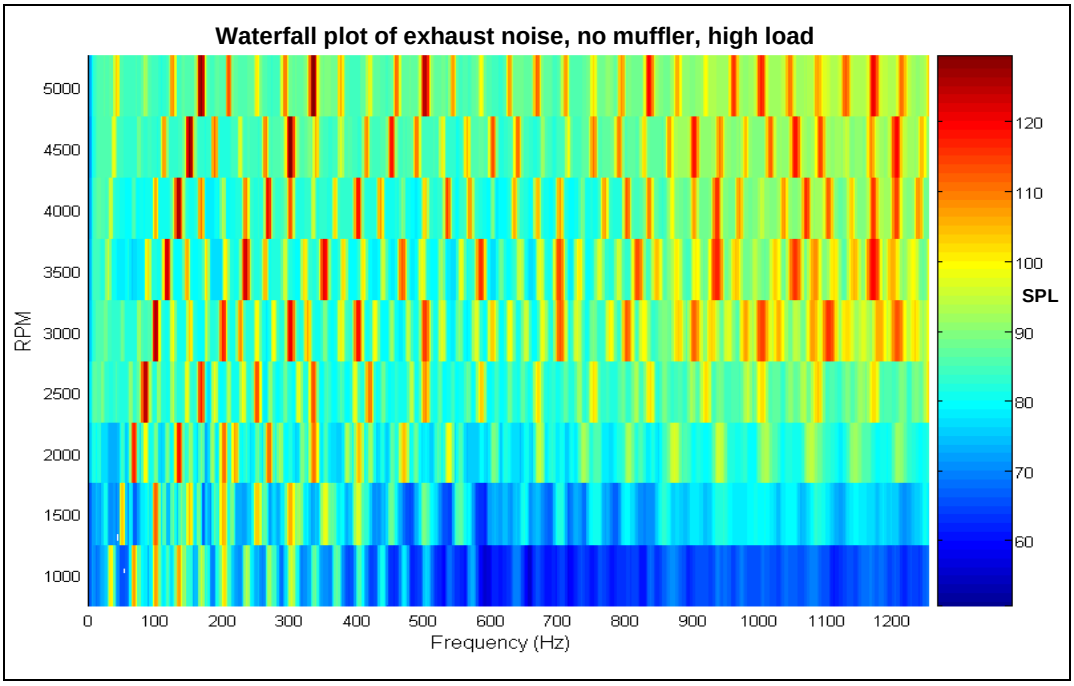

Figure 4.4-2 Waterfall plot of data

4.4.1.2 Muffled exhaust noise

Figure 4.4-3 shows the measured exhaust noise spectrum at 1000 RPM with the R2001 muffler installed. The firing harmonics are as predicted and there is a reduction in sound pressure level across the frequency range compared to the un-muffled case. Further data manipulation is required to give a measure of the performance of the muffler system itself.

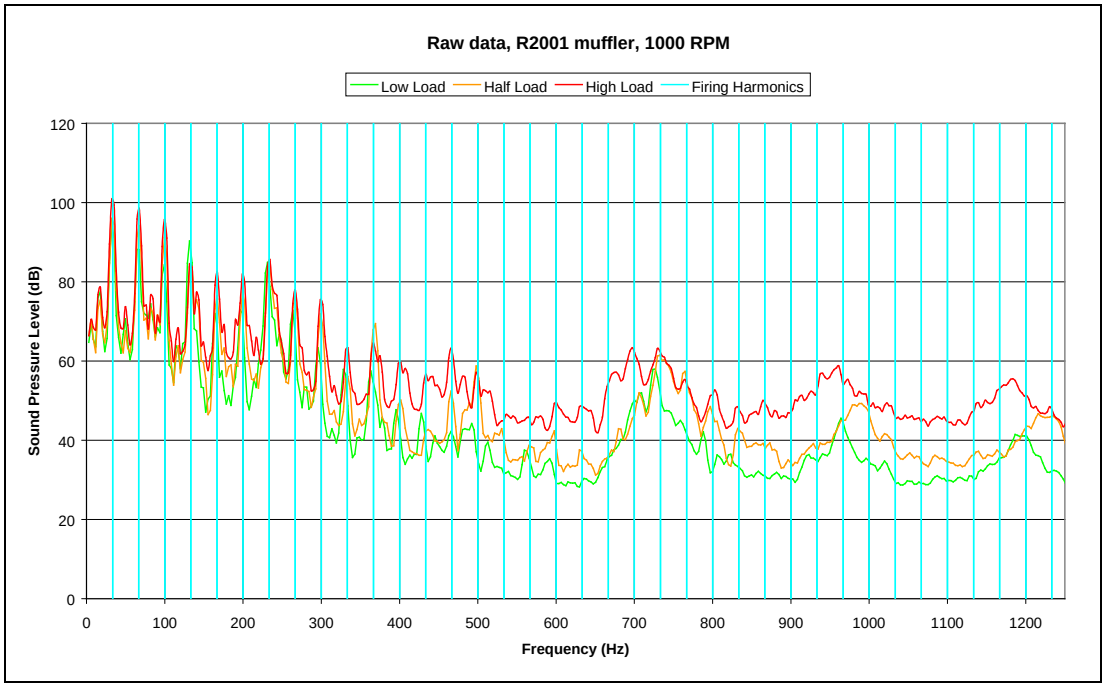

Figure 4.4-3 Muffled exhaust noise, R2001 muffler

4.4.1.3 Insertion loss of muffler

Insertion loss is the difference between sound pressure levels measured before and after a muffler has been inserted between the source and the measurement point. The measurement point is specified relative to the exhaust outlet, in this case, 500 mm from the exhaust outlet at 45°, in line with the top of the exhaust outlet. Insertion loss was calculated for each of the muffler systems tested with a speaker and an engine as the sources of excitation (separately). Figure 4.4-4 shows the insertion loss calculated using the data shown in Figures 4.4-1 and 4.4-3.

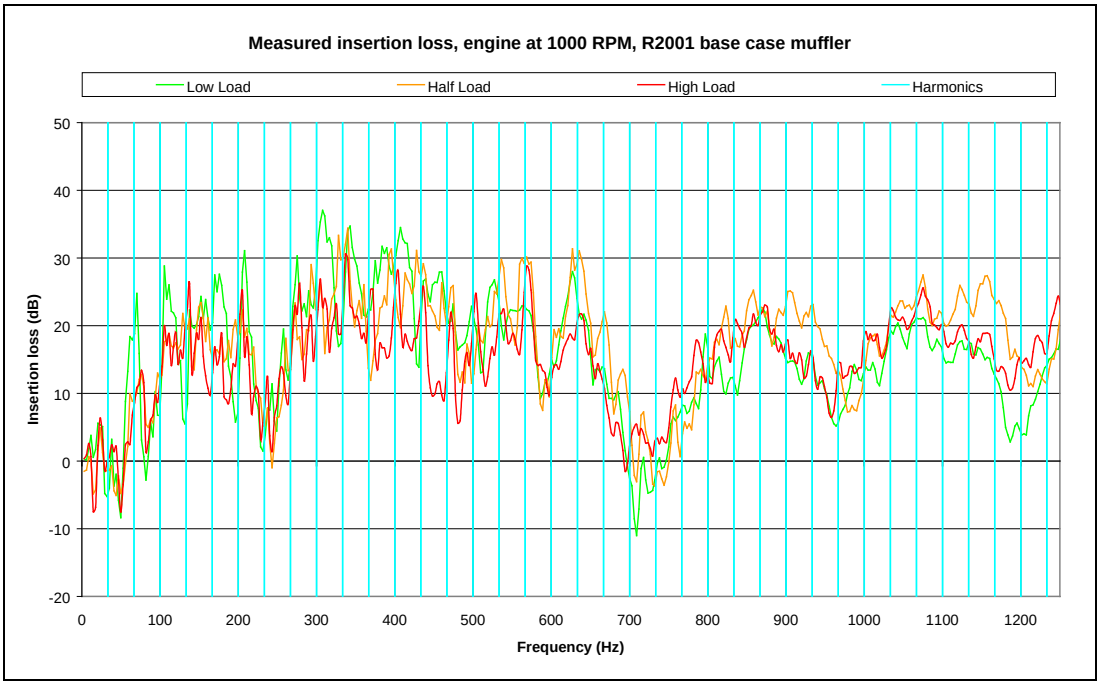

Figure 4.4-4 Insertion loss measured using the engine as the source

Insertion loss provides an insight into the performance of the muffler system itself and is to some extent independent of the source of excitation. This will be discussed further in Chapter 6. The three load cases (low, half, high) agree well and the insertion loss trend of the muffler can be seen. There are however, variations in the measurements.

4.4.1.4 Data smoothing

The removal of random variations from the data was investigated so that trends could be easily seen. Two smoothing schemes were considered; a moving average and a moving spline fit, both with variable degree of smoothing. The moving spline fit produced a marginally better result. However, due to the complexity of the spline algorithm, the 15 point moving average was used to smooth the data. Data that has been smoothed will be represented by a thicker line to differentiate it from that has not

been smoothed. Figure 4.4-5 below shows a comparison of smoothed data using the two smoothing schemes tested and the unsmoothed data for the R1002 muffler case at low load.

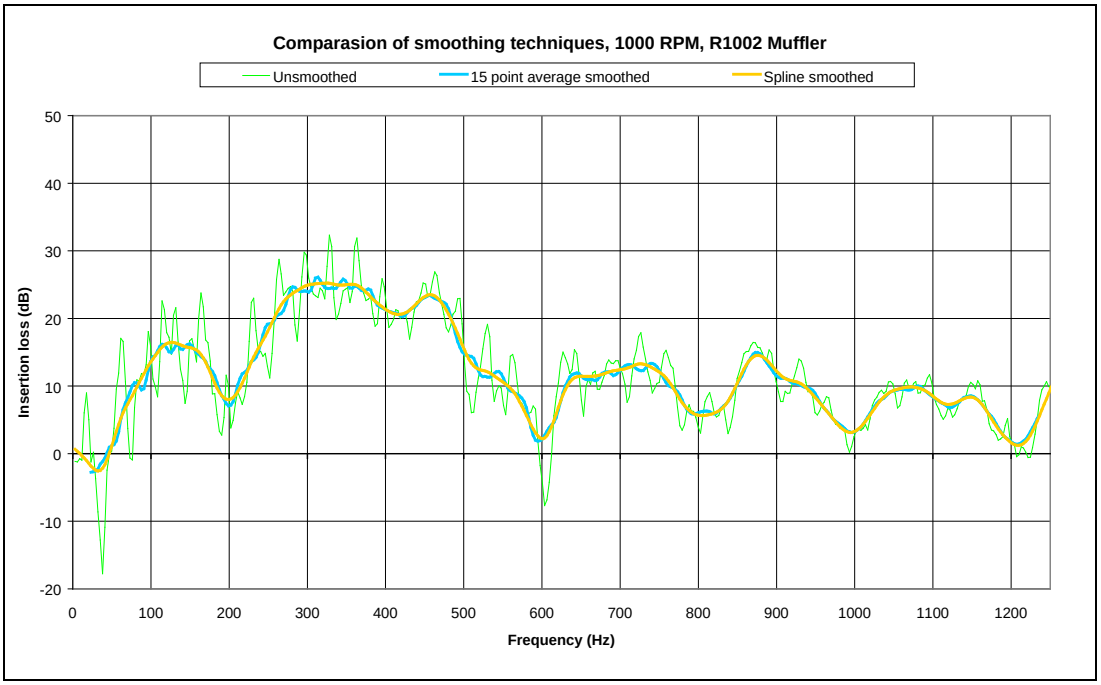

Figure 4.4-5 Comparison of smoothed and unsmoothed data

4.4.1.5 Repeatability

The accuracy of measurements was investigated by manufacturing and testing two nominally identical mufflers (R1000, R1002). There are a number of factors that will cause variation in measurements. Atmospheric variation of temperature and humidity both day to day and during a test period will change the efficiency of the engine and alter the firing characteristics. This will change the size and shapes of the pressure pulses released and hence alter the noise emitted from the exhaust outlet.

Variation of engine load and speed occurs during tests due to slight variations in dynamometer load and engine power output. The load is applied to the engine through a Froude dynamometer and controlled by varying engine throttle position and water flow through the dynamometer. Any variation in the water supply to the dynamometer causes small fluctuations in the load applied causing a change in engine speed. The control unit will compensate for this change by adjusting the throttle position and water flow which in turn varies the power produced by the engine. Engine power output may also change due to factors related to the engine itself such as fuel supply and water temperature. Varying the engine power output changes the magnitude of the harmonic peaks. A variation in engine speed blurs and lowers the peaks as they shift with the engine speed.

Manufacturing tolerances may result in baffle spacing or perforate location to change. This will change the insertion loss characteristic of the muffler. For example, a 1mm difference in baffle spacing at 400°C will cause a 2.3 Hz shift in the tuned frequency of the outlet quarter wave resonator. Variation in baffle spacing may be as much as ±2 mm in production mufflers.

The cooling of exhaust gas as its flows through the system is related to the ambient temperature in both the source and receiving rooms. Changes in ambient temperature both day to day and during test runs results in each run having a different temperature gradient down the exhaust system. An increase in exhaust gas temperature increases the speed that sound will propagate through the exhaust gas. This varies the insertion loss characteristic of the muffler, reducing the repeatability of testing. For example, a change in temperature from 400°C to 410°C increases the quarter wave resonant frequency of the R1000 muffler by 4.1 Hz. The factors described thus far represent variations that will occur day to day, long term changes such as engine wear, loss of calibration and seasonal changes both environmental and in fuel additives will cause additional variation between measurements.

Figure 4.4-6 below shows a comparison of insertion loss as calculated and smoothed for the nominally identical R1000 and R1002 mufflers. The two sets of data agree well with variation typically less than 5 dB, increasing at higher frequencies due to random flow noise.

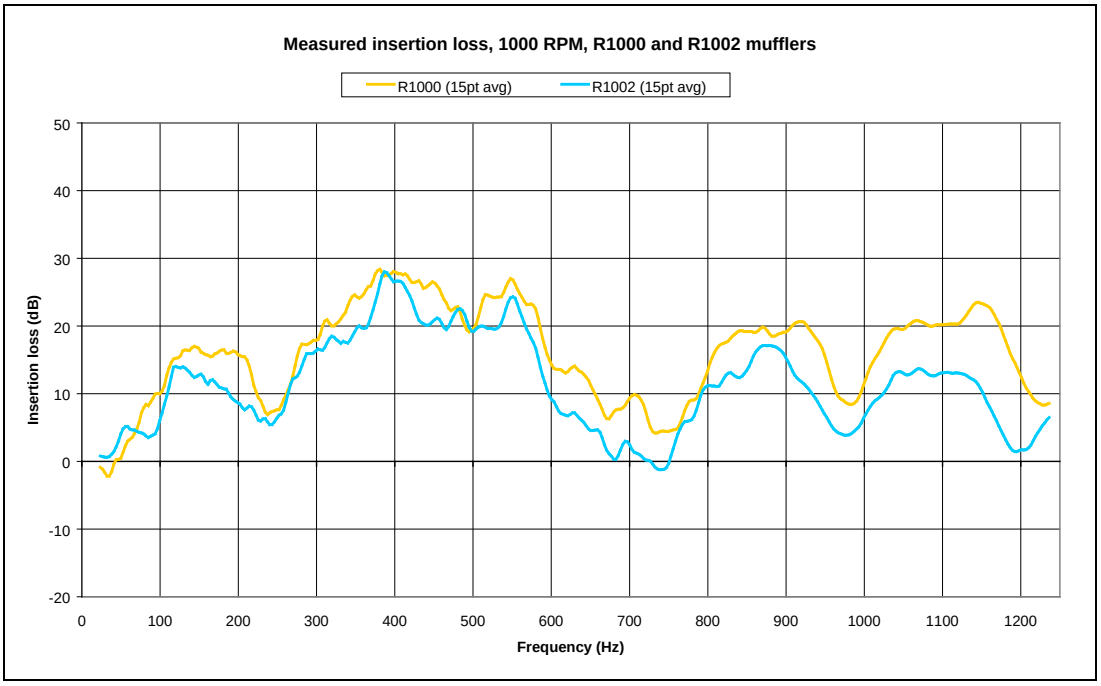

Figure 4.4-6 Comparison of measured insertion loss, engine as source of excitation

4.4.1.6 Pressure pulse analysis

Figure 4.4-7 shows the pressure change vs. time measured at the entry to the R2003 muffler. The data was recorded with the engine running at half load at 1000, 3000 and 5000 RPM.

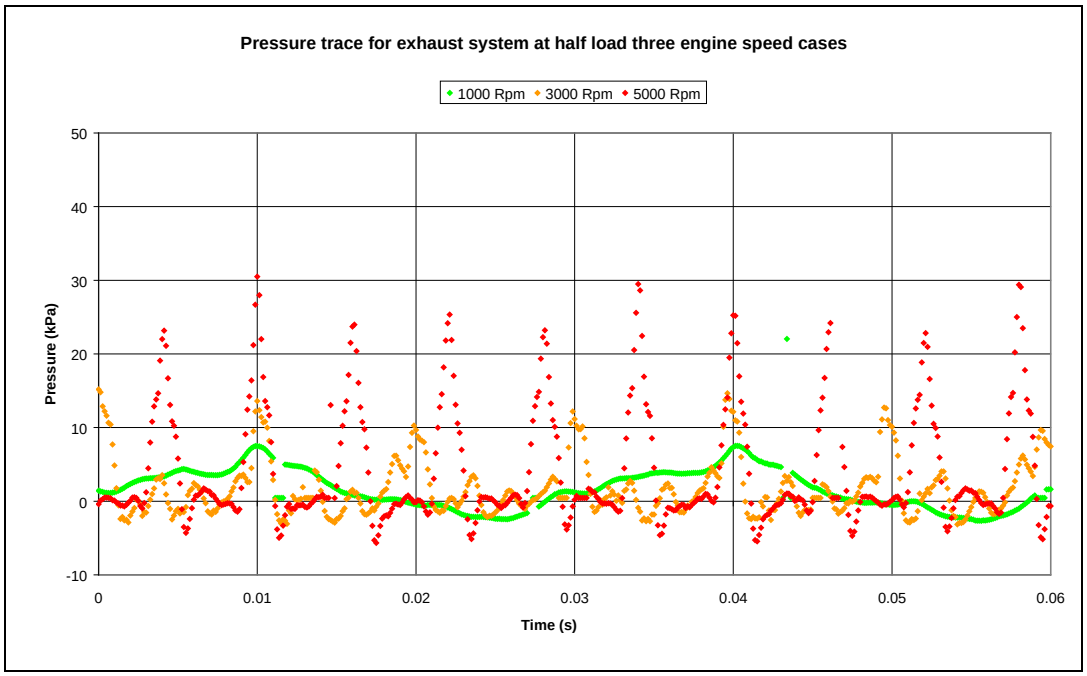

Figure 4.4-7 Pressure pulse analysis

The time interval measured between successive peaks shown in the plot above indicates the time between firing of each of the cylinders. Calculating the time between pressure pulses for the data above, we have 0.03s for 1000 RPM, 0.01s for 3000 RPM and 0.006s for 5000 RPM. These correspond to the fundamental firing frequencies measured at the exhaust outlet of 33.33, 100 and 166.66 Hz respectively.

The shape of the pressure pulse and its magnitude will determine the sound radiated from the system and have an effect on the performance of the muffler system. Figure 4.4-7 shows that as engine speed is increased the rise time of the pressure pulse is reduced resulting in a ‘steeper’ wave. A similar steepening effect was also observed with increasing engine load. These effects and their influence on muffler performance are discussed in detail in Chapter 6. Analysing the size and shape of successive pressure pulses shows that they are not identical. Closer examination reveals that every fourth pressure pulse is similar; corresponding to the firing of each of the four cylinders of the engine. There are a number of factors that may cause the pressure pulses from each cylinder to vary, including; cylinder compression, the unequal length inlet manifold, varying injector flow rates, engine wear, and ignition differences. As this variation is small and consistent it should not affect measurements.

4.4.2 Speaker testing

4.4.2.1 Measurements

Figure 4.4-8 below shows measurements made using the speaker as the source of excitation. The plot shows the input signal measured in the anechoic room (see section 3.5.1), the background noise level in the receiving room, and the signal measured at the exhaust outlet with and without the R2003 muffler system fitted.

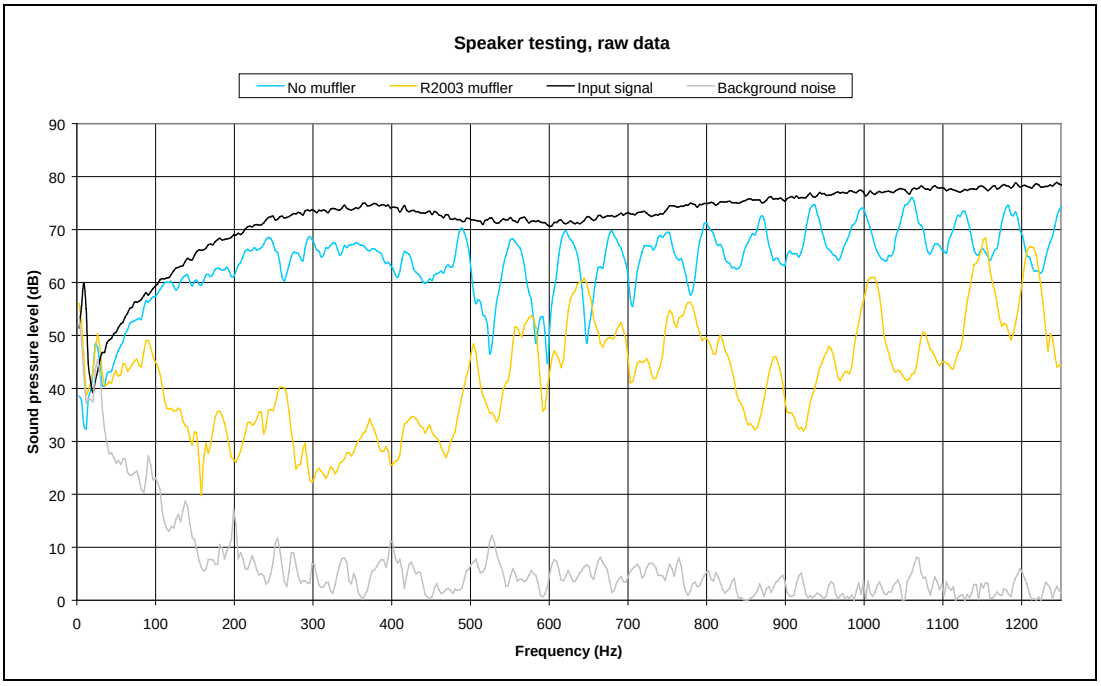

Figure 4.4-8 Measurements made with the speaker as the noise source

The signal measured with the speaker mounted at the inlet to the test exhaust system is reduced from that with no load present. At higher frequencies, pass bands associated with the inlet tube of the test system are exhibited, this will be discussed further in Chapter 6. Adding the R2003 muffler to the system further reduces the noise radiated. Figure 4.4-9 shows the insertion loss calculated using the data for the straight pipe and the R2003 muffler as shown in the plot above. Of note is that the maximum insertion loss that can be measured will be determined by the level of the straight pipe noise signal compared to that of the background noise. This is especially apparent at frequencies below 30 Hz where the background noise level is comparable to the input signal.

4.4.2.2 Repeatability

Figure 4.4-9 compares the insertion loss calculated from data collected on separate days, using the speaker as the source, for the R2003 muffler system.

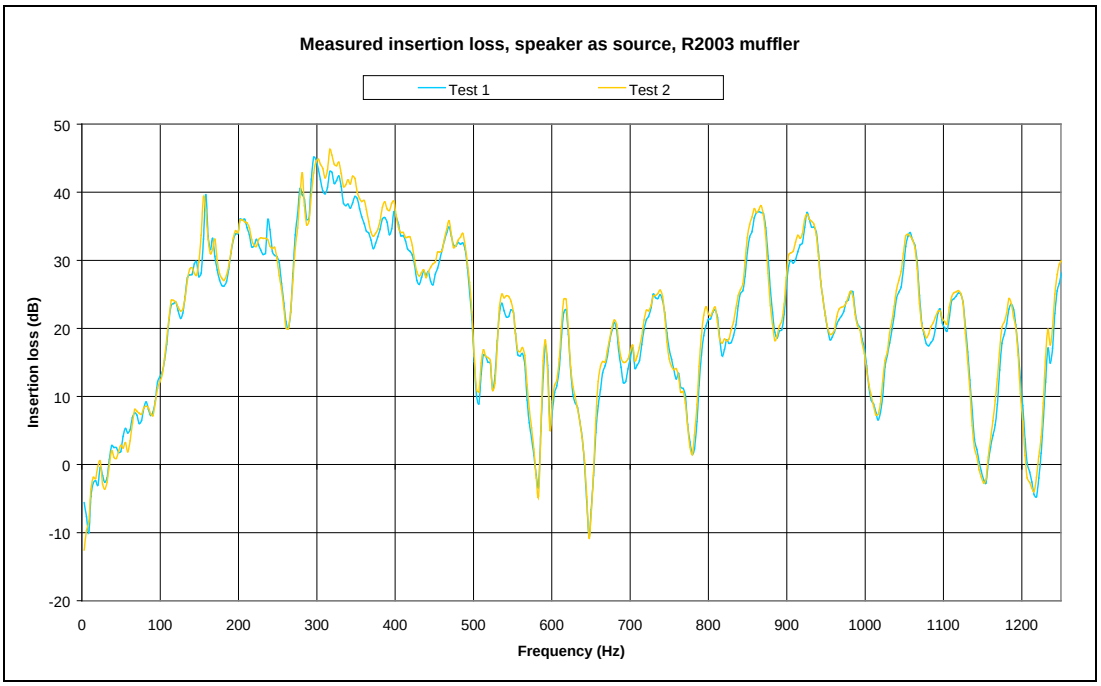

Figure 4.4-9 Comparison of insertion loss measured with a speaker

Variation between the two tests is much less than that shown in Figure 4.4-6 using the engine as the source of excitation. This is due to the stability of the input noise source, and the zero flow, uniform temperature environment.

One concern was that due to the direct mounting of the speaker on the test exhaust system, the varying acoustic load of the different muffler systems may affect the output of the speaker. A number of speaker mounting positions both direct and branched and also the use of a high impedance source, for selected tests by one author [1], are reported in the literature. Little to no justification was given in any of these publications regarding speaker position or discussion on the effect of the acoustic load on the speaker output. The lack of information on the effect of varying load on the source impedance and a statement by Munjal [2] that insertion loss does not have a strong dependence on source impedance suggests that speaker test arrangement is adequate. Chapter 6 contains further discussion of the accuracy of the insertion loss measurements with the speaker as the source of excitation with regards to those predicted by the modelling.

4.5 Conclusions

Results gathered using the test apparatus as described in Chapter 3 have been shown to be reasonably repeatable. Measurements gathered corresponded well with those expected showing firing harmonics, increases in noise level with load, and flow noise at higher frequencies. Comparing insertion loss measured with nominally identical mufflers produced acceptable agreement with some deviation due to experimental uncertainty.

A number of sources of random variation were identified with both the speaker and the engine as the sources of excitation. For the engine as the source, variation in load and engine speed change the magnitude and position of the firing harmonics. Variation in temperature throughout the exhaust system changes the speed that sound will propagate in the exhaust gas, changing insertion loss characteristics. A 15 point smoothing algorithm was used to remove the majority of variation. This allowed the true performance of the muffler to be easily assessed.

Analysis of the exhaust pressure pulse as it travelled into the muffler system showed the size and shape of the pressure pulses and how they change with engine speed and load. Analysis of sequential pressure pulses showed variation between the pulses from each of the four cylinders of the engine. This was attributed to variations in individual cylinder compression, flow and fuelling characteristics. The slight differences in pressure pulses released from each cylinder was not considered large enough to have any effect on the sound radiated, or the performance of the muffler systems tested.

4.6 References

[1] M. F. Harrison, "Time and Frequency Domain Modelling of Vehicle Intake and Exhaust Systems." Doctoral Thesis, Institute of Sound and Vibration Research, University of Southampton, 1994.

[2] M. L. Munjal, "Acoustic Characterization of an Engine Exhaust Source - A Review," presented at ACOUSTICS 2004, Gold Coast, Australia, 2004.

Chapter 5
Modelling

Summary

Modelling began by looking at the performance of single muffler components, specifically Helmholtz resonators. A suitable model for the attenuation of Helmholtz resonators was created based on early work by Davis et al. [1]. From this model, a spreadsheet was constructed that produced resonator performance curves to aid in muffler design. This model had two major drawbacks as it only considered the performance of a singular muffler component and did not consider the propagation of noise from the exhaust system.

In order to model the performance of an entire exhaust system a new model was created based on work by Davies [2]. The model calculated the insertion loss of a muffler system allowing for the interaction of muffler components, temperature gradients through the system and incorporated an end correction for radiation from the exhaust outlet to the surroundings. This model was written in MATLAB code due to the iterative nature of the calculations and the matrix algebra with complex numbers involved. Later the model was transferred to a spreadsheet.

In addition to the MATLAB code and the spreadsheet, a graphical user interface (GUI) was created that allowed experimental data to be displayed on a frequency vs. engine speed waterfall plot. Below this a secondary plot allowed data corresponding to specific engine speeds to be shown. The GUI was linked to the overall system model and the attenuated spectrum at temperatures corresponding to each engine speed could be calculated and displayed. An A-weighting feature was also incorporated into the GUI that allowed the A-weighting scheme to be imposed or removed from the data. The GUI can be used to quickly assess the performance of a number of muffler systems across the engine speed range for differing load cases.

Table of Contents

List of Figures

5.1 Introduction

This chapter describes the modelling process used to predict the performance of muffler systems containing resonant absorbers. Chapter 6 compares predictions from the modelling with experimental results as presented in Chapter 4.

Early modelling of muffler systems was performed by Davis et al. [1, 3]. Since then there has been a large amount of work performed and published in the literature on exhaust system modelling with both frequency domain and time domain methods in use by various groups. However, as the automotive market is incredibly large and competitive a vast amount of muffler system and modelling development is performed 'in house' by large manufacturing groups. As this information can be commercially sensitive, it is not readily available in the public domain.

There are a number of commercial packages available to predict muffler performance such as LAMPS3, Ricardo WAVE and STAR CD. These packages allow assessment of a number of muffler components in various configurations and can be used to optimise the design of a system. However, these packages are quite expensive and give results without the user necessarily understanding the process by which they have been calculated. The danger of these 'black box' programs is that the user may not have a full understanding of the assumptions used in the calculations and consequently the limitations of the predictions. This chapter will present the modelling used to model both single muffler components and systems of components, showing assumptions and justifications.

5.2 Helmholtz resonator model

5.2.1 Introduction

The first model created was of a simple Helmholtz resonator based on work by Davis et al. [1]. The equations presented were solved to give required tuning tube sizes for a given set of input data consisting of muffler size, baffle spacing, gas temperature and target tuned frequency. From these results, design curves were produced to allow selection of optimum tuning tube size. The theory, assumptions and equations used are presented in this section.

5.2.2 Assumptions

The assumptions required for analysis as a simple one-dimensional system are:

1. The sound pressures are small compared to the absolute value of the pressure in the system.
2. The tailpipe is terminated in its characteristic impedance; that is, there are no reflected waves and the termination is considered anechoic.
3. The muffler walls are rigid and do not conduct or transmit sound energy.
4. Only plane pressure waves are propagated.
5. Viscous effects are ignored. In addition to this, the boundary layer thickness in the connecting pipe is small compared to the diameter of the tube.
6. The dimensions of the resonator are small compared to the wave length of the sound considered.

Assumption 1 is generally valid for vehicle exhaust systems. This is discussed in detail in Chapter 6**.** Assumption 2 is required to analyse the performance of a single muffler component and implies an anechoic termination. Radiation from the tailpipe will be considered in later sections. Assumption 3 is a fair approximation as although some breakout will occur, the walls of the mufflers investigated are double walled and suitably rigid. Assumption 4 can be considered appropriate in most exhaust systems below the cut-off frequency. Wave steepening is assumed not to occur as the distance between discontinuities is relatively short [4]. This approximation is used widely in the design of exhaust systems and will be discussed further in Chapter 6. Assumption 5 is used to greatly simplify analysis. The effect of this assumption is discussed in detail in Chapter 6. Assumption 6 is valid for the muffler systems and frequencies of interest.

5.2.3 Modelling of Helmholtz resonator

Figure 5.2-1 shows a schematic of a Helmholtz resonator with symbols that will be used for analysis.

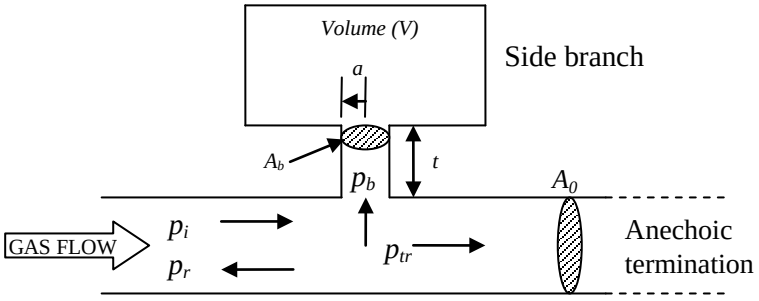

Figure 5.2-1 Helmholtz resonator diagram with symbols

Where: p = sound pressure (Pa)
A = area (m²)
V = volume (m³)
a = radius of connection tube
t = length of connection tube
$_{tr}$ = transmitted
$_b$ = branch
$_0$ = main pipe
$_i$ = incident
$_r$ = reflected

The impedance of the side branch is considered to be:

$$Z_b = R_b + iX_b \qquad (5.2\text{-}1)$$

Where: Z = impedance
R = real component of impedance
X = imaginary component of impedance

Pressure and particle velocity are conserved at the boundary between the exhaust pipe and the branch connector, giving:

$$p_i + p_r = p_b = p_{tr} \qquad (5.2\text{-}2)$$

$$v_i - v_r = v_b + v_{tr} \qquad (5.2\text{-}3)$$

Where: v = particle velocity

Using the fact that $p=Z_o v$, where Z_o is the characteristic impedance of the tube, equation 5.2-3 can be written as:

$$\frac{1}{Z_o}(p_i - p_r) = p_{tr}\left(\frac{1}{Z_b} + \frac{1}{Z_o}\right) \qquad (5.2\text{-}4)$$

Solving equations 5.2-2 and 5.2-4 simultaneously for the ratio p_i / p_{tr} gives:

$$\frac{p_i}{p_{tr}} = 1 + \frac{Z_o}{2Z_b} = 1 + \frac{Z_o}{2(R_b + iX_b)} \qquad (5.2\text{-}5)$$

The attenuation is therefore:

$$Attenuation = 10\log_{10}\left|\frac{p_i}{p_{tr}}\right|^2 = 10\log_{10}\frac{\left(R_b + \frac{Z_o}{2}\right) + X_b^2}{R_b^2 + X_b^2} \qquad (5.2\text{-}6)$$

Note that the impedances of the various components are:

$$Volume\ impedance = -i\frac{\rho c^2}{\omega V} \qquad (5.2\text{-}7)$$

$$Connector\ impedance = \frac{l_c}{\pi a^3}\sqrt{2\mu\rho\omega} + i\left(\frac{\omega\rho}{c_o} + \frac{l_c}{\pi a^3}\sqrt{2\mu\rho\omega}\right) \qquad (5.2\text{-}8)$$

Where: l_{eff} = the effective length of the connector = $t + 1.7a$
c_o = the conductivity of the connector = $\pi a^2/(l_{eff} + \beta a)$

As the connector and volume are arranged in series, the above expressions can be added to give the real and imaginary components of the branch impedance:

$$R_b = \frac{l_c}{\pi a^3}\sqrt{2\mu\rho\omega} \qquad (5.2\text{-}9)$$

$$X_b = \frac{\omega\rho}{c_o} - \frac{\rho c^2}{\omega V} + \frac{l_{eff}}{\pi a^3}\sqrt{2\mu\rho\omega} \qquad (5.2\text{-}10)$$

Setting $\mu = 0$ as per assumption 5 and substituting the components of Z_b into equation 5.2-6 gives:

$$Attenuation = 10\log_{10}\left(1 + \frac{Z_o}{4X_b^2}\right) \qquad (5.2\text{-}11)$$

At resonance, the branch impedance reduces to zero and the resonant frequency can be shown to be:

$$f_r = \frac{c}{2\pi}\sqrt{\frac{c_o}{V}} \qquad (5.2\text{-}12)$$

Using this expression and the value for X_b gives the attenuation of the Helmholtz resonator to be:

$$Attenuation = 10\log_{10}\left[1+\left(\frac{\frac{\sqrt{c_o V}}{2A_0}}{\frac{f}{f_r}-\frac{f_r}{f}}\right)^2\right] \qquad (5.2\text{-}13)$$

The equation above was solved for the geometric parameters of the connecting tube. The resulting equation was used to generate a spreadsheet that plotted attenuation vs. frequency and created design curves to allow the best tuning tube size to be selected for a resonator at a specific frequency.

5.3 Scattering matrix system model

5.3.1 Introduction

The scattering matrix system model works by assuming a radiated signal at the outlet and working back towards the source. At each discontinuity in the system, the signal is modified by a scattering matrix related to the geometrical features of that discontinuity. Once all muffler elements have been described, the resulting expression can be used to calculate the insertion loss of the system, or be coupled with a model of the source to obtain the radiated noise. As we are only concerned with the performance of the muffler system itself, the scattering matrix method will be used to calculate muffler insertion loss.

Assumptions 1, 3, 4 and 6 from section 5.2.2 are required for the analysis in this section. For this model, the exhaust outlet termination and radiation to the surroundings are considered using a mass end correction. The source is considered to be terminated at its characteristic impedance (anechoic termination). Insertion loss calculations for most frequencies have been shown to have very little dependence on the source impedance [5], and considering the source as anechoic greatly simplifies the calculations. The scattering matrix for each element will be shown in the following sections along with the process used to combine the matrices and obtain an insertion loss prediction. The theory presented in this section is based on work by Davies [2, 4, 6, 7].

5.3.2 Scattering matrices

5.3.2.1 Propagation of sound waves

Before the scattering matrices for each element can be derived, we must define expressions for sound waves propagating through the system. Beginning with the 1D Helmholtz equation:

$$\frac{\partial^2 p(x:t)}{\partial x^2} + k^2 p(x:t) = 0 \qquad (5.3\text{-}1)$$

Where p is a function of x and t, and k is the acoustic wave number = $\omega/c = (2\pi f)/c$. We can assume a separated solution of the form:

$$p(x:t) = P(x)T(t) \qquad (5.3\text{-}2)$$

Substituting equation 5.3-2 into equation 5.3-1 and eliminating T we obtain:

$$\frac{d^2 P}{dx^2} + k^2 P = 0 \qquad (5.3\text{-}3)$$

In complex exponential form a solution to equation 5.3-3 is:

$$P = P_o e^{\pm ikx} e^{i\psi} \qquad (5.3\text{-}4)$$

Where P_o is a real constant and ψ is the phase angle. It has been shown that the real part of this solution is the only part that has physical significance. If we accept the complex exponential solution of equation 5.3-1 and also write that $T = e^{i\omega t}$ we have:

$$p(x:t) = P_o e^{(\pm ikx + i\psi + i\omega t)} \qquad (5.3\text{-}5)$$

In the equation above it can be shown that the $+ikx$ solution corresponds to a wave travelling in the negative x-direction and the $-ikx$ to a wave travelling in the positive x-direction.

Therefore:

$$p^{+} = P_o^{+} e^{i(\omega t - kx + \psi^{+})} \quad \textit{(positive travelling wave)} \qquad \textit{(5.3-6a)}$$

$$p^{-} = P_o^{-} e^{i(\omega t + kx + \psi^{-})} \quad \textit{(negative travelling wave)} \qquad \textit{(5.3-6b)}$$

Defining $\widetilde{P}_o^{\pm}$ as the $P_o^{\pm}$ factor including $e^{i\psi^{\pm}}$ the solution to the Helmholtz equation 5.3-1 is:

$$p(x:t) = \widetilde{P}_o^{+} e^{i(\omega t - kx)} + \widetilde{P}_o^{-} e^{i(\omega t + kx)} \qquad \textit{(5.3-7)}$$

Using these expressions we can now create scattering matrices for the elements used for exhaust systems.

5.3.2.2 The scattering matrix for a straight pipe

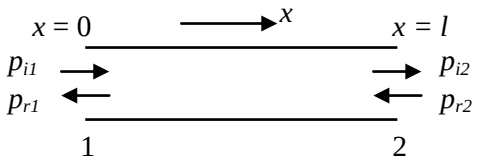

Figure 5.3-1 Straight pipe diagram with symbols

Using equations 5.3-6a and 5.3-6b to describe the incident and reflected waves for the straight pipe as shown in Figure 5.3-1 we can see that:

$$p_{i1} = p_{i2} e^{ikl} \text{ and } p_{r1} = p_{r2} e^{-ikl} \qquad \textit{(5.3-8)}$$

Expressing these equations in matrix form:

$$\begin{Bmatrix} p_{i1} \\ p_{r1} \end{Bmatrix} = \begin{bmatrix} e^{ikl} & 0 \\ 0 & e^{-ikl} \end{bmatrix} \begin{Bmatrix} p_{i2} \\ p_{r2} \end{Bmatrix} \qquad \textit{(5.3-9)}$$

The scattering matrix for the straight pipe section is therefore:

$$T_{pipe} = \begin{bmatrix} e^{ikl} & 0 \\ 0 & e^{-ikl} \end{bmatrix} \qquad \textit{(5.3-10)}$$

5.3.2.3 The scattering matrix for an abrupt area change

The derivation below accounts for an area change, which is the simplest of reactive elements. As no assumption is made for the relative sizes of areas, the model is applicable for both area expansions and contractions, even though the diagram below shows an area expansion.

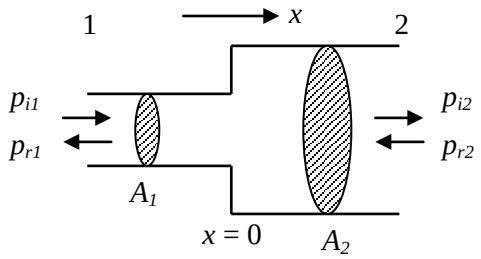

Figure 5.3-2 Area change diagram with symbols

At point x = 0 we must have continuity of sound pressure and continuity of volume velocity. For continuity of sound pressure:

$$p_{i1} + p_{r1} = p_{i2} + p_{r2} \qquad (5.3\text{-}11)$$

Using equations 5.3-6a and 5.3-6b, we have:

$$P_{i1}e^{i(\omega t - kx)} + P_{r1}e^{i(\omega t + kx)} = P_{i2}e^{i(\omega t - kx)} + P_{i2}e^{i(\omega t + kx)} \qquad (5.3\text{-}12)$$

As x = 0 the above reduces to:

$$P_{i1} + P_{r1} = P_{i2} + P_{i2} \qquad (5.3\text{-}13)$$

For continuity of volume velocity where:

$$\textit{volume velocity} = \textit{particle velocity} \times \textit{tube cross sectional area} \qquad (5.3\text{-}14)$$

Giving:

$$(u_{i1} + u_{r1})A_1 = (u_{i2} + u_{r2})A_2 \qquad (5.3\text{-}15)$$

Using a solution of the same form as for pressure:

$$(U_{i1}e^{i\omega t} + U_{r1}e^{i\omega t})A_1 = (U_{i2}e^{i\omega t} + U_{r2}e^{i\omega t})A_2 \qquad (5.3\text{-}16)$$

As:

$$U_i = \frac{P_i}{(\overline{\rho}c)} \text{ and } U_r = \frac{P_r}{(\overline{\rho}c)} \qquad (5.3\text{-}17)$$

Defining the area change as $\sigma = A_2/A_1$ equation 5.3-16 can be simplified to:

$$(P_{i1} - P_{r1}) = (P_{i2} - P_{r2})\sigma \qquad (5.3\text{-}18)$$

We now have two equations to solve being 5.3-18 and 5.3-11. Making use of the fact that x = 0 at the discontinuity we have:

$$p_{i1} + p_{r1} = p_{i2} + p_{r2} \qquad (5.3\text{-}19a)$$

$$p_{i1} - p_{r1} = (p_{i2} - p_{r2})\sigma \qquad (5.3\text{-}19b)$$

Writing these equations in matrix form:

$$\begin{Bmatrix} p_{i1} \\ p_{r1} \end{Bmatrix} = \begin{bmatrix} \frac{1+\sigma}{2} & \frac{1-\sigma}{2} \\ \frac{1-\sigma}{2} & \frac{1+\sigma}{2} \end{bmatrix} \begin{Bmatrix} p_{i2} \\ p_{r2} \end{Bmatrix} \qquad (5.3\text{-}20)$$

The scattering matrix for the abrupt area change is therefore:

$$T_{area} = \begin{bmatrix} \frac{1+\sigma}{2} & \frac{1-\sigma}{2} \\ \frac{1-\sigma}{2} & \frac{1+\sigma}{2} \end{bmatrix} \qquad (5.3\text{-}21)$$

5.3.2.4 The scattering matrix for a side branch junction

The following derivation is for the scattering matrix for a side branch junction, possibly involving an area change as shown in Figure 5.3-3. The impedance of the side branch (Z_3) is required.

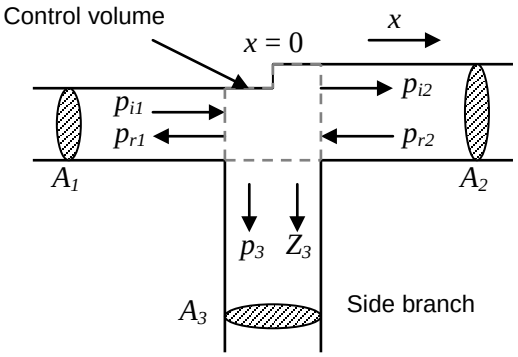

Figure 5.3-3 Side branch with area change diagram with symbols

As for the straight pipe and the area change, sound pressure and volume velocity through the control volume must be conserved. For continuity of sound pressure:

$$p_{i1} + p_{r1} = p_{i2} + p_{r2} = p_3 \qquad (5.3\text{-}22)$$

And for continuity of volume velocity:

$$A_1(u_{i1} + u_{r1}) = A_2(u_{i2} + u_{r2}) + A_3 u_3 \qquad (5.3\text{-}23)$$

Substituting in equations 5.3-6a and 5.3-6b, and making use of the fact that x = 0. Equation 5.3-23 may be expressed in terms of pressures as:

$$(p_{i1} - p_{r1}) = \left(\frac{A_2}{A_1}\right)(p_{i2} - p_{r2}) + \frac{A_3 u_3 \bar{\rho} c}{A_1} \qquad (5.3\text{-}24)$$

Again defining $\sigma = A_2/A_1$ and writing $u_3 = p_3/(A_3 Z_3)$ we obtain by combining 5.3-22 and 5.3-24:

$$p_{i1} = p_{i2}\left(\frac{1+\sigma}{2} + \frac{\bar{\rho} c}{2A_1 Z_3}\right) + p_{r2}\left(\frac{1-\sigma}{2} + \frac{\bar{\rho} c}{2A_1 Z_3}\right) \qquad (5.3\text{-}25a)$$

$$p_{r1} = p_{i2}\left(\frac{1-\sigma}{2} + \frac{\bar{\rho} c}{2A_1 Z_3}\right) + p_{r2}\left(\frac{1+\sigma}{2} - \frac{\bar{\rho} c}{2A_1 Z_3}\right) \qquad (5.3\text{-}25b)$$

Writing these equations in matrix form we have:

$$\begin{Bmatrix} p_{i1} \\ p_{r1} \end{Bmatrix} = \begin{bmatrix} \left(\frac{1+\sigma}{2} + \frac{\bar{\rho}c}{2A_1Z_3}\right) & \left(\frac{1-\sigma}{2} + \frac{\bar{\rho}c}{2A_1Z_3}\right) \\ \left(\frac{1-\sigma}{2} - \frac{\bar{\rho}c}{2A_1Z_3}\right) & \left(\frac{1+\sigma}{2} + \frac{\bar{\rho}c}{2A_1Z_3}\right) \end{bmatrix} \begin{Bmatrix} p_{i2} \\ p_{r2} \end{Bmatrix} \qquad (5.3\text{-}26)$$

The scattering matrix for a side branch possibly involving and area change is therefore:

$$T_{branch} = \begin{bmatrix} \left(\frac{1+\sigma}{2} + \frac{\bar{\rho}c}{2A_1Z_3}\right) & \left(\frac{1-\sigma}{2} + \frac{\bar{\rho}c}{2A_1Z_3}\right) \\ \left(\frac{1-\sigma}{2} - \frac{\bar{\rho}c}{2A_1Z_3}\right) & \left(\frac{1+\sigma}{2} + \frac{\bar{\rho}c}{2A_1Z_3}\right) \end{bmatrix} \qquad (5.3\text{-}27)$$

5.3.2.5 Impedance of side branch elements

Shown below are the impedances for side branch elements for use with equation 5.3-27. Expressions are only shown for side branch elements as used in the exhaust systems tested.

For a Helmholtz resonator:

$$Z_{helm} = i\bar{\rho}\left(\frac{\omega L}{A_{neck}} - \frac{c^2}{\omega V}\right) \qquad (5.3\text{-}28)$$

The resonant frequency is at:

$$f_{res} = \frac{c}{2\pi}\sqrt{\frac{A_{neck}}{L_{eff}V}} \qquad (5.3\text{-}29)$$

For a quarter wave resonator:

$$Z_{qtr} = -i\frac{\bar{\rho}c}{A_{branch}}\cot kL \qquad (5.3\text{-}30)$$

5.3.3 Modelling procedure using scattering matrices

This section will present the modelling procedure used to calculate the insertion loss (*IL*) for a typical exhaust system used in this work. The system to be analysed is shown in Figure 5.3-4 below.

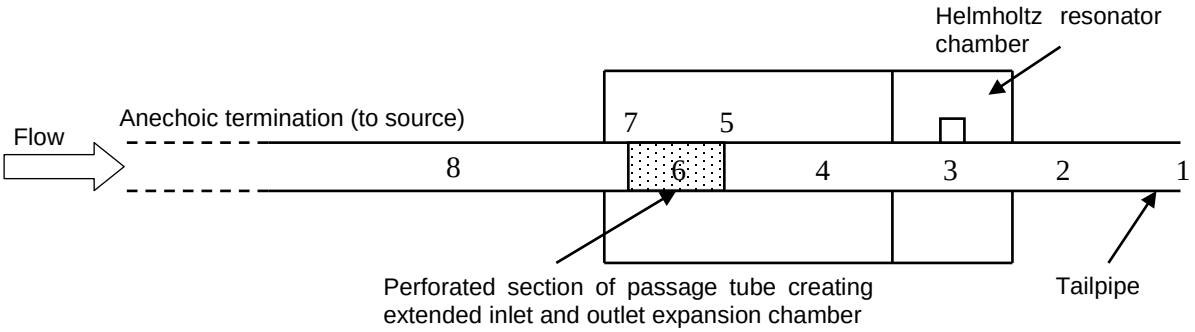

Figure 5.3-4 Muffler system to be analysed

The muffler system above consists of an inlet pipe to a muffler with two separate chambers and a tail pipe that terminates to the open environment. Entry to the first chamber is through a perforated section of the main pipe which will be assumed to be acoustically transparent. This assumption is considered valid area over frequency range considered for perforates with greater than 20% open. The second chamber has a tuned tube as entry to an enclosed volume creating a Helmholtz resonator. Each element in the system will be represented with a scattering matrix and these will be combined to form an expression for the entire system. From this the insertion loss of the system can be calculated assuming the source is anechoic.

We will first assume an outlet signal of:

$$p_{i1} = 1 + i0 \qquad (5.3\text{-}31)$$

Using equations developed by Levine and Schwinger [8] and simplified by Davies [2] the component of the assumed outlet signal that is reflected back towards the source by the tail pipe termination can be found. The proportion of sound reflected by the tailpipe termination is proportional to the diameter of the exhaust outlet and frequency of interest is given by:

$$\frac{P^-}{P^+} = -Re^{i2k\delta} \qquad (5.3\text{-}32)$$

Where R is the reflection coefficient, for Helmholtz number (ka) less than 1.5:

$$R = 1 + 0.01336ka - 0.59079(ka)^2 + 0.33576(ka)^3 - 0.06432(ka)^4 \qquad (5.3\text{-}33)$$

And δ is the mass end correction defined piecewise:

$$\delta = 0.6133a - 0.1168a(ka)^2 \quad , \quad ka < 0.5 \qquad (5.3\text{-}34a)$$

$$\delta = 0.6393a - 0.1104a(ka) \quad , \quad 0.5 \leq ka < 1.5 \qquad (5.3\text{-}34b)$$

Using these equations the component of the incident wave to the tailpipe that is reflected is:

$$p_{r5} = -Re^{i2k\delta} \qquad (5.3\text{-}35)$$

We now have the incident and reflected sound waves in the system at point 1. Using the scattering matrices as presented in previous sections for each muffler element we can modify the outlet signal working back towards the source. This gives the following expression for the inlet signal:

$$\begin{pmatrix} p_{i8} \\ p_{r8} \end{pmatrix} = T^8_{inletpipe} T^7_{branch(1/4wave)} T^6_{chamber} T^5_{branch(1/4wave)} T^4_{pipe} T^3_{branch(Helmholtz)} T^2_{tailpipe} \begin{pmatrix} p_{i1} \\ p_{r1} \end{pmatrix} \qquad (5.3\text{-}36)$$

The insertion loss of the muffler system can be calculated by dividing the sound power radiated from the system without a muffler present with that radiated from the system with the mufflers in place as shown below:

$$IL = 10\log\left[\frac{W^{unmuffled}_{rad}}{W^{silenced}_{rad}}\right] \qquad (5.3\text{-}37)$$

With no silencer:

$$W^{unmuffled}_{rad} = C \times \left|p_{i8}\right|^2 \text{ (C = constant)} \qquad (5.3\text{-}38)$$

With silencer:

$$W^{silenced}_{rad} = C \times \left|p_{i1}\right|^2 \qquad (5.3\text{-}39)$$

As we have assumed $p_{i1} = 1 + i0$ the insertion loss can be expressed as:

$$IL = 10\log[|p_{i8}|^2] \qquad (5.3\text{-}40)$$

As the end corrections and scattering matrices are dependant on $\omega = 2\pi f$, the insertion loss must be calculated for each frequency of interest. Due to this, and the matrix algebra involving complex numbers, the calculations were initially performed using MATLAB. Later the model was transferred to a spreadsheet for ease of use. A typical insertion loss curve for a muffler as per the one shown in Figure 5.3-4 is shown in Figure 5.3-5 below.

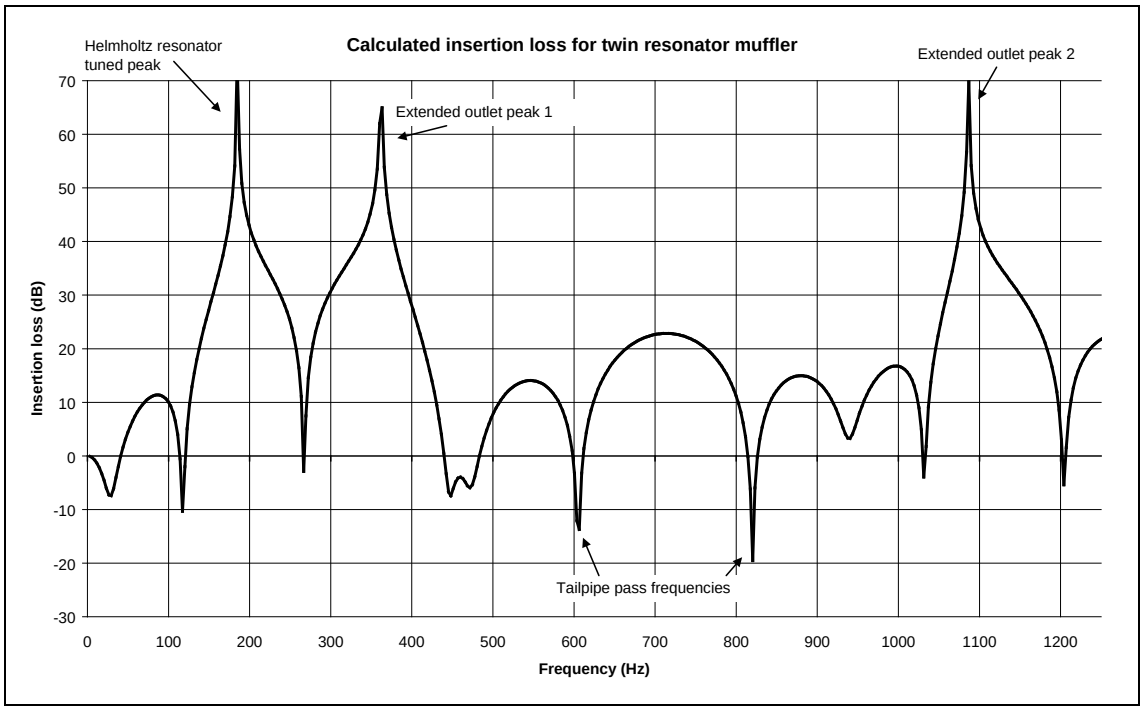

Figure 5.3-5 Example of calculated insertion loss for example muffler system

5.4 Graphical user interface

Due to the large amount of data gathered for each muffler system, and the large number of mufflers tested, a program '*exhaustperformance*' and an associated graphical user interface (GUI) were created to facilitate data assessment and analysis. Data collected was downloaded as a text file and then imported into a spreadsheet that ordered the data into matrices. The spreadsheet created plots of sound pressure level vs. frequency for each engine speed showing the three load cases. The matrices of data were then be exported into a script file and used with the '*exhaustperformance*' program.

The '*exhaustperformance*' GUI is shown in Figure 5.4-1 below.

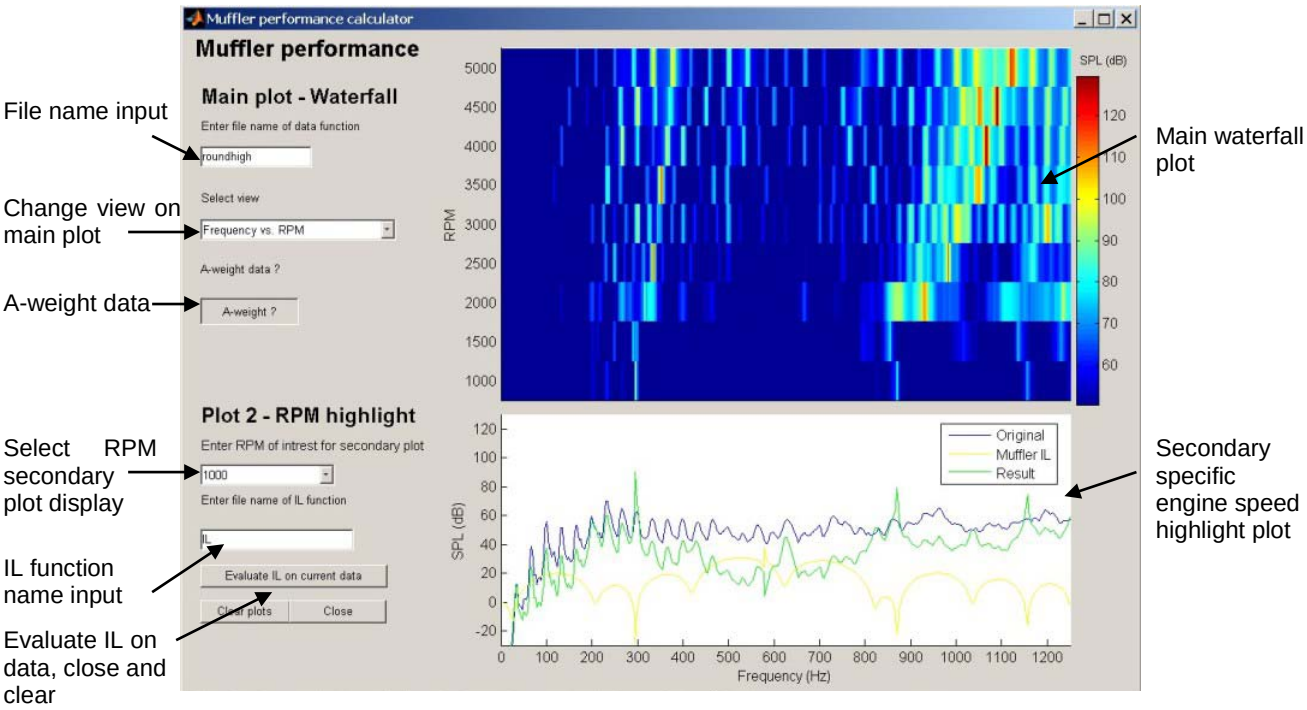

Figure 5.4-1 Screen shot of graphical user interface showing plots generated

Filenames for the measured spectrum and muffler system predictions are entered into the fields on the left. Using the 'select view' tab five different views can be selected for the main plot to display the measured data. The 'select RPM' tab plots data corresponding to a specific engine speed on the secondary frequency vs. sound pressure level plot. The 'evaluate IL on current data' button evaluates the effect of the muffler system of interest on the current data. The resultant muffled spectrum will be shown in the main window and both the resultant and the original data will be shown on the secondary plot. Selection of the 'A-weight' button evaluates the A-weighting scheme on the data and displays the result on both the main and secondary plots. The A-weighting will be removed if button is toggled off. The '*exhaustperformance*' program and GUI proved to be a useful tool to create waterfall plots and evaluate and compare the performance of different muffler systems on measured data.

5.5 References

[1] D. D. J. Davis, G. M. Stokes, D. Moore, and G. L. J. Stevens, "Theoretical and Experimental Investigation of Mufflers: with Comments on Engine-Exhaust muffler Design," U.S National Advisory Committee for Aeronautics Langley Aeronautical Laboratory, Report 1192, 1954.

[2] P. O. A. L. Davies, "Practical Flow Duct Acoustics," *Journal of Sound and Vibration*, vol. 124, pp. 91-115, 1988.

[3] D. D. J. Davis and G. M. Stokes, "The Attenuation Characteristics of Four Specifically Designed Mufflers Tested on a Practical Engine Setup," NACA, Technical Note 2943, 1953.

[4] P. O. A. L. Davies, "Piston Engine Intake and Exhaust System Design," *Journal of Sound and Vibration*, vol. 190, pp. 677-712, 1996.

[5] M. L. Munjal, "Acoustic Characterization of an Engine Exhaust Source - A Review," presented at ACOUSTICS 2004, Gold Coast, Australia, 2004.

[6] P. O. A. L. Davies, "The Observed Aeroacoustic Behaviour of Some Flow-Excited Expansion Chambers," *Journal of Sound and Vibration*, vol. 239, pp. 695-708, 2001.

[7] P. O. A. L. Davies and M. F. Harrison, "Predictive Acoustic Modelling Applied to the Control of Intake/Exhaust Noise of Internal Combustion Engines," *Journal of Sound and Vibration*, vol. 202, pp. 249-274, 1997.

[8] H. Levine and J. Schwinger, "On the radiation of sound from an unflanged circular pipe," *Physics Review*, vol. 73, pp. 373, 1948.

Chapter 6
Project Findings and Analysis

Summary

Comparing experimental results to predictions gives insight into the accuracy of the predictions, the validity of experimental results, and the performance of the muffler systems themselves. Insertion loss measured with the engine as the source of excitation for single chamber, base case mufflers, at low engine speeds and loads showed good agreement with predicted insertion loss. The major deviation from predicted performance was at points where muffler impedance tended asymptotically towards peak or pass frequencies. Increasing engine speed and load reduced the performance of the muffler most likely due to increases in viscous damping. This behaviour was not accounted for in the model and resulted in a reduction of accuracy of the predictions.

Insertion loss measured using the speaker as the source of excitation gave closer agreement to that predicted as temperature, pressure and flow effects were not present as with the engine. At higher frequencies (above 500 Hz) standing waves between the speaker and the muffler were observed, reducing the accuracy of the prediction. This phenomenon was a result of the speaker test arrangement and was not observed with the engine as the source of excitation. An alternative speaker test arrangement was proposed that will most likely yield results closer to those predicted and measured with the engine as the source of excitation.

A number of mufflers with varying internal geometry and secondary Helmholtz chambers (in various configurations) were tested. With the engine as the source of excitation the addition of the secondary Helmholtz chamber had no measurable effect on muffler performance in all but one case. This was attributed to the extremely high sound pressure levels and high flow speeds created by the engine. With the speaker as the source of excitation the performance of Helmholtz resonators with varying connection tube geometry and connection to the main chamber were assessed. Helmholtz resonators with large punched hole connection tubes, arranged in series with the main chamber, had the best performance that was accurately predicted by the model.

Table of Contents

List of Figures

6.1 Introduction

This chapter compares the results obtained using the experimental arrangement and methods presented in Chapters 3 and 4 to predicted results obtained using the modelling procedures presented in Chapter 5. Results are as presented in Chapter 4 with the data smoothed for clarity using a 15 point moving average, the smoothed data indicated by a thicker line. Details of mufflers referred to throughout this chapter are shown in Appendix A. Predicted and measured results for all muffler systems tested are shown in Appendix B.

Comparisons are made between different muffler systems to investigate the effect of mid-pipe length, chamber curvature, and tuned resonators on muffler performance. Experimentally derived insertion loss using either the engine or the speaker as the source of excitation is compared to predicted insertion loss for a number of muffler systems. The differences between predicted and experimental results due to temperature, flow and load effects are discussed.

6.2 Accuracy of modelling

6.2.1 Introduction

Comparing experimentally derived results with predicted results offers insight into both the validity of the model and the repeatability and accuracy of experimental tests. As described in previous chapters, the insertion loss of the muffler systems was measured using either the engine or the speaker as the source of excitation. The accuracy of the model and how muffler performance changes with engine conditions are discussed in the following section. Throughout this section single chamber mufflers will be used as examples, with the performance of specific resonator components discussed in subsequent sections.

6.2.2 Comparison to engine data

6.2.2.1 Base case

Figure 6.2-1 shows the predicted and measured insertion loss for the R2001 base case muffler, with the engine as the source of excitation at 1000 RPM. The three load cases are shown, smoothed for clarity, using the 15 point average smoothing technique.

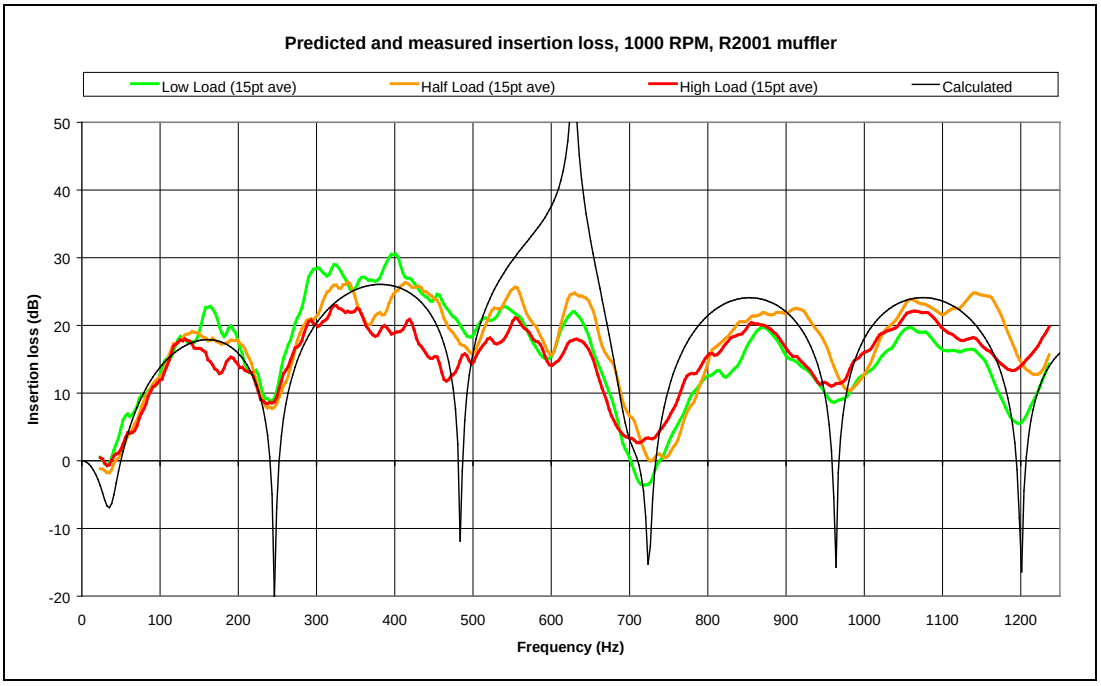

Figure 6.2-1 Predicted and measured insertion loss for base case muffler

The predicted and measured insertion loss agrees well over the range of interest. The most noticeable deviation being that the tuned quarter wave peak and tailpipe pass frequencies are reduced. The modelled peaks and passes ideally tend asymptotically towards the maxima or minima frequency. The 15 point average smoothing scheme used to process the data also smoothes over the peaks and troughs, somewhat but this effect is minimal (see Figure 4.4-5). The primary reason that the peak and pass frequencies are not realised in practice is due to viscous damping. Viscous damping within the system restricts the peak and pass, maxima and minima, as the dissipation of energy prevents resonances from increasing unbounded. Of note is that the addition of the muffler, in particular the perforated section within the muffler, will provide further viscous attenuation. This behaviour is not predicted by the model and leads to the deviations seen in Figure 6.2-1 above. At higher frequencies, the accuracy of the prediction is further reduced due to flow noise.

6.2.2.2 Effect of engine load and speed

Figures 6.2-2 and 6.2-3 show the predicted and measured insertion loss for the R1002 muffler with the engine as the source of excitation at 1000 and 5000 RPM respectively. The three load cases are shown, with the data smoothed for clarity.

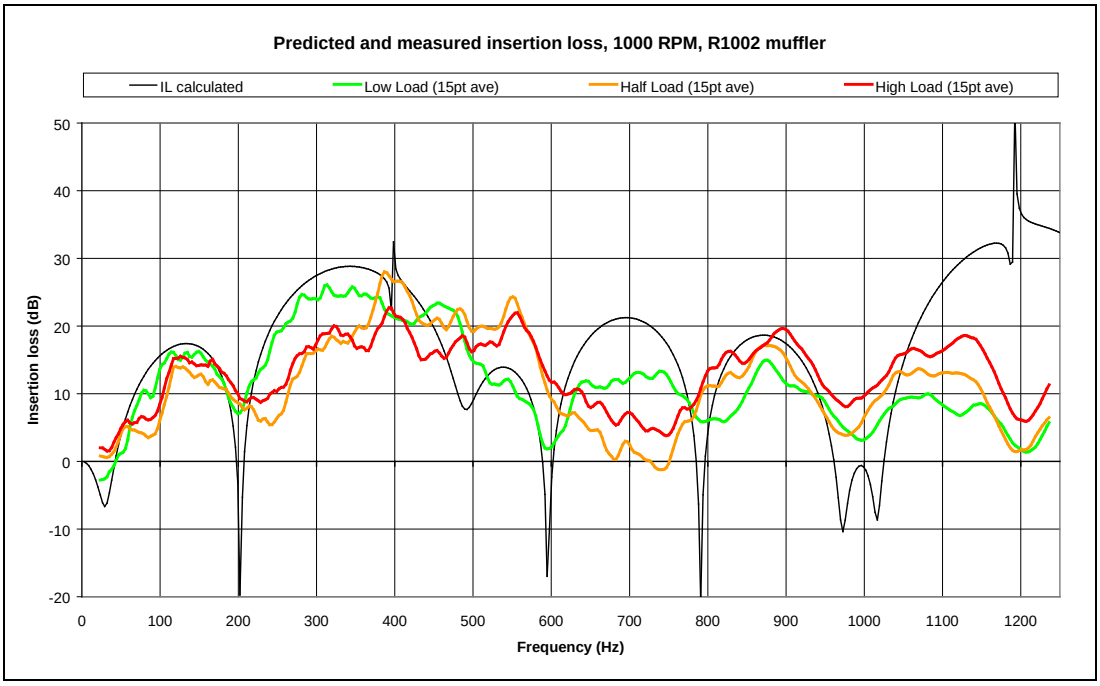

Figure 6.2-2 Predicted and measured insertion loss, 1000 RPM, R1002 muffler

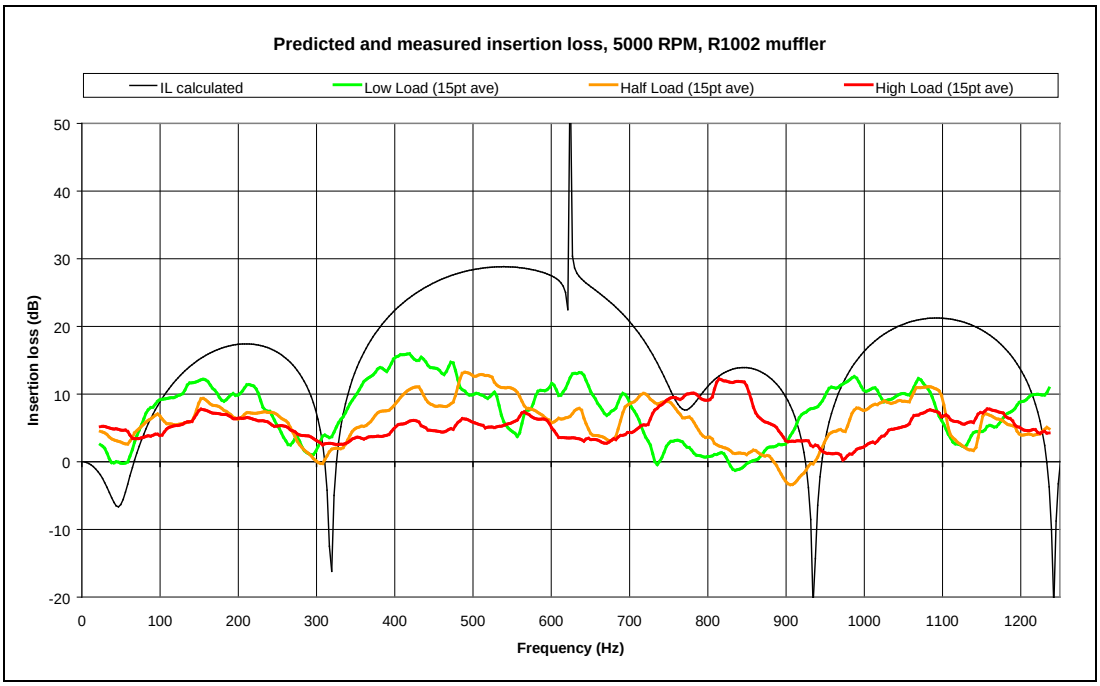

Figure 6.2-3 Predicted and measured insertion loss, 5000 RPM, R1002 muffler

The R1002 muffler is a single expansion chamber muffler, of circular cross section, with extended inlet and outlet. Entry to the expansion chamber is through a perforated section of the passage tube. The perforate consisted of a total of 608, 3 mm holes arranged in 32 rows, giving an open area of 29 percent. Comparing the measured and predicted insertion loss shown in Figures 6.2-2 and 6.2-3, a number of observations can be made about the effects of engine load and speed on the accuracy of the model and the performance of the muffler. As for the base case shown in Figure 6.2-1, the predicted peak and pass maxima and minima are not fully realised due to viscous damping for both the 1000 and 5000 RPM cases.

At 1000 RPM, correlation between predicted and measured insertion loss is good across the frequency range of interest for the three load cases. This suggests that the assumptions made in modelling the exhaust system and experimental uncertainties are acceptable.

At 5000 RPM there is larger variation between measured and predicted insertion loss, and differences between the three load cases. The measured insertion loss follows the general trend of the predicted insertion loss, exhibiting reduced minima at the tailpipe pass frequencies and reduced maxima, which are reduced further with increasing load. At higher frequencies, the measured insertion loss becomes more random as flow noise becomes significant.

As engine speed and load are increased, flow through the exhaust system increases. A grazing flow boundary condition occurs on the perforate causing the orifice resistance to increase significantly [1, 2]. An increase in orifice resistance leads to a decrease in insertion loss as less acoustic energy is transferred through the perforate to the expansion chamber. An increase in flow will also increase viscous damping, further reducing insertion loss at attenuation peaks. These effects were not included in the modelling and in part lead to the differences between the 1000 and 5000 RPM cases.

Comparing the low, half and high load cases in Figure 6.2-3 shows a decrease in muffler performance with increasing load. As load is increased, both the size of the pressure pulse and the flow velocity through the exhaust system will increase. Increasing flow will reduce muffler performance as previously described. Furthermore, a change in load will change the size and shape of the pressure pulse travelling down the system, leading to a change in muffler performance. Figure 6.3-4 shows the pressure pulse measured at entry to the muffler, at 3000 RPM, for the three load cases.

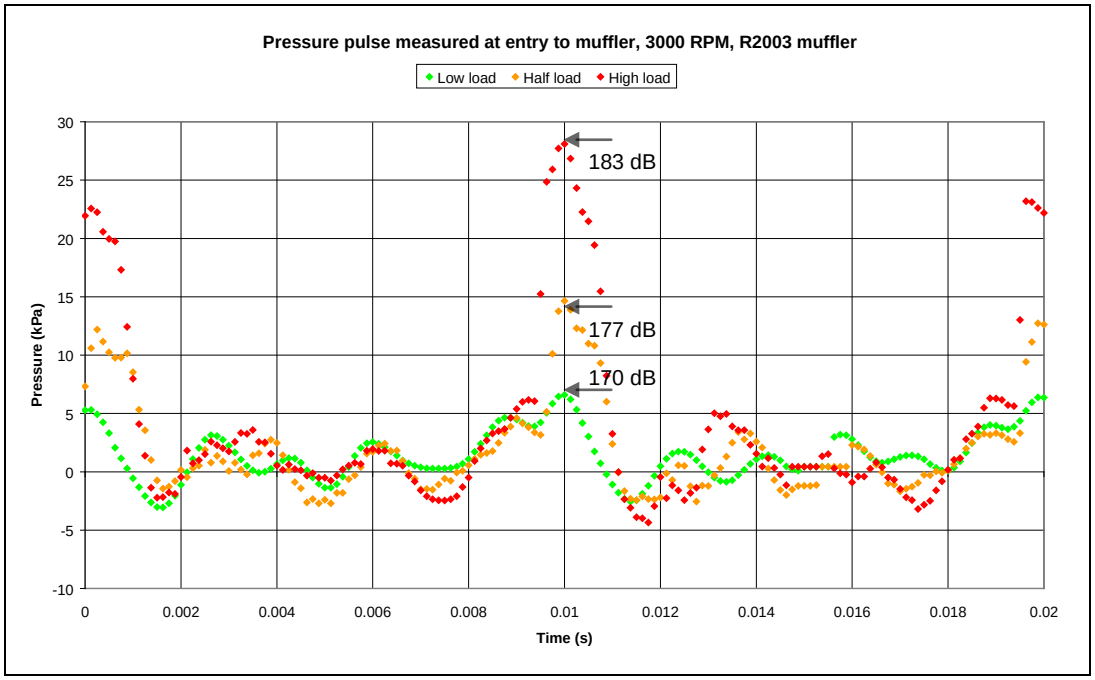

Figure 6.2-4 Pressure pulse measured at entry to muffler, 3000 RPM, R2003 muffler

At lower sound pressure levels, the perforate will act as acoustically transparent, having a very low resistance. As the model assumes the perforate to be perfectly acoustically transparent, at low sound pressure levels, agreement between predicted and measured results is good. As load is increased, the size of the pressure pulse increases, creating a higher pressure differential between each side of the perforate. As the pressure differential is increased, flow separation occurs as the pressure wave passes through the perforate resulting in the generation of vortices [2]. The generation of vortices results in energy loss as the pressure wave passes through the perforate. This increases the resistance of the perforate and reduces the reactive quality of the muffler. The resistance of perforates has been shown to increase nonlinearly, dependant on the local sound pressure level [1]. To model the pressure and flow effects shown in this section a more complex model than the one used in this study would be required.

6.2.3 Comparison to speaker data

Figure 6.2-5 below shows the predicted and measured insertion loss with the speaker as the source of excitation for the R1002 muffler.

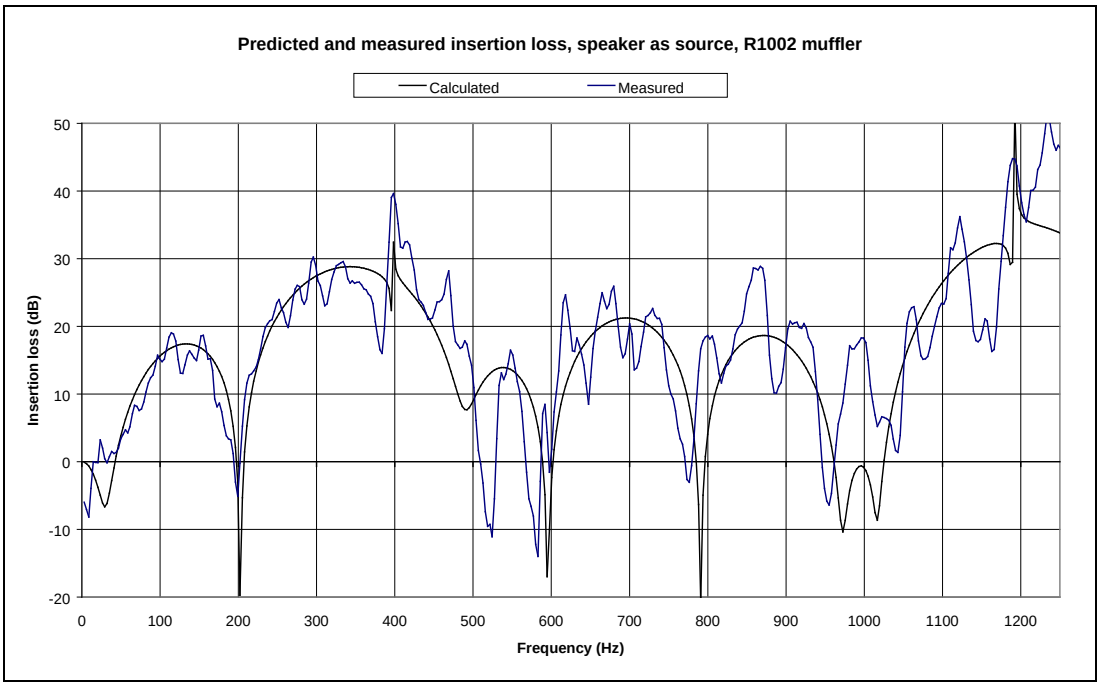

Figure 6.2-5 Predicted and measured insertion loss, speaker, R1002 muffler

Agreement between predicted and measured insertion loss is good for frequencies below 500 Hz with increasing deviation at higher frequencies. Variation between the predicted and measured results may be in part due to the behaviour of the perforated section of the muffler. However, these effects are unlikely to be significant at the comparatively low sound pressure levels generated by the speaker.

As the model assumes one dimensional wave propagation, a possible source of variation is two or three dimensional wave propagation within the muffler. As the frequencies of interest are below the cut-off frequency of the muffler, higher order modes are not of concern. The model assumes an instantaneous expansion or contraction at area discontinuities which will not occur in practice. This is investigated further in section 6.3.

The primary reason the experimental data varies from that predicted is attributed to the assumption that the source is anechoic and independent of the acoustic load. As the speaker is mounted directly on the end of the exhaust system it may act like a reflective termination, dependant on the acoustic load and the frequency of interest. Reflections from the source will result in standing waves being set up between the speaker and muffler.

Figure 6.2-6 below shows the muffler system modelled with a fully reflective source. The reflective source results in a number of pass frequencies in the insertion loss curve due to resonances within the inlet tube to the muffler. At frequencies above 500 Hz, the predicted pass frequencies relating to the inlet pipe resonances correlate well to the experimental data, indicating that the source is reflective at these frequencies.

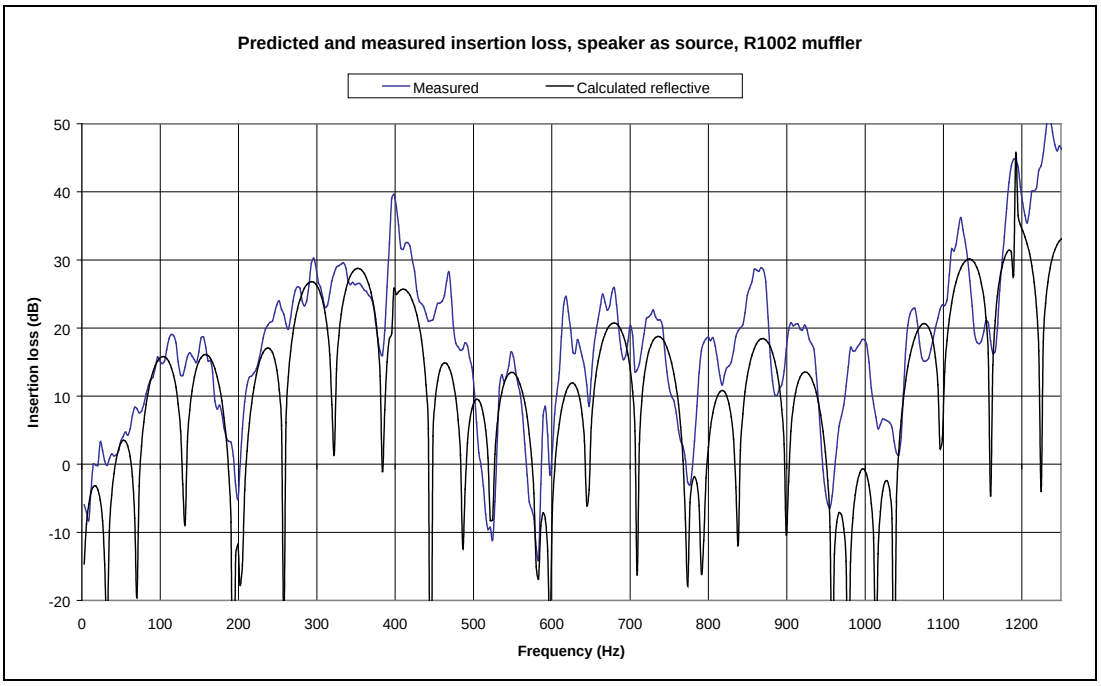

Figure 6.2-6 Predicted with reflective source and measured insertion loss, speaker, R1002 muffler

This same phenomenon is not exhibited with the engine as the source. This indicates that the engine is acting closer to an anechoic source as assumed in the model. This is most likely due to viscous dissipation of acoustic energy as the reflected sound from the muffler travels back towards the valves and is split up by the 4-2-1 exhaust manifold and between the eight exhaust ports.

An improvement to the speaker test arrangement would be to mount the speaker as a branch element and use an anechoic termination at the source end, as shown in the diagram below. This would almost certainly result in better agreement between insertion loss measured with the speaker, and that predicted and measured with the engine.

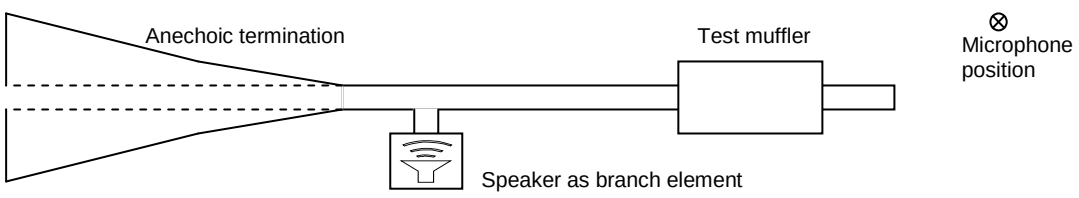

Figure 6.2-7 Possible alternative speaker test arrangement

6.2.4 Multiple mufflers

To assess the performance of the model with a larger number of reactive elements, testing was performed with an intermediate and rear muffler. Figure 6.2-8 shows the predicted and measured insertion loss for the R1002 muffler in series with the R1021 intermediate muffler.

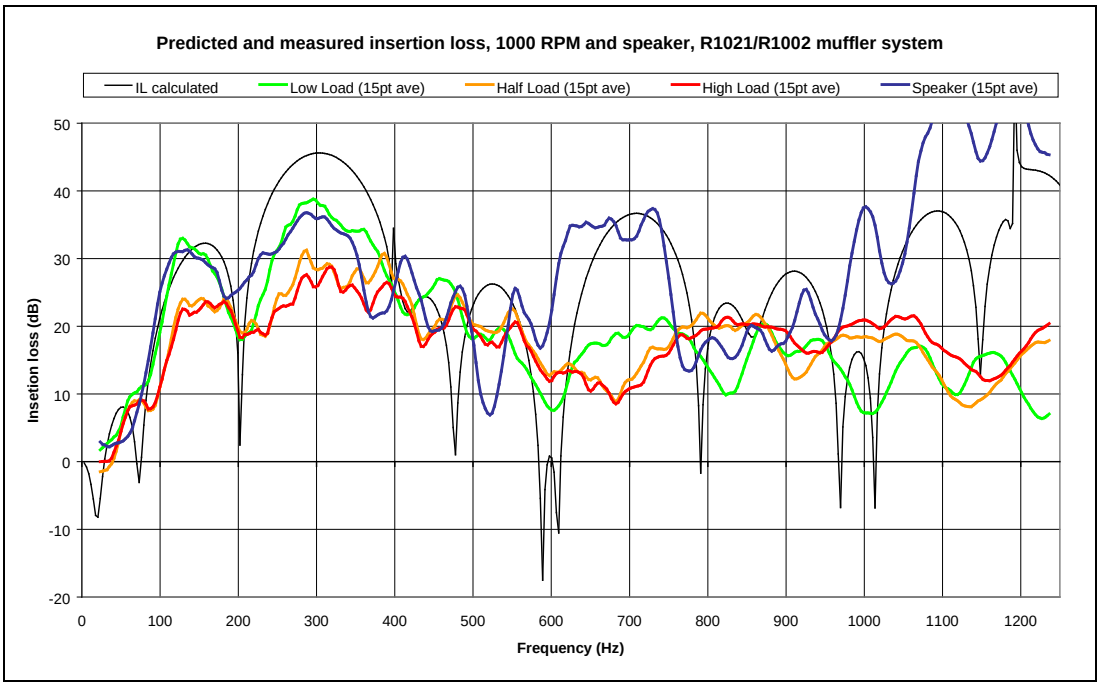

Figure 6.2-8 Predicted and measured insertion loss for twin muffler system

Agreement between predicted and measured insertion loss for the twin muffler system is not as good as for the single resonator system. The insertion loss measured with the speaker as the source of excitation exhibits pass frequencies above 500 Hz relating to standing waves in the inlet tube, as per in the previous section. When flow noise generated downstream of the muffler or at exit from the system becomes the dominant source of noise, the maximum level of insertion loss that can be achieved will be restricted. This phenomenon can be seen in Figure 6.2-8 where above 700 Hz the measured insertion loss with the engine as the source becomes very flat with the maxima levels clipped.

The measured insertion loss peak at approximately 300 Hz is lower than that predicted with both the speaker and the engine as the source of excitation. The measured insertion loss across the frequency range of interest is lower than that predicted suggesting that this trend is not related to flow or high sound pressure effects. This deviation is most likely caused by the assumption that the perforated section of the muffler is fully acoustically transparent. As the perforate has some resistance this will lower the insertion loss maxima due to a reduction in transmission to and from the muffler chambers. In addition to this, as with resonators previously presented, the peak and pass frequencies will not be realised due to viscous damping.

6.3 Performance of quarter wave resonators

This section focuses on the performance of expansion chamber mufflers with extended inlet and outlet quarter wave resonators. A number of resonators were tested to observe the effect of changing the length of the outlet extended tube quarter wave resonator. Other studies [3] have shown that tuning the quarter wave resonator to the pass frequencies of the expansion chamber provides an improvement in the overall insertion loss of the muffler. The predicted and measured insertion loss with the engine as the source of excitation for the R2002 muffler (tuned to the second expansion chamber pass frequency) and the R2001 muffler (tuned to the third attenuation peak of the expansion chamber) are shown in Figure 6.3-1 below.

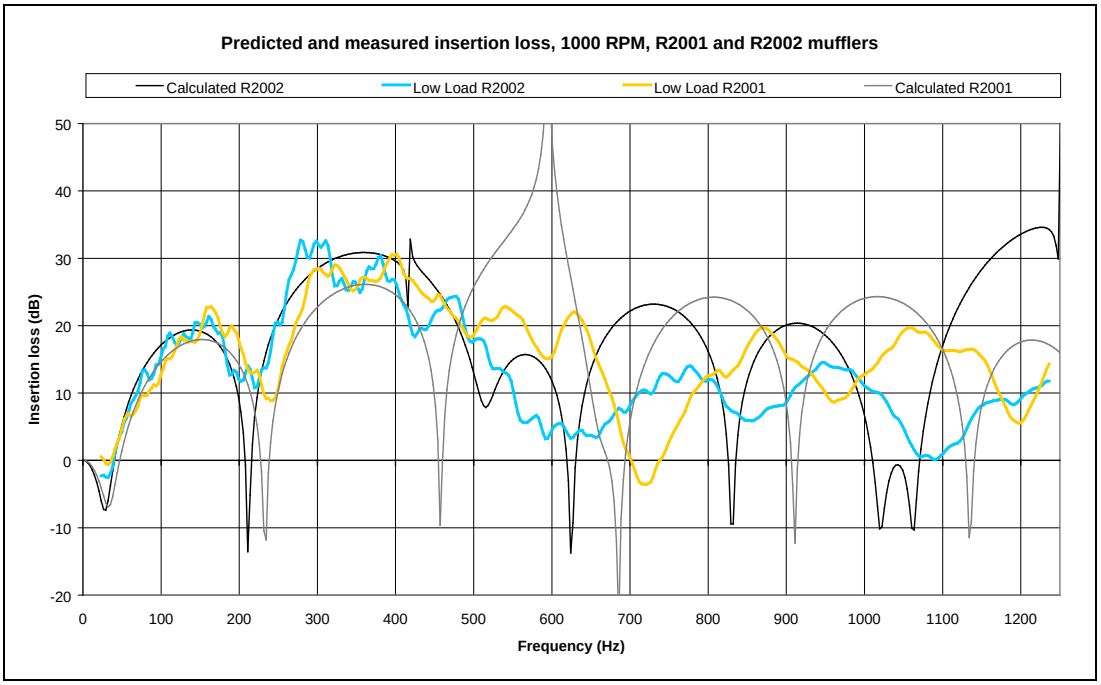

Figure 6.3-1 Comparison quarter wave resonator performance

As for mufflers previously presented, the peak and pass maxima and minima are not fully realised for both mufflers shown in above due to viscous damping. The performance of the outlet extend tube resonator at approximately 600 Hz for the R2001 muffler is very poor compared to that of the R2002 muffler at approximately 425 Hz. Overall, the performance of the R2001 muffler is better than that of the R2002 muffler. This is primarily due to the predicted pass frequency at approximately 450 Hz for the R2001 muffler that is not realised in practice and the reduction in performance of the R2002 muffler between 500 and 700 Hz. This result is contradictory to the hypothesis that the R2002 muffler would have the best performance.

Figure 6.3-2 shows the insertion loss measured using the speaker as the source of excitation for the R2001 and R2002 mufflers. It is worth noting that the predicted insertion loss curve is different to that shown in Figure 6.3-1 due to the difference in temperature between the engine and speaker tests as further discussed in section 6.5.2.

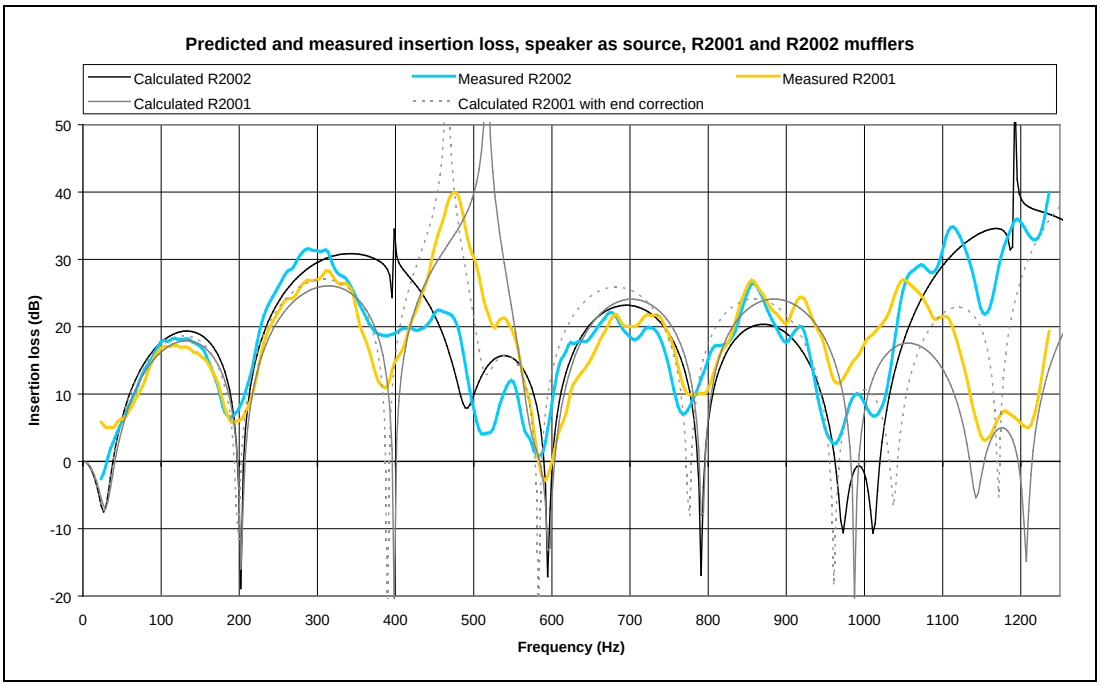

Figure 6.3-2 Comparison of quarter wave resonator performance, speaker as the source

As there is no flow through the muffler with the speaker as the source of noise, the measured results show better agreement to the predictions, with higher insertion loss evident at tuned frequencies. For the R2002 muffler the second chamber pass frequency at 400 Hz is eliminated by tuning of the quarter wave resonator. The resonant frequency at approximately 520 Hz for the quarter wave resonator of the R2001 is slightly over predicted. This is most likely due to the plane wave approximation used in the model. This approximation assumes an instantaneous expansion at area discontinuities which in practice will not occur. Davies [4] used an end correction to account for non-instantaneous expansions and contractions. This was incorporated into the model and is shown for the R2001 muffler in the above figure by the grey dashed line. The incorporation of the end correction improves the accuracy of the prediction at the tuned frequency.

Overall the hypothesis that tuning to the chamber pass frequency would result in improved muffler performance was neither proved nor disproved. The prediction with the incorporation of an end correction agreed well with the measured data, with the speaker as the source. With the engine as the source, the level of attenuation is over predicted. Further development of the model is required to fully incorporate these effects by including viscous damping.

6.4 Performance of Helmholtz resonators

6.4.1 Introduction

A number of Helmholtz resonators were constructed and tested with varying connecting tube geometry and connector positions. Cummings [2] stated that the effective stiffness of the volume is insensitive to flow and pressure effects. Taking this into consideration, all resonators were tuned by varying chamber volume to eliminate a problem noise component at 333 Hz corresponding to a second order firing harmonic at 5000 RPM, high load. Each Helmholtz resonator chamber was incorporated into the base case mufflers, either connected in series or in parallel to the main chamber. Figure 6.4-1 below shows the basic layout of mufflers tested. The Helmholtz chamber is shown shaded in grey with the series and parallel connector positions indicated by solid and dashed lines respectively.

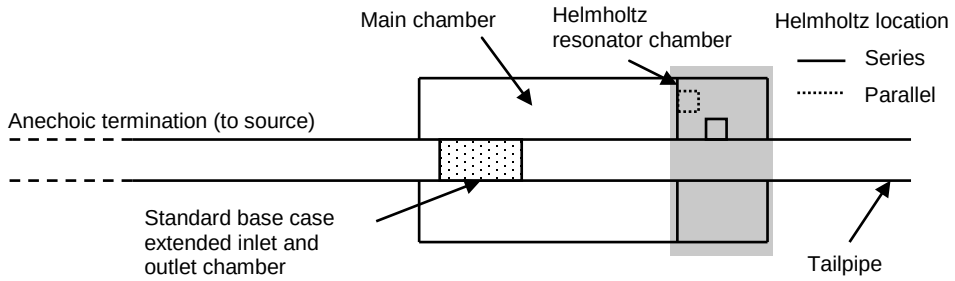

Figure 6.4-1 Layout of muffler showing Helmholtz resonator positions

6.4.2 General performance

Figures 6.4-2 and 6.4-3 show the predicted and measured insertion loss with the engine and the speaker as the source of excitation, for the R1001 and R1003 mufflers. The R1001 and R1003 mufflers have identical main chambers however the R1003 muffler also contains a Helmholtz resonator connected in series. As the Helmholtz chamber was placed on the outlet end of the muffler, the effective tailpipe length is reduced, increasing the distance between the tailpipe pass frequencies and shifting them to higher frequencies.

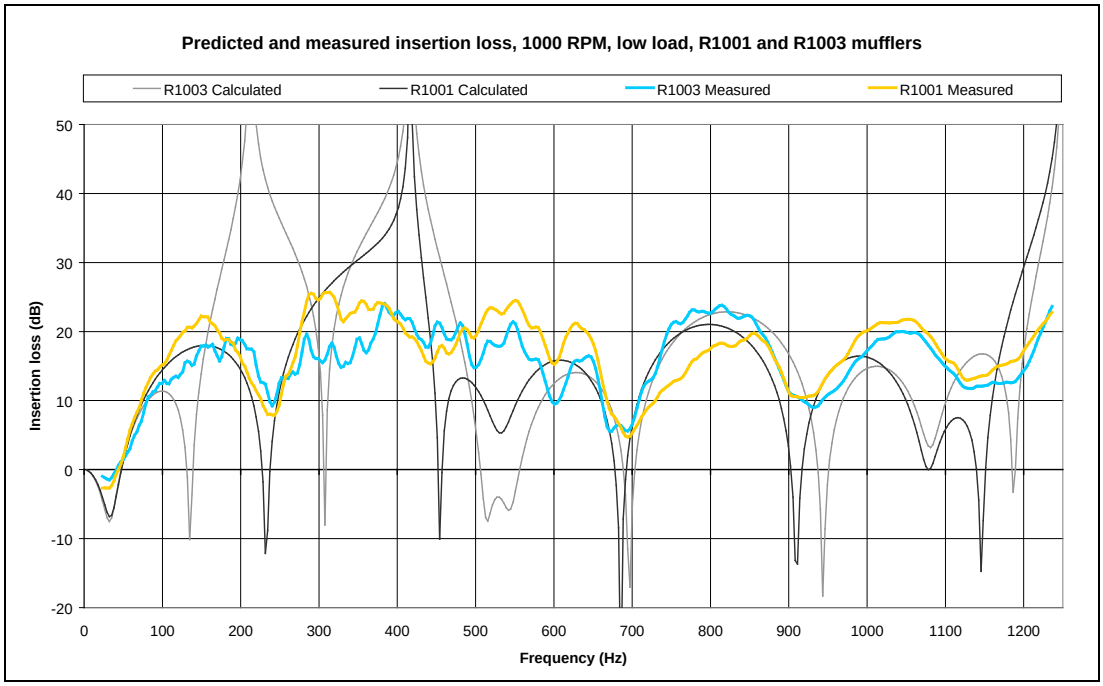

Figure 6.4-2 General performance of Helmholtz resonator, engine as source of excitation

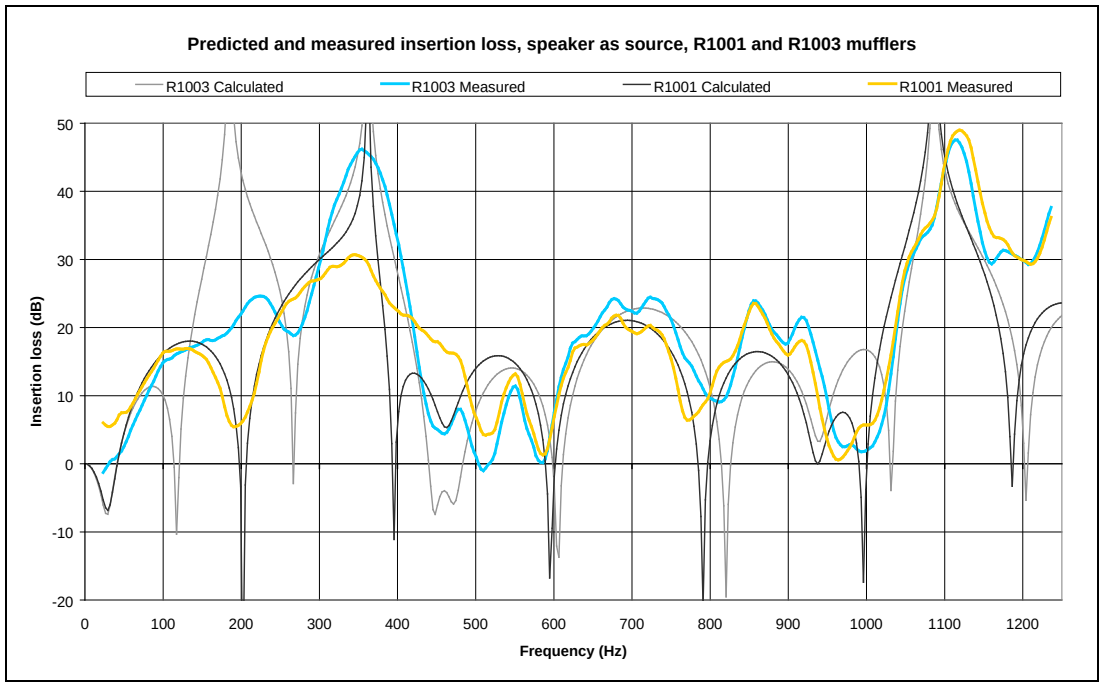

Figure 6.4-3 General performance of Helmholtz resonator, speaker as source of excitation

Comparing the predicted and measured insertion loss for each of the two mufflers with the speaker and the engine as the source of excitation shows substantial variation between the two cases. As with the results presented thus far the speaker data is closer to that predicted with the peak and pass, maxima and minima reduced with the engine as the source of excitation.

A peak in the insertion loss curve of the R1003 muffler related to the resonant frequency of the Helmholtz resonator is predicted at 215 Hz. This corresponds to the 333 Hz target frequency at the low load, 1000 RPM muffler temperature. Comparing the predicted and measured insertion loss shown in Figures 6.4-2 and 6.4-3 shows substantial variation at the resonant frequency of the Helmholtz chamber, as well as variation between results obtained with the speaker and with the engine.

With the engine as the source of excitation the measured insertion loss for the R1003 muffler shows no Helmholtz resonant peak as predicted. Comparing the measured insertion loss of the R1003 muffler to that of the R1001 muffler shows little variation between the two cases. This indicates that the addition of the Helmholtz chamber had no effect on the muffler performance. With the speaker as the source of excitation, the Helmholtz resonant peak predicted at 215 Hz is present. This improves the overall performance of the muffler by eliminating the pass frequency at 200 Hz.

The trends illustrated for the R1003 muffler are consistent throughout the testing of mufflers with Helmholtz resonators (see Appendix B). The only deviation from this trend was muffler R1011 that showed an improvement over the base case muffler, at the tuned frequency of the Helmholtz resonator, with the engine as the source of excitation. As with the quarter wave resonators the reduction in performance of the Helmholtz resonators with the engine as the source was most likely due to flow and pressure effects.

Davis et al. [5] stated that if the connection tube was too small, the required flow into and out of the chamber could not be achieved. This is analogous to the size of a mass spring system and the force that this system can impart at resonance. If the system cannot impart enough force (in this case sound pressure) it will be unable to counteract the input force. The model assumes that viscosity in the system is zero, simplifying the analysis. Viscous damping limits the speed that the effective mass can oscillate, thus reducing the attenuation at high sound pressures.

Sindhupak et al. [6] showed that in the presence of flow, the attenuation of a Helmholtz resonator will be reduced and the resonant peak moved to a higher frequency. The performance of the resonator is reduced in the presence of flow as increased damping caused by the flow limits the amplitude to which the effective mass can oscillate. As the mass oscillates in the presence of flow, a portion of the mass is lost with the flow into the main pipe. This causes a reduction in effective mass and results in an increase in the resonant frequency of the muffler. El-Rahman et al. [1] presented a study on the non-linear behaviour of Helmholtz resonators at high sound pressures. The study proposed reducing the end correction for the effective mass from 0.8 to 0.4 to account for this behaviour. At extremely high sound pressures the end correction depends on the instantaneous hole velocity and is therefore variant with position and time.

6.4.3 Effect of connecting tube geometry

6.4.3.1 Introduction

As the performance of mufflers containing Helmholtz resonators measured with the engine as the source of excitation is indistinguishable from that of nominally identical mufflers with no Helmholtz resonators, the following sections concerned with the effects of varying the connection tube geometry will use results with the speaker as the source of excitation to support the discussion.

6.4.3.2 Effect of connecting tube length

Mufflers R1011 and R1012 contain the base case chamber and a Helmholtz resonator connected in series. The connecting tube inside diameter for both resonators was 23 mm. The connecting tube length for the R1011 muffler is 36.20 mm. For the R1012 muffler a punched hole was used giving a connecting tube length of 1.6 mm, the wall thickness of the main pipe. The volume of the resonator chambers was set so both mufflers were tuned to 185 Hz at 20°C, using a 0.85 end correction. The predicted and measured insertion loss for these mufflers, and the base case, are shown in Figure 6.4-4.

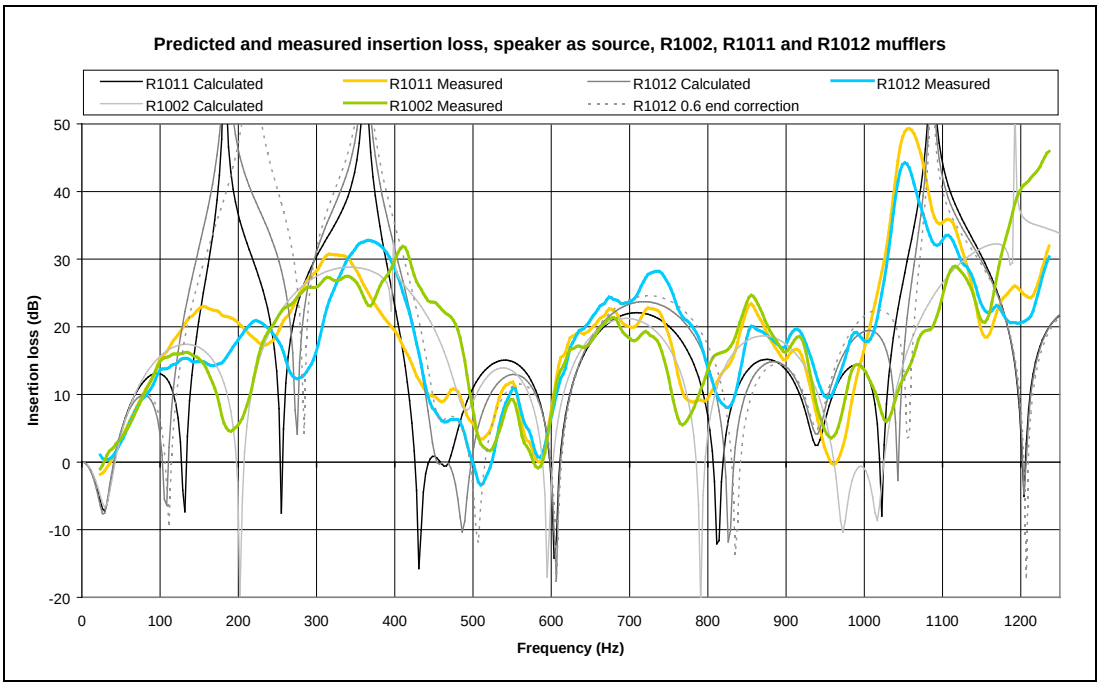

Figure 6.4-4 Performance of Helmholtz resonators with varying length connection tubes

The resonant peak measured at 225 Hz for the punched hole Helmholtz resonator (R1012) agrees with that predicted with a modified end correction of 0.60. The resonant peak measured for the tuned tube Helmholtz resonator (R1011) at approximately 160 Hz is lower than that predicted for the range of end correction considered (0.60-0.85 giving a resultant frequency range of 195-185 Hz).

This behaviour was consistent throughout the testing for all punched hole vs. connecting tube Helmholtz resonators, and was especially evident with larger diameter connecting tubes. As the connection tube diameter increases and becomes comparable to that of the passage tube, the length perpendicular to the defined length becomes significant as shown in Figure 6.4-5. To account for this, the end correction for tuned tubes could be modified.

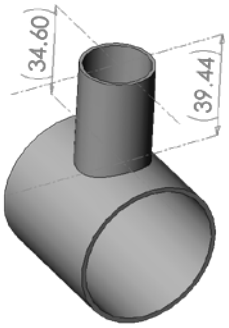

Figure 6.4-5 Connection tube, R1011 muffler

6.4.3.3 Effect of hole size

Three hole sizes were tested being 15.9, 23, and 32 mm in diameter corresponding to mufflers R1003, R1012 and R2003 respectively. The connection element in all cases was a punched hole in the main tube. The hypothesis was that the larger the connection holes would have better insertion loss at the resonant frequency of the Helmholtz chamber due to proportionally lower viscous losses. Figure 6.4-6 shows the predicted and measured insertion loss for the R1003, R1012 and R2003 mufflers.

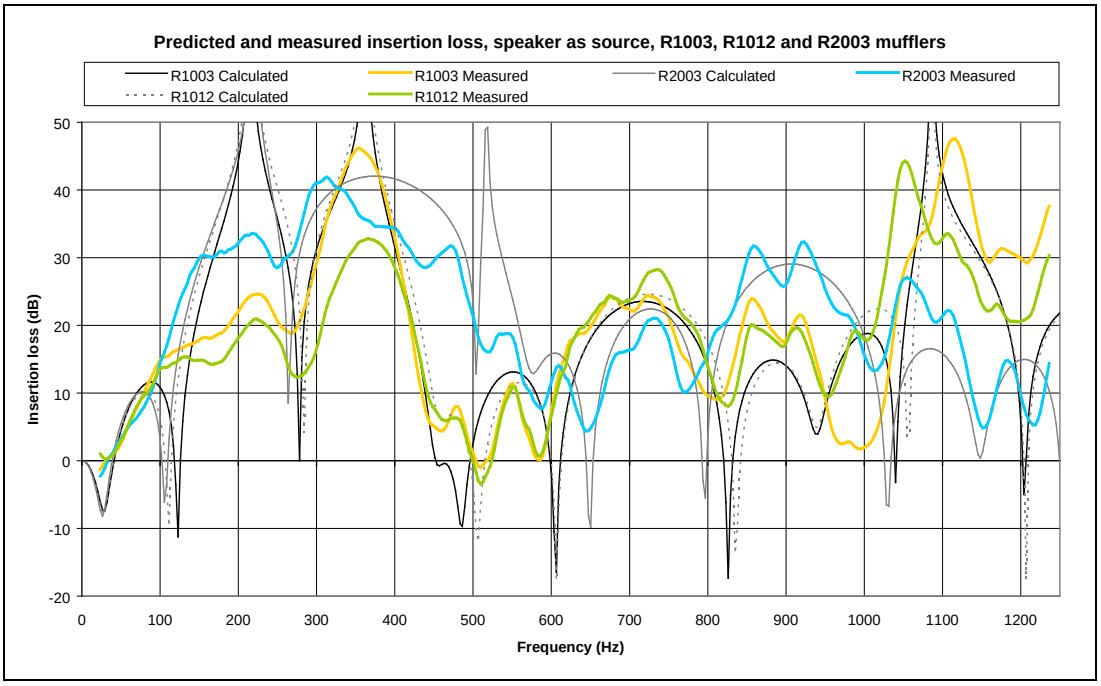

Figure 6.4-6 Effect on performance of varying connection hole size

The resonance peak due to the Helmholtz resonator chamber in each of the mufflers is present as predicted at 216 Hz using an end correction of 0.60. Comparing the performance of the three resonators at the tuned frequency the R2003 muffler (32 mm ID) has the best performance followed by the R1003 muffler (15.9 mm ID). The R1012 muffler (23 mm ID) had the worst performance. This result is somewhat contradictory to the hypothesis as although the largest hole had the best performance the smallest hole outperformed the intermediate sized hole. Further analysis and testing of various sized tuning holes is required to fully understand these effects.

6.4.3.4 Placement of connection tube

Two tuned chambers being the extended inlet and outlet expansion chamber, and the Helmholtz resonator, were tested connected in series and in parallel (see diagram 6.4-1). The purpose of this testing was to observe the effect of Helmholtz resonator location on the performance of the muffler and compare the performance of the two different types of tuned reactive chamber. Placement of the connection tube in parallel with the quarter wave resonator results in a two degree of freedom system which is unable to be analysed by the current model. Figures 6.4-7 and 6.4-8 show the performance of mufflers containing Helmholtz resonators in series and parallel along with the base case muffler. Figure 6.4-7 shows mufflers R2005 and R2003 containing Helmholtz resonators in parallel and series respectively with 32 mm punched holes as entry to the Helmholtz chambers. The R2001 base case muffler is also shown for comparison.

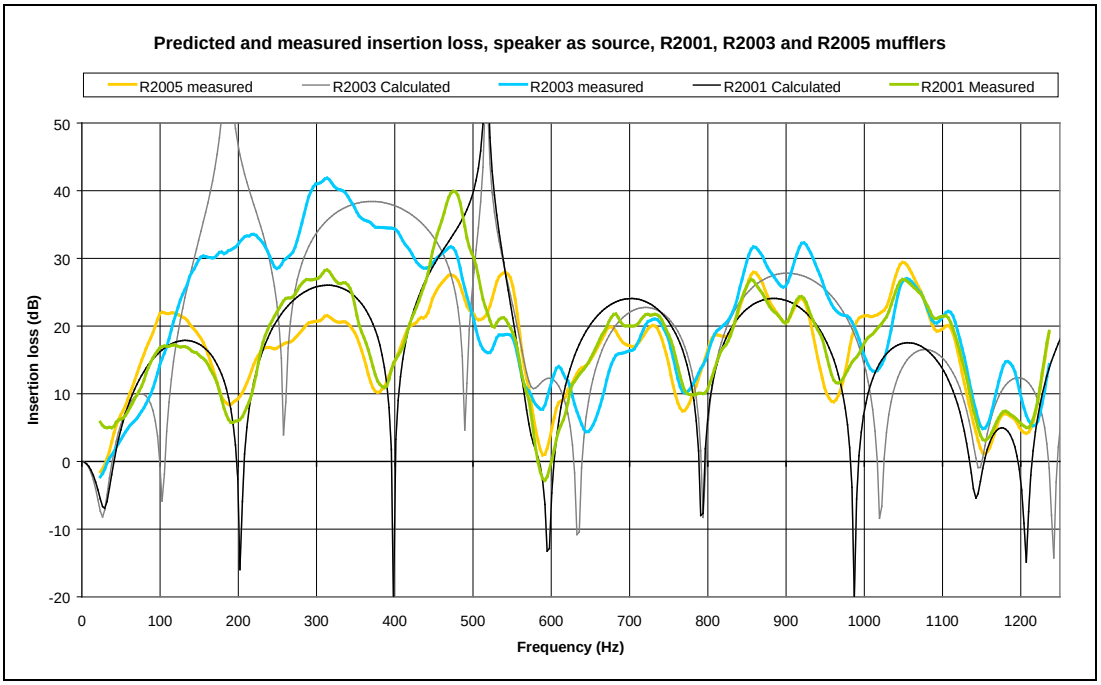

Figure 6.4-7 Series and parallel Helmholtz resonators, punched holes, oval cross-section

Figure 6.4-8 shows mufflers R1006 and R1011 containing Helmholtz resonators in parallel and series respectively with 23 mm inside diameter tubes as connecting elements to the Helmholtz chambers. The R1001 base case muffler is also shown for comparison.

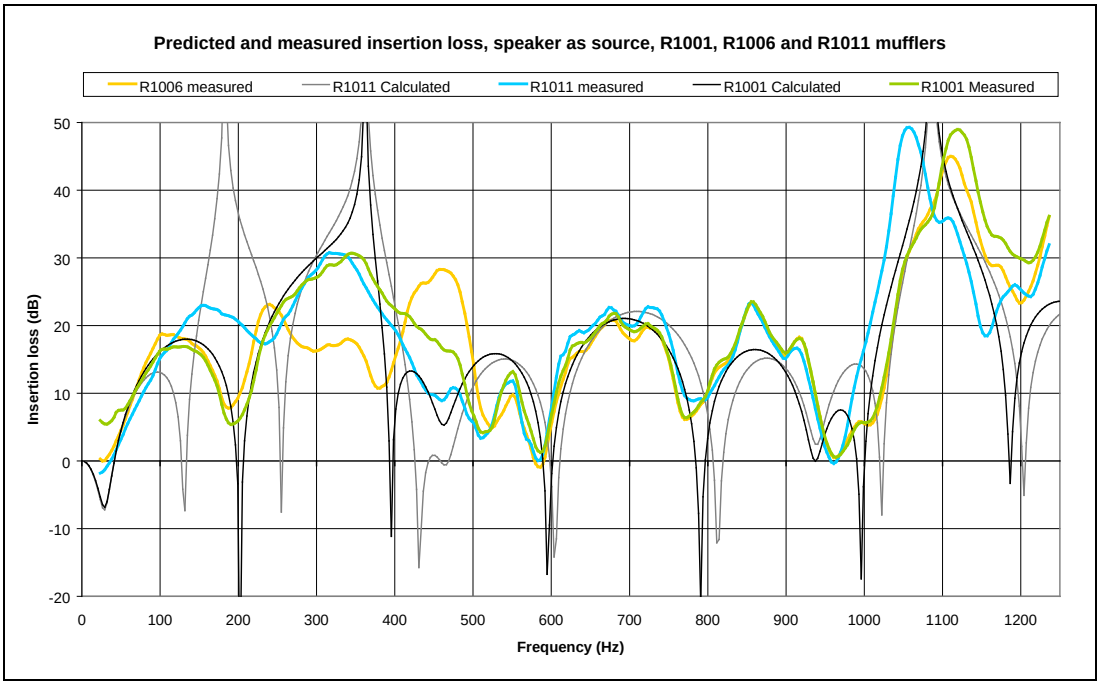

Figure 6.4-8 Series and parallel Helmholtz resonators, tuned tubes, round cross-section

As the parallel Helmholtz resonator chamber muffler is a two degree of freedom system it will have a resonant frequency related to both the quarter wave resonator and the Helmholtz chamber. Due to this the performance of the series and parallel chamber mufflers cannot be directly compared at the resonant frequency of the Helmholtz chamber.

From the measurements taken it is seen that the performance of the base case resonator is modified by the Helmholtz chamber in parallel. The addition of the chamber in parallel has reduced the performance of the muffler overall and is much less effective than placing the Helmholtz chamber in series. For both the tuned in parallel mufflers, the first quarter wave tuned peak frequency is reduced and shifted to a higher frequency. There is no peak observed at the resonant frequency of the Helmholtz chamber for either of the tuned in parallel mufflers. This reduction in performance is most likely due to the longer transmission path to the parallel chamber reducing its effect.

6.5 Resonator performance parameters

6.5.1 Introduction

The aim of this section is to show using experimental results, the performance change of mufflers caused by effects not considered by the model. The change in performance of mufflers with changing gas temperature, differing muffler cross section and varying mid-pipe length will be considered.

6.5.2 Gas temperature

As exhaust gas temperature increases, the speed of sound increases, elongating the insertion loss curve. As the temperature of the exhaust gas is dependant on engine load, speed, and atmospheric conditions, the exhaust temperature can vary over a large range. A variation of 60-810°C was observed during dynamometer tests. It is worth nothing that exhaust temperatures encountered on an engine dynamometer will be in excess of those for normal operating conditions due to the cooling effect of the airflow under the car. Harrison [7] refers to the catalytic converter as being a 'thermal choke' in the exhaust system regulating the input temperature to the remainder of the system. No catalytic converter was present for this work. These factors indicate that the range of exhaust temperatures encountered is larger than the range that may be encountered on a road tested vehicle. Figure 6.5-1 shows the change in muffler performance with increasing exhaust gas temperature. The exhaust gas temperature was measured at the inlet to the muffler and was increased by increasing engine speed.

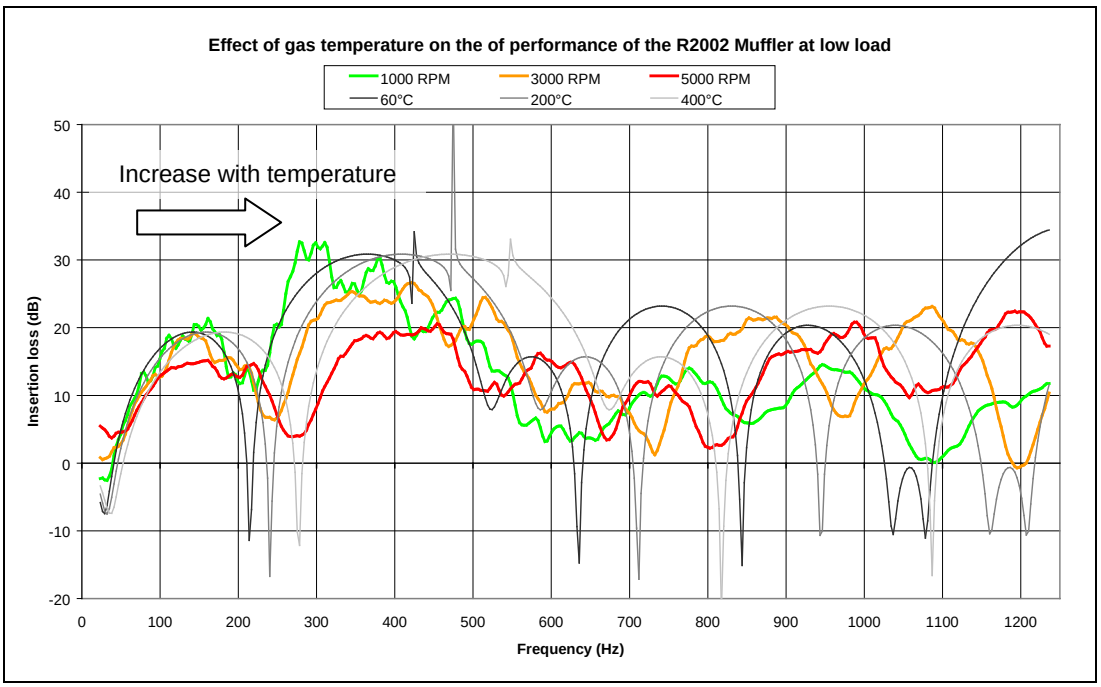

Figure 6.5-1 Change in insertion loss with increase in temperature

As environmental conditions, engine speed and engine load are extremely variable; exhaust gas temperature is also highly variable. To ensure adequate muffler performance, the insertion loss curve must not have any points of low attenuation (e.g. pass frequencies) that intersect with engine firing harmonics over the operating temperature range.

6.5.3 Muffler casing geometry

One of the initial objectives of the project was to investigate the effect of casing geometry on muffler performance. The muffler systems were analysed assuming one dimensional plane waves to be propagated through the system. The model calculates impedance changes at area discontinuities assuming instantaneous area expansions and contractions (see section 6.3), without considering the actual cross sectional shape. Mufflers R1002 and R2002 have identical baffle spacing, perforates, and lengths of extended tube features. The R1002 muffler has a round cross section and the R2002 muffler has an oval cross section with a slightly higher cross sectional area. Figure 6.5-2 below shows the difference in performance between the round and oval mufflers.

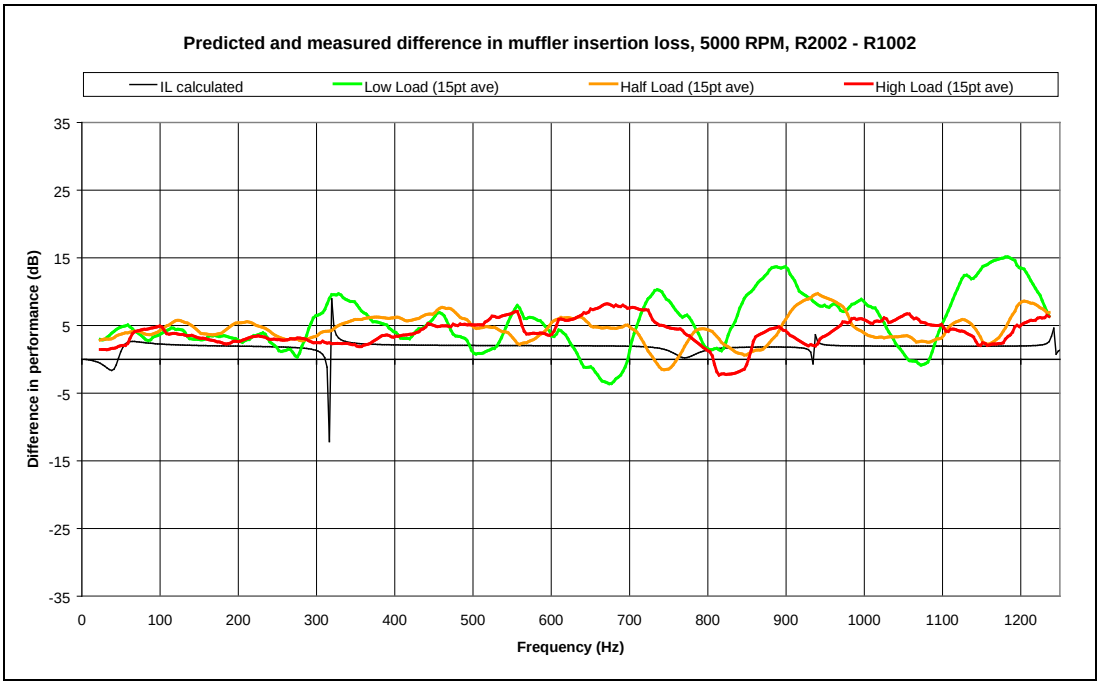

Figure 6.5-2 Difference in performance between oval and round mufflers

The above figure shows that the difference in performance between the two mufflers is very low with the oval cased muffler just slightly out performing the round casing due to its larger cross sectional area. This indicates that for the frequencies of interest and cross-sections considered, the performance of the muffler is insensitive the cross sectional shape.

6.5.4 Mid-pipe length

The mid-pipe is the connection tube between the rear and intermediate mufflers. Resonances or standing waves within the mid-pipe result in pass frequencies in the insertion loss curve. The R1002 muffler was tested with an intermediate muffler (R1021/R1022) with three different mid-pipe lengths. The object of this was to assess the performance of the model with two mufflers present in the system and observe the effect of changing mid-pipe length on muffler system performance. Figure 6.5-3 shows the predicted and measured insertion loss with the engine as the source of excitation for the R1002/R1021 muffler system with 300, 450 and 600 mm mid-pipe lengths.

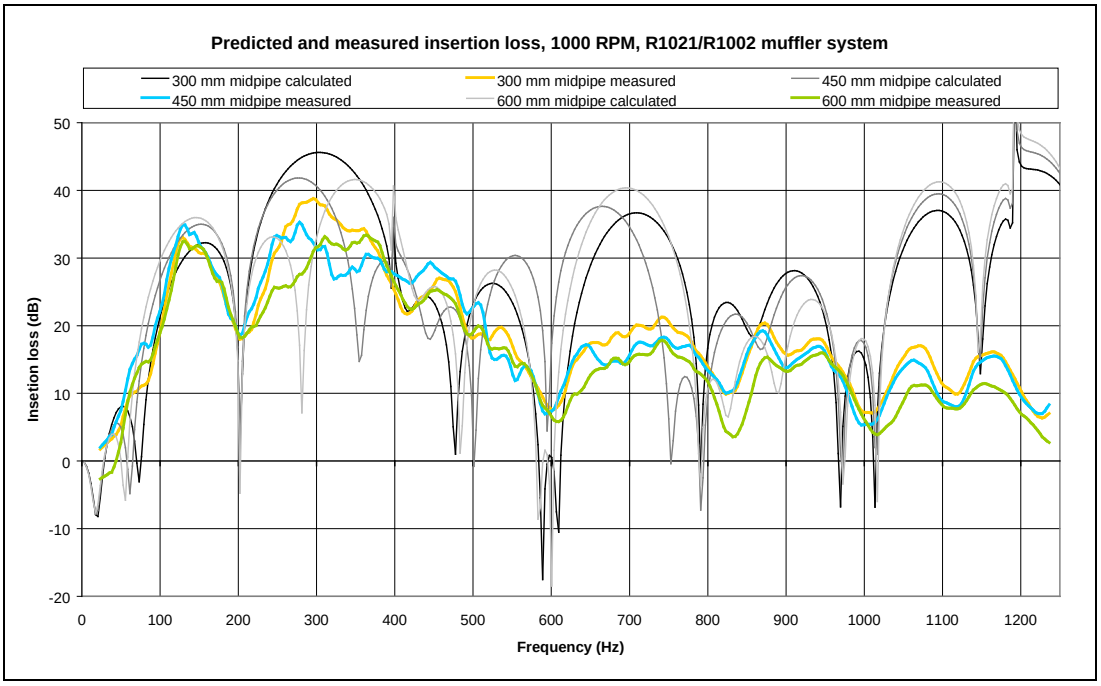

Figure 6.5-3 Measured and predicted data for twin resonator system with varying mid-pipe length

Resonance within the mid-pipe will be exhibited at the fundamental frequency and at higher order modes at integer multiples of the fundamental. A longer mid-pipe has a lower first order resonant frequency and hence more pass frequencies over the range of interest. The higher the number of pass frequencies, the lower the performance of the muffler. This is evident in the above figure when comparing the 300 mm mid-pipe case to the 600 mm mid-pipe case. From a design point of view the distance between discontinuities in the system should be kept as short as possible so that pass frequencies due to resonance within the connecting pipes are spaced further apart and located at higher frequencies.

6.6 Conclusion

Insertion loss measured using the engine as the source of excitation at low engine speeds and loads agrees well with that predicted for the base case mufflers. As engine speeds and loads are increased, agreement between predicted and measured insertion loss decreases. Flow and pressure effects at high engine speed and load are likely to cause an increase in the resistance of the perforate section. This reduces transmission to the reactive elements of the muffler, reducing its performance. Flow through the muffler is likely to cause an increase in viscous damping in the muffler chambers, further reducing the performance of the muffler. The reduction in muffler performance is manifested through reduced maxima and minima with the general insertion loss trend (peak and pass frequency locations) still shown. As the model only considers impedance changes in the system and not dissipative or nonlinear pressure and flow effects, increases in engine speed and load result in a reduction of accuracy of the model.

Agreement between predicted and measured insertion loss is good with the speaker as the source of excitation for frequencies below 500 Hz. At frequencies above 500 Hz, variations attributed to the presence of standing wave resonances between the muffler and the speaker were observed. An assumption used in the modelling was that the source is anechoic. As there is a standing wave in the pipe related to reflections from both the source and the muffler, this indicates that the source is not fully anechoic. A modification to the speaker test arrangement with the speaker mounted as a branch element was proposed. This should improve agreement between the results measured with the speaker and those predicted and measured with the engine.

The effect of varying quarter wave resonator length was investigated. The hypothesis was that tuning the quarter wave resonator for chamber pass frequencies would result in an overall improvement in muffler performance. The results were inconclusive with further testing required. With the engine as the source of excitation, the measured performance of mufflers containing Helmholtz resonators, for all but one case, was indistinguishable from nominally identical mufflers with no Helmholtz resonators. This result was attributed to flow and pressure effects similar to those presented in other studies [1, 5, 6]. Further work is required to clarify the effect of varying connection tube geometry and under what conditions Helmholtz resonators will improve muffler performance on an engine.

Mufflers containing Helmholtz resonators with varying connection tube geometry arranged in series and parallel with the main chamber were tested with a speaker as the source of noise. The tuned frequency of Helmholtz resonators connected in series with punched hole connection tubes was as predicted. The largest connection hole significantly outperformed the smaller holes, however no clear

relationship between hole size and resonator performance was found. The resonant frequency of Helmholtz resonators connected in series with tuned tube connecting elements was over predicted by the model. This suggests that the end correction for these resonators requires modification. Mufflers with Helmholtz resonators located in parallel with the main chamber had no performance gain over the base case mufflers containing no Helmholtz resonators. The transmission path to the Helmholtz resonator in parallel is much longer than that with the resonator in series. The resulting transmission losses to and from the chamber are higher, reducing its effect. With the Helmholtz chamber arranged in parallel the muffler becomes a two degree of freedom system and must be analysed as such.

A number of muffler systems were investigated experimentally with the engine as the source of excitation to investigate muffler performance characteristics. The effects of changing muffler temperature, muffler cross section and mid-pipe length were investigated. Increasing gas temperature was shown to elongate the insertion loss curve. Exhaust gas temperature is highly variable with engine speed and load, as well as with atmospheric conditions. The muffler system must therefore be analysed at a variety of muffler temperatures to ensure adequate muffler performance over a variety of operating conditions. Mufflers with oval and round cross sections were tested to analyse the effect of cross sectional shape on muffler performance. No differences were observed that was not related to the slight difference in expansion ratio between the oval and round mufflers. Changing the length of the mid-pipe between the intermediate and rear mufflers affects the overall performance of the muffler system. Standing wave resonances within the mid-pipe are manifested as pass frequencies in the insertion loss curve. Resonance within the mid-pipe is related to its length and an improvement in muffler performance can be obtained by ensuring the length between discontinuities in the system is as short as possible.

Overall, the performance of the model used to predict muffler performance was good. Damping and dissipative behaviour within the muffler reduced the performance of the reactive elements. This dissipative behaviour was not included in the model, reducing the accuracy of the predictions at high engine speeds and loads. Investigating the performance of mufflers with an engine and a speaker as the source of excitation gave insight into the effectiveness of different reactive elements for automotive applications. Temperature, flow and pressure effects were shown to be of paramount importance and must be considered when designing muffler systems.

6.7 References

[1] A. A. I. El-Rahman, A. S. Sabry, and A. Mobarak, "Non-Linear Simulation if Single Pass Perforated Tube Silencers Based on thr Method of Characteristics," *Journal of Sound and Vibration*, vol. 278, pp. 63-81, 2004.

[2] A. Cummings, "The Response of a Resonator Under a Turbulent Boundary Layer to a High Amplitude Non-Harmonic Sound Feild," *Journal of Sound and Vibration*, vol. 115, pp. 321-328, 1987.

[3] A. Selamet and Z. L. Ji, "Acoustic Attenuation Performance of Circular Chambers with Extended Inlet/Outlet," *Journal of Sound and Vibration*, vol. 223(2), pp. 197-121, 1999.

[4] P. O. A. L. Davies, "Practical Flow Duct Acoustics," *Journal of Sound and Vibration*, vol. 124, pp. 91-115, 1988.

[5] D. D. J. Davis, G. M. Stokes, D. Moore, and G. L. J. Stevens, "Theoretical and Experimental Investigation of Mufflers: with Comments on Engine-Exhaust muffler Design," U.S National Advisory Committee for Aeronautics Langley Aeronautical Laboratory, Report 1192, 1954.

[6] A. Sindhupak, M. Lokitsangtong, B. Silapakijwongkul, T. Wada, S. Murakami, M. Maeda, and S. Hagi, "Acoustical Characteristics of Helmholtz Type Resonators," Ladkrabag, Bangkok, Thailand.

[7] M. F. Harrison, "Time and Frequency Domain Modelling of Vehicle Intake and Exhaust Systems." Doctoral Thesis, Institute of Sound and Vibration Research, University of Southampton, 1994.

Chapter 7
Conclusion and Recommendations

7.1 Conclusion

A literature review was conducted identifying sources of exhaust noise and its propagation, muffler elements both reactive and dissipative, sound measurement techniques, applicable ISO and SAE standards, and modelling techniques for the prediction of muffler performance. Test facilities were constructed that allowed the testing of muffler systems with either an engine or a speaker as the source of excitation. The test arrangement separated the source of noise from the measurement position to obtain a very good signal to noise ratio. A number of tests were performed to quantify the acoustics of the receiving room to ensure that results obtained were reliable. Using temperature and pressure sensors the characteristics of the exhaust gas pressure pulse were analysed and related to noise measurements made at the exhaust outlet.

A number of mufflers were constructed and their insertion loss measured. Insertion loss was predicted for each muffler system using a scattering matrix technique. Simple mufflers with one chamber were initially tested and set as the 'base case' mufflers. With the engine as the source of excitation, agreement between measured and predicted insertion loss for base case mufflers was very good at low engine loads and speeds, with some flow noise at higher frequencies. As engine speed and load were increased, the performance of the mufflers decreased due to flow and pressure effects. These effects most probably reduce muffler performance by increasing viscous damping and the resistance of the perforated section that links the main pipe to the outer chamber. The reduction in muffler performance was manifested through reduced maxima and minima, with the general insertion loss trend (peak and pass frequency locations) still shown. This behaviour was not accounted for by the model as dissipative and damping effects were not included. With the speaker as the source of excitation agreement between predicted and measured performance was improved. At frequencies above 500 Hz, a standing wave was observed within the inlet tube to the muffler system. This was attributed to a characteristic of the test arrangement.

The performance of mufflers containing Helmholtz resonators with varying connection tube geometry and location were assessed. With the engine as the source of excitation, the predicted resonant peak associated with the Helmholtz resonator was not present for all but one muffler. This result was similar to others presented in literature and was attributed to flow and pressure effects not allowing the

resonator to create a high enough sound pressure to counter the incoming sound field. With the speaker as the source of excitation the measured and predicted insertion loss showed much better agreement. From this data a number of trends were identified relating connection tube geometry to the performance of the Helmholtz resonator.

Of the reactive muffler components tested, extended inlet and outlet expansion chambers had the best performance. The insertion loss of these mufflers was accurately predicted using a one dimensional scattering matrix technique. Any dissipative behaviour within the muffler reduces the reactive quality of the muffler. This reduces the performance of the muffler and as this behaviour was not accounted for in the modelling also reduces the accuracy of the prediction.

7.2 Recommendations for further work

7.2.1 Testing

This section describes testing that could be performed to further understand muffler performance and aid in the development of modelling techniques. Using the test apparatus developed during the course of this project a number of tests could be carried out to further investigate the performance of automotive muffler systems. For many of these tests, all that would be required would be to manufacture and test a batch of mufflers varying a parameter of interest. Further test apparatus may be required to isolate effects occurring with the engine.

Testing of Helmholtz resonators during this project showed that for all but one isolated case the addition of a Helmholtz resonator to a muffler system gave no measurable improvement in muffler performance. Further testing is required to understand why one Helmholtz resonator gave an improvement in performance and others did not. Testing could also be performed for Helmholtz resonators with two or more connecting tubes into a single volume. This testing could be performed using the existing experimental arrangement.

The mufflers tested in this project contained a perforated section of pipe that served as entry to the main outer chamber. The perforation consisted of 608, 3 mm holes, giving an open area of 29 percent. It was observed that with increasing engine speed and load, muffler performance was reduced. This reduction in performance was in part attributed to the resistance of the perforate increasing. An improvement in muffler performance could be attained by using a perforate with a lower resistance. Using the existing experimental arrangement the performance of nominally identical mufflers with different perforates could be assessed at with varying engine speeds and loads.

Testing of mufflers with varying length quarter wave resonators showed that the accuracy of the prediction could be improved by the incorporation of an end correction. The model assumed an instantaneous expansion into the main chamber. The incorporation of an end correction improved the prediction by accounting for the non-instantaneous expansion that occurs in practice. The end correction used was fairly approximate and could be possibly improved through testing of mufflers with a variety of quarter wave resonators and expansion ratios.

High pressure wave effects on muffler performance could be investigated. Through the use of two or more pressure transducers the pressure waves released from the cylinders could be analysed as they travel though the system. High pressure wave effects on perforates could also be investigated. Understanding how muffler components and systems react to high pressure waves would aid in understanding how to design systems that will perform over a range of engine operating conditions.

The effect of flow on muffler performance could be investigated. The flow velocity through the exhaust system could be measured and the conditions replicated on a cold flow bench. This would separate flow effects from other effects occurring with the engine as the source of excitation. The effect of steady flow and pulsating flow could be investigated and differences between the two and their effect on muffler performance obtained. A test apparatus used for duct testing is available in the Department of Mechanical Engineering and could be easily modified to accommodate cold flow muffler testing.

7.2.2 Modelling

Models need to be developed in conjunction with experimental testing to allow the modelling to be verified and to gain a greater understanding of processes that are being modelled. The current model could be improved in at least the following areas:

- Damping (this may be very difficult)
- Flow and high pressure effects
- The range of reactive, dissipative and absorptive muffler elements modelled
- Reactive elements in parallel and parallel path mufflers e.g. for a system with twin outlets
- Inclusion of the source of excitation

Various computational modelling techniques could also be investigated.

Appendix A
Muffler Drawings

This appendix contains drawings of all mufflers tested. Dimensions, volumes and cross sectional areas (were required) are shown.

Table of contents

Table A-1 Muffler description

Muffler	Description	Profile	Layout	Details
R1001	Base case round	155 Round	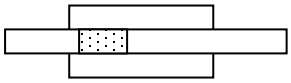	47.6 to 150.5 mm expansion 95.5 mm perforate, extended inlet (38.5 mm) and outlet (237 mm)
R1002 R1000	Modified tuned outlet extend tube	155 Round	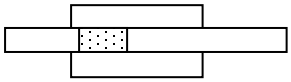	As per round base case with length of outlet extend tube decreased to 216 mm
R1003	Tuned Helmholtz chamber in series	155 Round	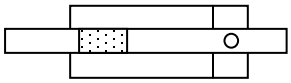	R1000 + Helmholtz chamber with Ø15.9 mm punched hole (series) 1145948 mm³ chamber volume
R1004	Tuned Helmholtz chamber in series	155 Round	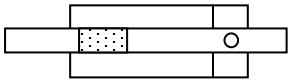	R1000 + Helmholtz chamber with 13.5 ID x 11 mm tube (series) 906355 mm³ chamber volume
R1005	Tuned Helmholtz chamber in parallel	155 Round	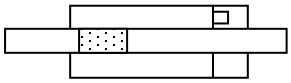	R1000 + Helmholtz chamber with Ø25.4 mm punched hole (parallel) 1145948 mm³ chamber volume
R1006	Tuned Helmholtz chamber in parallel	155 Round	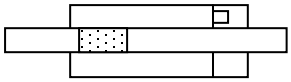	R1000 + Helmholtz chamber with 23 ID x 20 mm tube (parallel) 645594 mm³ chamber volume
R1011	Tuned Helmholtz chamber in series	155 Round	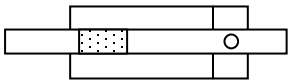	R1000 + Helmholtz chamber with 23 ID x 36 mm tube (series) 649419 mm³ chamber volume
R1012	Tuned Helmholtz chamber in series	155 Round	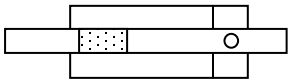	R1000 + Helmholtz chamber with Ø23 mm punched hole (series) 1713642 mm³ chamber volume
R1021 R1022	Intermediate muffler (two positions)	155 Round	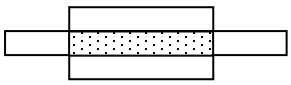	Perforated along entire length of expansion chamber (400 mm)
R2001 R2000	Base case oval	220x119 Oval	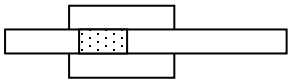	Ø50.9 to Ø150.5 mm expansion 95.5 mm perforate, extended inlet (38.5 mm) and outlet (166 mm)
R2002	Modified outlet extend tube	220x119 Oval	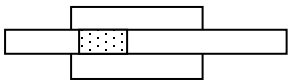	As per oval base case with length of outlet extend tube increased to 216 mm
R2003	Tuned Helmholtz chamber in series	220x119 Oval	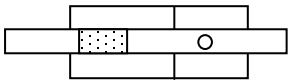	R2000 + Helmholtz chamber with Ø32 mm punched hole (series) 2405242 mm³ chamber volume
R2004	Tuned Helmholtz chamber in series	220x119 Oval	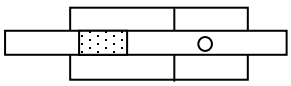	R2000 + Helmholtz chamber with 30.8 ID x 15 mm tube (series) 1442269 mm³ chamber volume
R2005	Tuned Helmholtz chamber in parallel	220x119 Oval	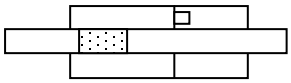	R2000 + Helmholtz chamber with Ø32 mm punched hole (parallel) 2405242 mm³ chamber volume
R2006	Tuned Helmholtz chamber in parallel	220x119 Oval	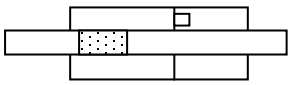	R2000 + Helmholtz chamber with 30.8 ID x 20 mm tube (parallel) 126447 mm³ chamber volume

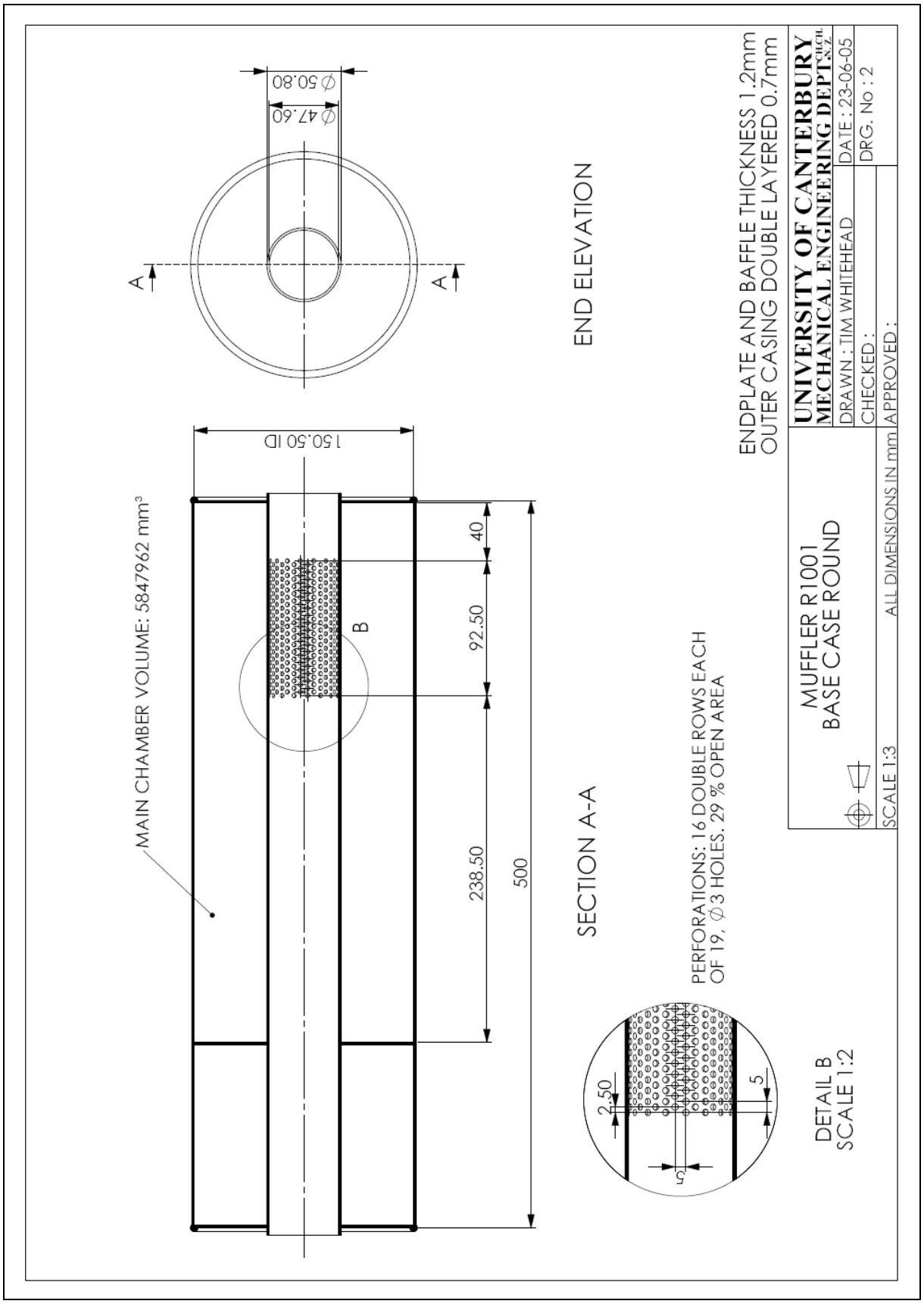

Figure A-1 R1001 base case muffler

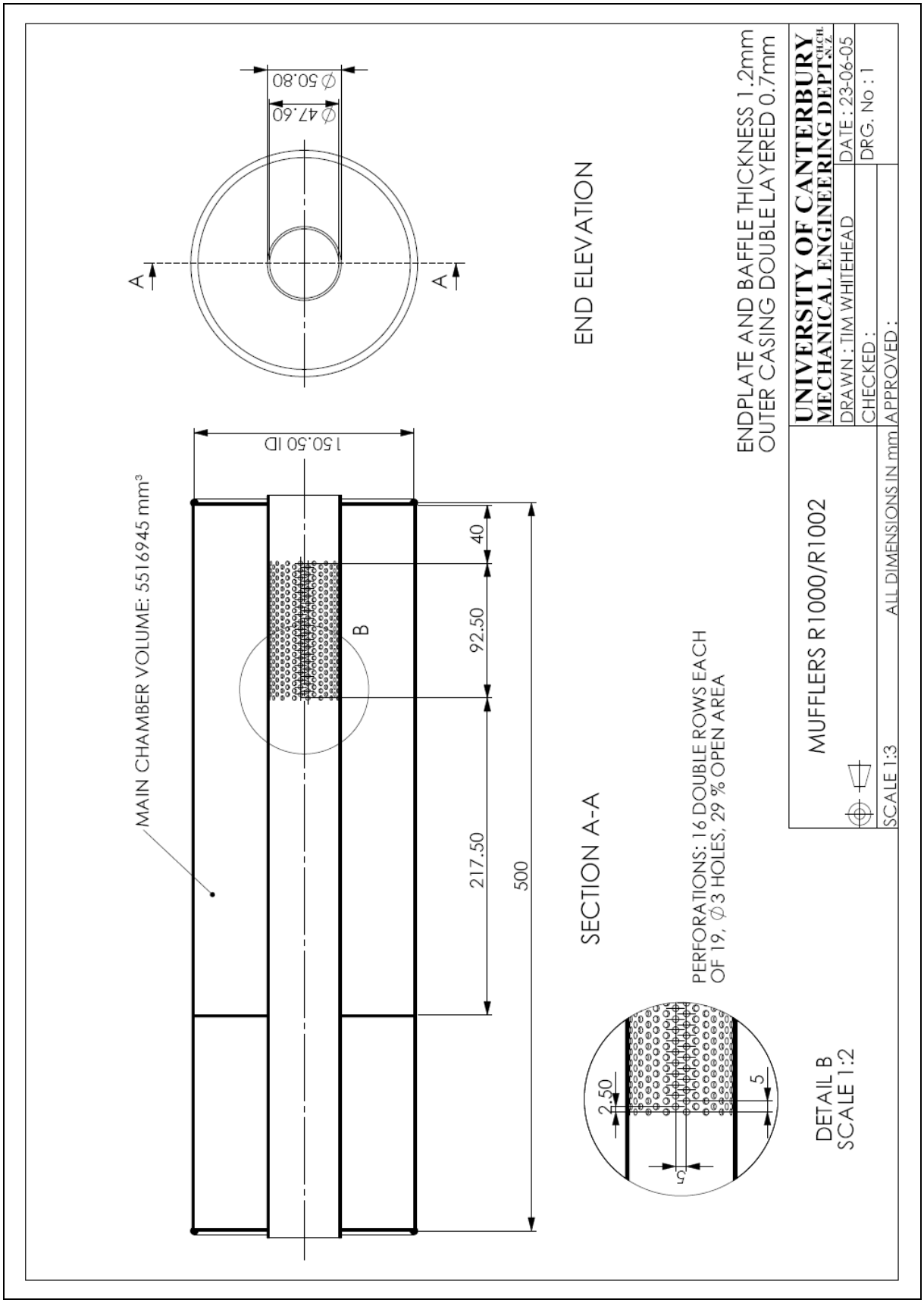

Figure A-2 R1000/R1002 mufflers

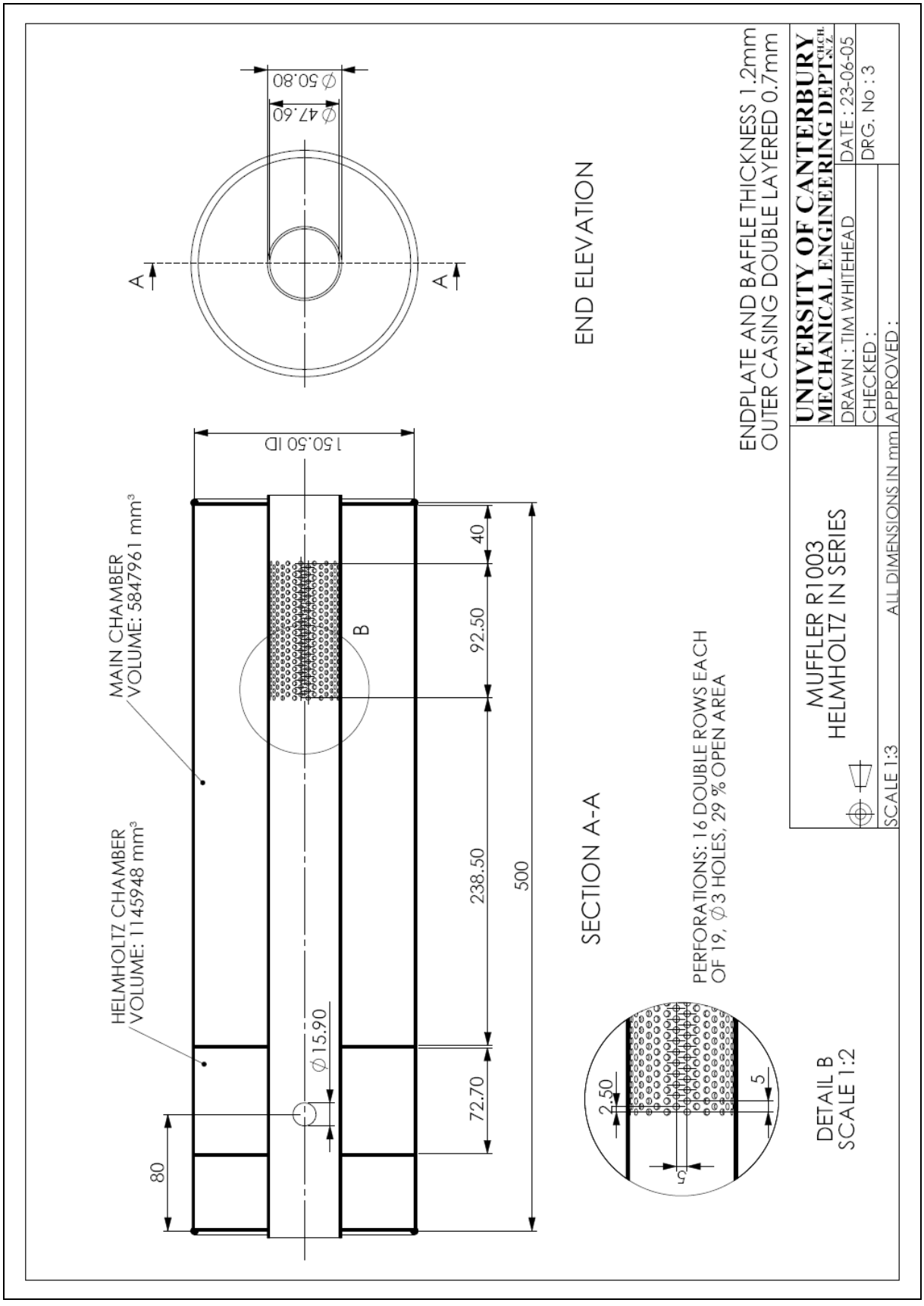

Figure A-3 R1003 muffler

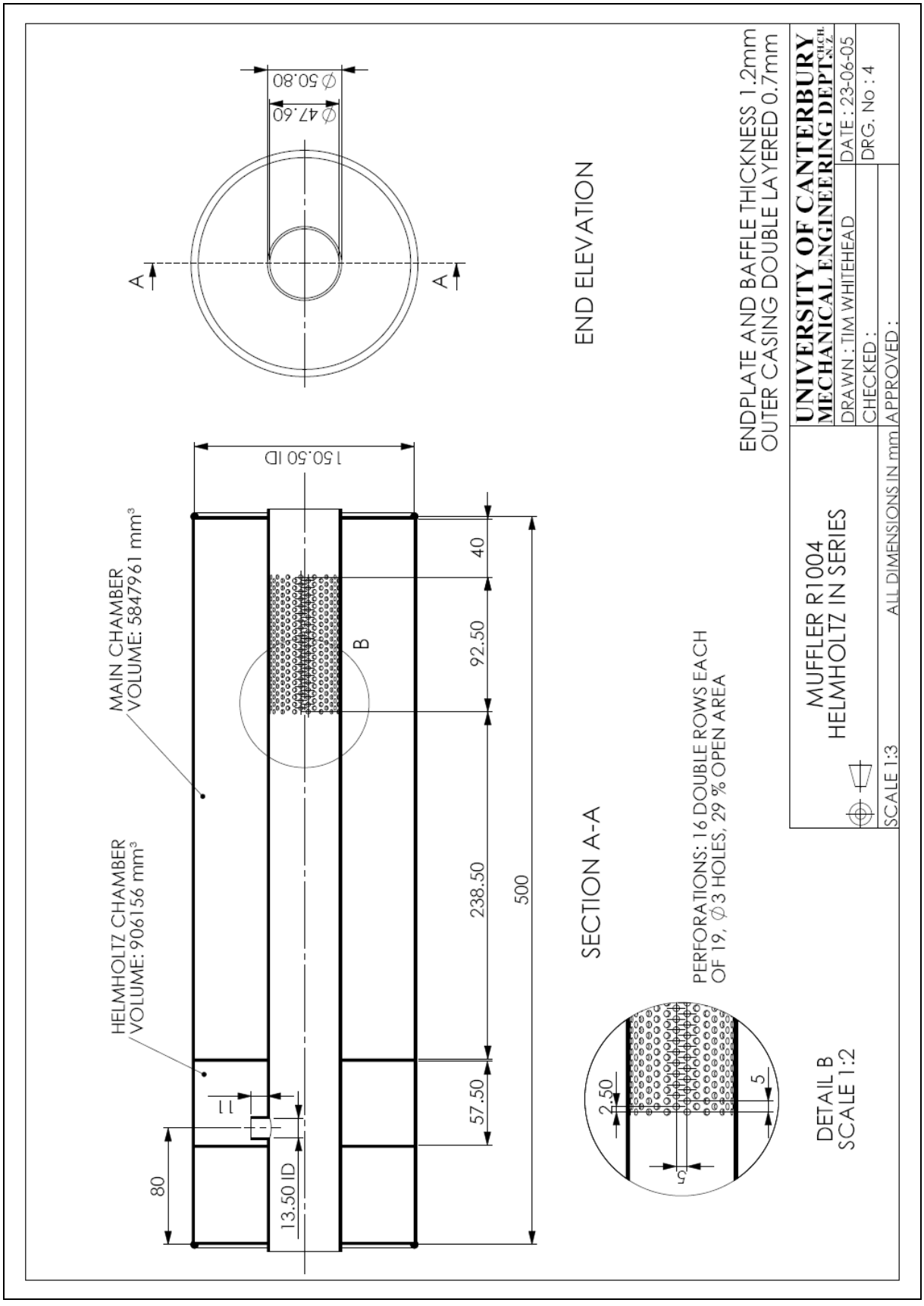

Figure A-4 R1004 muffler

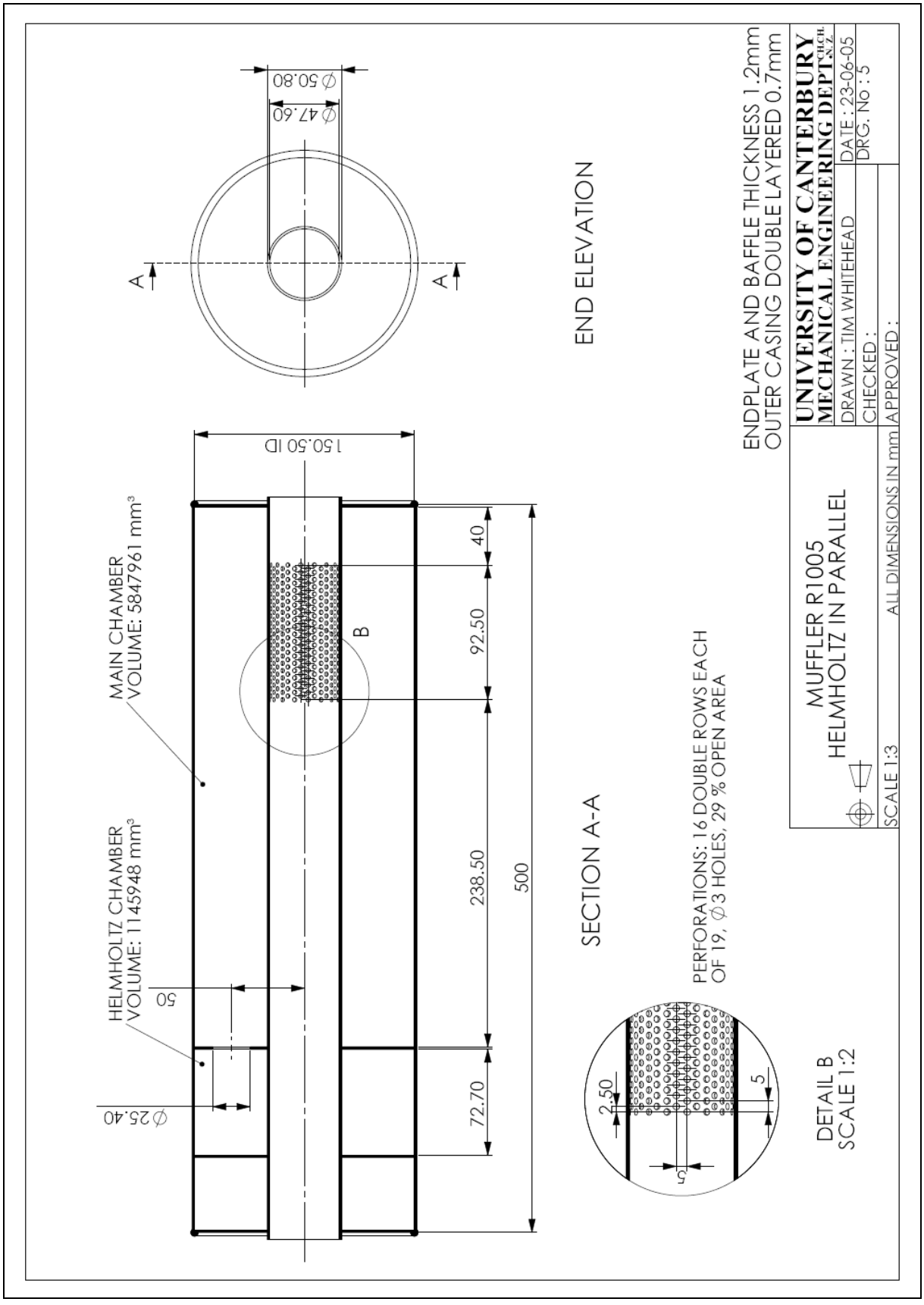

Figure A-5 R1005 muffler

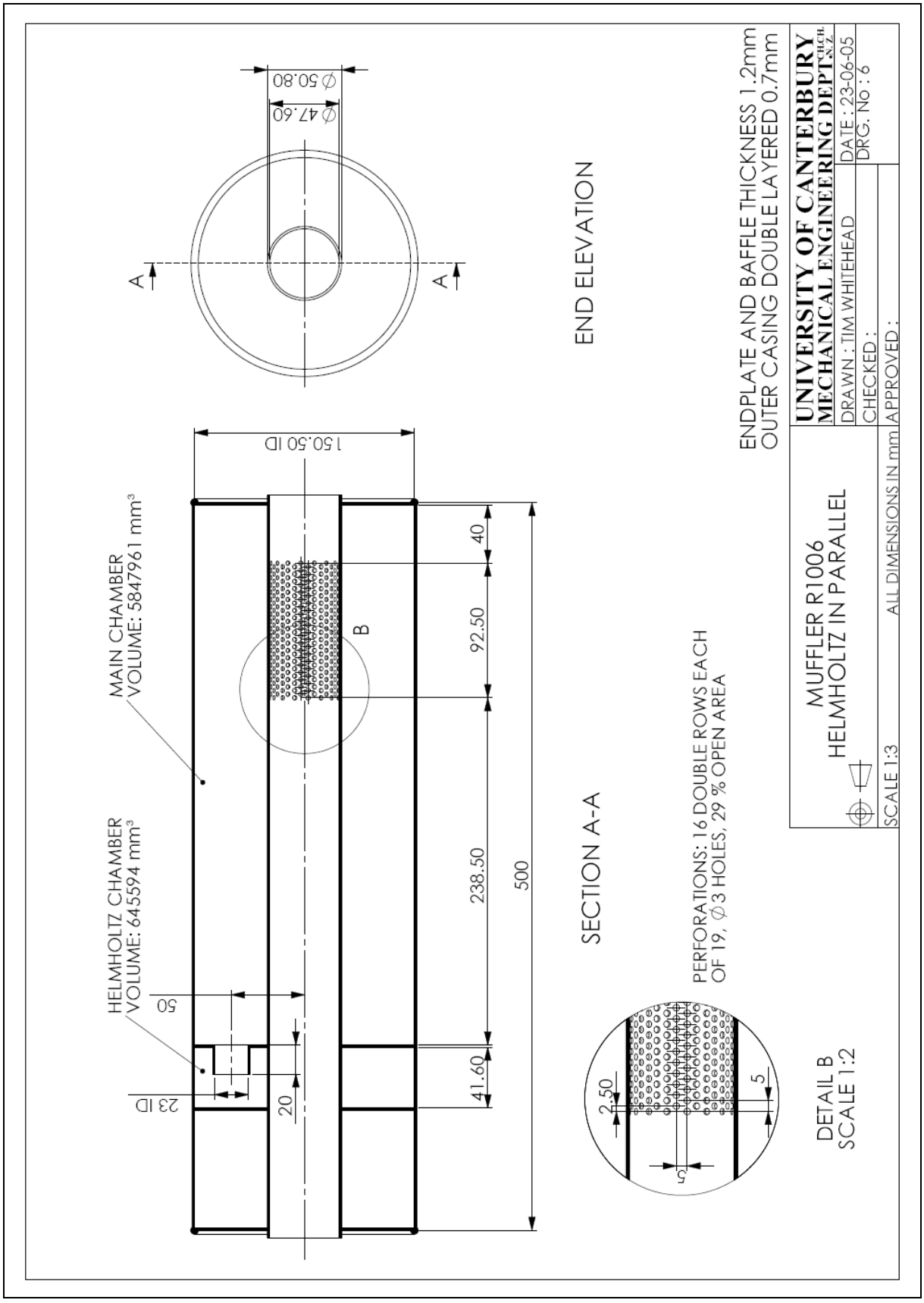

Figure A-6 R1006 muffler

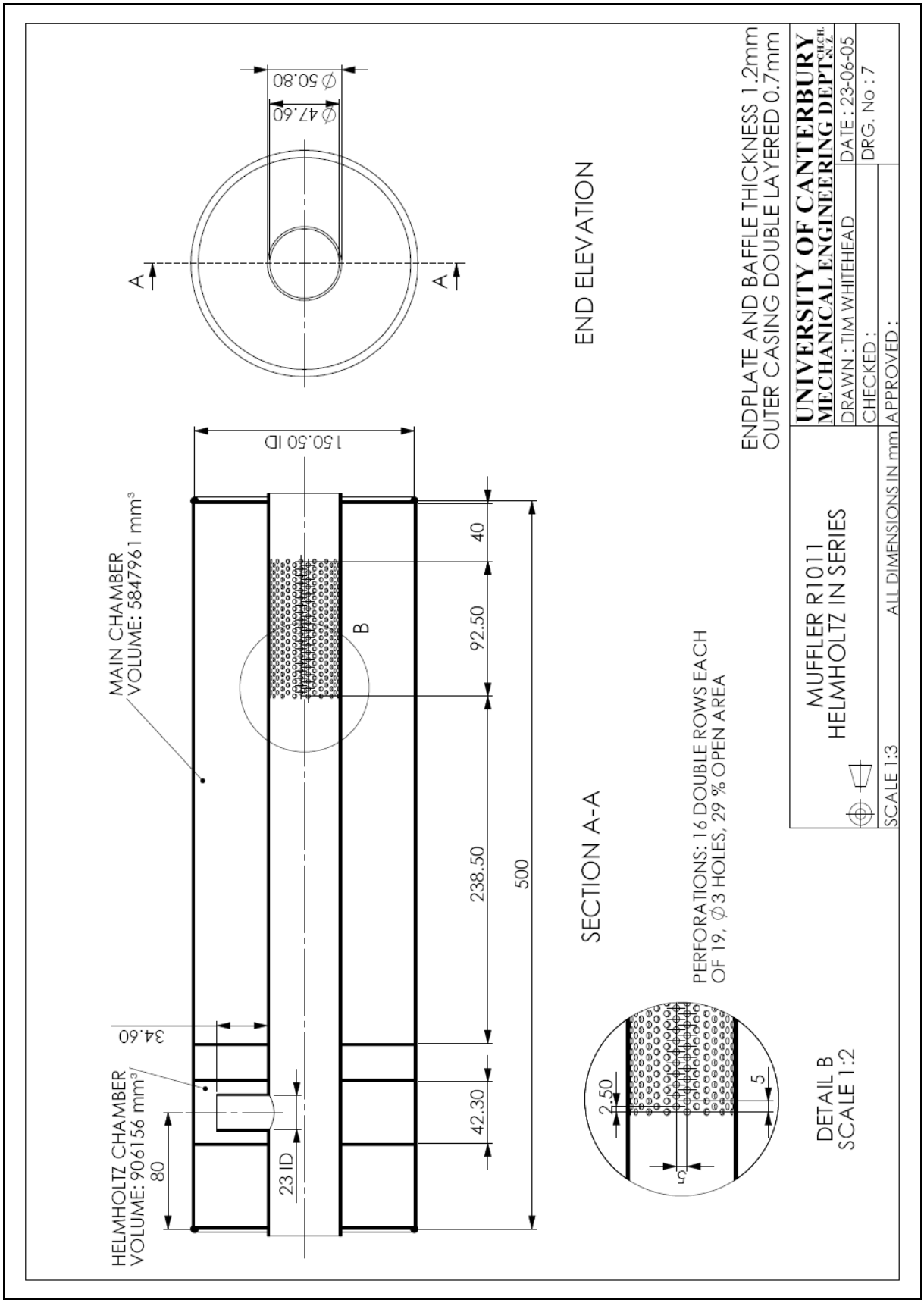

Figure A-7 R1011 muffler

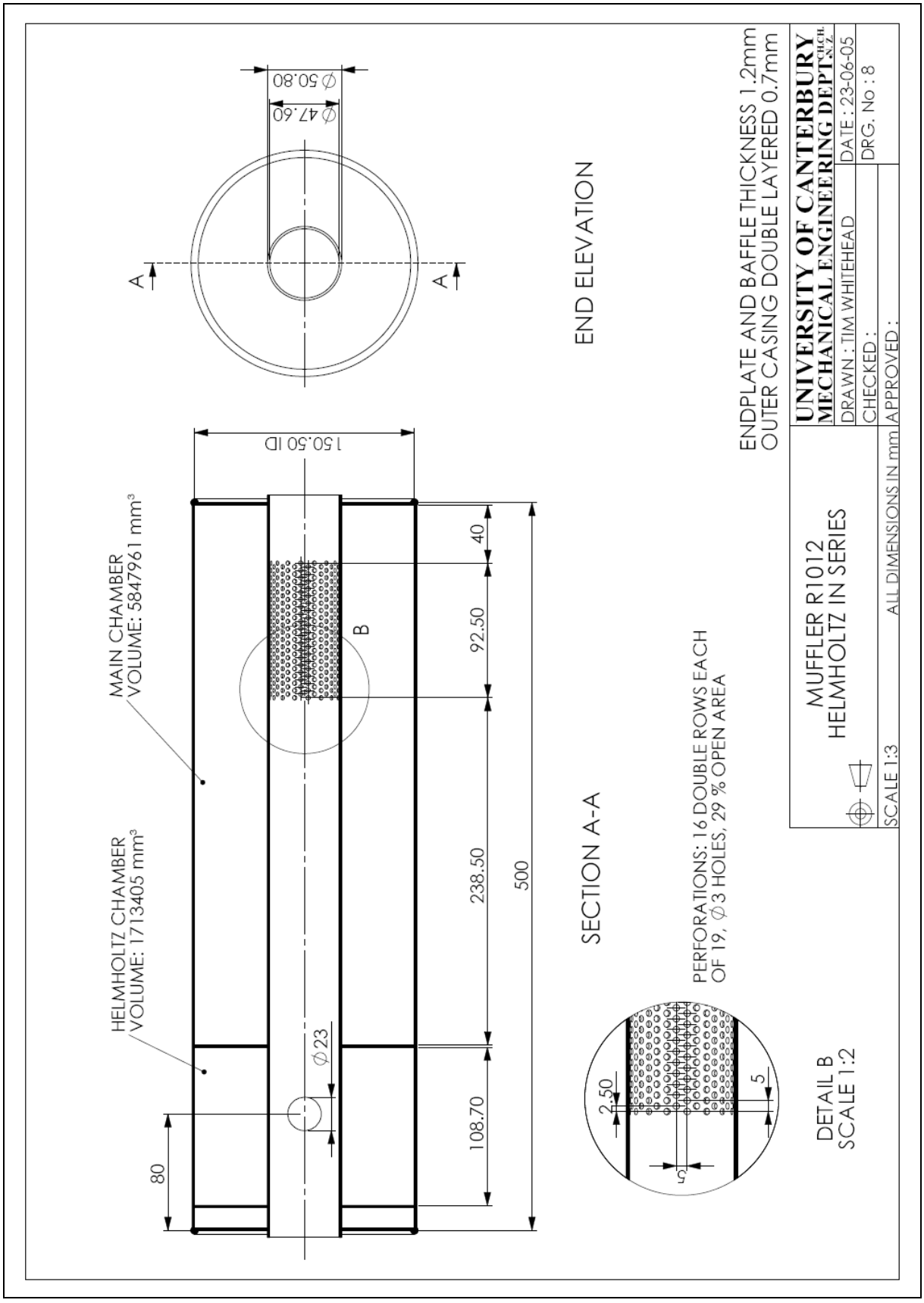

Figure A-8 R1012 muffler

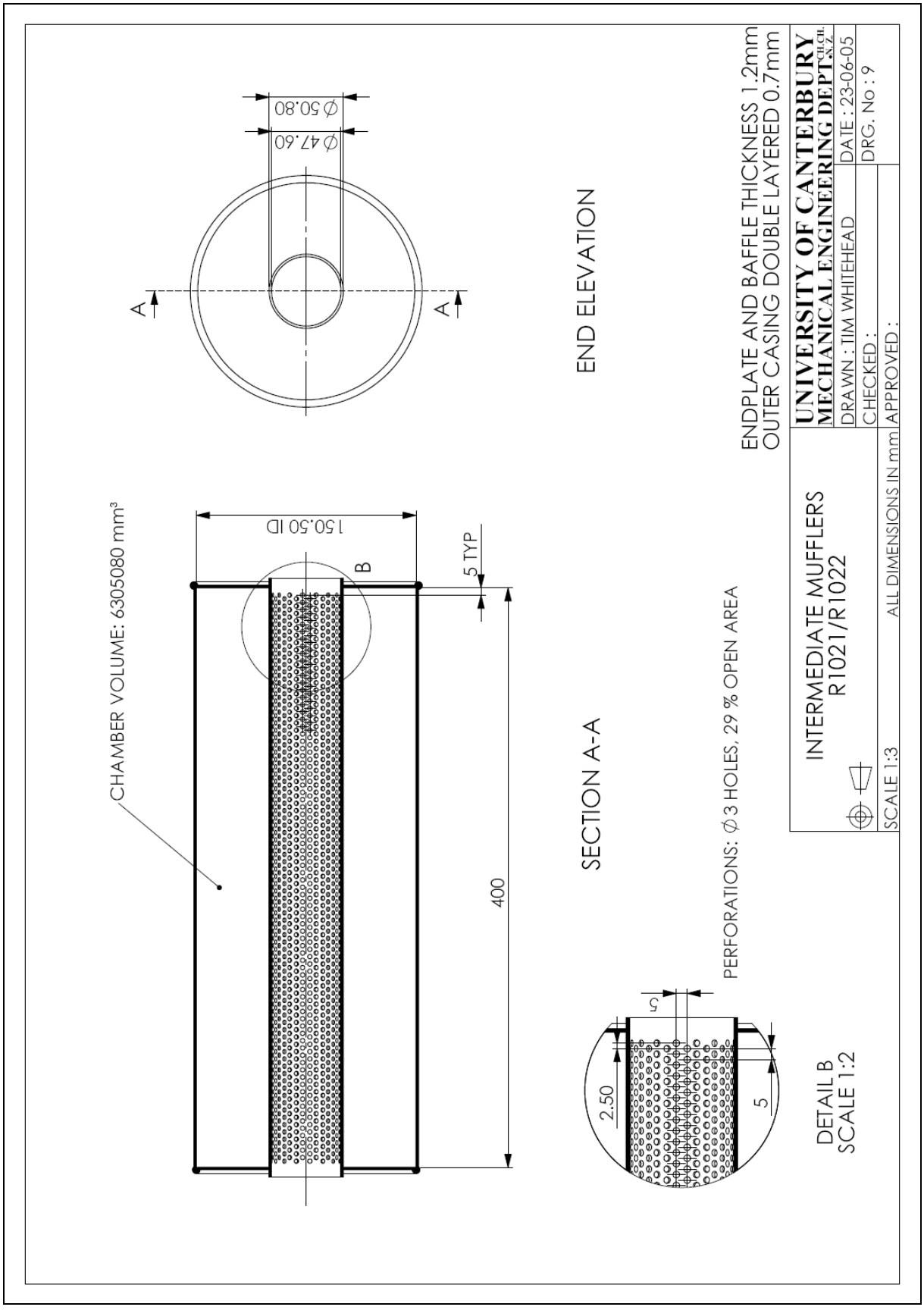

Figure A-9 R1021/R1022 mufflers

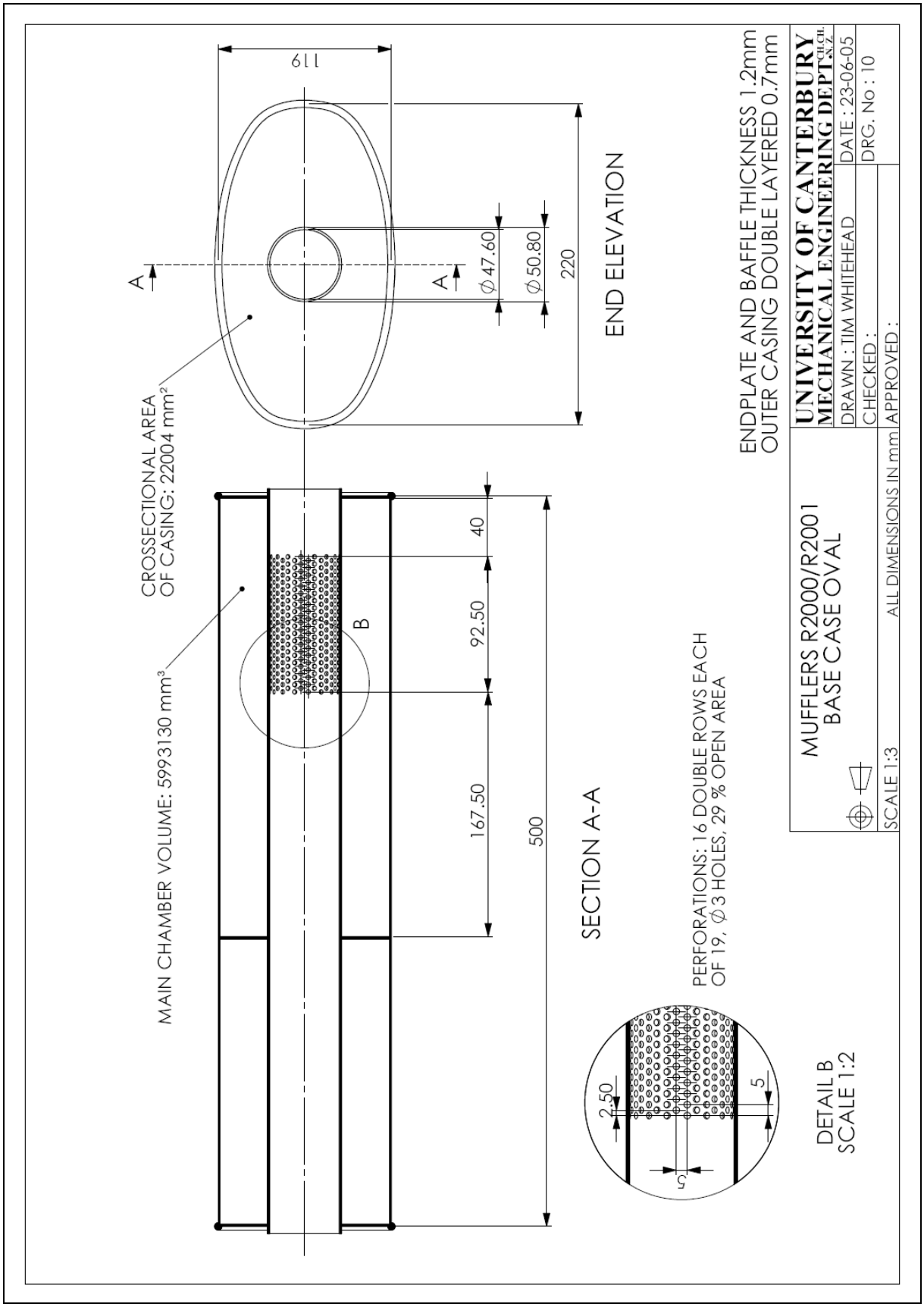

Figure A-10 R2000/R2001 base case mufflers

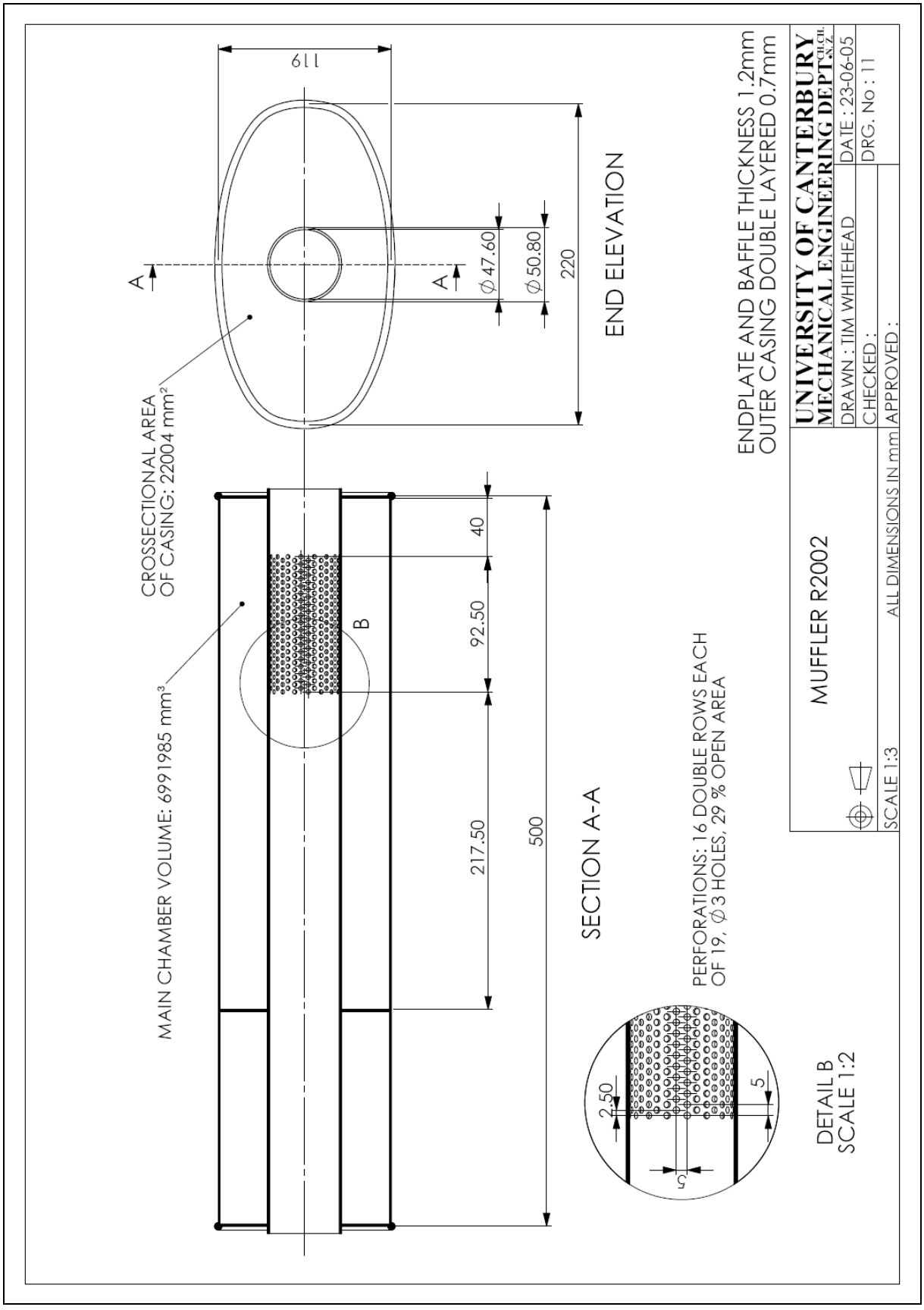

Figure A-11 R2002 muffler

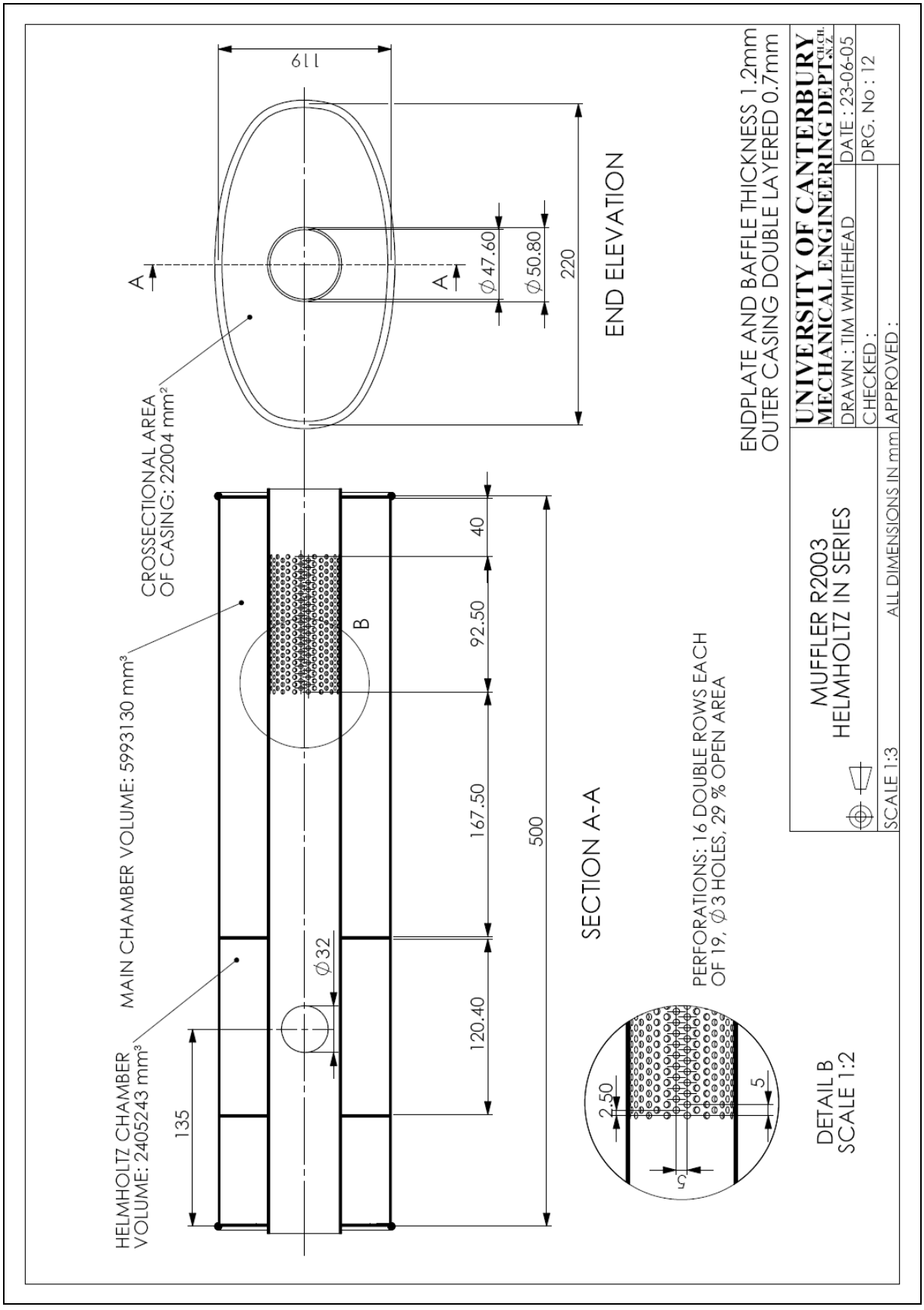

Figure A-12 R2003 muffler

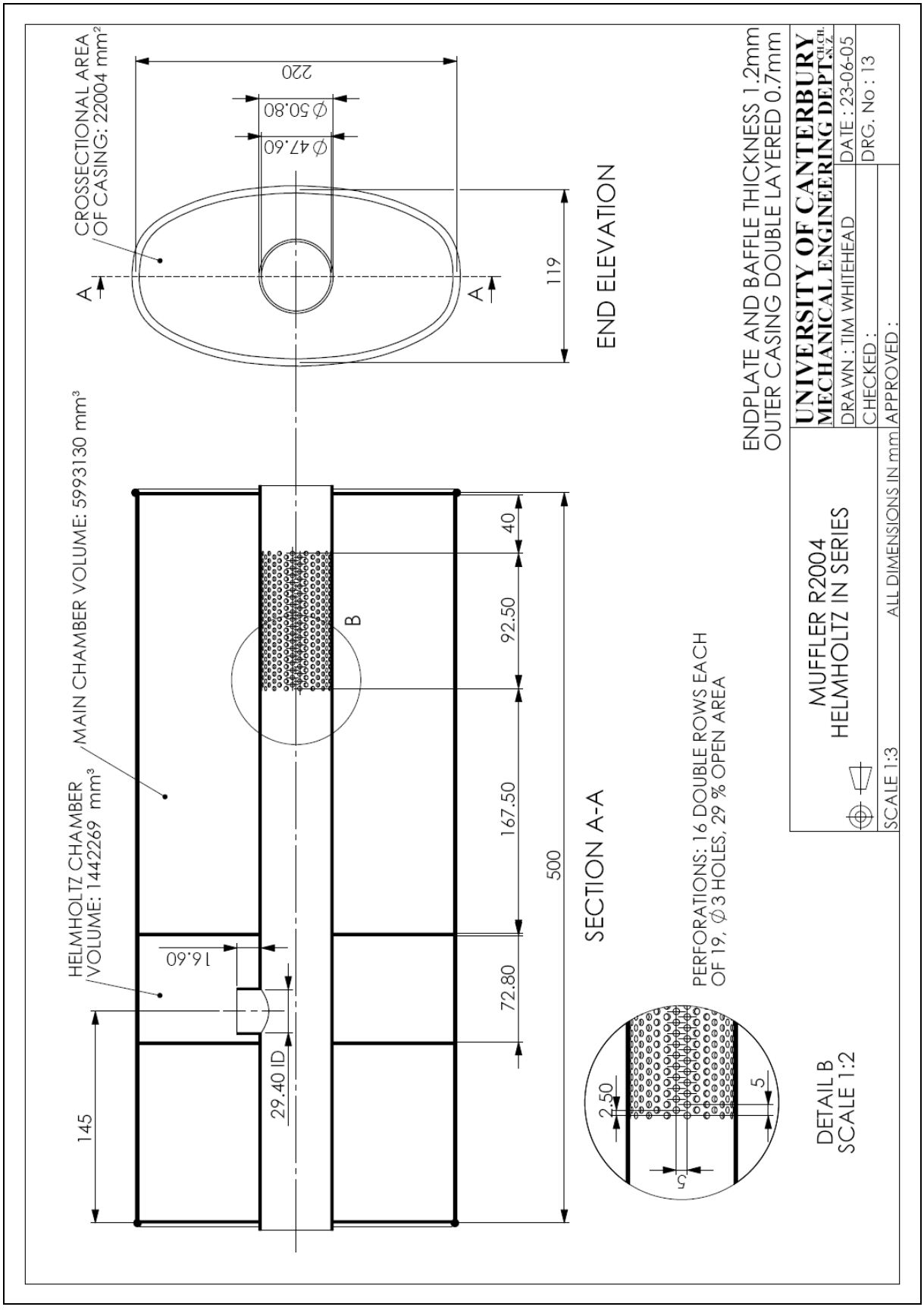

Figure A-13 R2004 muffler

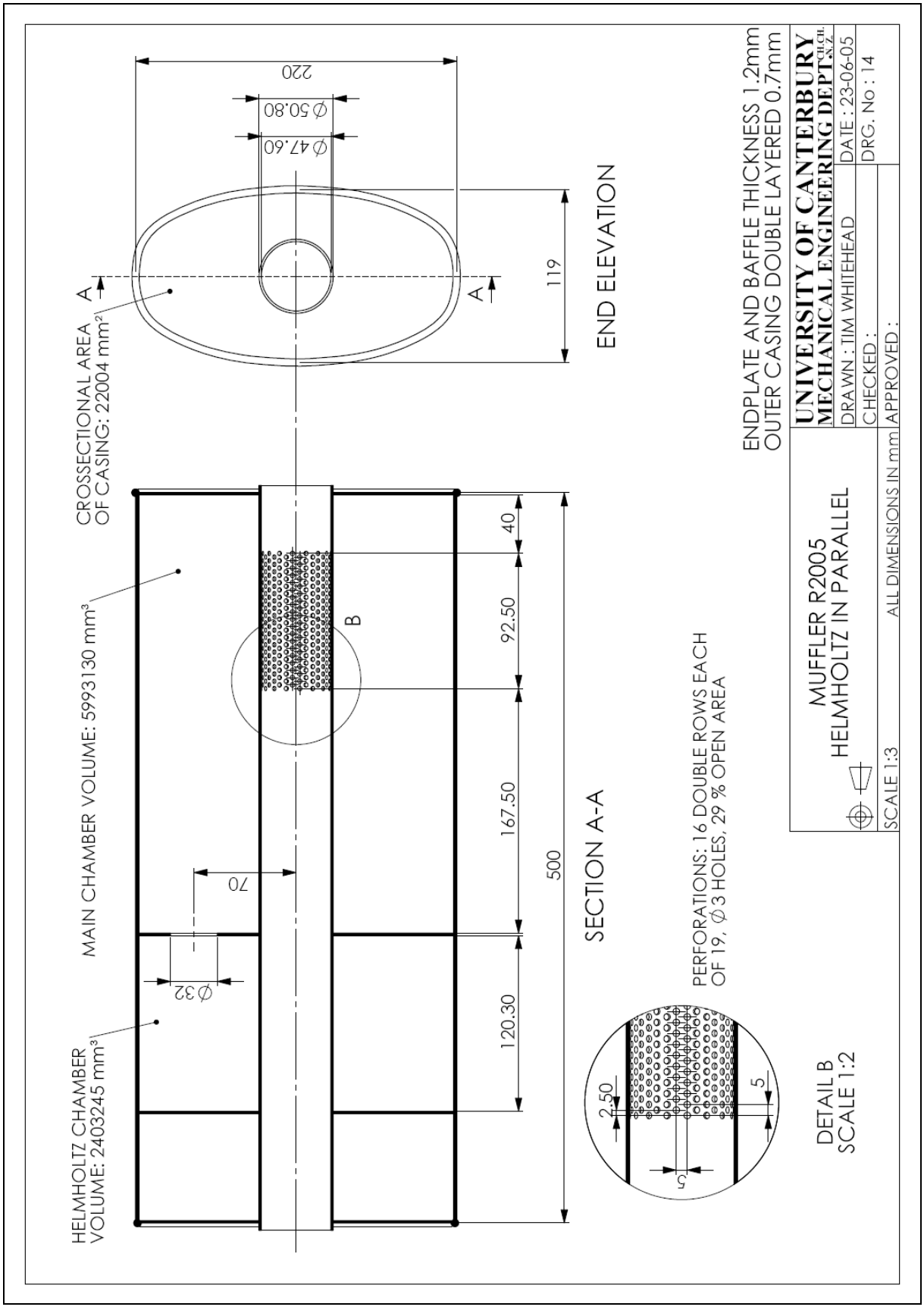

Figure A-14 R2005 muffler

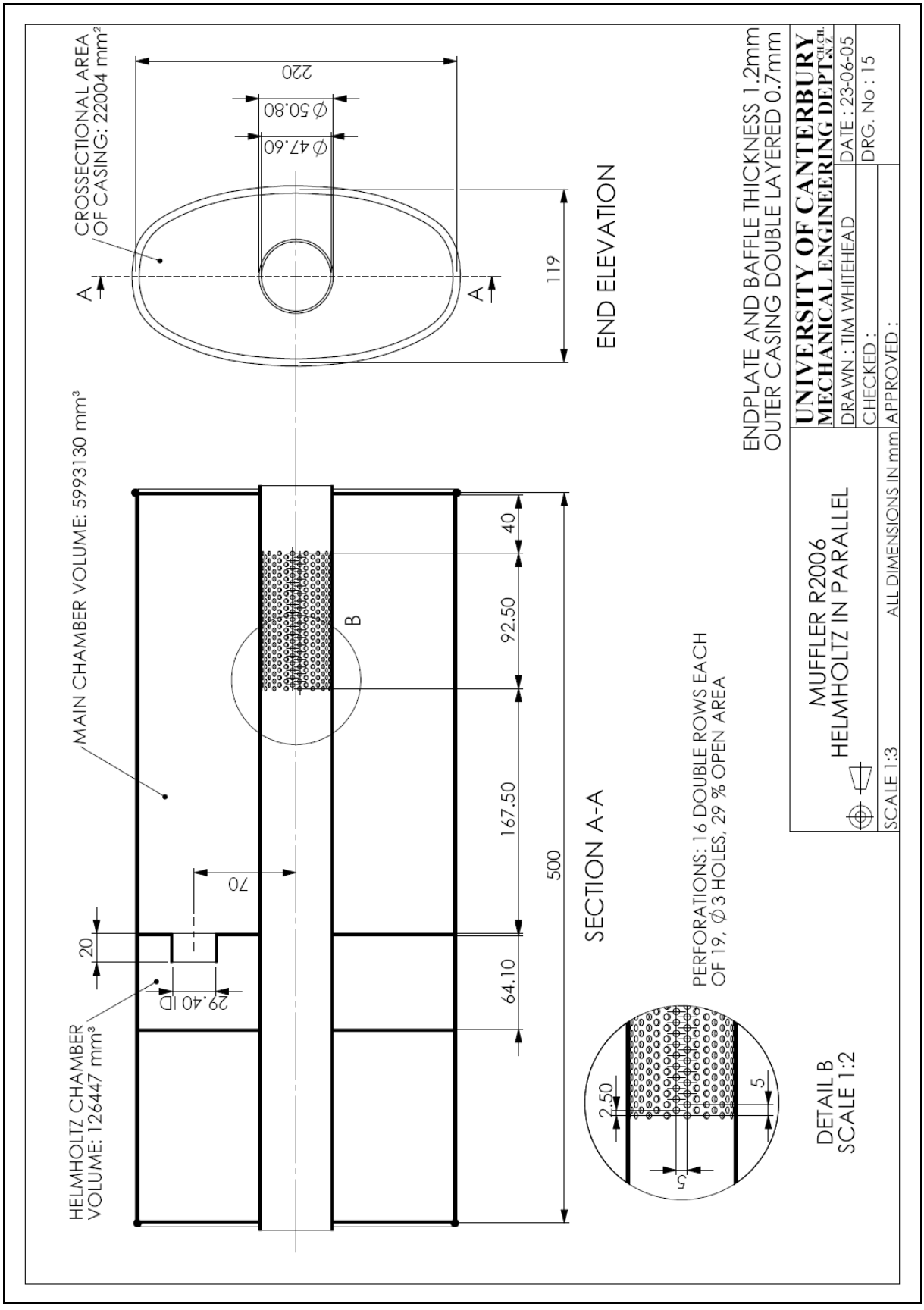

Figure A-15 R2006 muffler

Appendix B
Experimental Results

This appendix contains the predicted and measured insertion loss of all the muffler systems tested. Data was gathered for each muffler system from 1000 to 5000 RPM at increments of 500 RPM. Due to the large amount of data gathered, results are only shown for with the engine as the noise source at 1000, 3000 and 5000 RPM, and with the speaker as the noise source (on 1000 RPM graph).

Table of contents

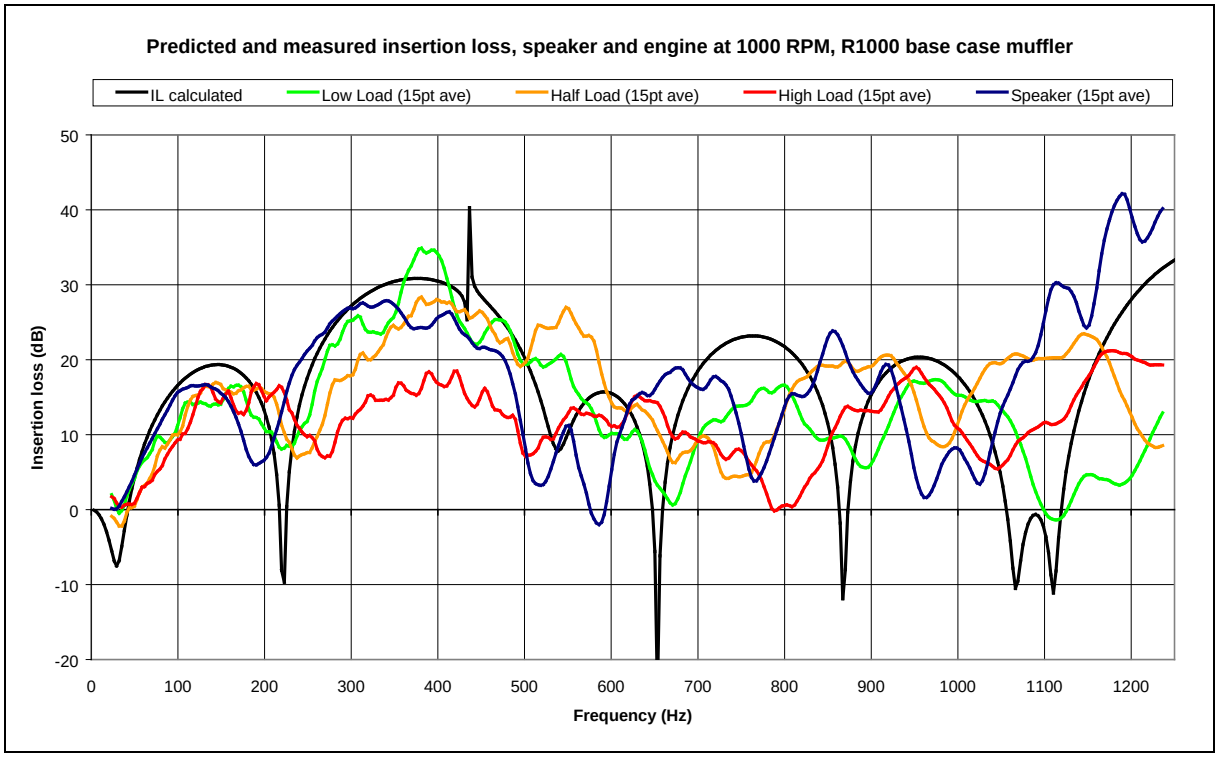

Figure B-1 Predicted and measured insertion loss, speaker and engine at 1000 RPM, R1000 base case muffler

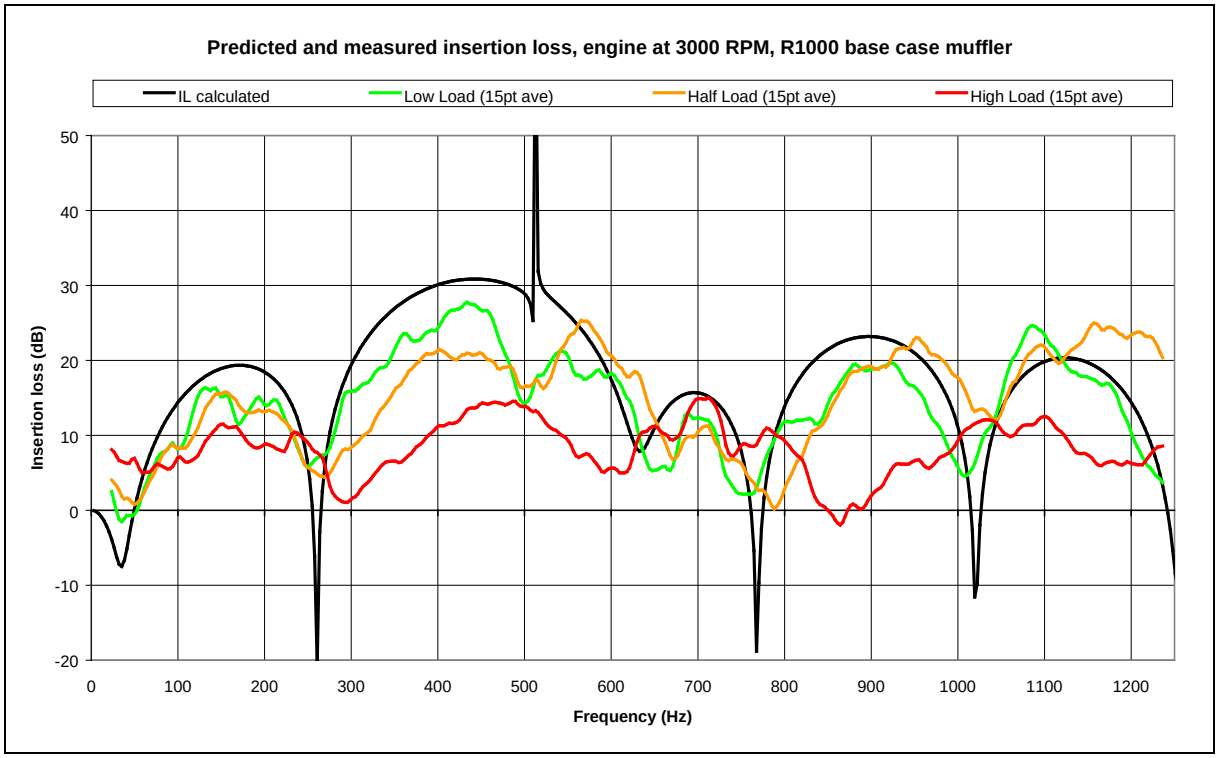

Figure B-2 Predicted and measured insertion loss, engine at 3000 RPM, R1000 base case muffler

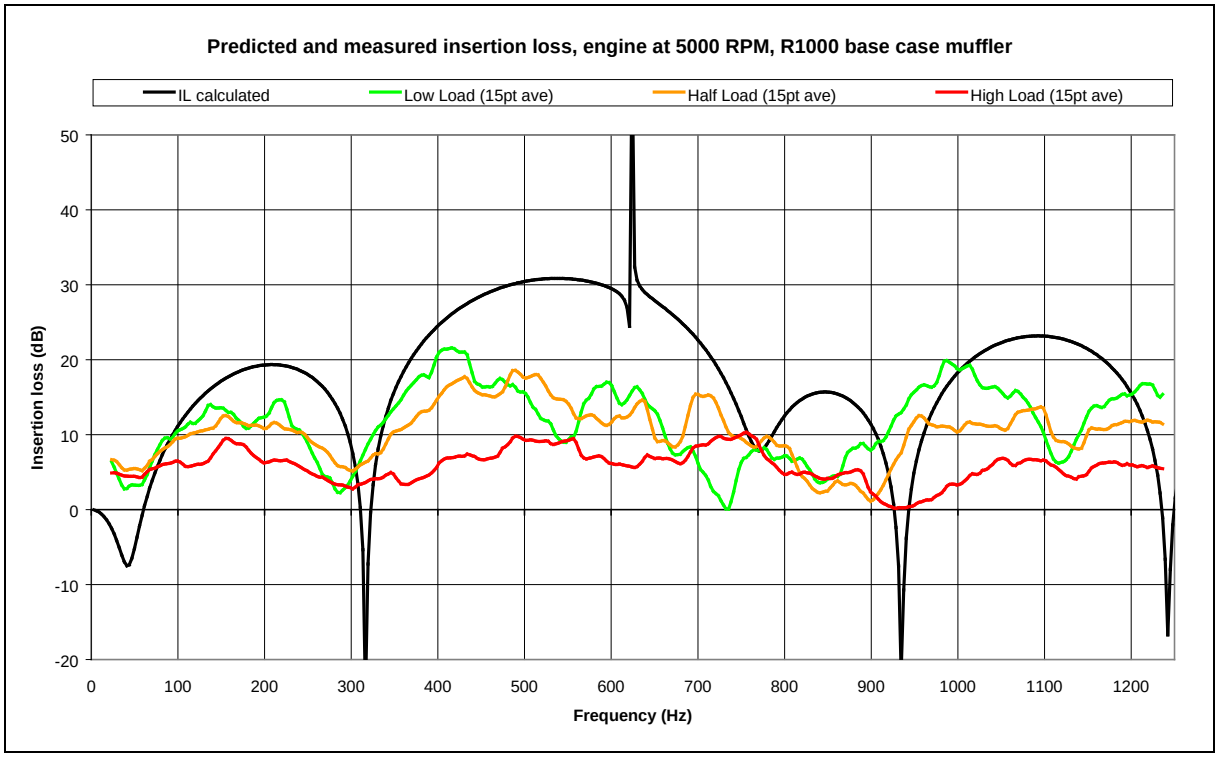

Figure B-3 Predicted and measured insertion loss, engine at 5000 RPM, R1000 base case muffler

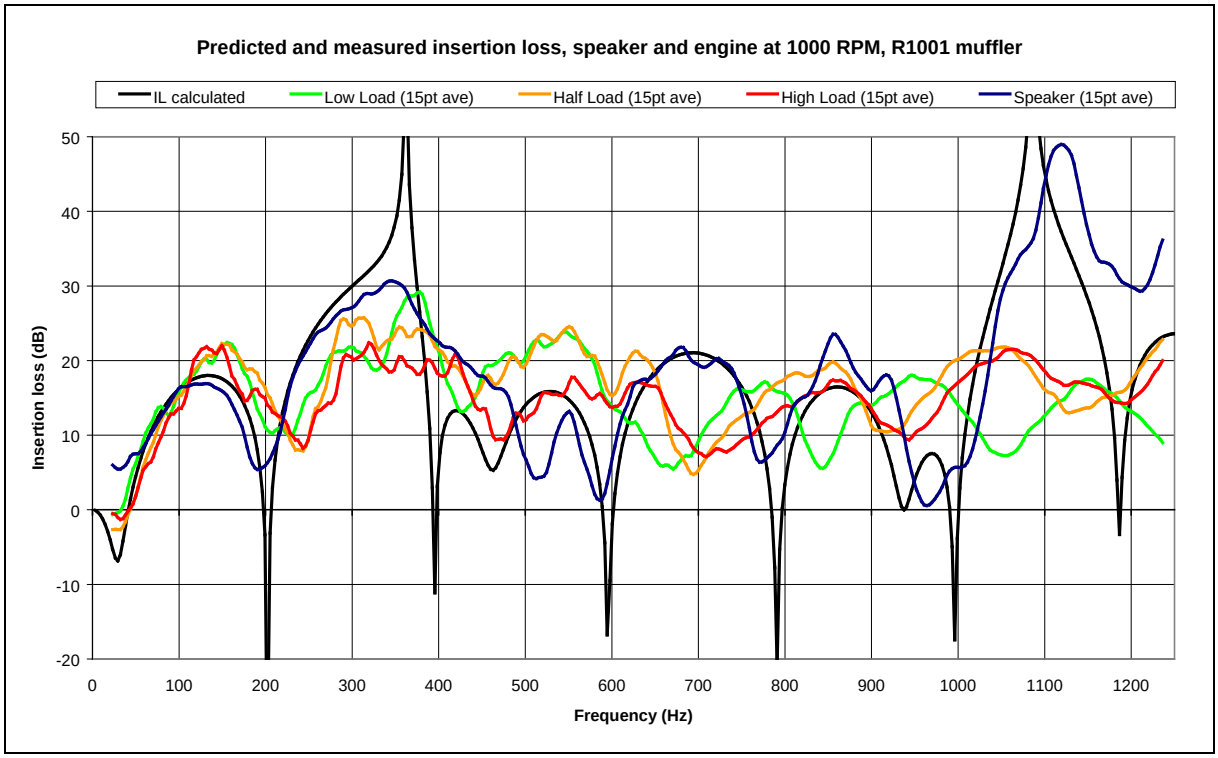

Figure B-4 Predicted and measured insertion loss, engine at 1000 RPM, R1001 muffler

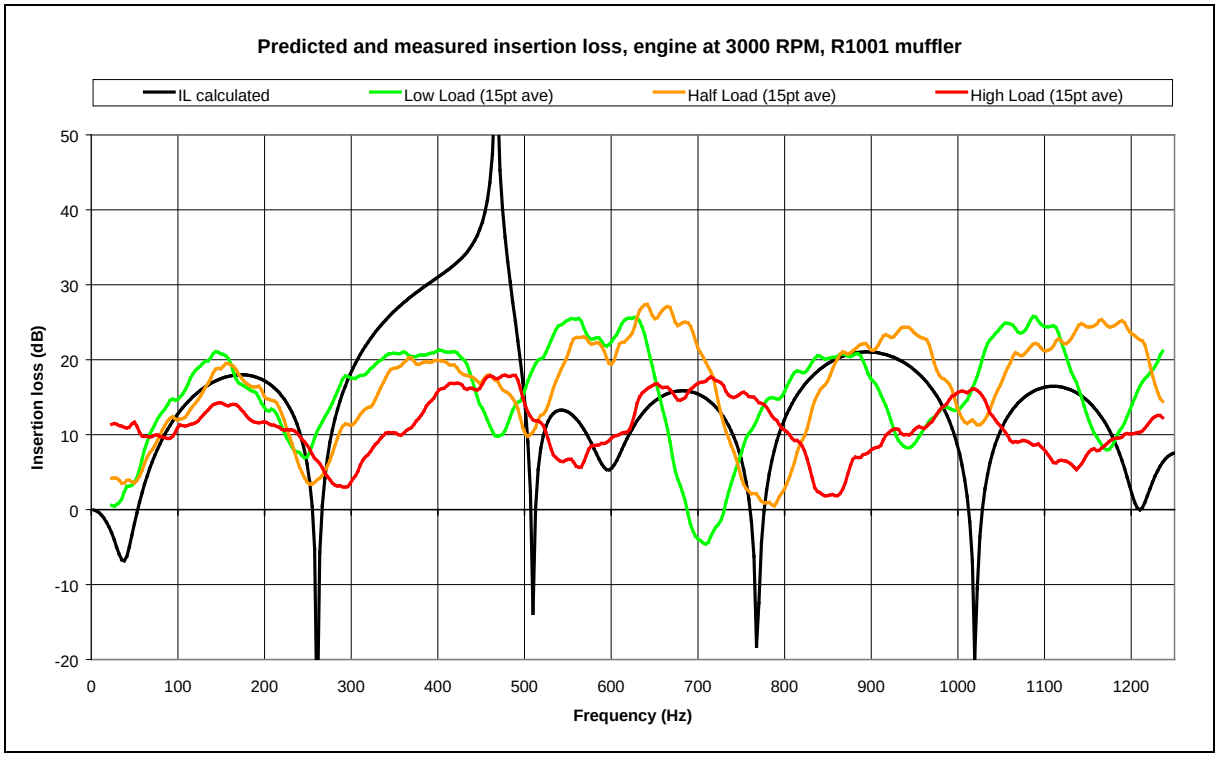

Figure B-5 Predicted and measured insertion loss, engine at 3000 RPM, R1001 muffler

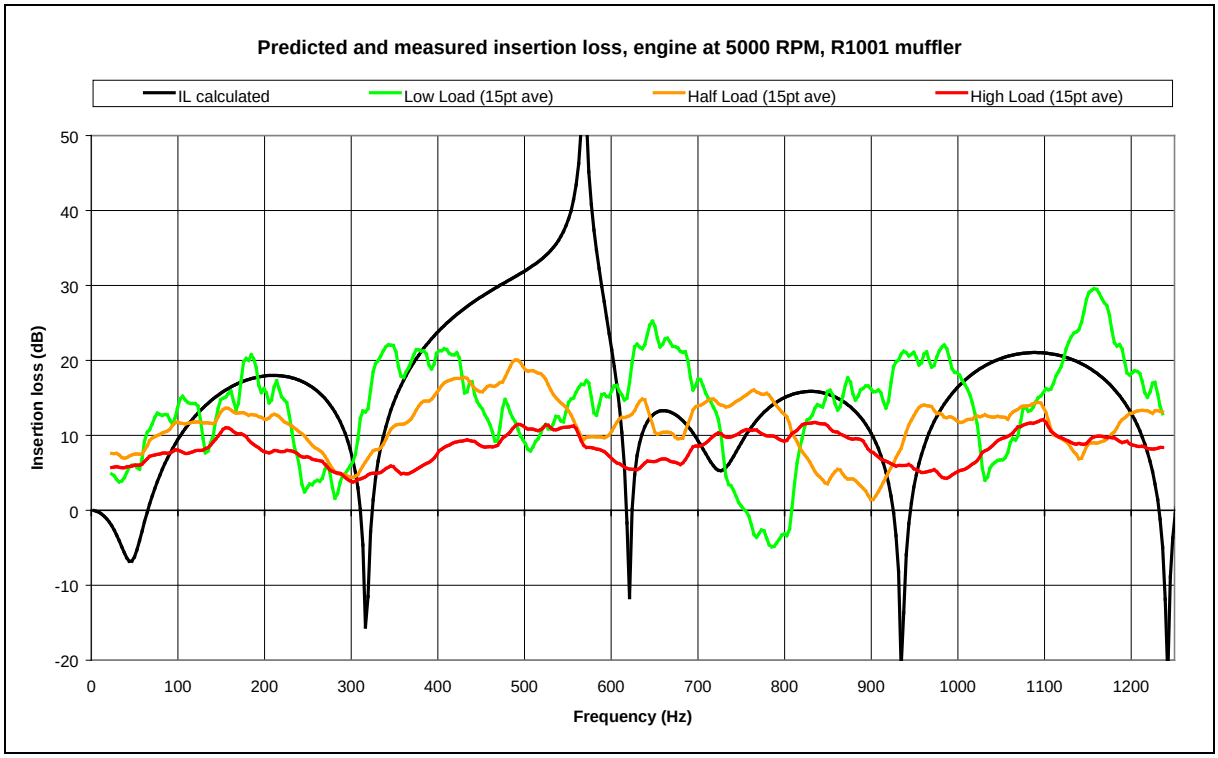

Figure B-6 Predicted and measured insertion loss, engine at 5000 RPM, R1001 muffler

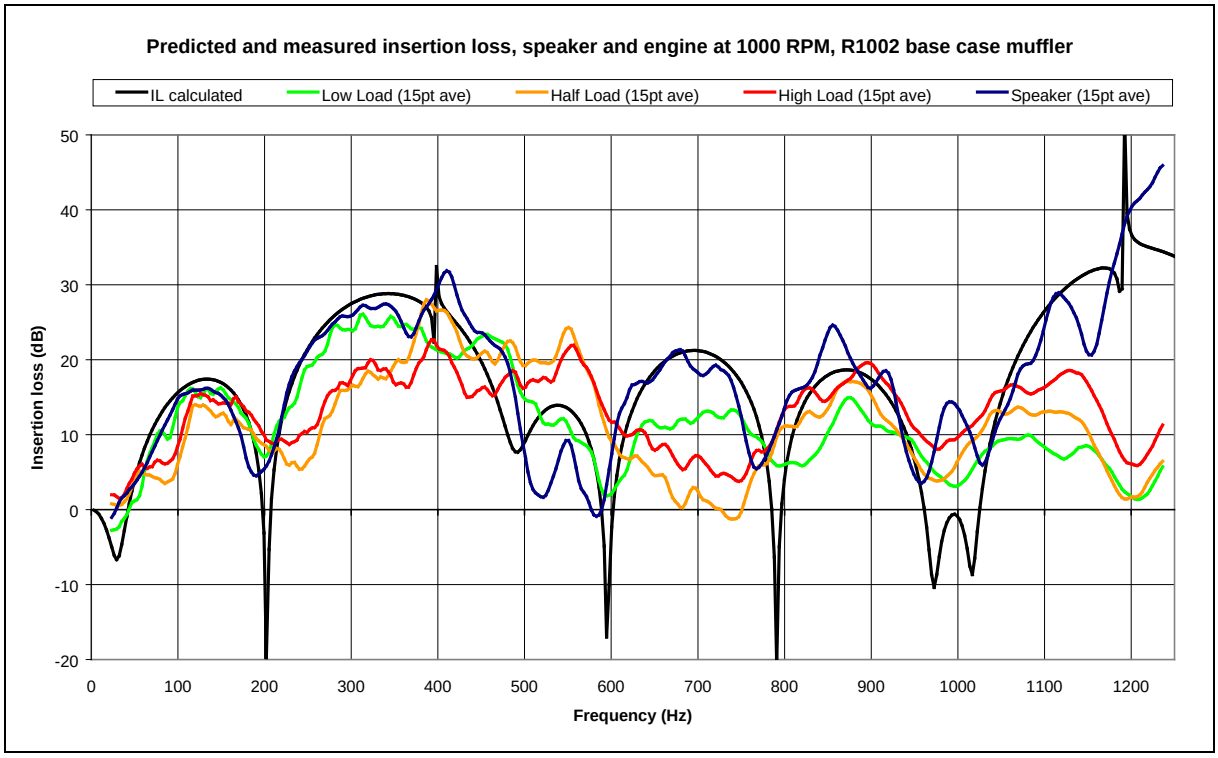

Figure B-7 Predicted and measured insertion loss, speaker and engine at 1000 RPM, R1002 base case muffler

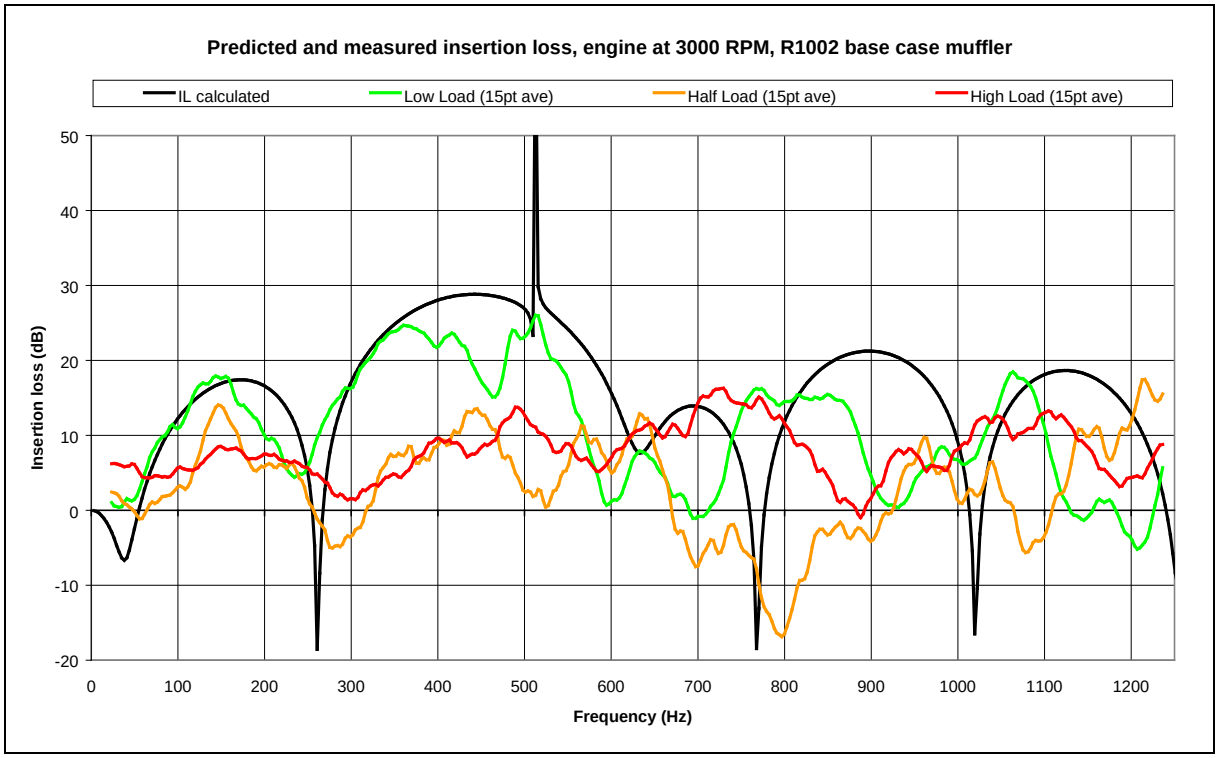

Figure B-8 Predicted and measured insertion loss, engine at 3000 RPM, R1002 base case muffler

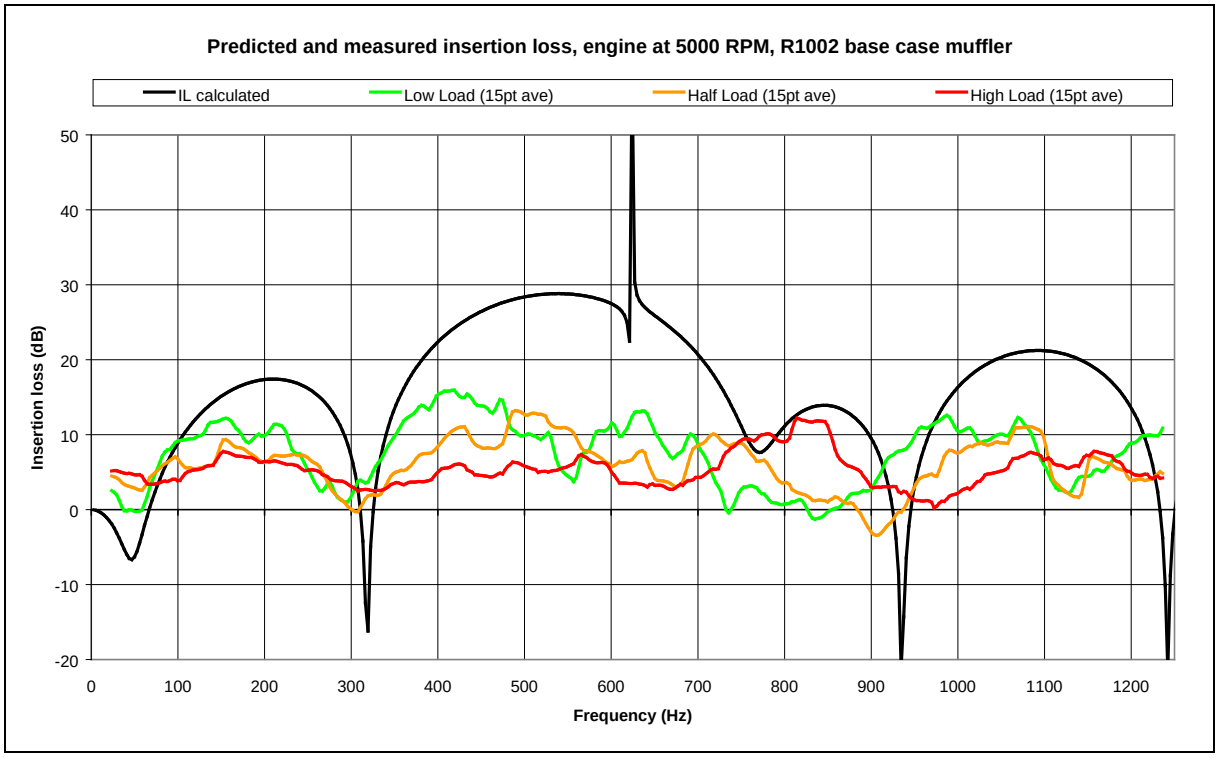

Figure B-9 Predicted and measured insertion loss, engine at 5000 RPM, R1002 base case muffler

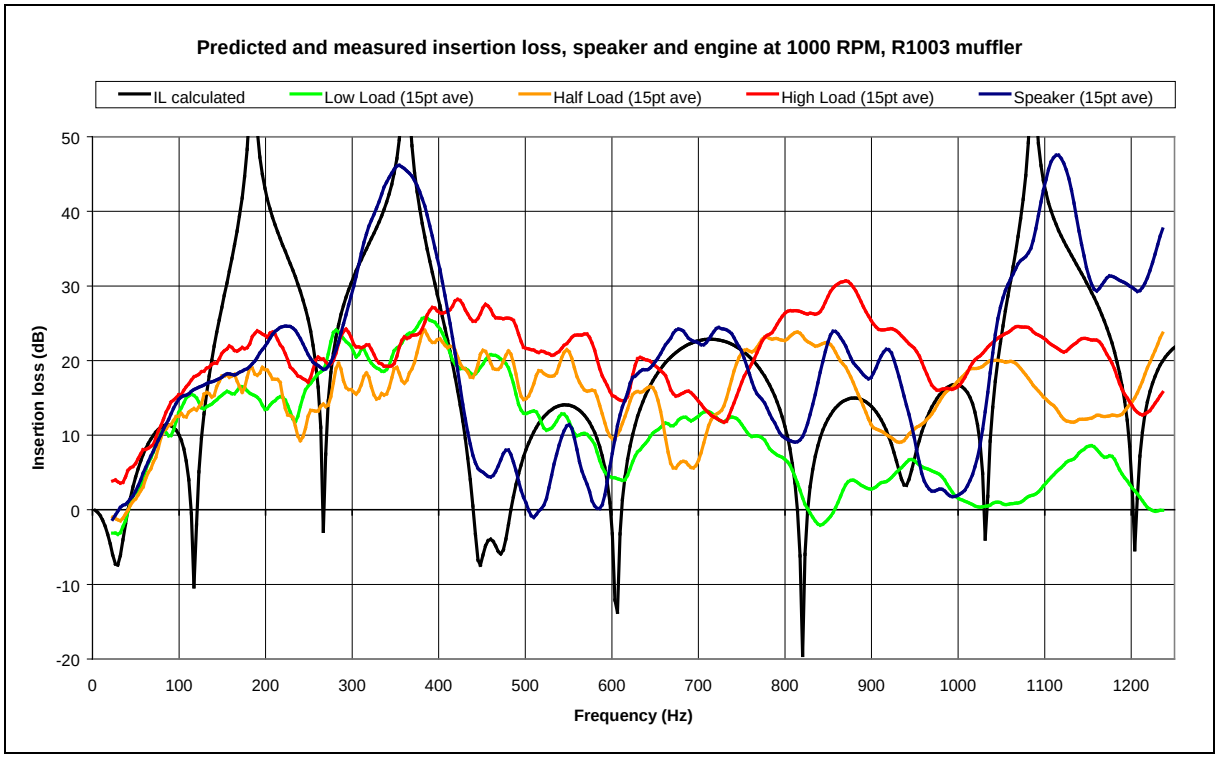

Figure B-10 Predicted and measured insertion loss, speaker and engine at 1000 RPM, R1003 muffler

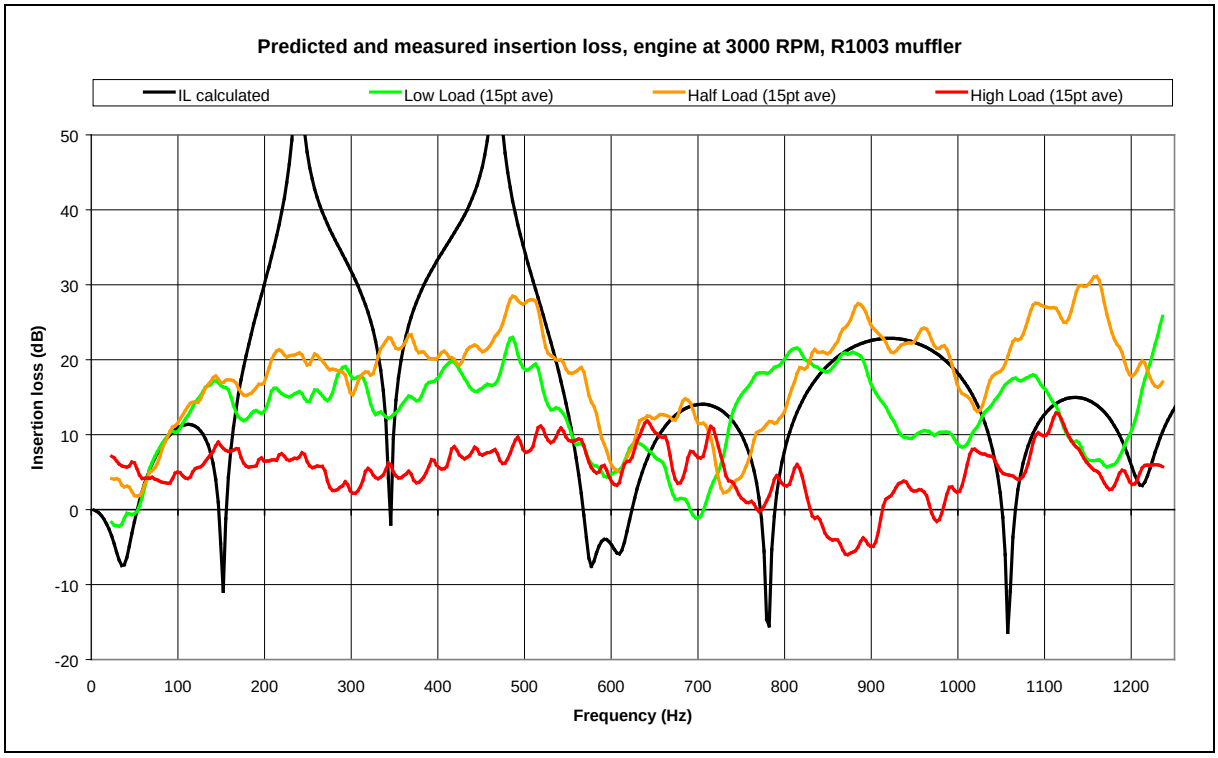

Figure B-11 Predicted and measured insertion loss, engine at 3000 RPM, R1003 muffler

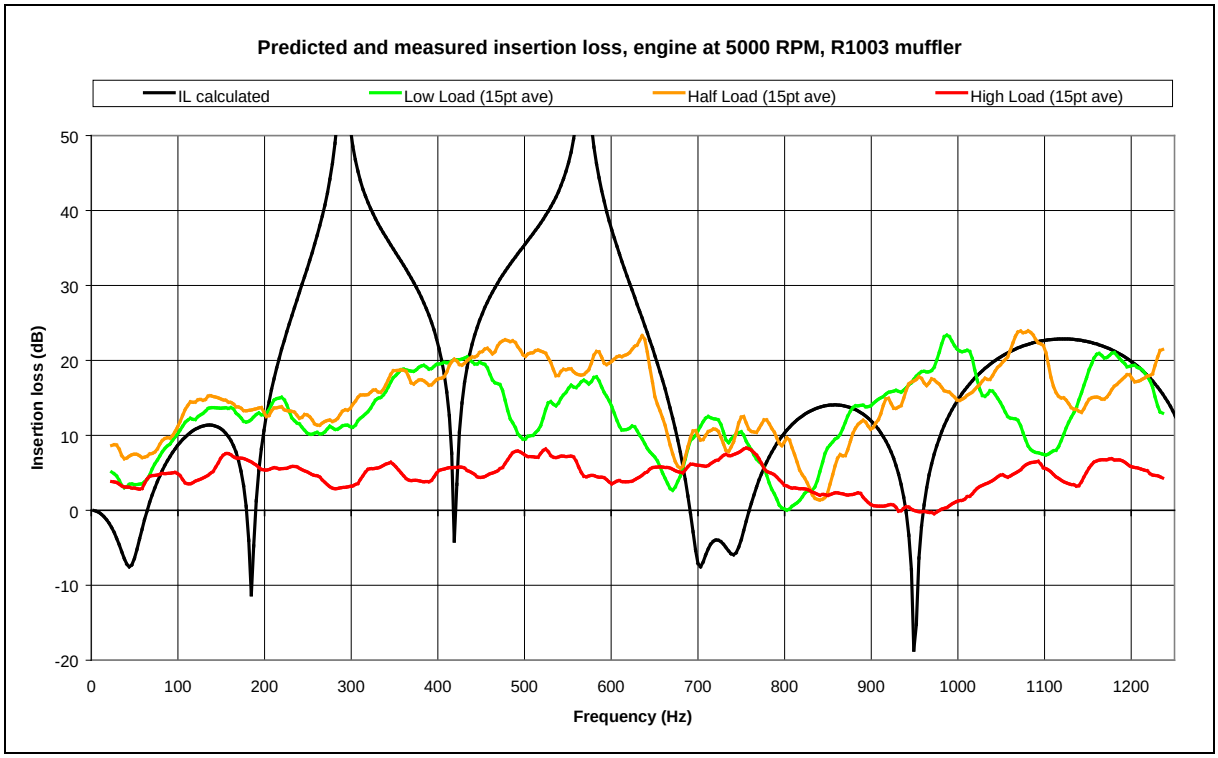

Figure B-12 Predicted and measured insertion loss, engine at 5000 RPM, R1003 muffler

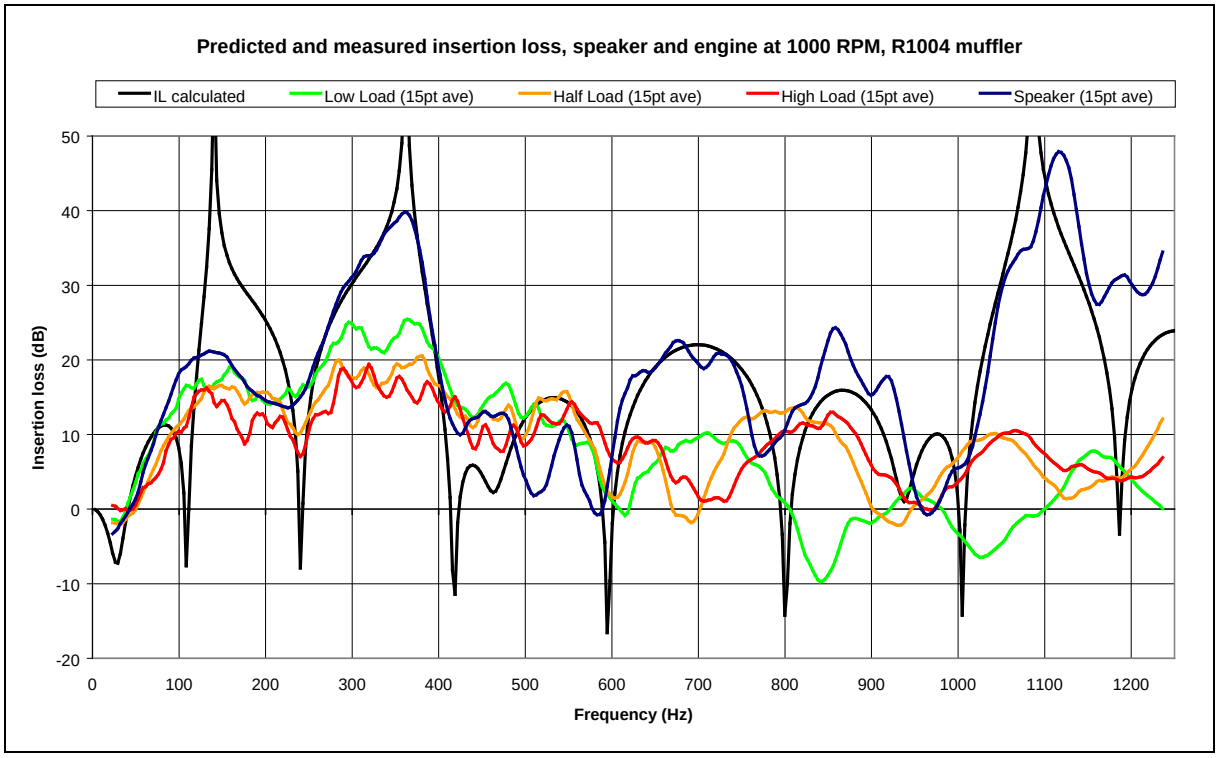

Figure B-13 Predicted and measured insertion loss, speaker and engine at 1000 RPM, R1004 muffler

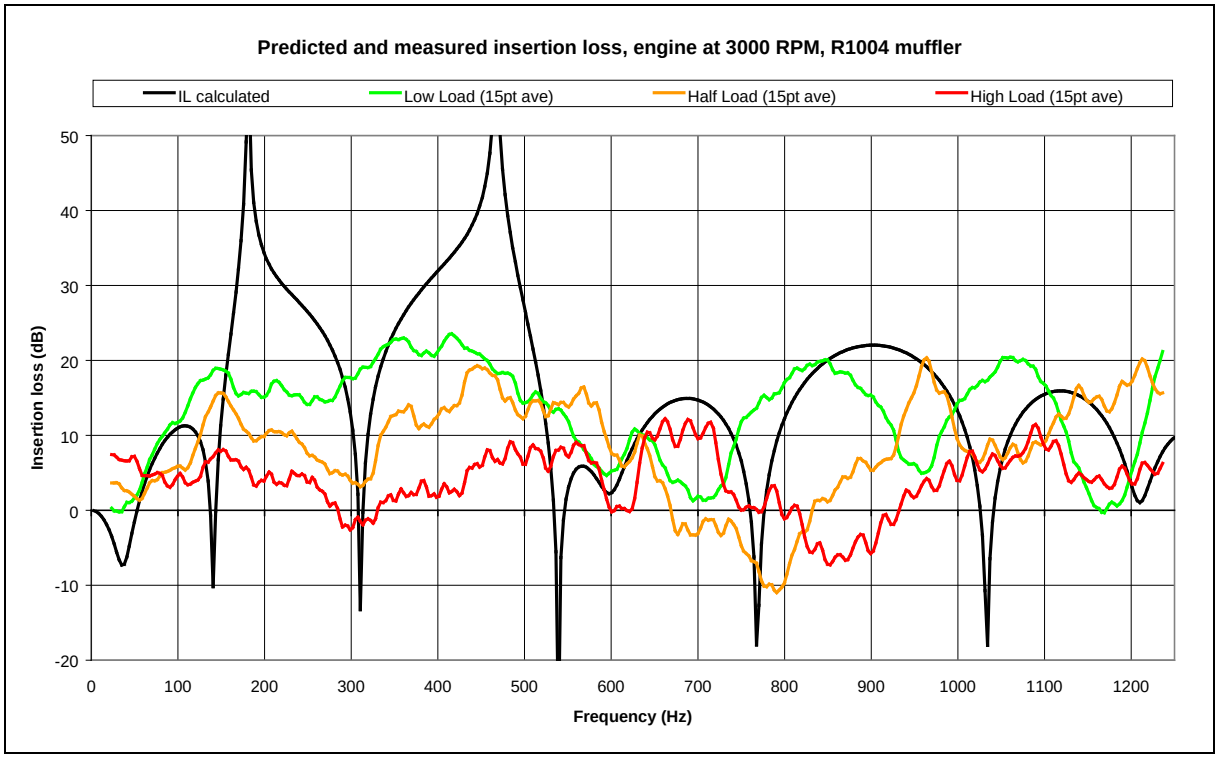

Figure B-14 Predicted and measured insertion loss, engine at 3000 RPM, R1004 muffler

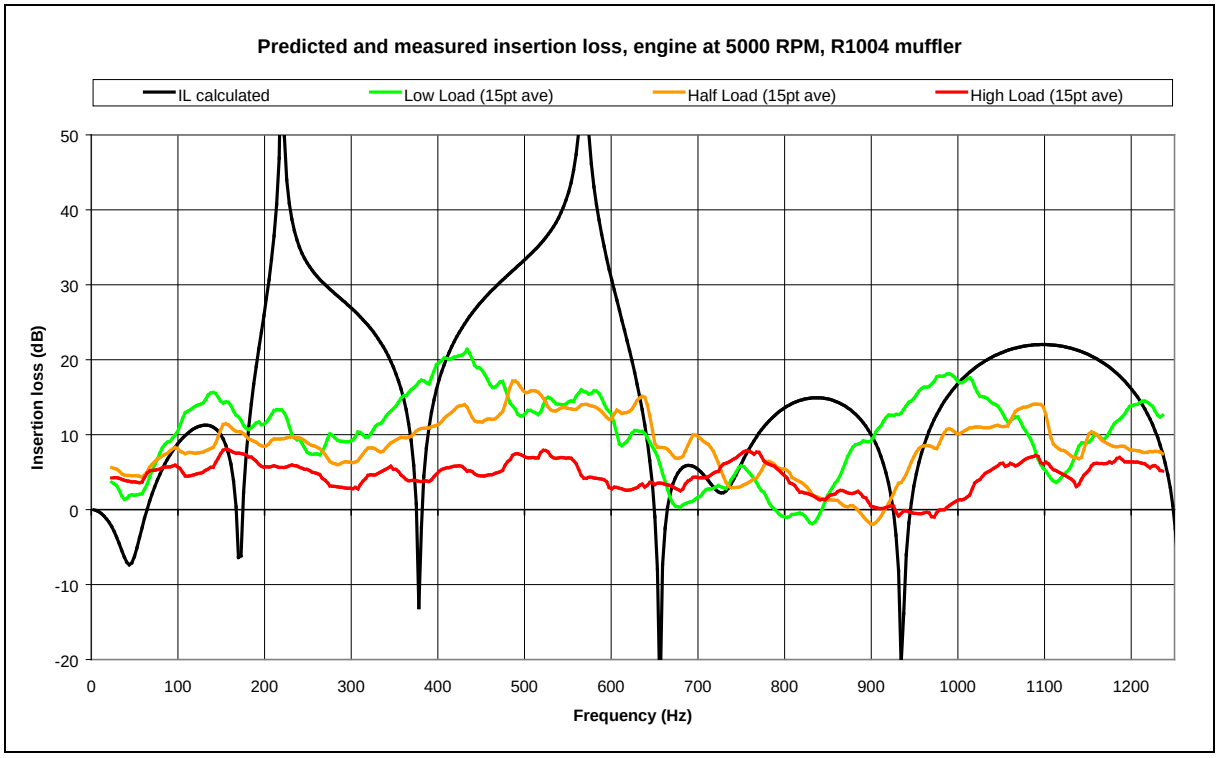

Figure B-15 Predicted and measured insertion loss, engine at 5000 RPM, R1004 muffler

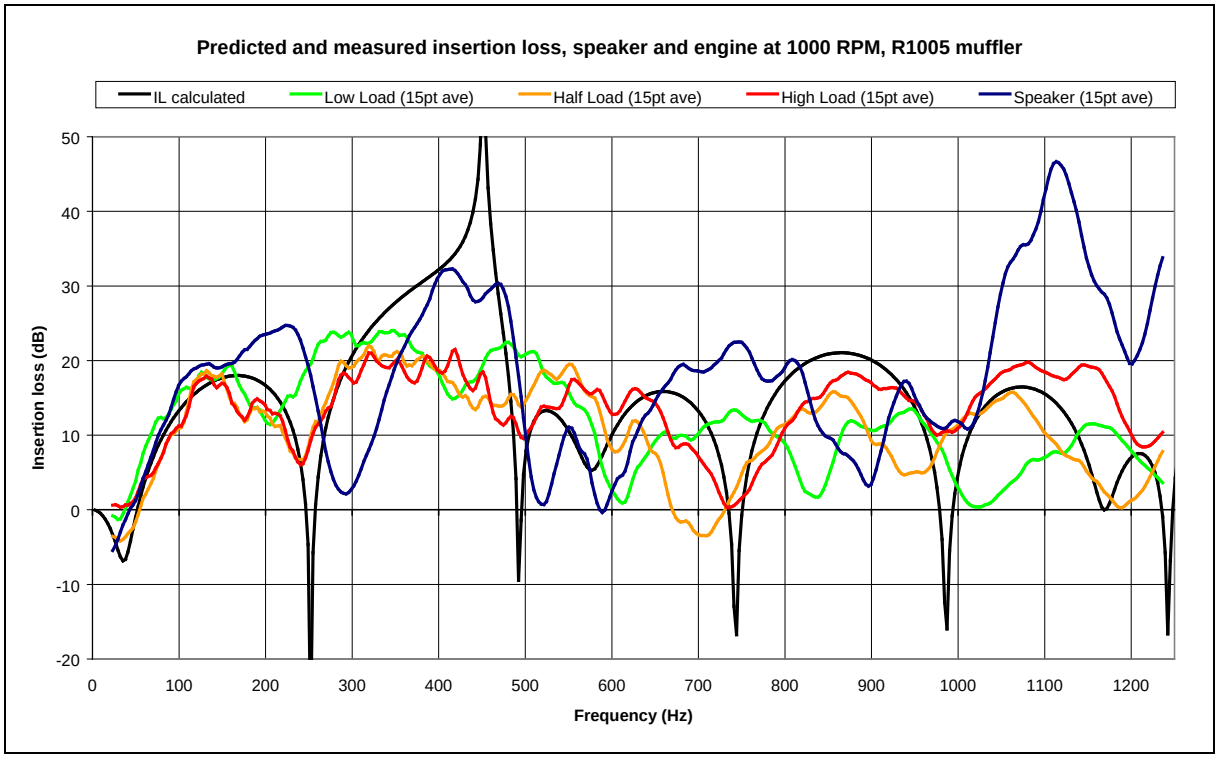

Figure B-16 Predicted and measured insertion loss, speaker and engine at 1000 RPM, R1005 muffler

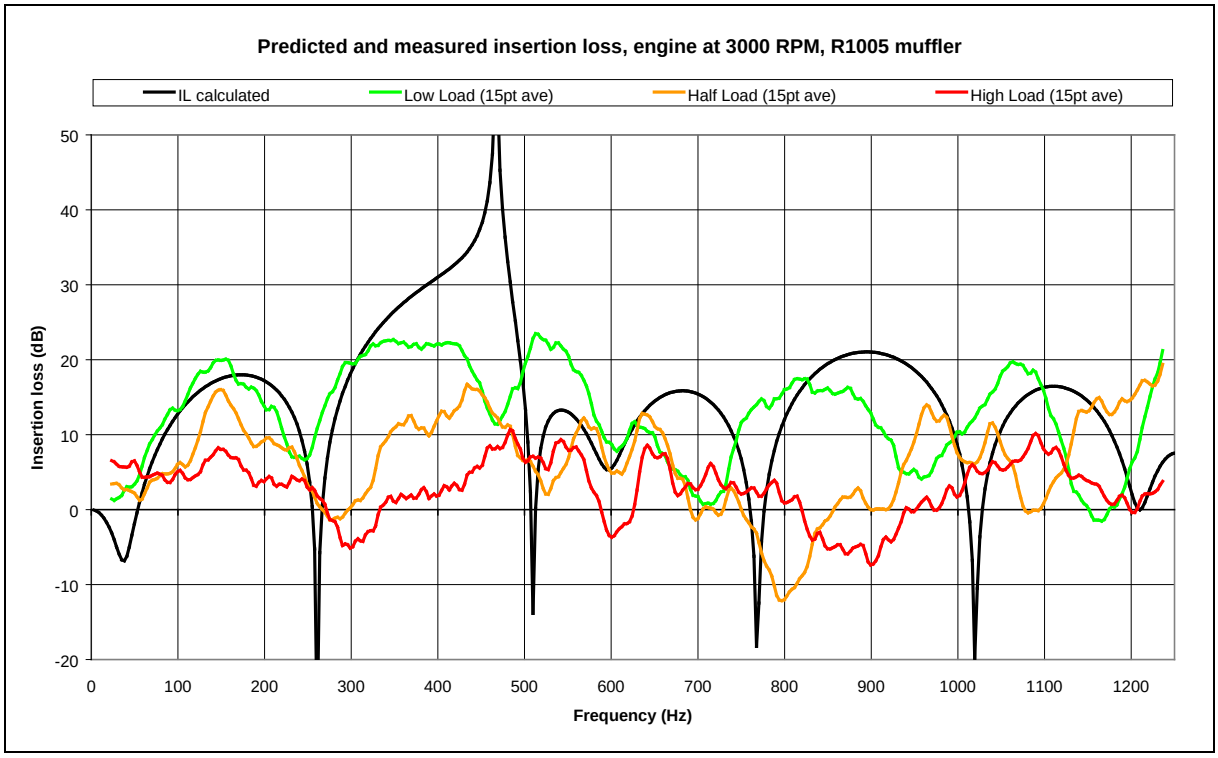

Figure B-17 Predicted and measured insertion loss, engine at 3000 RPM, R1005 muffler

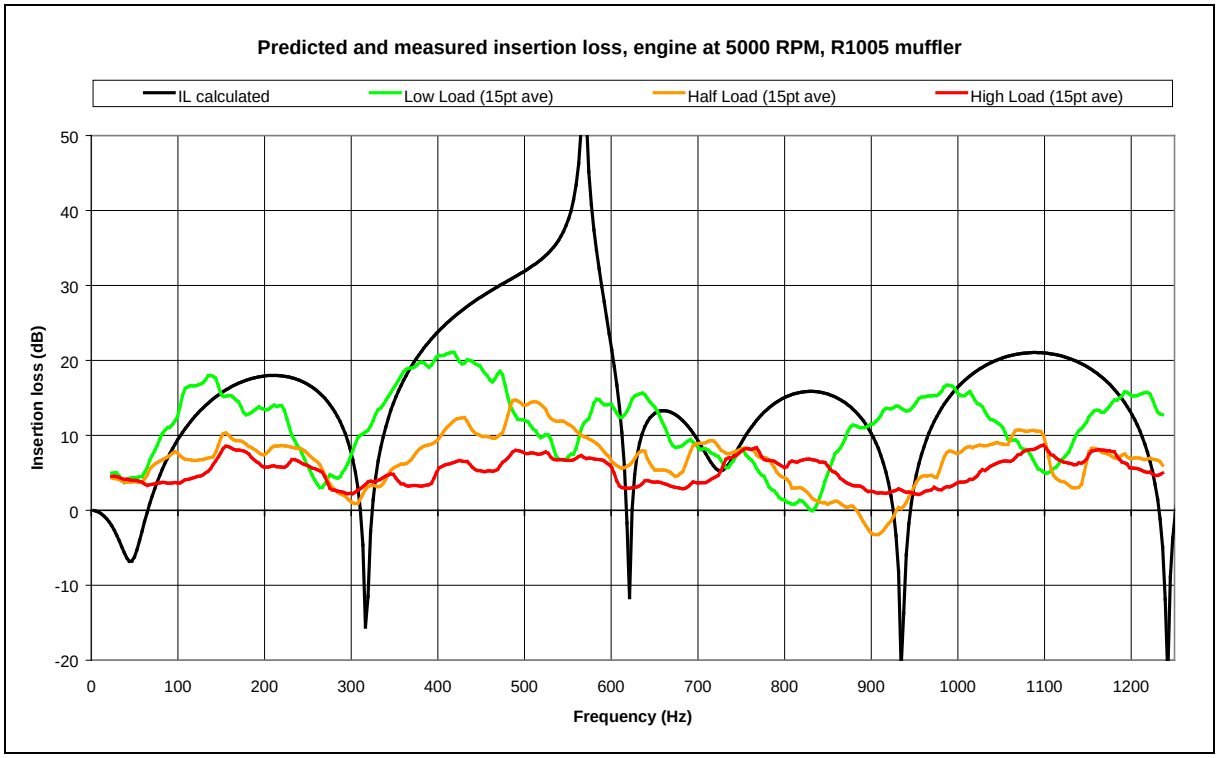

Figure B-18 Predicted and measured insertion loss, engine at 5000 RPM, R1005 muffler

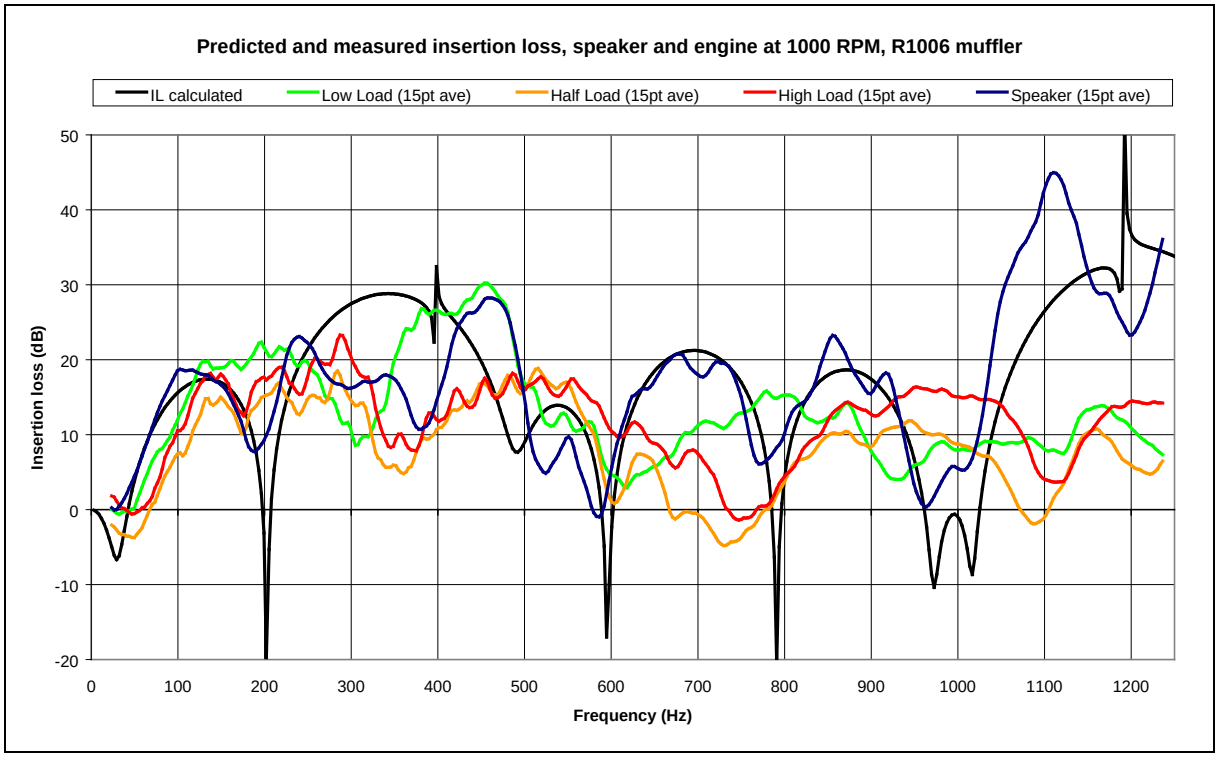

Figure B-19 Predicted and measured insertion loss, speaker and engine at 1000 RPM, R1006 muffler

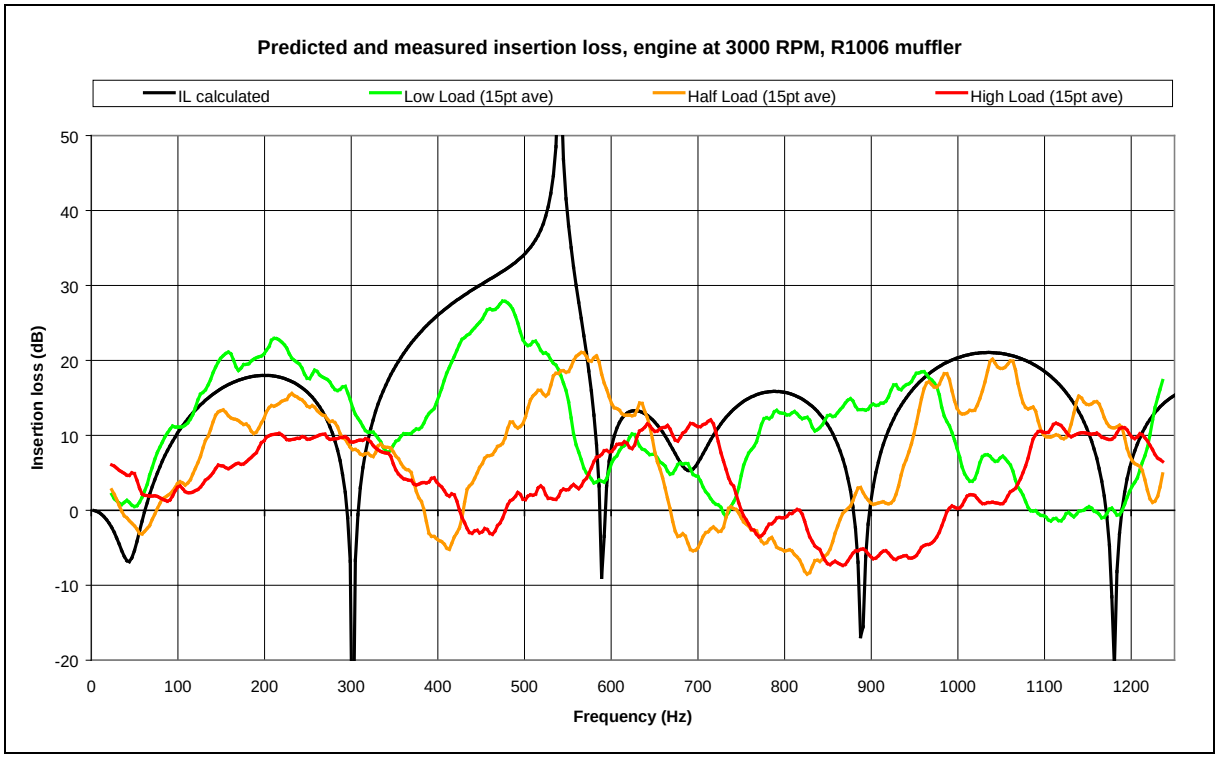

Figure B-20 Predicted and measured insertion loss, engine at 3000 RPM, R1006 muffler

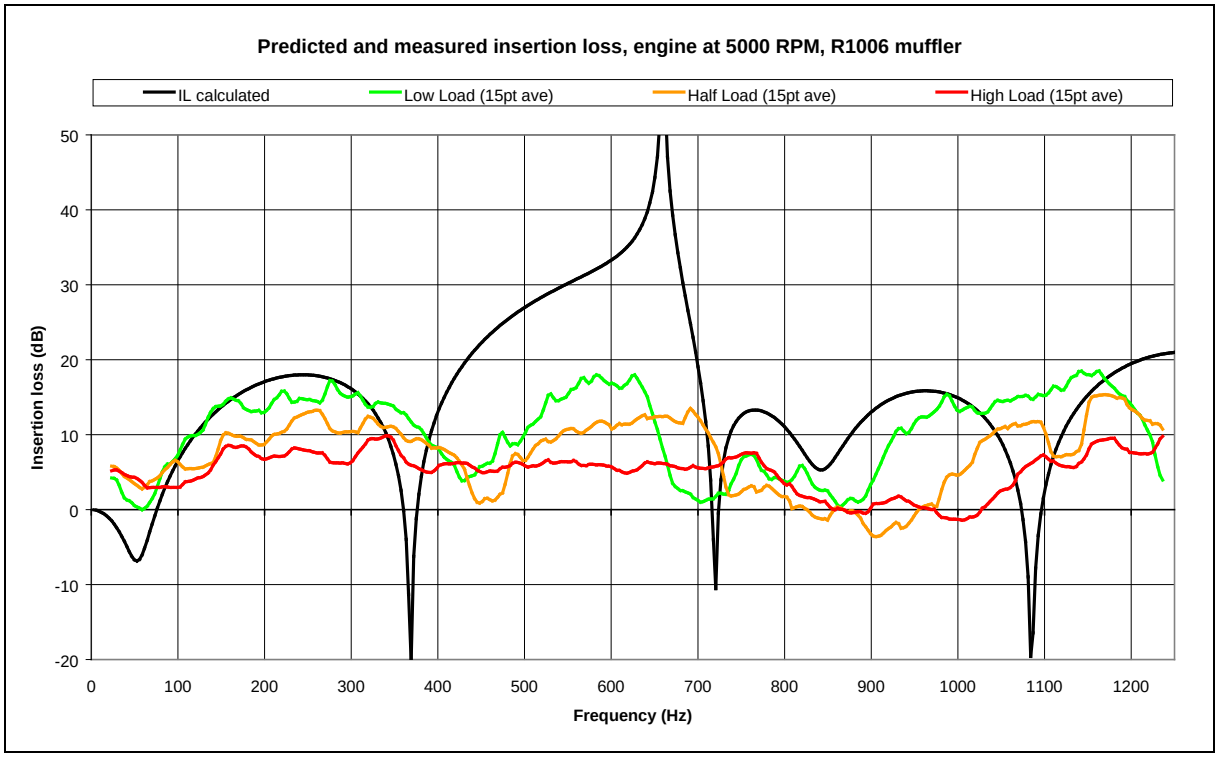

Figure B-21 Predicted and measured insertion loss, engine at 5000 RPM, R1006 muffler

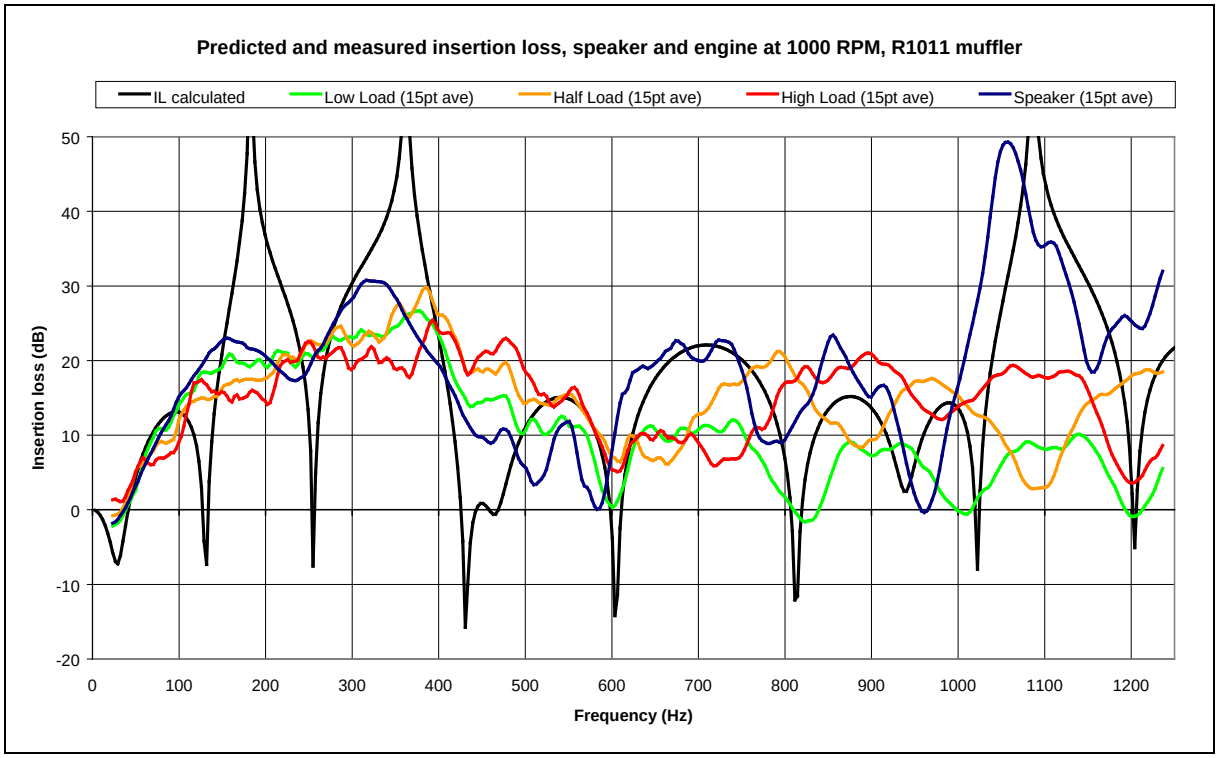

Figure B-22 Predicted and measured insertion loss, speaker and engine at 1000 RPM, R1011 muffler

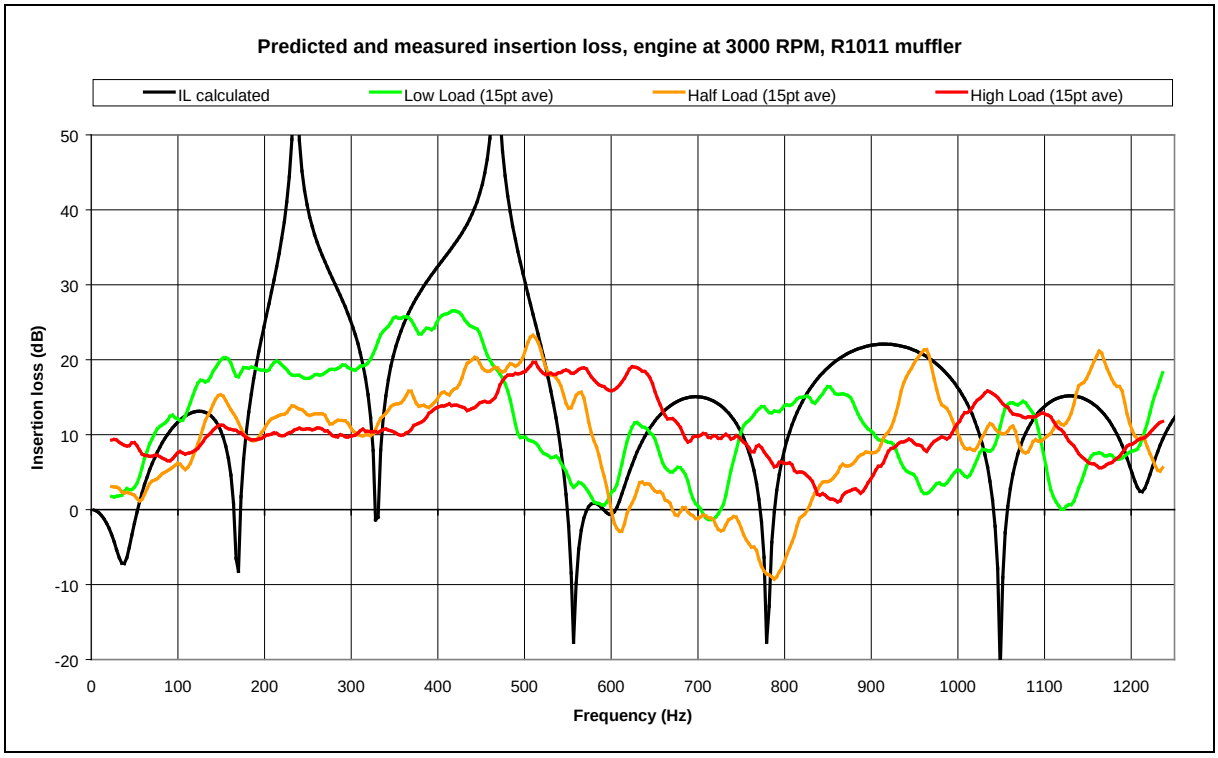

Figure B-23 Predicted and measured insertion loss, engine at 3000 RPM, R1011 muffler

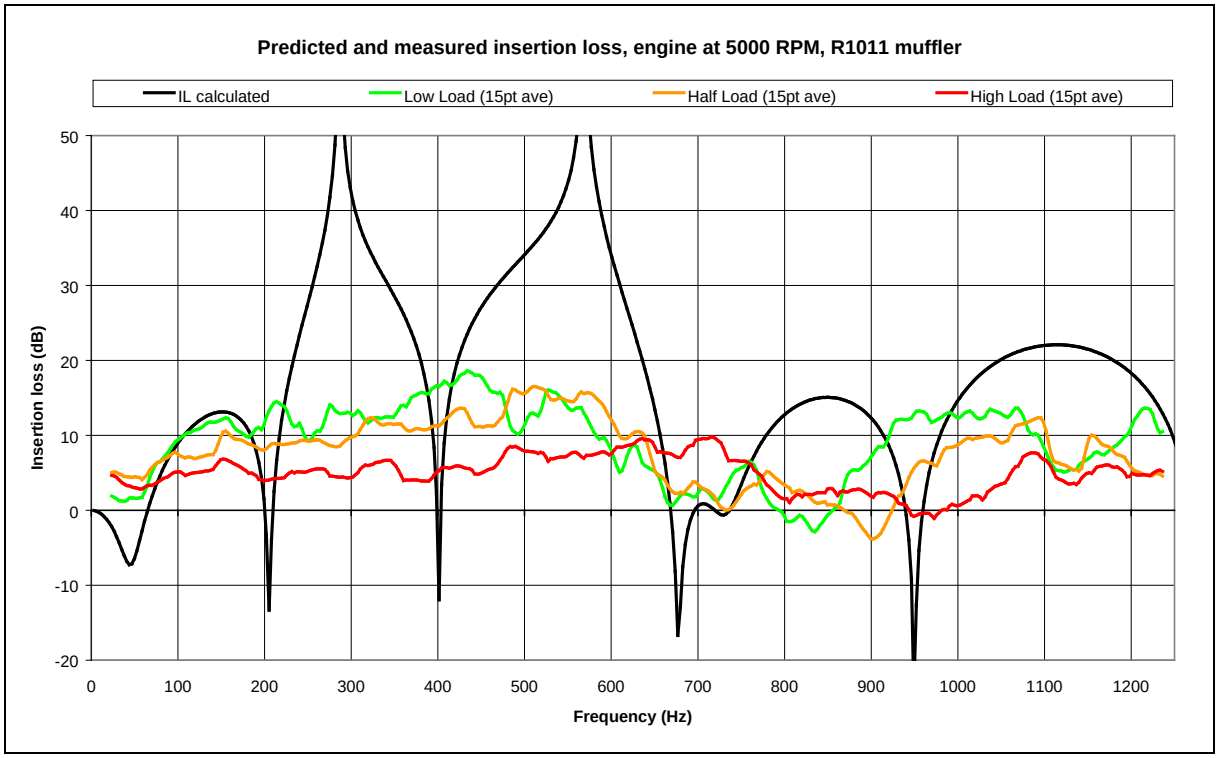

Figure B-24 Predicted and measured insertion loss, engine at 5000 RPM, R1011 muffler

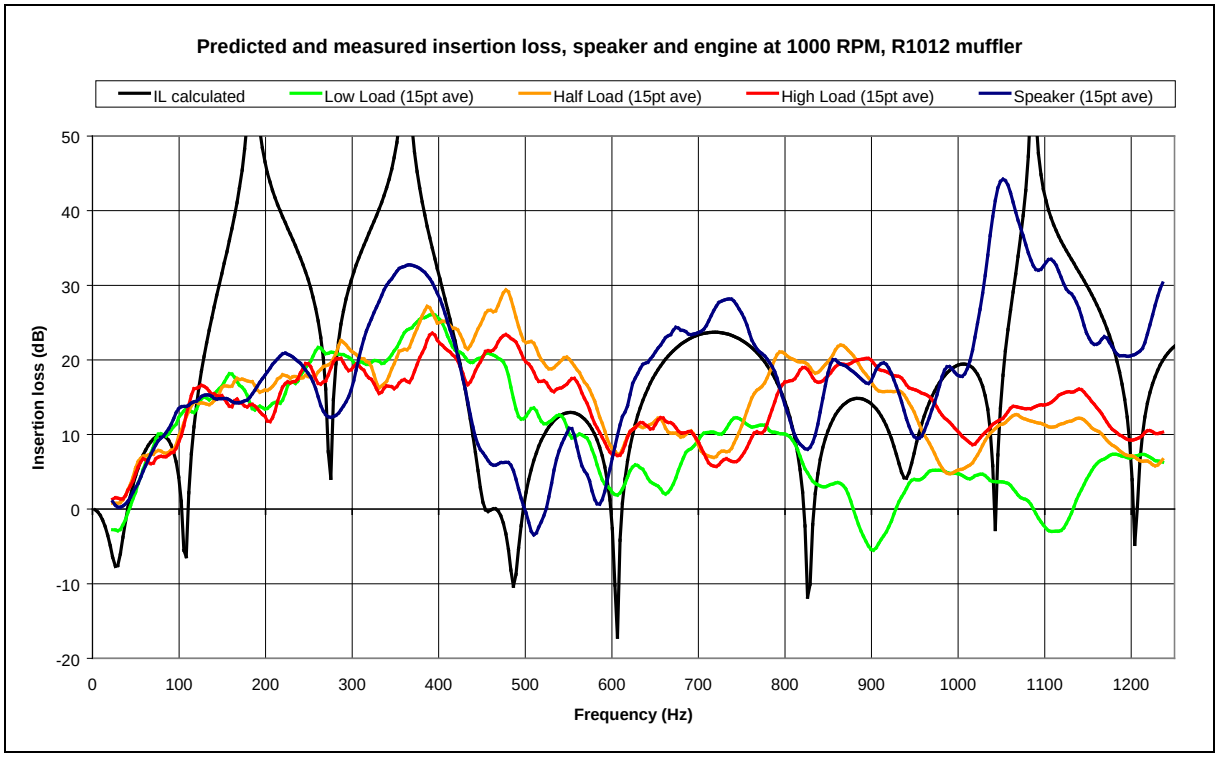

Figure B-25 Predicted and measured insertion loss, speaker and engine at 1000 RPM, R1012 muffler

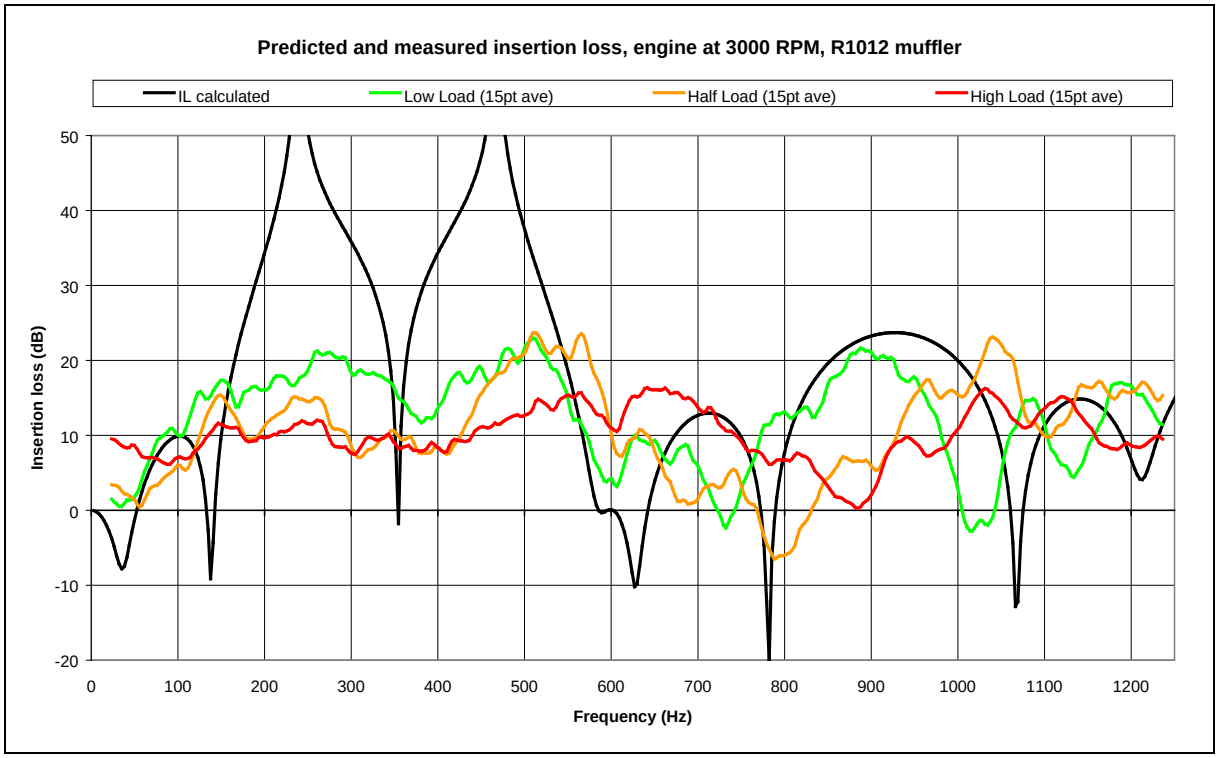

Figure B-26 Predicted and measured insertion loss, engine at 3000 RPM, R1012 muffler

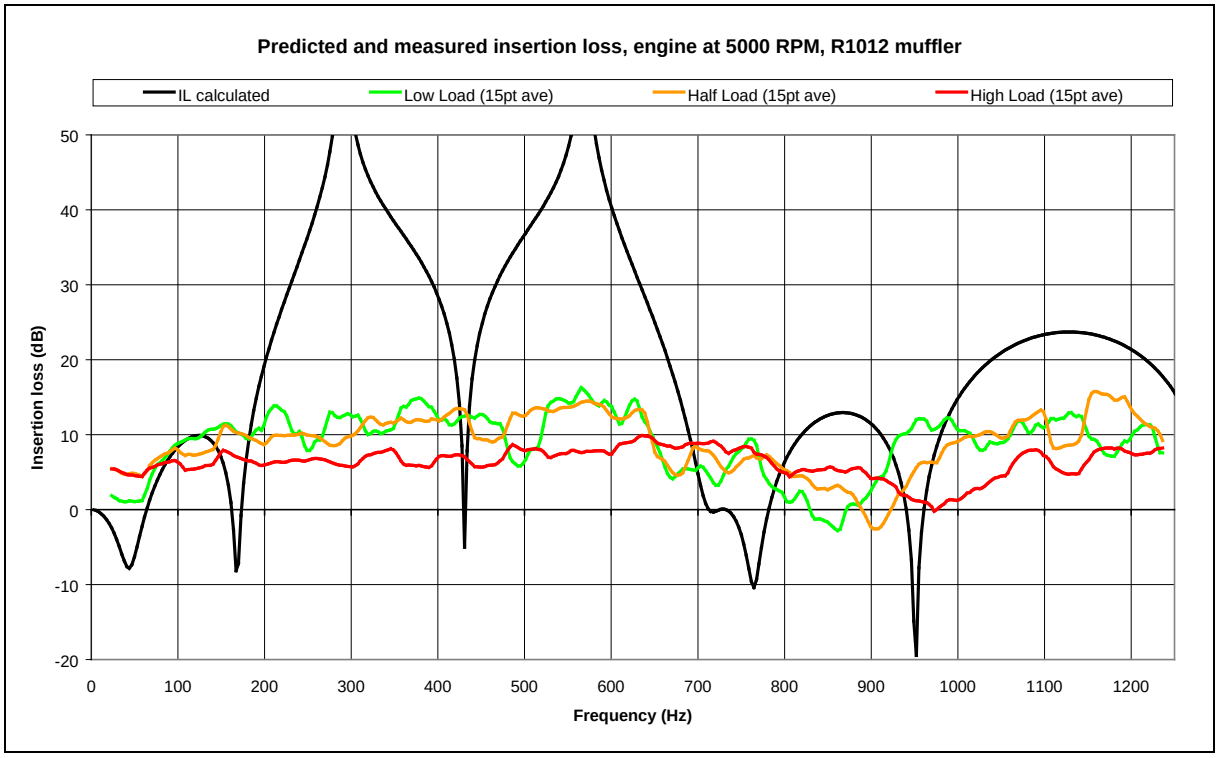

Figure B-27 Predicted and measured insertion loss, engine at 5000 RPM, R1012 muffler

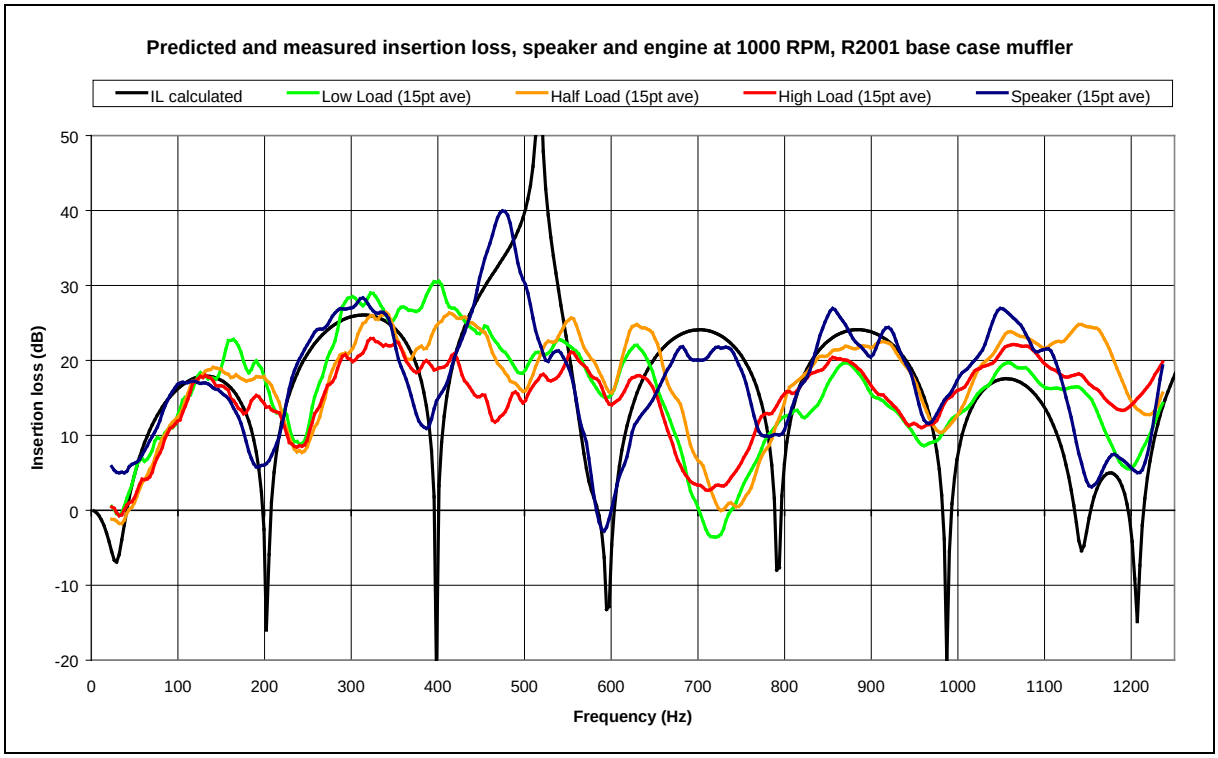

Figure B-28 Predicted and measured insertion loss, speaker and engine at 1000 RPM, R2001 base case muffler

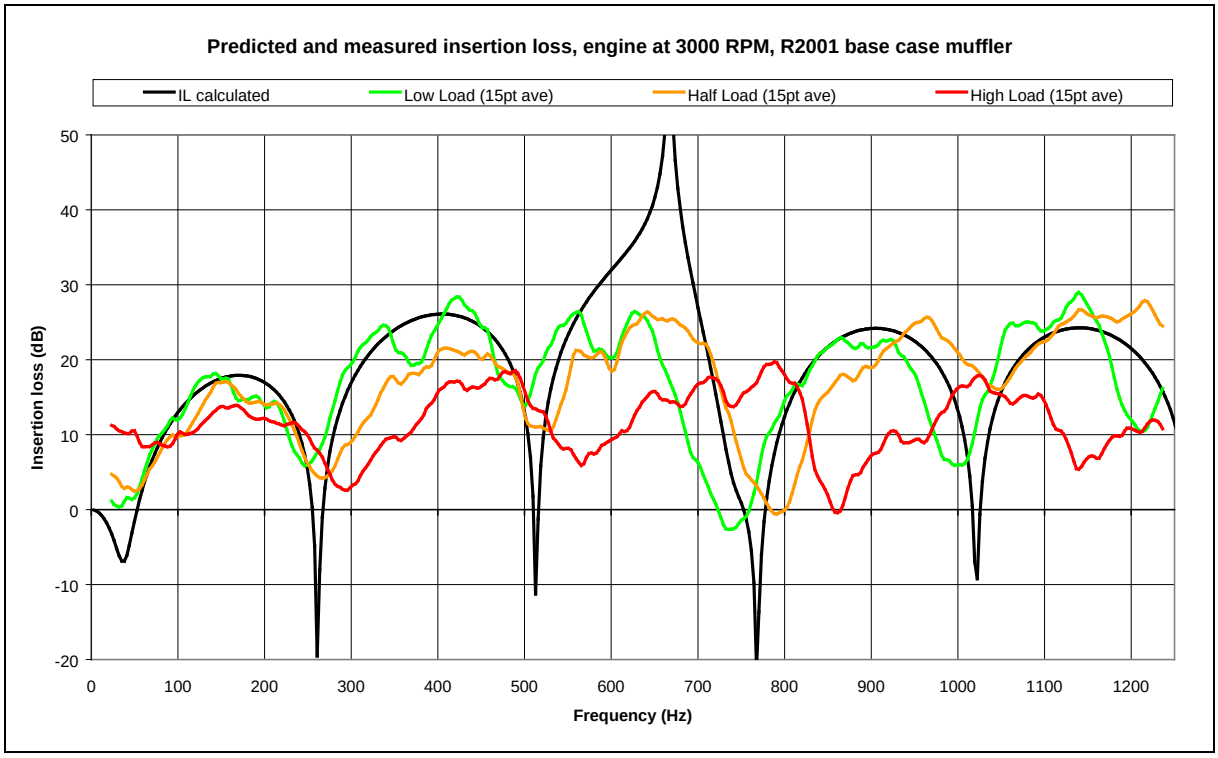

Figure B-29 Predicted and measured insertion loss, engine at 3000 RPM, R2001 base case muffler

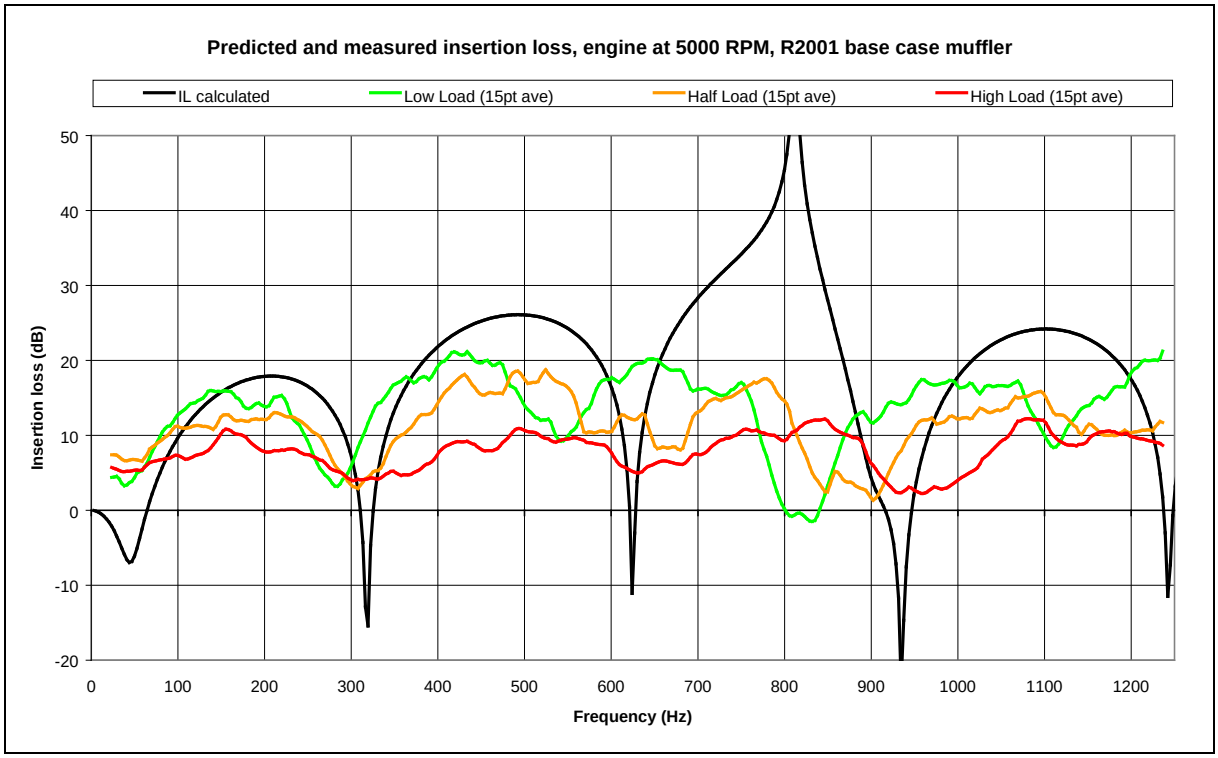

Figure B-30 Predicted and measured insertion loss, engine at 5000 RPM, R2001 base case muffler

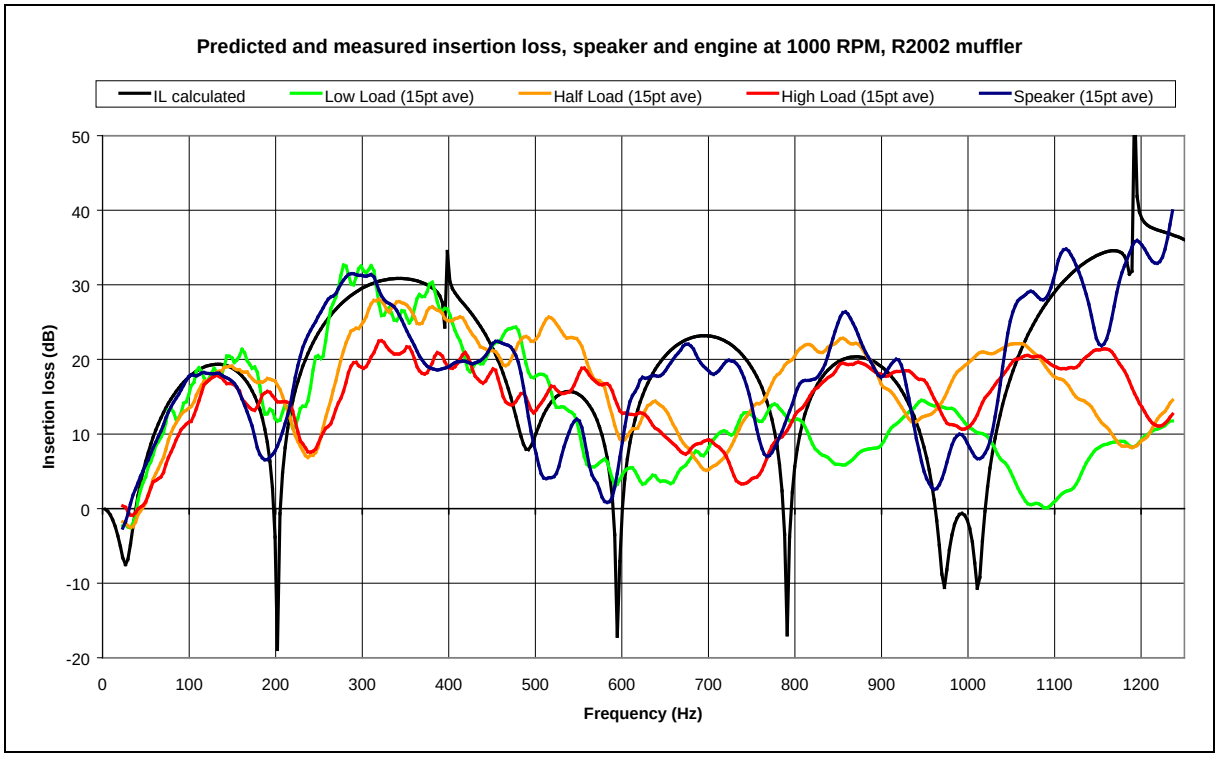

Figure B-31 Predicted and measured insertion loss, speaker and engine at 1000 RPM, R2002 muffler

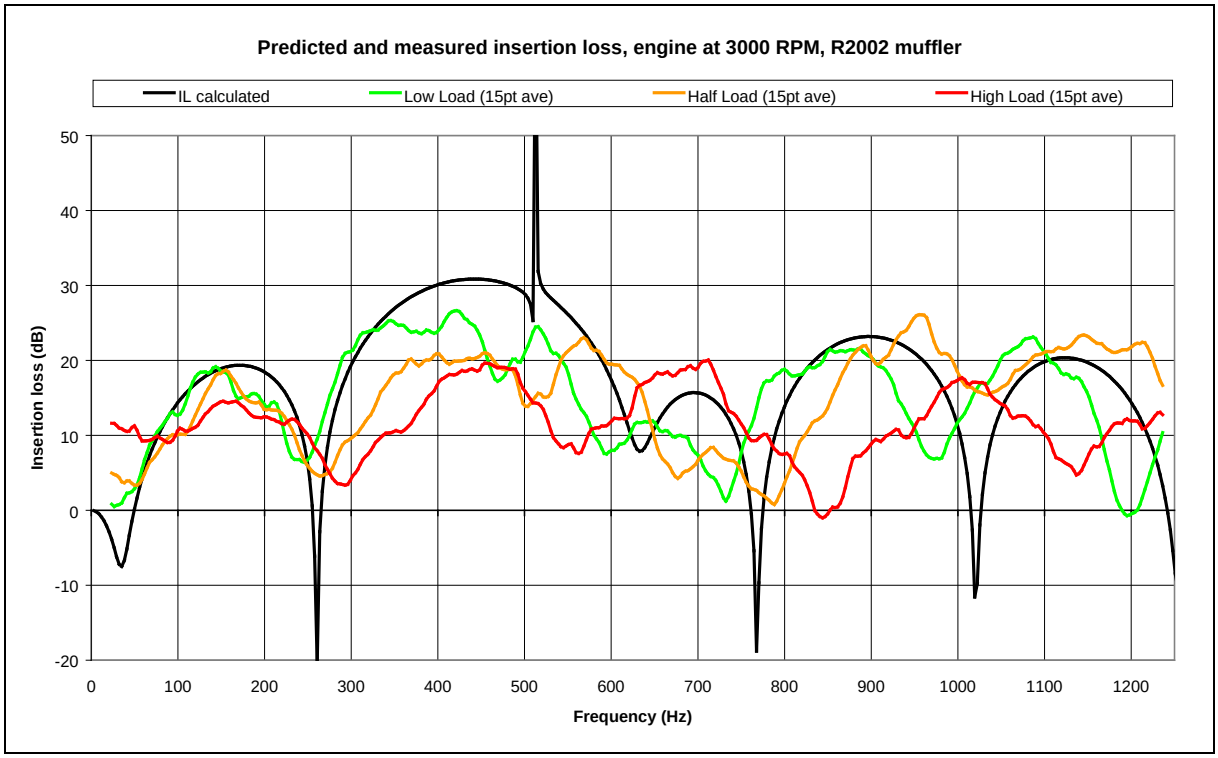

Figure B-32 Predicted and measured insertion loss, engine at 3000 RPM, R2002 muffler

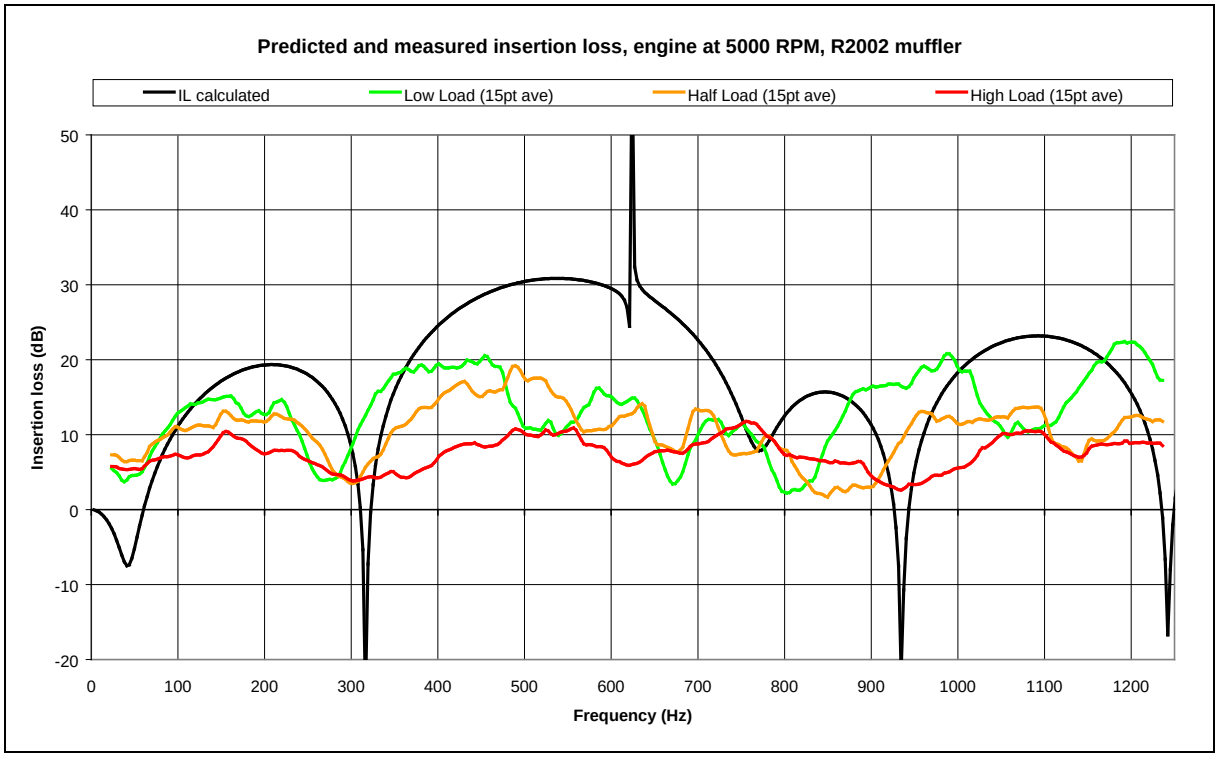

Figure B-33 Predicted and measured insertion loss, engine at 5000 RPM, R2002 muffler

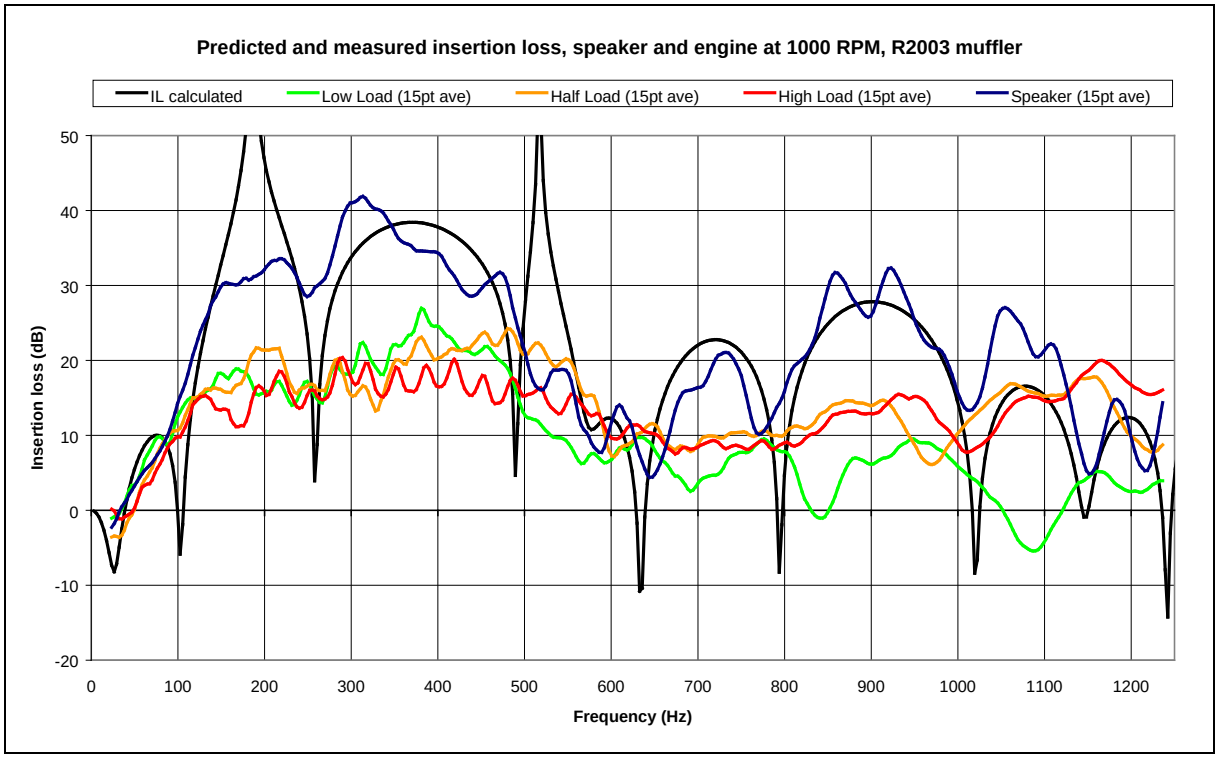

Figure B-34 Predicted and measured insertion loss, speaker and engine at 1000 RPM, R2003 muffler

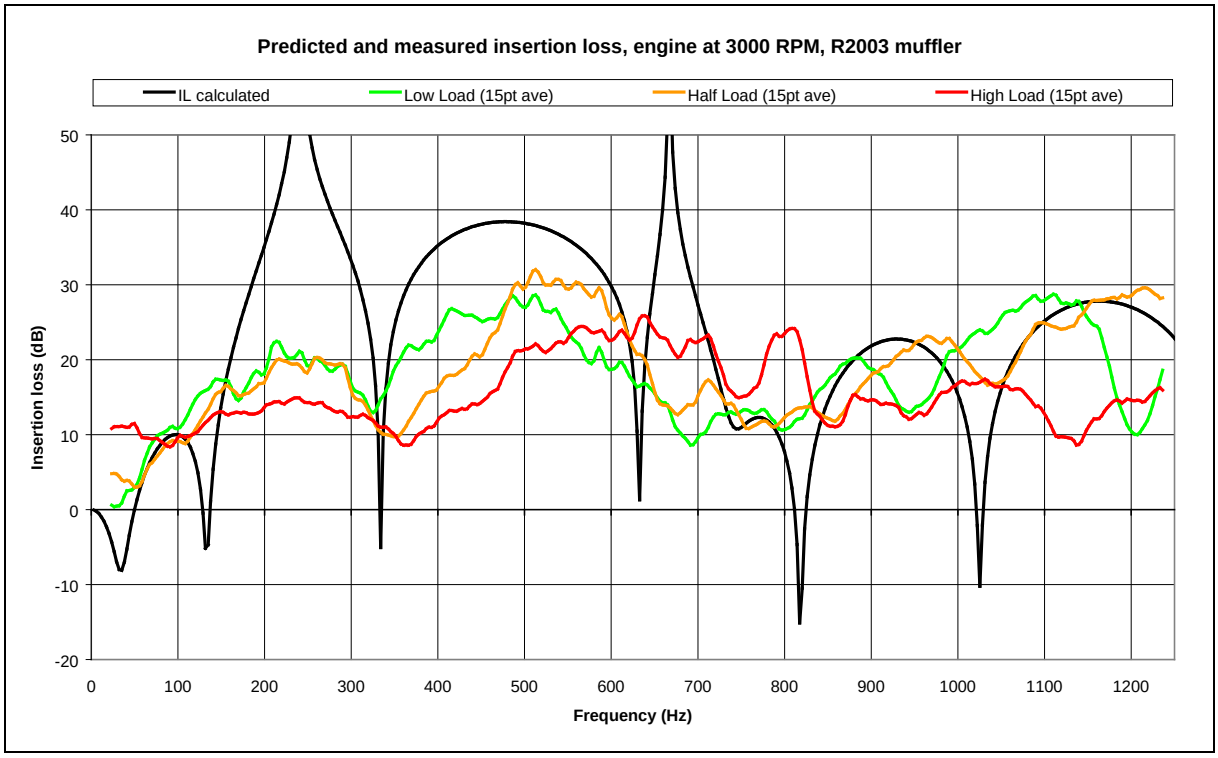

Figure B-35 Predicted and measured insertion loss, engine at 3000 RPM, R2003 muffler

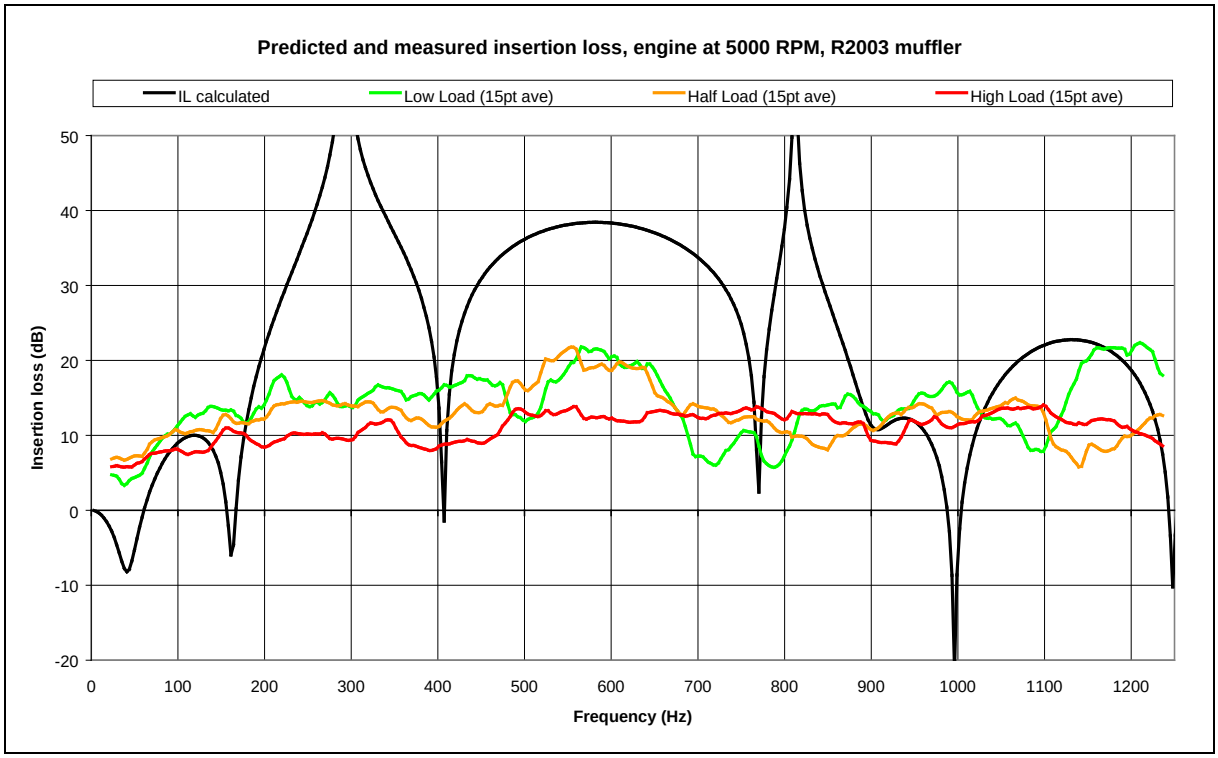

Figure B-36 Predicted and measured insertion loss, engine at 5000 RPM, R2003 muffler

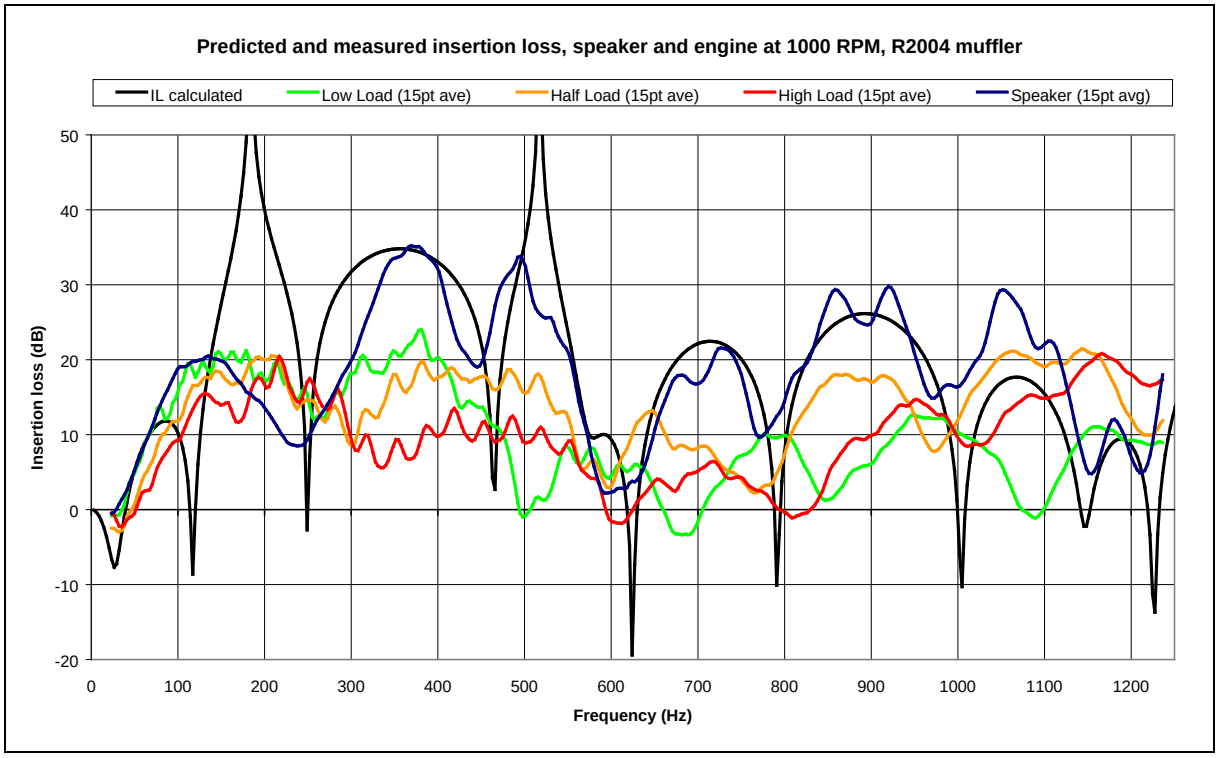

Figure B-37 Predicted and measured insertion loss, speaker and engine at 1000 RPM, R2004 muffler

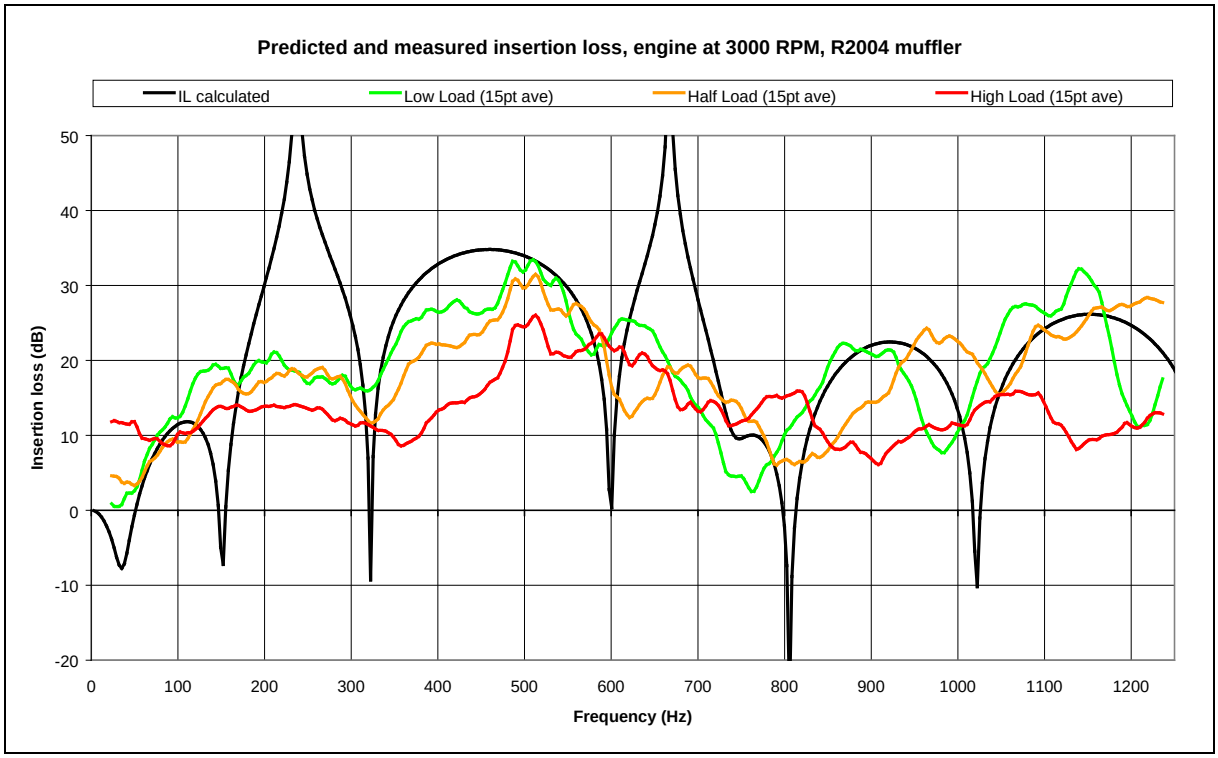

Figure B-38 Predicted and measured insertion loss, engine at 3000 RPM, R2004 muffler

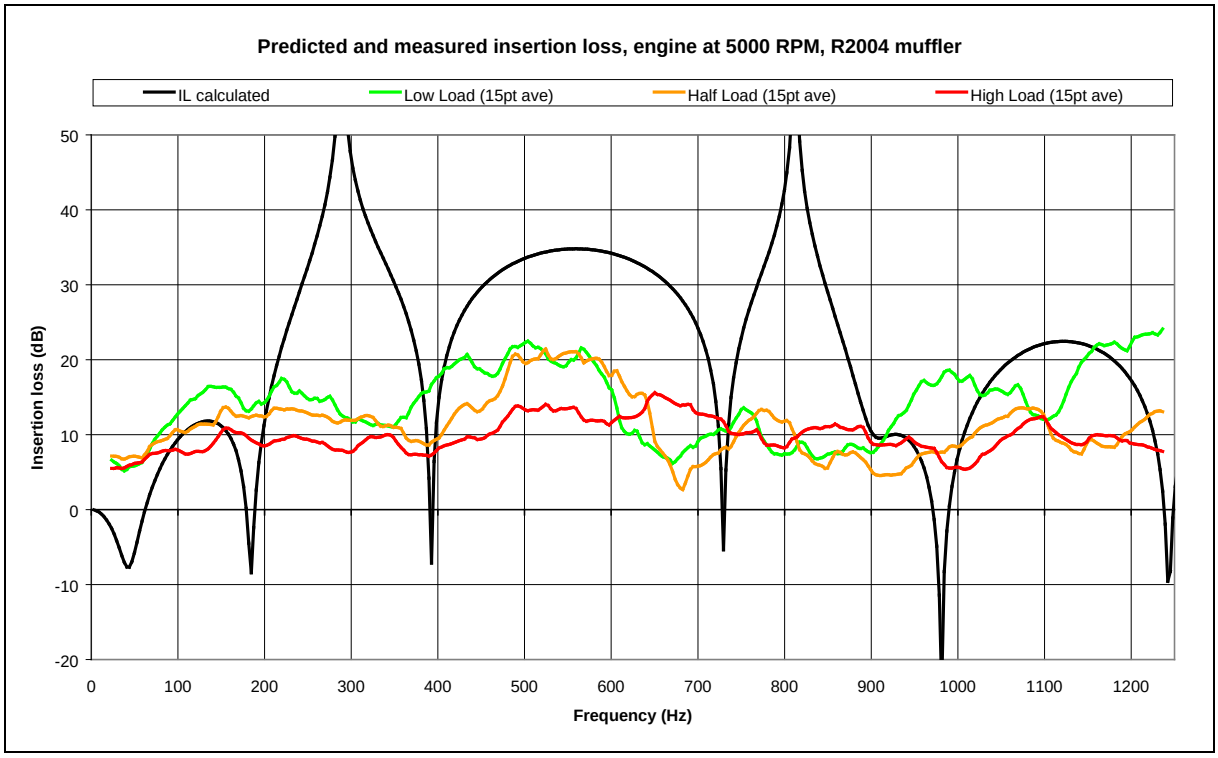

Figure B-39 Predicted and measured insertion loss, engine at 5000 RPM, R2004 muffler

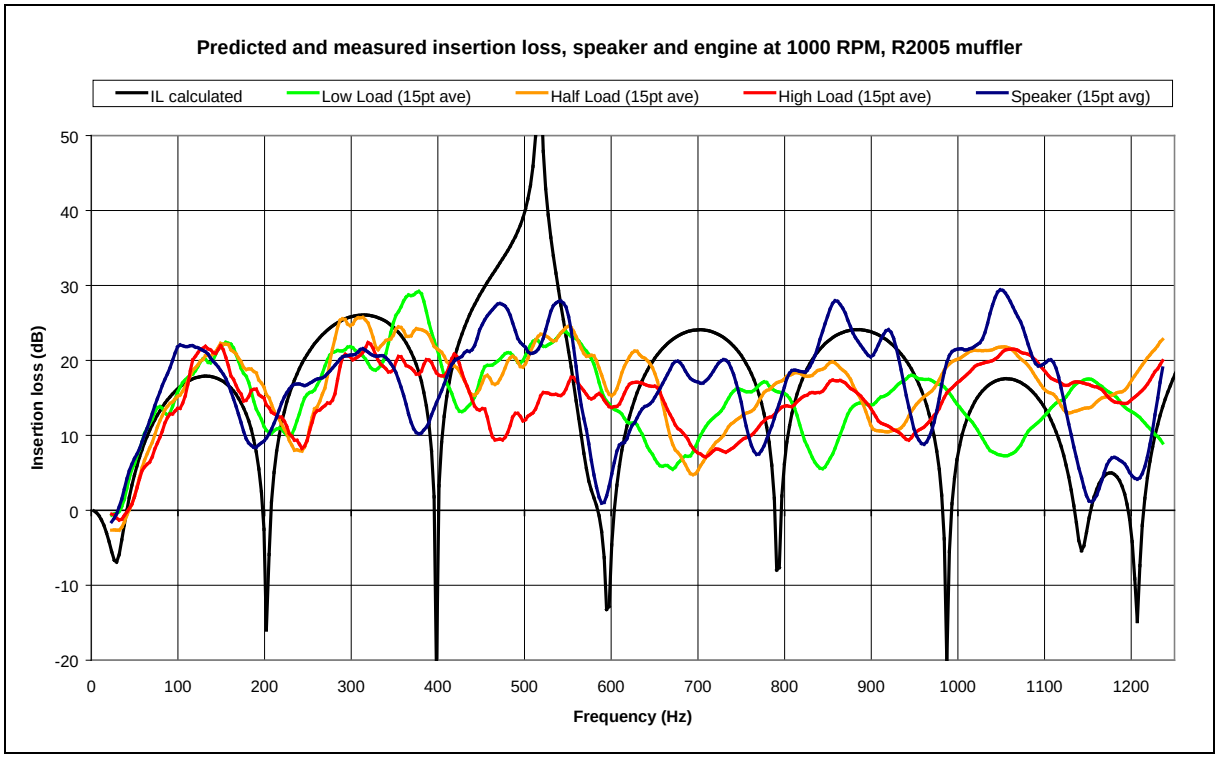

Figure B-40 Predicted and measured insertion loss, speaker and engine at 1000 RPM, R2005 muffler

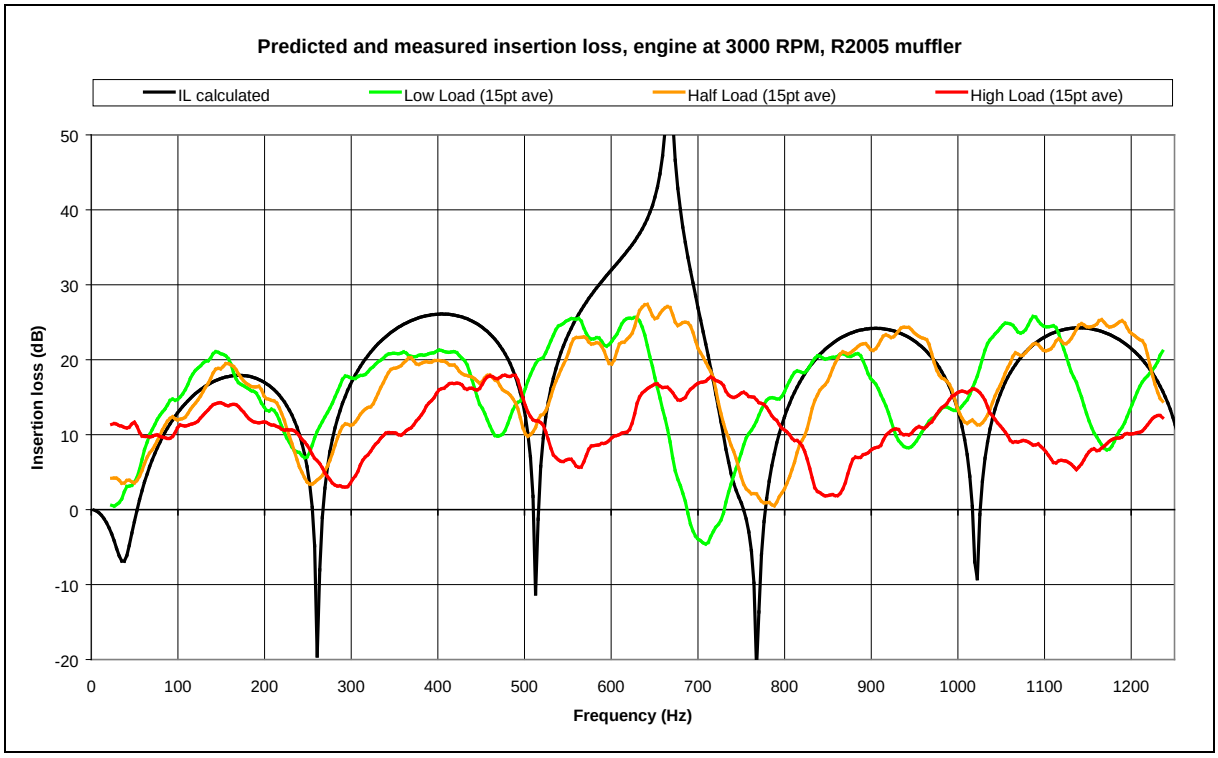

Figure B-41 Predicted and measured insertion loss, engine at 3000 RPM, R2005 muffler

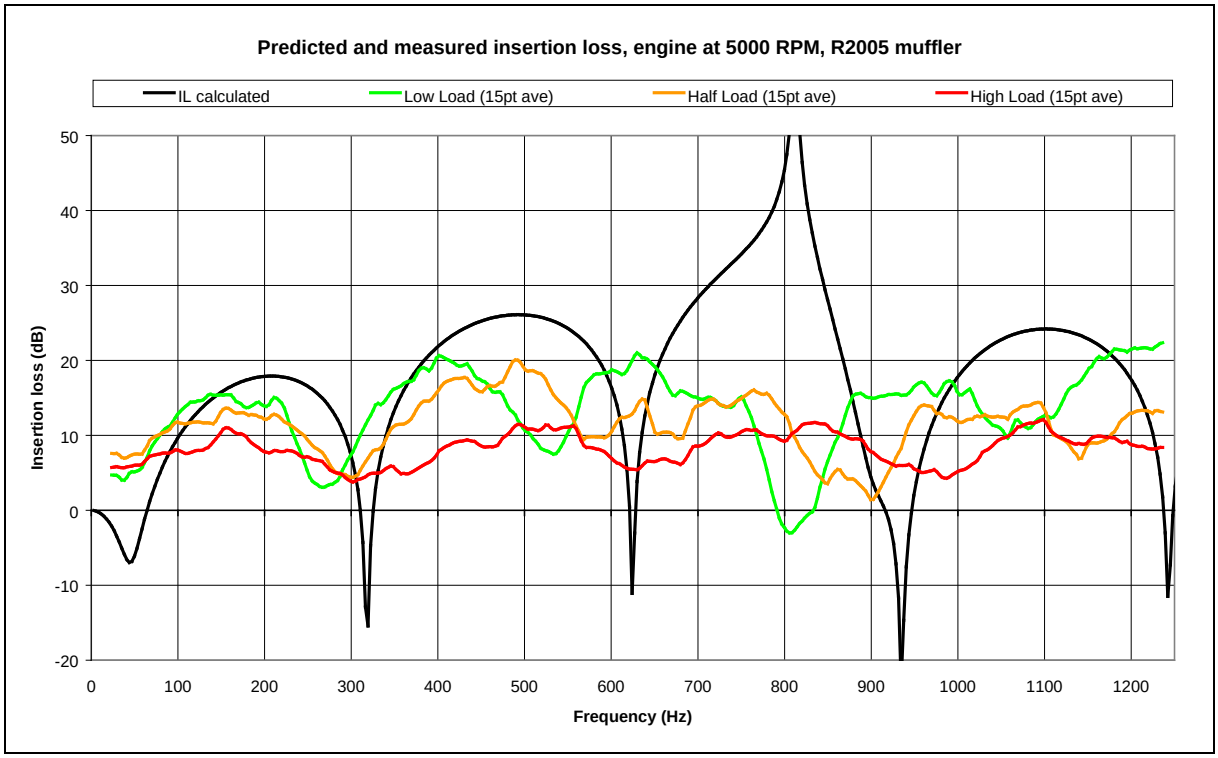

Figure B-42 Predicted and measured insertion loss, engine at 5000 RPM, R2005 muffler

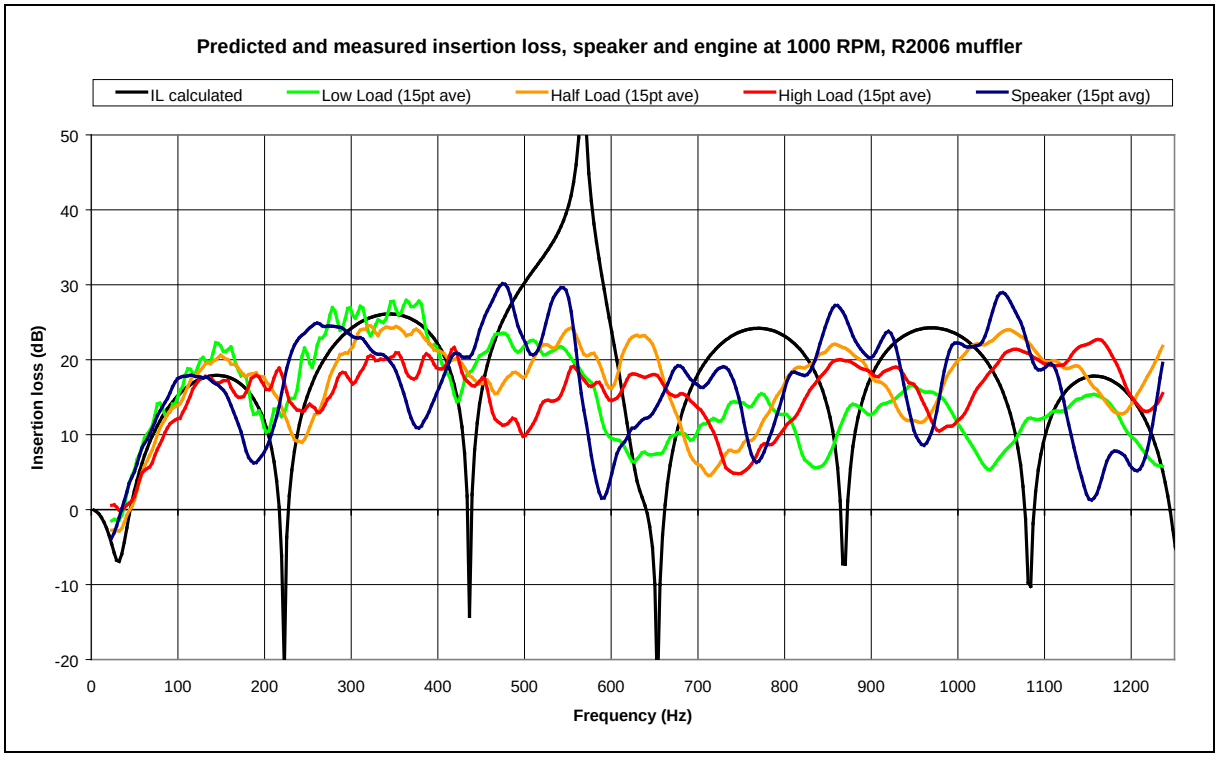

Figure B-43 Predicted and measured insertion loss, speaker and engine at 1000 RPM, R2006 muffler

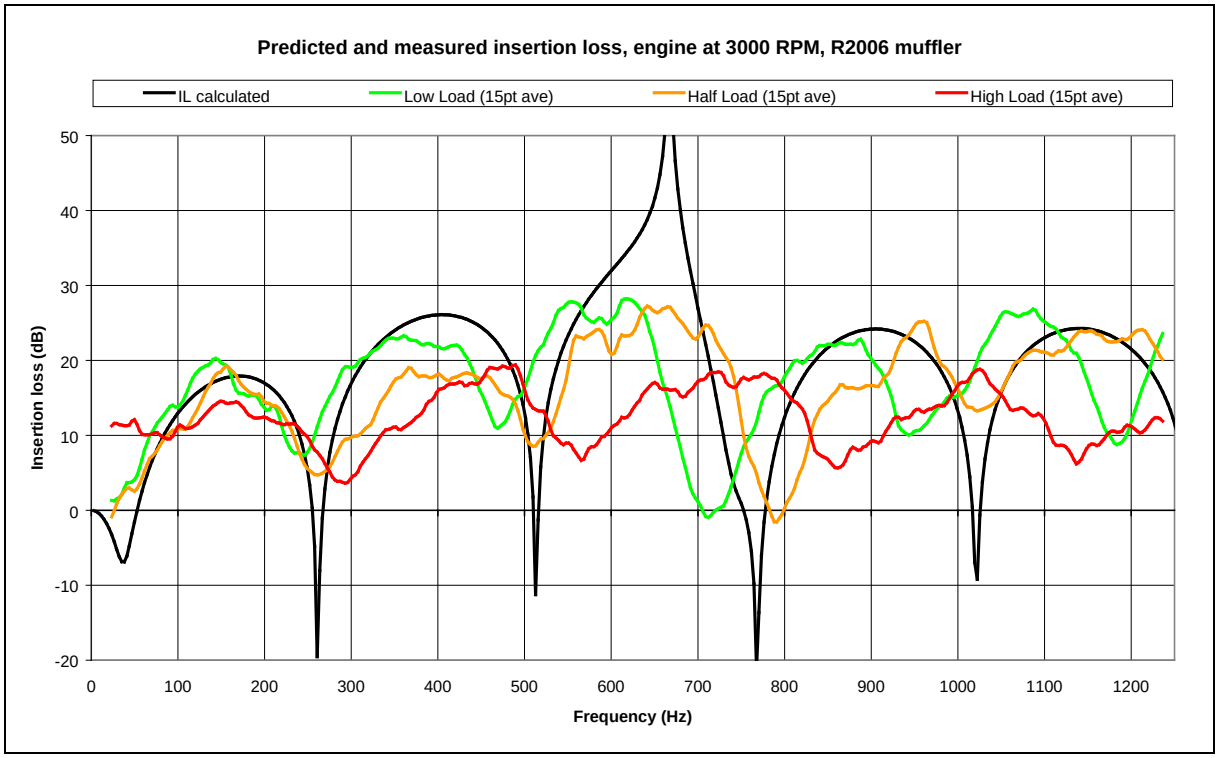

Figure B-44 Predicted and measured insertion loss, engine at 3000 RPM, R2006 muffler

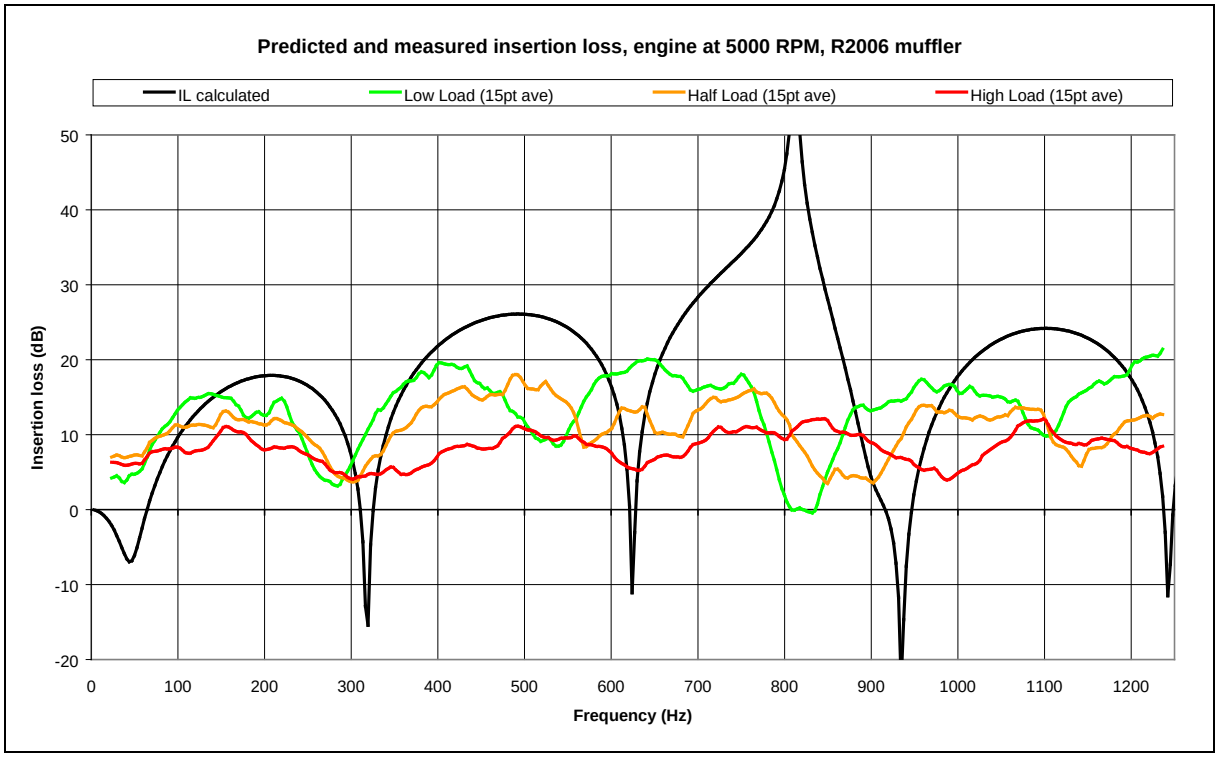

Figure B-45 Predicted and measured insertion loss, engine at 5000 RPM, R2006 muffler

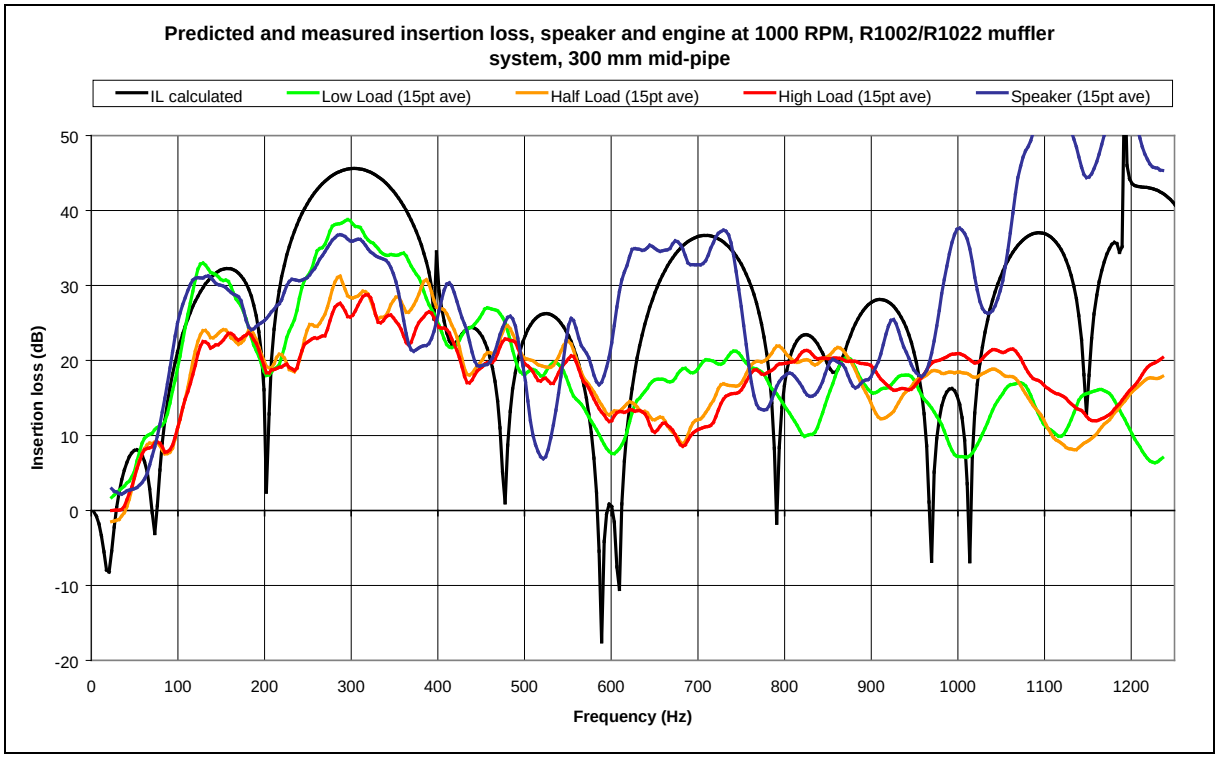

Figure B-46 Predicted and measured insertion loss, speaker and engine at 1000 RPM, R1002/R1022 muffler system, 300 mm mid-pipe

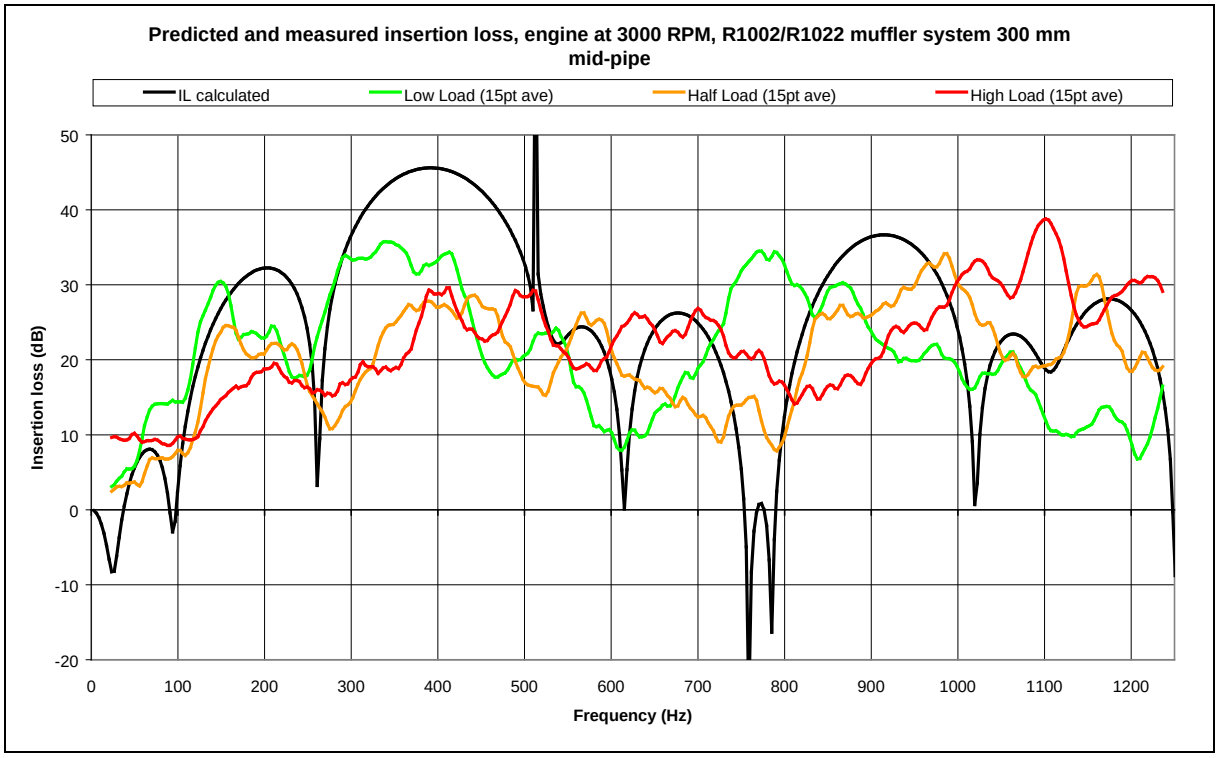

Figure B-47 Predicted and measured insertion loss, engine at 3000 RPM, R1002/R1022 muffler system 300 mm mid-pipe

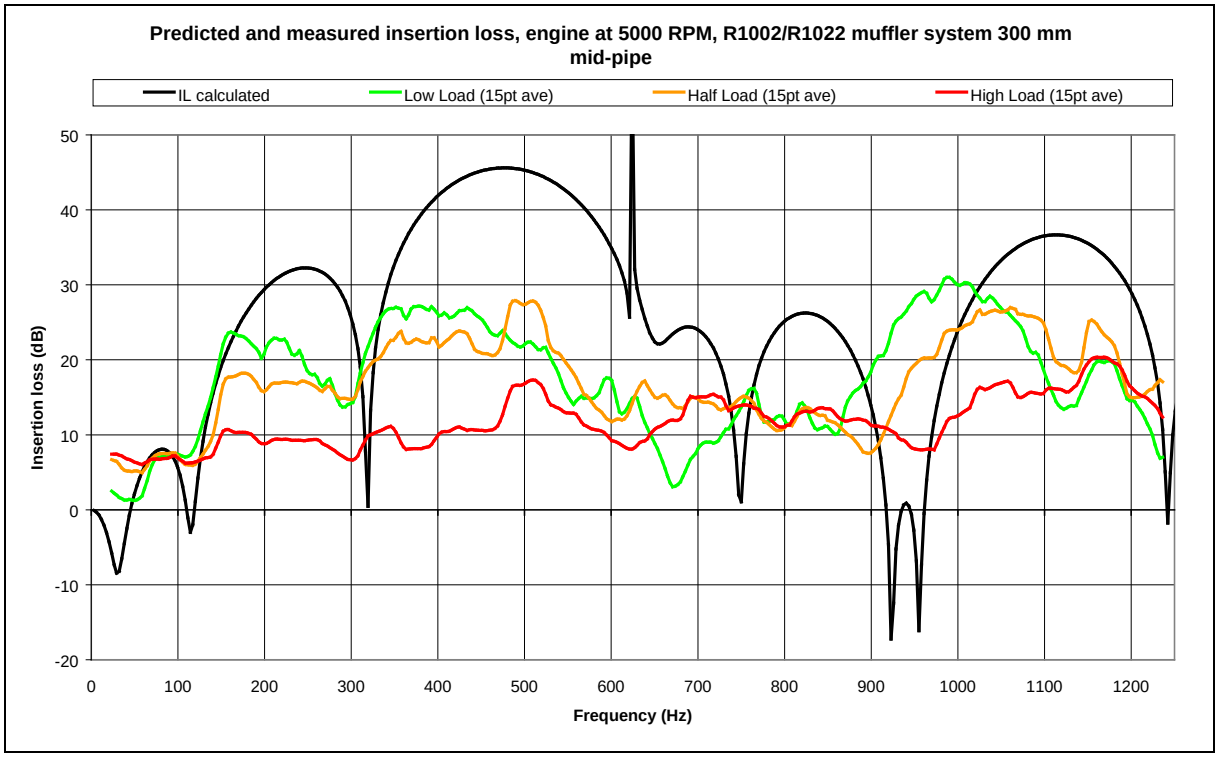

Figure B-48 Predicted and measured insertion loss, engine at 5000 RPM, R1002/R1022 muffler system 300 mm mid-pipe

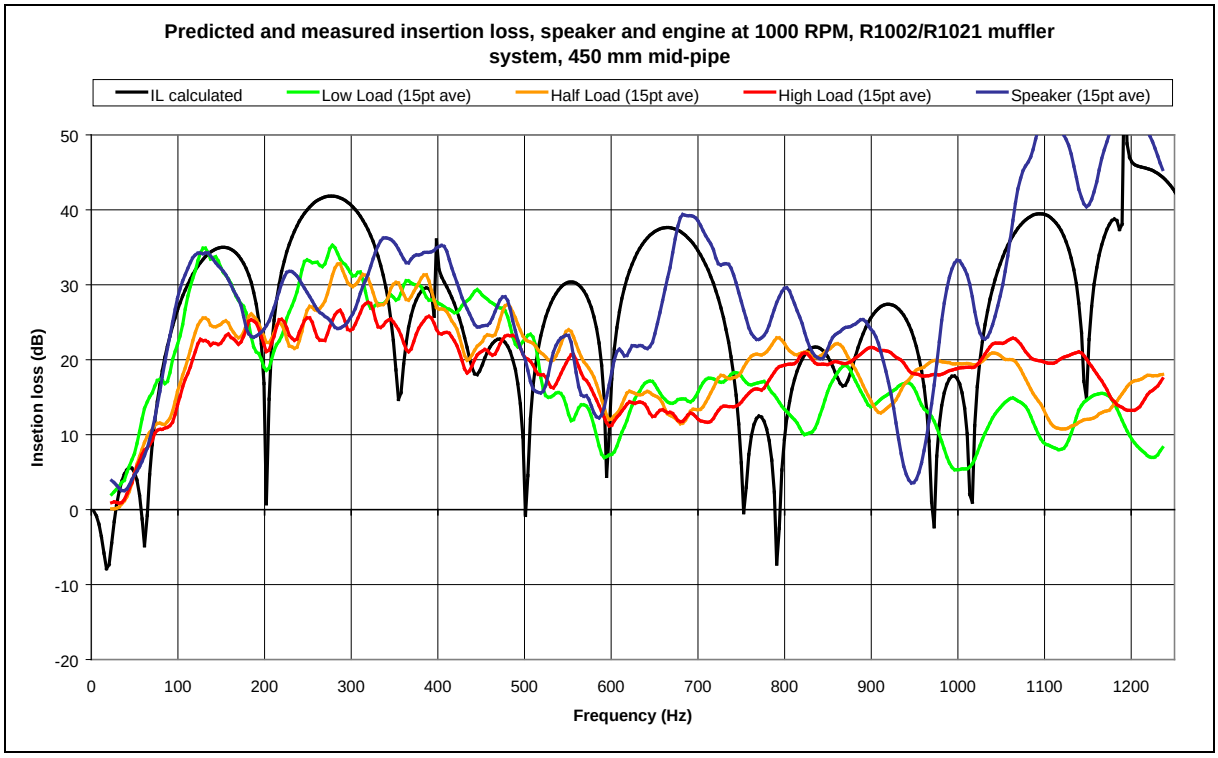

Figure B-49 Predicted and measured insertion loss, speaker and engine at 1000 RPM, R1002/R1021 muffler system, 450 mm mid-pipe

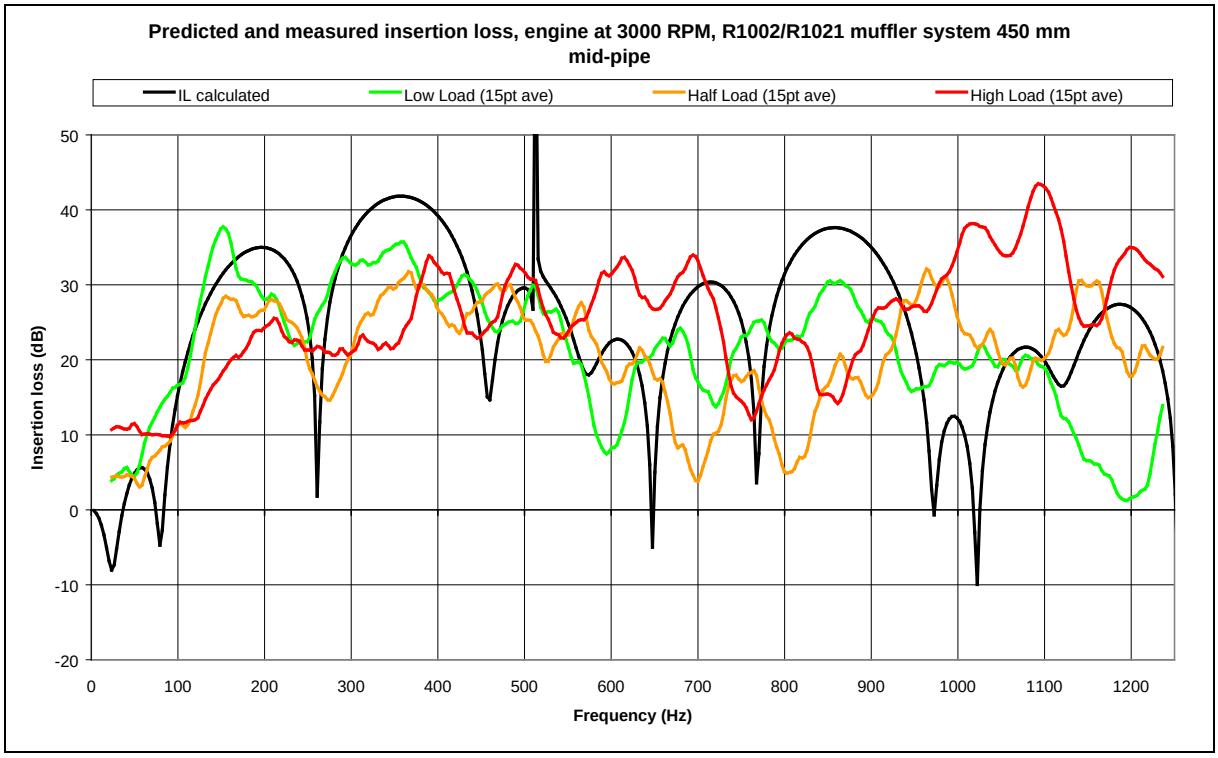

Figure B-50 Predicted and measured insertion loss, engine at 3000 RPM, R1002/R1021 muffler system 450 mm mid-pipe

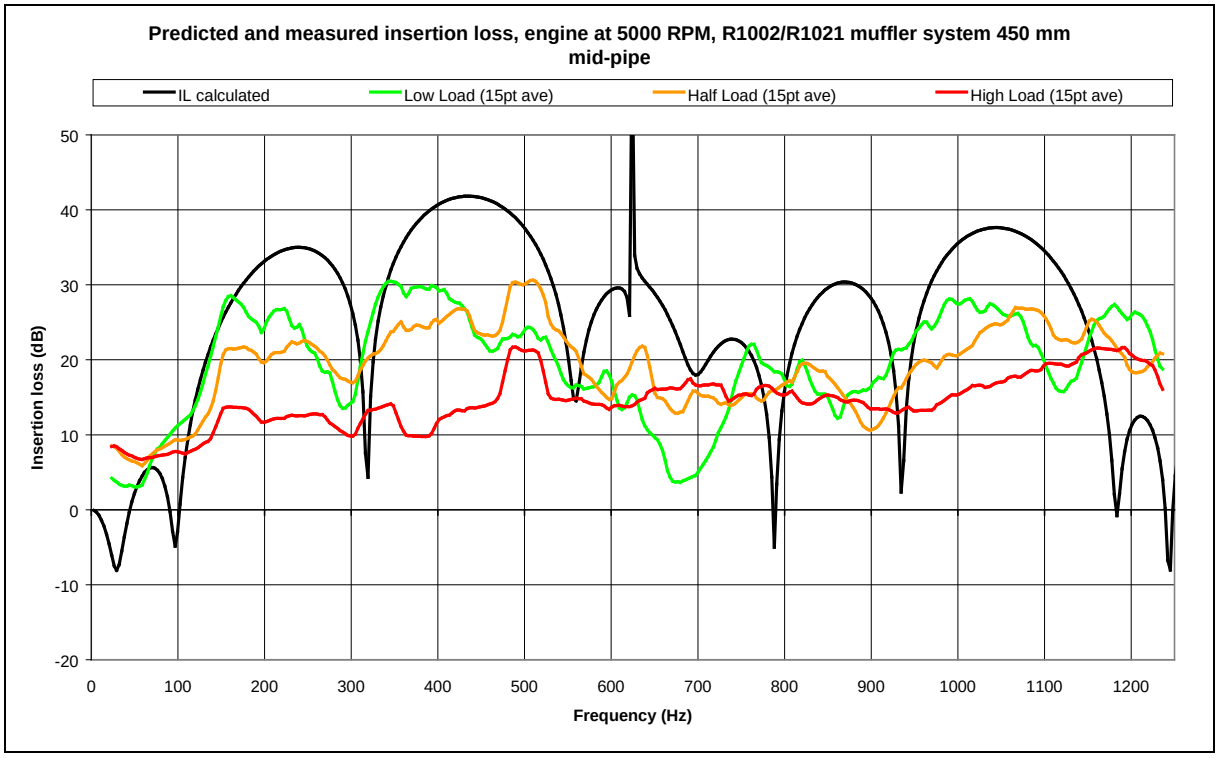

Figure B-51 Predicted and measured insertion loss, engine at 5000 RPM, R1002/R1021 muffler system 450 mm mid-pipe

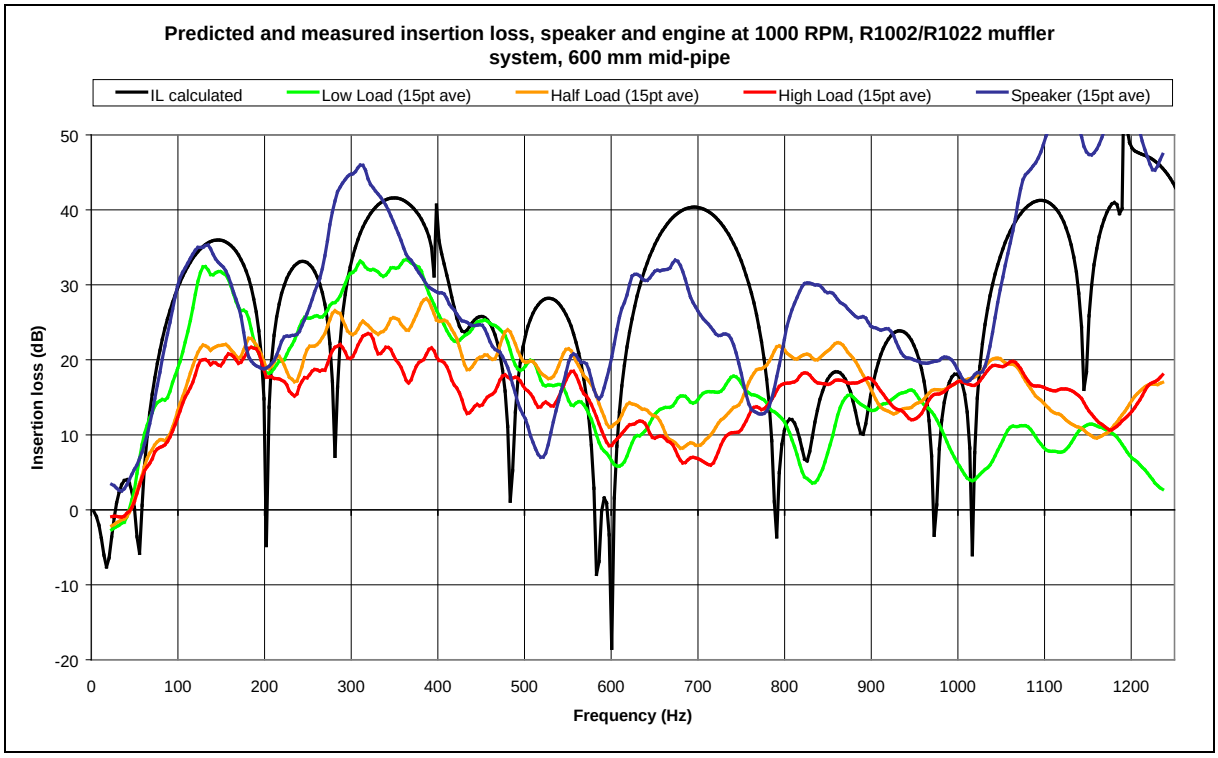

Figure B-52 Predicted and measured insertion loss, speaker and engine at 1000 RPM, R1002/R1022 muffler system, 600 mm mid-pipe

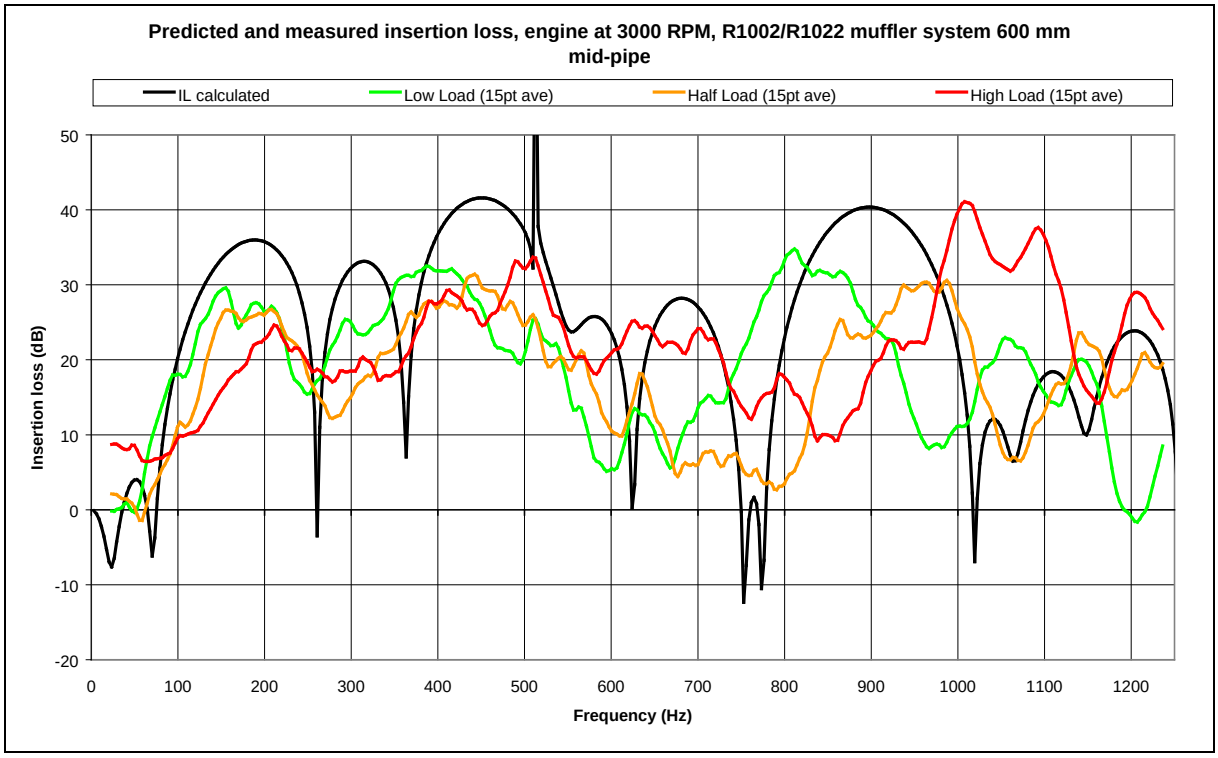

Figure B-53 Predicted and measured insertion loss, engine at 3000 RPM, R1002/R1022 muffler system 600 mm mid-pipe

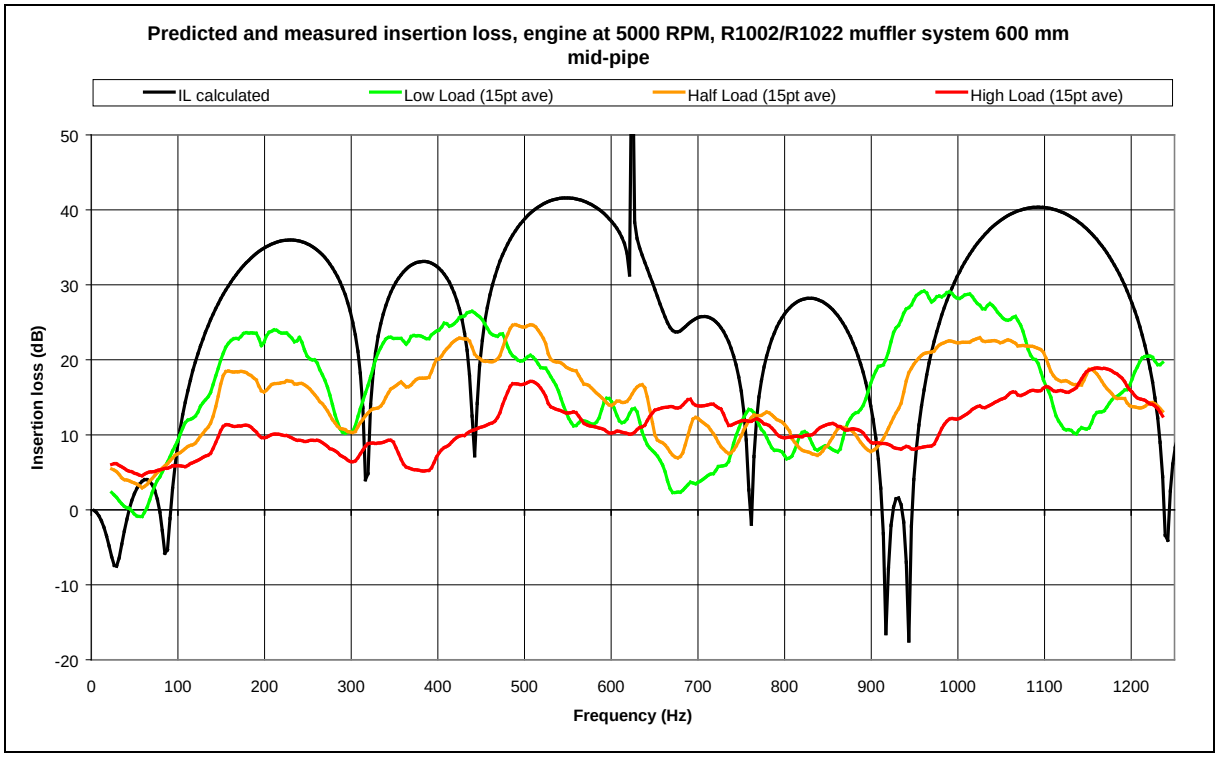

Figure B-54 Predicted and measured insertion loss, engine at 5000 RPM, R1002/R1022 muffler system 600 mm mid-pipe